Multi-Layer Polymer-Metal Laminate as Fire Protection for Lightweight Transport Structures

Sandra Christke

Thesis submitted in accordance with requirements of Newcastle University
for the degree of Doctor of Philosophy

Supervisors: Prof A.G. Gibson and Dr G. Kotsikos

School of Mechanical and Systems Engineering
Newcastle University
Newcastle upon Tyne, UK

June, 2016

Abstract

This study describes the development both of a new surface thermal insulation system, the experimental investigations into its fire protection mechanism and efficacy and a new thermal response modelling program.

The use of multi-layer polymer metal laminates (PML) draws on the general principle common in conventional insulation methods, such as mineral-fibre and intumescent coatings, of immobilising high fractions of gas within the material and using the gas' low thermal conductivity, harnessing the insulating effect. PMLs have the advantage over these systems in that they also form an integral part of the structure thereby contributing to the structural performance.

With the view of taking this concept from laboratory scale to manufacture, material characterisation experiments were carried out to determine thermal and expansion characteristics of the PML material as these properties significantly influence fire performance.

The PML_FIRE model predicts the thermal response of PML-insulated substrates and was developed to take account of PML-specific effects such as expansion and foil melting.

A series of small-scale fire tests were performed over wide heat flux ranges and on various PML designs, which included variations of PML ply numbers, foil thicknesses as well as the front face appearance, in order to gain insights into the PML fire protection mechanism and to validate the PML_FIRE model.

Fire-structural experiments on non-reactive and combustible PML-protected substrates commonly used in lightweight structures demonstrated the lower temperature transfer and the greatly improved structural resilience of the underlying substrate achieved.

Good correlation of experimental and modelled temperature curves using PML_FIRE has been obtained. The thermal state of specimens during heat exposure experiments up to structural failure can now be accurately predicted.

Comparison of PML against other insulation methods illustrated the PML's equivalent or superior behaviour in reducing underlying substrate temperatures and prolonging structural life during fire-structural testing.

Acknowledgements

My sincere gratitude goes towards my supervisors Prof Geoff Gibson and Dr George Kotsikos for their continued support, encouragement and discussion to assist me on my way throughout these years.

A great thank you is owed to my colleagues of the composites office, namely Pietro, Johannes, James, Maria, Katerina and Sheila. Their companionship, helpful comments and practical assistance is highly appreciated.

I am grateful to all technical and clerical staff at the School of Mechanical and Systems Engineering. Special thanks go to our workshop technicians Brian and Stevie for their excellent work.

This research was part of the FIRE-RESIST project funded as a Framework 7 program by the European Commission. I would also like to acknowledge the financial support given through the Endeavour Research Fellowship awarded by the Australian Government, Department of Education and Training.

Finally, I would like to express my greatest thanks to my family and friends for their limitless trust, enthusiasm and patience over the last years.

Contents

List of Figures

List of Tables

Nomenclature

Abbrevations	**Description**
1D, 2D, 3D	1-, 2-, 3-dimensional
AA2024	Aluminium alloy of type 2024/T351
CFRP	Carbon fibre reinforced polymer
COM_FIRE	Program modelling thermal behaviour of composites in fire
DSC	Differential scanning calorimetry
FD	Finite difference
FIGRA	Fire growth rate
FR	Flame retardant
GLARE	Glass laminate aluminium reinforced epoxy
GNUPLOT	Function and data plotting software
HR10, HR20, HR40	Heating rates of $10\,\mathrm{K\,min^{-1}}$, $20\,\mathrm{K\,min^{-1}}$, $40\,\mathrm{K\,min^{-1}}$
HRR	Heat release rate
HTC	Heat transfer coefficient
LVDT	Linear variable differential transformer
MARHE	Maximum average rate of heat emission
ML	Mass loss
PML	Polymer-metal laminate
PML_FIRE	Program modelling thermal behaviour of PML-insulated specimen in fire
QI	Quasi-isotropic
SEA	Smoke extinction area
T600	Time to reach 600 °C
TC	Thermocouple
TGA	Thermogravimetric analysis
THR	Total heat release
TTF	Time to failure
TTI	Time to ignition

Symbols	**Description**
A	Pre-exponential factor
α	Thermal diffusivity
α_s	Material absorbtivity
a, b	Thickness
β	Expansion factor
Bi	Biot number
c_p	Specific heat capacity
Δ	Increment, difference
ΔH	Enthalpy
E_a	Activation energy

Symbols (contd.)	**Description**
ϵ	Emissivity
Fo	Fourier number
h	Heat transfer coefficient
h_g, h_s	Enthalpy of volatiles, solid
H_m	Latent heat of melting
k	Thermal conductivity
m	Mass
m_0, m_f	Initial and final mass
n	Order of reaction
φ	Constituent volume fraction
q	Heat flux
Q_p	Heat of decomposition
R	Gas constant
ρ	Density
σ	Stefan-Boltzman constant
t	Time
T	Temperature
T_0	Initial temperature
T_{amb}, T_∞	Ambient temp
T_{fl}	Temperature of flame or heat source
T_g	Glass transition temperature
T_{max}	Temperature at point of maximum mass loss rate
T_{melt}	Melting point
T_{onset}, T_{offset}	Temperature at start and end of reaction
$T_{\%}$	Temperature at point of specific residual mass
θ	Dimensionless temperature
w	Constituent weight fraction
x	Spatial location, distance
y_c	Char yield

Sub-/Superscripts	**Description**
0	Initial
1	Final
alu	Aluminium
eff	Effective
fl	Flame
g	Gas
Int	Intumescent
k	Reaction
pc	Passive coating
PML	Polymer Metal Laminate
res	Resin
s	Solid, substrate
$t-1, t, t+1$	Time increment
x	X-direction
$x-1, x, x+1$	Spatial, nodal location

Chapter 1

Introduction

1.1 Application of Lightweight Materials

Over the last century, materials used in mass transportation industries such as aerospace, marine and railway have seen pioneering evolution. Continued advances in vehicle design and manufacturing processes led to the emergence of new materials such as aluminium, magnesium and titanium alloys as well as fibre-reinforced composite materials that replaced the traditional metal and wood structures used at the beginning of mass transportation in the 1930s.

One of the main reasons for technological progress was the drive to find lightweight substitutes which could significantly reduce the overall mass. Weight reduction has been and continues to be an important driving force in the development of passenger and freight transportation as it is one of the major aspects that has direct impact on vehicle performance. Further advantages that new, lighter but also stronger materials bring is a reduction of the vehicle's structural weight enabling vehicles to carry a higher proportionate payload as well as longer range, greater fuel economy and higher speeds.

Lower fuel consumption as a direct result of weight reduction is a critical economic aspect as cost savings play an important factor alongside ever-increasing fuel expenses. Another benefit arising from reduced fuel consumption is the reduced emission of greenhouse gases, mainly CO_2, and with global efforts to reverse climate change imposed by government regulations this is a major objective.

1.1.1 Aerospace

Since the first powered flight that the Wright Brothers made in 1903 with their motorised and controlled *Wright Flyer*, one of the main driving forces for development in aviation has been the search for lighterweight materials. From the beginning of mass transportation in the 1930s aluminium alloys have been the choice of materials used in aircrafts. They offer high strength-to-weight ratios which makes them favourable in weight sensitive applications. Improvements in aluminium alloys through the introduction of new alloying elements, new manufacturing methods and heat treatment processes led to the development of aircraft alloys such as the 2024-T3 which features Al-Cu-Mg, moderate strength and good damage tolerance as well as the 7075 alloy comprising Al-Zn-Mg-Cu rated for having the highest alloy strength but with poor corrosion resistance [1]. A series of accidents in 1954 caused by premature fatigue failure prompted a rethink of the state-of-the-art development strategies. Improvements in structural performance simply through lighter materials was not as important a consideration because other aspects such as damage tolerance, i.e. fatigue resistance and fracture toughness, became essential criteria in material selection and alloy development.

The 1970s and 1980s saw diverse approaches in material developments because upcoming

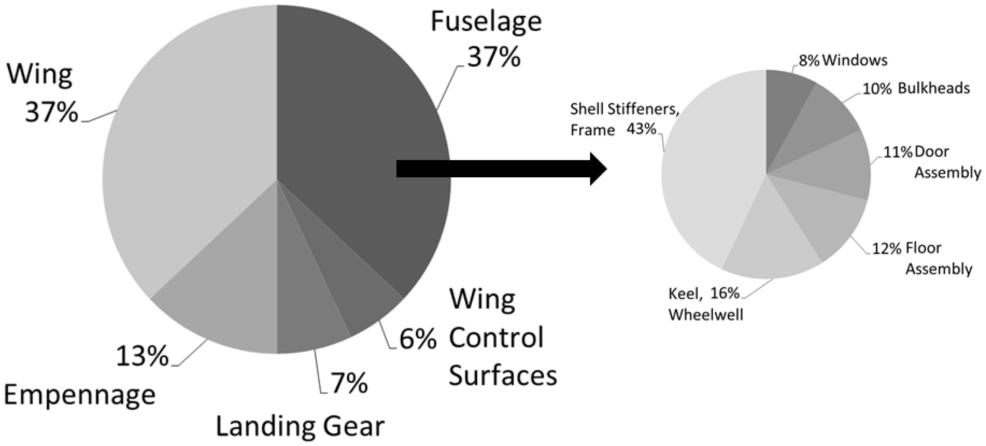

Figure 1.1: Contributions of individual structural elements to the overall weight of a commercial transport aircraft. Data from [4].

challenges such as fuel cost, increased range and landing weight fees added to the burden of suitable material selection. One approach to overcome these challenges was the development of aluminium-lithium alloys. For every 1 % of lithium added to the alloy the material density is reduced by 3 % which results in high specific material properties. Typical Al-Li alloys (8090/1, 2090/1) comprise of a lithium content of around 2 % which leads to optimum strength, corrosion and damage resistance. Disadvantages such as high material cost, high property anisotropy and thermal instability limit the widespread use of Al-Li alloys [2]. Even today Al-Li are only used for specific applications in commercial aircrafts, with the noteworthy exceptions of the EH101 helicopter and space craft tank applications which make extensive use of Al-Li alloys [3].

Titanium alloys present an alternative to Al-Li alloys because of their increased strength-to-weight ratio. They also provide thermal stability compared to aluminium alloys which is specifically attractive in temperature sensitive areas such as engine applications of rotating and static components, e.g. fan discs, blades, vane materials and in airframe components located close to the engine [5]. The use of titanium has increased significantly comprising up to 10 % total weight of a Boeing 777 as well as higher percentages in military aircraft [6].

With the development of new aluminium alloys being virtually exhausted the focus has shifted to new hybrid materials. In the 1980s fibre-metal laminates emerged combining metals and new composite materials. Fibre-metal laminates consist of alternating layers of high-strength aluminium alloys and fibre-reinforced epoxy polymers. The two most common types are ARALL (aramid reinforced aluminium laminate) and GLARE (glass reinforcement). Various laminate configurations exist which feature tailored volume fractions or fibre orientations to meet versatile design requirements, combining properties of high strength and stiffness. Fibre-metal laminates have been especially developed because of their high fatigue resistance, bearing in mind that nearly 58 % of repairs to fuselages are due to fatigue cracks [7]. Cracks developing in individual aluminium sheets can be bridged by the undamaged fibres of the composite layers which slows down the crack growth by a factor 10-100 compared to monolithic aluminium alloys [8]. Probably the most well-known application of fibre-metal laminates today is the fuselage of the A380 that is entirely manufactured from GLARE material.

With the advent of composite materials being used in all transport sectors, fibre-reinforced polymers were firstly introduced into aircrafts in the 1970s as secondary structures, e.g. doors, spoilers, rudders and fairing, due to their weight saving potential, see figure 1.1. Advances specifically directed at the development of fibre-reinforced composites and the manufacturing processes have led

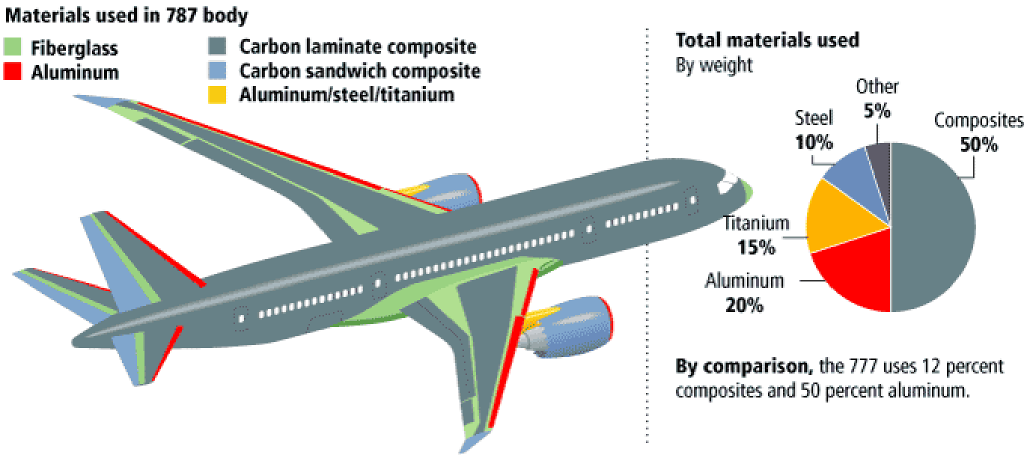

Figure 1.2: Detailed material breakdown for a Boeing 787 Dreamliner [14].

to the emergence of high-strength and high-modulus carbon fibre structures which are compatible substitutes for aluminium and titanium alloys for use in primary structures [9]. Besides the weight saving potential of up to 40 % of the secondary structure and 20 % of the primary structure [10], further advantages in the use of composite materials lie in the simplification of the assembly process by reducing the number of component parts and in their use for repairs of metal parts of the aircraft. Eventually in the early 1980s, the first all-composite small business aircrafts were launched with the LearFan and the Beech Starship [11]. The increasing advances and hence the more widespread application of composites over the last decade culminated in the launch of the super jet airliner Airbus A380 and Boeing 787 that are manufactured using nearly 50 % of composite materials, see figure 1.2, and more recently the A350XWB made from 52 % [12]. The military sector generally has been more amenable to new technologies and material types due to the lack of commercial pressure. Current examples of composite applications include the V22-Osprey helicopter which comprises nearly 70 % composite materials of its overall weight as well as the A400M cargo transport aircraft which makes extensive use of composites [13].

1.1.2 Rail

Compared to the aerospace sector, the uptake of composite materials within the railway sector has been slow in the past. This is true for the substitution of traditional steel with new materials in particular in the rail car body structure, however, in modern tram and monorail systems composites comprise the main proportion of the overall material list [15].

Composites have been used for several decades in the manufacture of secondary elements, such as the interiors of trains with weight savings of up to 40 % of the total weight being achieved. Traditional material systems have comprised of glass fibre reinforced polymers made of polyester or phenolic resin which meet the high fire, smoke and toxicity requirements needed to guarantee passenger safety. Further developments have led to the development of new composites including carbon fibre materials as well as sandwich structures of thin high-performance skins with a thick low-density core [16] leading to the introduction of a vast range of interior components such as doors, window frames, ceilings, flooring, side panels, partition walls, seats and luggage storage.

The advantage clearly lies in the flexibility of the shaping and forming processes of the composite materials to meet the complex needs of the customers and train operators. Advances have also been made by major train manufacturers such as Siemens, Bombardier and Alstom to expand the use of composites to the exterior of the rail cars. The front-ends of most high speed trains nowadays are made of composite materials because they offer a simplified manufacturing process for the complex curvature, in comparison to metal structures, which also has the significant benefits of meeting the high aerodynamics and aesthetic requirements of the nose design; an example of such a composite design is shown in figure 1.3. Notable examples are the German ICE, French TGV and Eurostar trains as well as their counterparts in South Korea and the USA [17]. Some of the drawbacks in using composites on a larger scale, in particular, for load-bearing structures arise from concerns due to lack of research data regarding the long term material performance characteristics over the expected life span of 30 to 40 years. Especially, the performance during a vehicle crash is an important aspect as impact and energy absorption in collision scenarios have been probed [15]. Additionally, questions of higher front loading of investment and manufacturing costs together with uncertainties in maintenance and repair presented significant obstacles for a faster uptake of composite materials. In the past, uncertainties with regard to standards and regulations, i.e. the lack of relevant rail industry standards for certifying composite designs, have also hindered progress. Much progress was achieved through the harmonisation of a multitude of national standards contained in European-wide legislation, which lowers trade barriers and allows for interoperability across borders. For example, all materials in rail applications have had to comply with standards regarding the structural performance of a vehicle under static load, EN-12663 [19], in a collision, EN-15227 [20], as well as having to fulfil stringent fire safety regulations, EN-45545 [21] which represents the most recent European standardisation.


Figure 1.3: Composite nose design in Siemens Velaro train family used as Eurostar, ICE3, AVE or CRH3 [18].

However, research efforts over the last two decades have shown the possibility and feasibility of manufacturing rail vehicles that are predominantly manufactured from composite materials. The impetus for this research has been the light railway sector. For example, the body-shells for numerous monorails in theme parks such as Florida and Las Vegas as well as the Copenhagen metro are all manufactured from composite materials [15, 22]. A major break-through in the field of heavy railway development was the first full-composite prototype of a body-shell of a three car tilting train designed by Schindler Waggon in the mid-1990s [22] which facilitates faster cornering. Further examples of the application of composite materials to the body-shell of rail cars include the Korean TTX, the Amtrac NEC in the USA and the Japanese APM Otis [23].

1.1.3 Marine

The US navy pioneered the use of composites in the marine sector in the early 1950s. Although only used for small boats and non-critical structures in the early stages, the advantages of improved operational performance that composites offered quickly led to extended applications to a variety of all-composite vessels including private boats, patrol boats and landing crafts [24].

Besides the universal advantages when using composites instead of steel structures of reducing weight and inducing fuel savings, one especially advantageous aspect for the marine sector is the much reduced maintenance costs because of the corrosion resistance inherent in composites which avoids extensive repainting and consequently reduces maintenance time. Of further importance in naval applications are the enhanced stealth properties due to the non-magnetic properties of composite materials [25].

Advances in design, manufacturing and mechanical performance resulted first in the naval application in larger vessels, hovercrafts, mine hunters and corvettes [24]. The largest all-composite

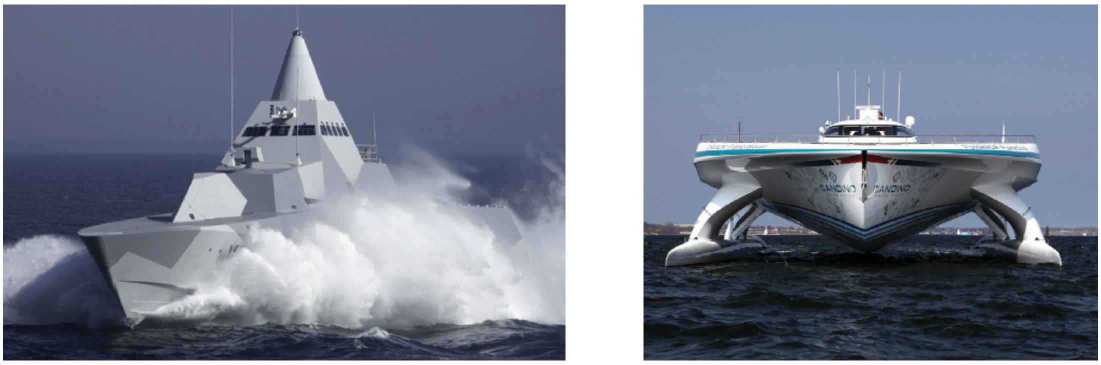

(a) Visby class naval vessel **(b)** TURANOR PlanetSonar

Figure 1.4: Two examples for large-scale composite marine application: a) Swedish corvette-type warship [26], b) the first solar-powered boat to circumnavigate the globe [27].

naval prototypes were commissioned around the turn of the millennium with the Norwegian Skøld and the Swedish Visby class pictured in figure 1.4a. Both of these vessels make extensive use of high performance carbon fibre laminates in combination with sandwich structures.

Traditionally, glass fibre reinforced polyesters were the materials of choice in smaller boats. Vinyl esters and epoxies offer superior matrix properties of resistance to hydrolysis and higher mechanical properties, respectively [28]. However, the higher material cost for both polymeric matrices limits their application to the mass market.

Developments in reinforcement led to the use of Aramid or Kevlar fibres especially for improved impact behaviour, with carbon fibres being used for their high strength and stiffness properties. Sandwich structures of high-strength laminate skins and traditional polyvinylchloride (PVC) foam are widespread [29].

In civilian ship building, small boats and yachts are almost exclusively manufactured from composite materials. Glass fibre-reinforced composites are still the preferred choice for mainstream constructions, but carbon fibres as well as epoxy resins are also popular especially in the luxury or high-performance niche vessels, where specific design requirements need to be met for individual commisions, be it based on aesthetics, strength or stiffness qualities [30]. With the existing variety of matrix systems in combination with the number of reinforcement and core materials, composites can be tailored to meet the required properties accordingly. This resulted in the development of superyachts like the Mirabella V which is the largest single-mast yacht ever built with an overall length of 75 m [31] and the TURANOR, see figure 1.4b, which is solely powered by solar energy.

1.2 Principle of PML Fire Protection

Most of the materials used in lightweight transport applications summarised above suffer from one major drawback: their poor fire performance. Aluminium alloys exhibit low softening and melting temperatures whereas polymer-matrix composites soften and then suffer thermal decomposition due to their organic constituents. These effects pose a major obstacle in the wider implementation of lightweight metal and polymeric materials.

Upon exposure to heat these composite materials first undergo softening which greatly reduces their mechanical strength before the onset of decomposition at higher temperatures for organic components. Besides the potential structural collapse under mechanical loading within a short time frame when exposed to heat, by-products released during decomposition present additional hazards. Smoke not only reduces visibility and impedes evacuation, toxic fumes have a huge impact on survival rates due to the risk of suffocation and intoxication, particular due to the inhalation of

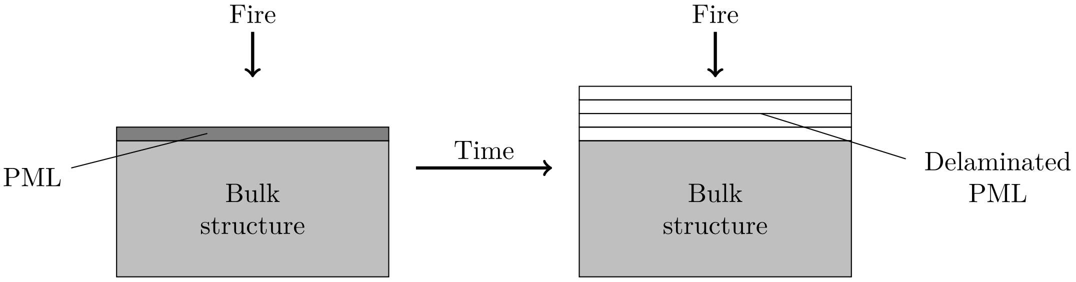

Figure 1.5: Fire protection principle of PML insulation systems.

CO_2. Flammable reaction products add to the total heat release which can further fuel a fire and cause increased flame spread.

In fires multi-micro-layered polymer-metal laminates (PML) are designed to overcome these drawbacks when used as a fire protection barrier on lightweight metallic and polymeric structures. PML are multi-layered laminates consisting of thin metal foils separated by polymeric resin. The concept of hybrid materials assembled in alternating layers is not new. Fibre-metal laminates were the first material class to successfully exploit the synergetic effects of combining completely different material types in order to maximise system performance. The PML concept is derived from the fibre-metal laminate lay-out, however, its primary application to fire protection has not been explored so far. One of the major aspects of the PML concept is to convert the inherently adverse effect of resin decomposition that is accompanied by mass loss and gas production into the advantage of forming a thermal insulation shield.

When exposed to heat, PML undergo great transformation as schematically shown in figure 1.5. The individual polymer layers within the laminate progressively decompose and release gaseous by-products. Extensive delamination is caused as the metallic foils form an impermeable barrier that traps the decomposition gases resulting in an expansion of the whole of the PML. This provides an effective insulating fire barrier to the underlying structure because the rate at which heat is transferred through the PML into the substrate is slowed down due to a drastic reduction in the PML thermal transport properties.

1.3 Assessment of Fire Behaviour

1.3.1 Standards and Regulations

Transportation systems inherently present situations of high fire risks through the presence of high volumes of fuel, the risk of collision or maliscious damage. This in combination with the potential of a great number of fatalities makes fire safety an issue of high priority. Standards and regulations have been developed implementing safety limits on the performance of materials to ensure maximum passenger safety in case of a fire.

Historically, all legislation was based on the performance of metallic materials and structures which usually excluded the use of the composite materials as an alternative to metallic structures. With the acceptance of composites as alternative materials, specific regulations were developed with regard to the use of non-metallic, combustible materials. These guidelines specify the procedures and exact test methods as well as fire protection measures that need to be undertaken for the use of the material to be permitted.

Over the last couple of decades a change from the multiplicity of autonomous national safety codes to globally applicable fire legislation has been undertaken. Most notably here are the Safety of Live at Sea SOLAS convention Chapter II part 2 [32] regulated by the International Marine Organization IMO which defines the fire safety standards applied to all non-metallic materials used in civil ship construction. Similar to the marine sector, in the aerospace industry the US Federal Aviation Administration defines the fire behaviour characteristics for large, wide-bodied aircraft to ensure passenger safety. Here, FAR-25 [33] regulates fire performance limits for heat release, smoke and toxicity of cabin material for specific fire scenarios in order to allow safe evacuation of the passengers within a set period of time after a crash without them being incapacitated, injured, or hindered by heat, smoke or fumes. The rail sector has brought together European national regulations with the implementation of the EN-45545 [21] in 2012 to ensure consistency across nations' borders. The counterpart for the EN-45545 in the US is overseen by the Federal Rail Administration.

1.3.2 Fire Reaction and Fire Resistance

The properties describing a material's behaviour during fire exposure can be grouped into two categories: Fire reaction properties and Fire resistance properties.

The Fire reaction characteristics of a material can be determined during the initial phase of exposure to fire. Some of the main parameters that are used to classify a material's fire reaction include time-to-ignition, heat release, flame spread and smoke and gas toxicity.

The Fire resistance properties are used to describe the fire behaviour of a material after flashover has occurred and the fire is in a fully developed state. Fire resistance is widely defined as the ability to withstand a fire. This encompasses the ability to retain mechanical integrity in order to avoid structural collapse and to restrict the fire spread into the environment. Assessment of the fire resistance capability of a material includes the measurement of post-fire mechanical properties as well as the evaluation of burn-through resistance via heat conduction observations.

1.3.3 Test Procedures

Methods for the determination of fire reaction properties involve the use of coupon-sized specimens which allow bench-scale tests to yield fast and cost-efficient results. They are however limited in their simplification of the problem as they are tailored to measure specific aspects of the fire process only. Effects that arise from the fire growth and turbulent gas flow which would evolve in a real fire are not taken into account. Therefore, the fire reaction properties do not reflect the true fire behaviour which needs to be taken into consideration whilst assessing the material's overall fire risk potential. This also presents difficulties for extrapolating real structural behaviour from the results obtained from the coupon-sized samples.

Fire resistance tests on the other hand are typically carried out on larger-scale items that are representative of the structure in end-use applications, see for example figure 1.8. These tests can overcome some of the drawbacks of the bench-scale methods as a more accurate replication of a real fire scenario is achieved. The use of furnace, pool fire or jet fire tests as experimental methods to assess fire resistance requires more complex setups and resources, which involve higher cost and are more time consuming.

Cone Calorimeter

One of the most versatile and widely used methods to determine fire reaction properties is the Cone Calorimeter apparatus [35], illustrated in figure 1.6. According to ISO-5660 [34], small samples with a $100\,\mathrm{mm}^2$ surface area are exposed to a conical shaped radiant heater that can emit a heat flux of up to $100\,\mathrm{kW\,m^{-2}}$. After an electrical spark initiates ignition of the evolving gases released from the decomposing specimen upon irradiance, the sample is left to burn until the flames are extinguished and all combustible material is spent. The gases produced during decomposition are analysed in the exhaust system to ascertain composition and quantity while the sample's mass loss

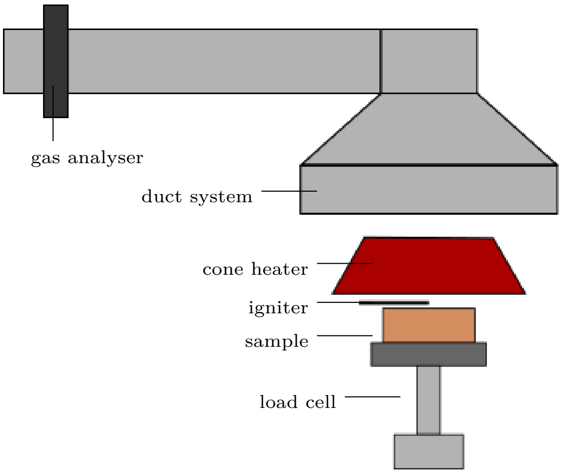

Figure 1.6: Schematic of a Cone Calorimeter apparatus according to ISO-5660 [34].

is simultaneously recorded by a load cell. The single-most important fire reaction property [36], the heat release rate of a material, can be directly deduced from the oxygen concentration in the exhaust gases by the oxygen consumption method.

The reason for selecting the cone calorimeter is that it is capable of measuring many different aspects from the combined measurement of additional fire reaction properties to that of average and peak heat release rates, such as time-to-ignition, mass loss, smoke production as well as CO and CO_2 yields.

The choice of variable heat flux in combination with a horizontal or vertical orientation makes it a very adaptable test procedure in replicating various real case scenarios. The option of an atmosphere controlled cone calorimeter is largely unneccessary because most fire events happen under normal atmospheric conditions with an oxygen concentration of 21 %. One of the drawbacks of this method is however being unable to measure the flame spread.

Flame Spread

The Radiant Panel Test, ASTM-E162 [37], is the most commonly used method to evaluate the rate at which a flame can spread over the surface of a material [33]. A flat specimen inclined at 45° towards the heater is subjected to a constant heat flux of $25\,\mathrm{kW\,m^{-2}}$. A flame spread index is calculated from the time of flame propagation downwards along the sample and the temperature increase in the exhaust. The flame spread index is used to rank the potential of flame propagation in comparative material studies.

Many variations of this test have been developed, including the Horizontal/Vertical Flame Chamber, UL-94 [38], the Upward Flame propagation test, NASA-STD-6001 [39] or the Lateral Flame spread test, ASTM-E1321 [40] and ISO-5658 [41], to account for different orientations and directions of flame travel.

Limiting Oxygen Index

Information about ignition and flammability can be obtained through the Limiting Oxygen Index (LOI) test according to ISO-4589 [42–44] and ASTM-D2863 [45]. During this test a vertically orientated specimen is placed in a glass chamber within an atmosphere of controlled levels of oxygen and nitrogen, and is ignited at the top. Through a series of tests during which the oxygen content is continuously increased the material's LOI is determined. LOI is defined as the minimum amount of oxygen needed to sustain combustion for three minutes or to support a flame spread of 50 mm. High values of LOI indicate higher resistance to ignitability and a low flammability. This test has

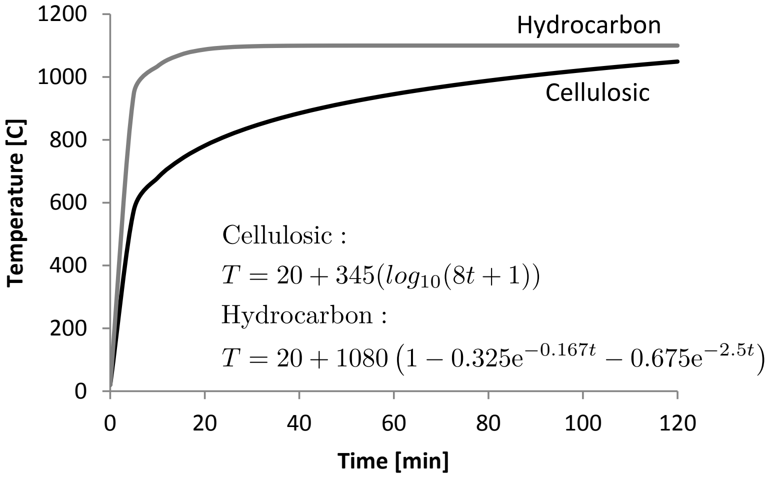

Figure 1.7: Standardardised heating curves as employed during furnace tests [48].

the shortcoming that the LOI value and its validity have not been related to full-scale scenarios. However, it is still commonly used to rank the flammability of materials in comparative studies.

Smoke Density

The optical density of smoke generated during the fire exposure of a combustible material is measured with the NBS Smoke Density Chamber, ISO-5659 [46]. The transmission of a laser beam is monitored during the exposure of a vertically orientated specimen to a $25\,\mathrm{kW\,m^{-2}}$ heat flux from a radiant heater with or without a pilot flame. Conclusions about a material's potential for smoke production are measured inversely according to the degree of visibility. Drawbacks arise from the inherent problem that laboratory combustion conditions do not replicate real fire exposures.

Furnace Test

The fire resistant properties of intermediate and large scale structures are measured in furnace tests where fully-fitted flat panels are attached to the open side of a furnace. Thermocouples bonded to and embedded at various points of the structure monitor the heat conduction during heat exposure. The parameter of fire resistance is defined as the time taken to reach a certain temperature at the unexposed rear face of the specimen. Observation of the specimen's mechanical integrity can be simultaneously carried out when the structure is subjected to a compressive or bending load whilst under fire exposure.

The fire scenarios during a furnace test are standardised by the application of predefined heating rates or temperature increases with time, where the temperature inside the furnace follows one of the standard fire curves. The cellulosic fire curve resembles a fire that arises from burning wood or fabric. The temperature rise is defined through a time dependency function given in ASTM-E119 [47] and ISO-834 [48]. Another curve that is commonly applied is the hydrocarbon curve, UL-1709 [49], which is used to replicate intense petroleum or oil based fuel fires. The severity of the hydrocarbon fire in comparison to the cellulosic fire is evident when comparing the temperature-time curves as shown in figure 1.7. The hydrocarbon curve features a steep increase in temperature exceeding 1000 °C within five minutes whereas this mark is only reached after four hours during a cellulosic fire.

(a) Furnace [50]
(b) Pool fire [51]
(c) Jet fire [52]

Figure 1.8: Different types of fire resistance tests from medium to large scale.

Pool Fire

During pool fire tests, the specimen is placed over a horizontally orientated fuel bed which, upon ignition, can release a heat flux of up to $150\,\mathrm{kW\,m^{-2}}$. For the purpose of assessing the mechanical response, a structural load can be applied during the test. This arrangement is taken from practical aspects of the accidental ignition of evaporating fuel from a spillage or leakage. A high variability in the results of pool fire tests makes replication difficult because of the unsteady heat flow that is caused due to the nature of the unaided combustion.

Jet Fire

In a jet fire test, by way of contrast, a high pressure flame that can exceed a heat flux of $180\,\mathrm{kW\,m^{-2}}$ is directed at the test specimen which commonly is a full size structural element. The high heat flux in combination with the high gas velocity leads to severe fire damage to the specimen. Jet fires are mostly used to replicate situations of accidents during which high pressurised fuel containers burst such as pipelines or fuel storage vessels used in the oil and gas industry.

1.4 Objectives of Study

The principal objectives of the present study include:

- The development of multi-micro-layered metal laminates, including the manufacturing process and optimisation of such.
- Determination of the thermal characteristics of the newly-developed material.
- Characterisation of the fire protection effect of PML via fire exposure tests and fire-structural testing.
- Development and application of a material model to predict the temperature profiles during fire exposure.

Chapter 2

Literature Review

2.1 Material Response to Fire Exposure

2.1.1 Metal Structures

Aluminium and its alloys are chosen for many structural applications due to their high specific strength, corrosion resistance, ease of fabrication and processing as well as relative low cost. One of the main drawbacks however is the rapid degradation of the mechanical properties when exposed to high temperatures which is caused by a combination of its low melting point, low density and high thermal conductivity. Many aluminium alloys melt around 600 °C to 660 °C but experience a reduction in mechanical properties at much lower temperatures. A noticeable degradation in structural properties such as yield strength and Young's modulus can be observed from temperatures as low as 150 °C. This typically leads to a 50 % loss of structural strength at around 250 °C [53] which is shown in figure 2.1 for aluminium alloys of the 5000er series. The inferior behaviour of aluminium alloys is evident when compared to structural steel which retains about 90 % of its ambient-condition mechanical properties up to 300 °C [54].

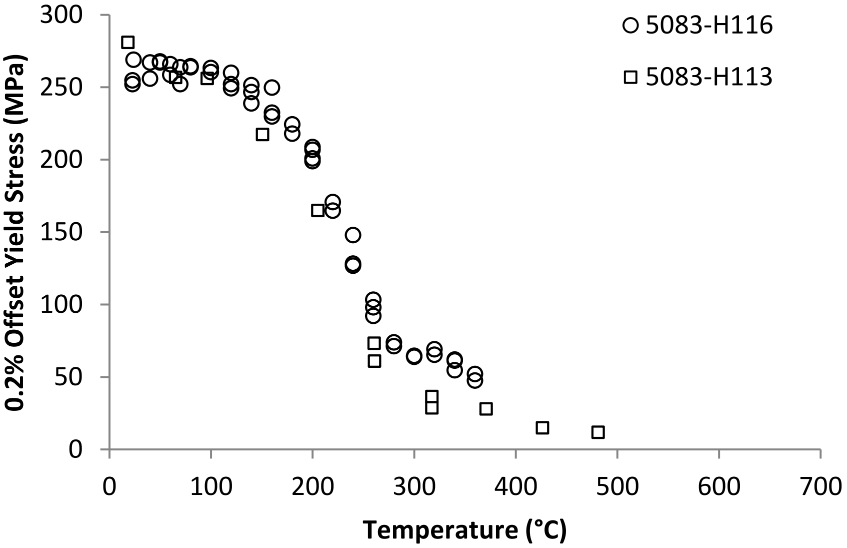

Figure 2.1: Temperature dependence of structural property for marine aluminium alloys. Reproduced from Fogle et al. [53].

The decrease in mechanical strength is accompanied by a high risk of structural collapse because the load-bearing capacity of the aluminium structure is significantly reduced. The structural deformation behaviour is determined by mechanically induced distortions as shown in figure 2.2.

With prolonged heat exposure additional thermal deformations develop which contribute to the structural deterioration. Therefore, aluminium alloy structures in load-bearing applications are commonly insulated in order to decelerate the temperature increase in structural members so that they conform with the requirements for fire resistance times of 30, 60, 90 or 120 minutes outlined in the standards such as the Eurocode 9 (EN-1999, part 2) which sets the structural safety levels for a requisite period of time.

The EN-1999 defines a set of safety criteria based on the temperature dependency of the 0.2 % proof stress obtained from steady-state experiments at elevated temperatures [56]. The Ramberg-Osgood relationship [57] is used to describe the stress-strain curves whilst taking into account the strain hardening effect of the alloy. This is commonly used at room temperature and can be extended to higher temperatures through the application of temperature-dependent relationships of the mechanical parameters. However, steady-state tests do not reflect the conditions of a true fire scenario. Transient tests with designated heating rates are considered to be better representative of a real-case scenario. Based on findings that at high temperatures the structural behaviour of aluminium alloys is dominated by creep, Dorn [58] established the first constitutive model including creep effects which was extended to comprise of the primary and secondary creep stages and is known as the Dorn-Harmathy [59] creep model.

Figure 2.2: Deformed H-column specimen after structurally loaded heating test. Reproduced from [55].

Over the last decade numerous experimental and analytical studies have been carried out on aluminium to analyse the deformation behaviour and determine failure characteristics at elevated temperatures and during exposure to fire. These advances are intended to overcome the erroneous or conservative approaches applied in the Eurocode standard and provide analytical models that can accurately predict the structural behaviour under real fire conditions. Suzuki [55] derived analytical expressions that can be used to predict the critical temperatures which lead to compressive failure of aluminium alloy structures exposed to fire. Maljaars [60, 61] and Feih [62] developed failure models based on creep behaviour in combination with time-independent elastic and plastic softening. Their approaches are used to describe the dependency of deformation on time and temperature as well as failure characteristics. Kandare [63] successfully employed the Larsson-Miller relationship which utilises the Arrhenius equation for the description of the creep rate in order to predict creep-based softening and rupture leading to compressive failure of aluminium structures. Whereas many studies, including the aforementioned papers, mainly concentrated on the analysis of compressive failure, few studies deal with the failure behaviour under flexural [64] or tensile [65] conditions.

2.1.2 Polymeric Materials

This section will discuss the effects of heat exposure on polymeric materials. The subsequent remarks are not exclusively applicable to monolithic polymers but also apply to multi-component materials where all organic constituents contribute towards the thermal performance. Examples are fibre-reinforced composites that are comprised of a polymer matrix in combination with organic or inorganic fibres or organic core materials in sandwich structures.

One of the main disadvantages which limits the wider use of composite materials is their poor fire performance. Whilst polymeric composites are widely used in aerospace, marine and offshore applications, all of these pose problems because of the significant risk of a fire occurring. Although the overall fire performance of an organic material is assessed before it is cleared for specific use in

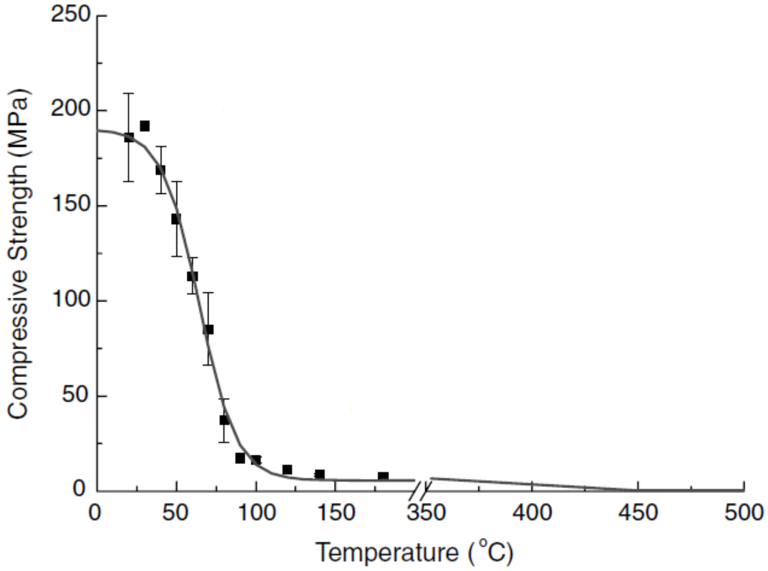

Figure 2.3: Softening behaviour of a carbon-epoxy composite characterised by a rapid strength loss with increasing temperature. Reproduced from Burns et al. [66].

certain applications, the maintenance of structural integrity becomes the main safety concern.

Due to their organic nature polymeric materials are inherently combustible. The fire behaviour of polymers and polymeric composites is mainly influenced by the process of thermal decomposition of the organic constituents. Under heat exposure, polymeric materials begin to soften readily at moderate temperatures of 100 °C and above upon exceeding the material's glass transition temperature. This leads to a reduction in mechanical strength and the introduction of deformations resulting ultimately in the failure of load-carrying structures. Characteristic strength loss behaviour of a fibre-reinforced composite material is shown figure 2.3. With further exposure to radiant heat, decomposition is initiated at temperatures around 300 °C for most thermoset polymers such as epoxy, phenolic, polyester and vinyl ester [67]. The decomposition reaction occurs over a wide temperature range but mostly comes to an end at around 650 °C.

Polymers and composites experience a steep temperature gradient across their through-thickness plane when exposed to one-sided heating because of their low thermal transport properties in comparison to metals. This has the advantage of a slow burn-through effect of composites [68] during which a thin decomposition front slowly progresses through the sample to the rear face. Heat induced thermal decomposition (pyrolysis) entails the breaking down of the polymer chains via various scission mechanisms in order to generate low molecular-weight species that are able to form vaporised gases. The chain scission reaction is endothermic in absorbing energy from the pyrolysis process. Therefore, the heat conduction into the material is delayed and the decomposition rate reduced.

During this decomposition reaction a complete transformation of the polymeric material into carbon-rich residue (char), flammable and/or non-flammable volatile gases as well as soot particles (smoke) takes place. The release of the volatiles from the decomposition zone towards the surface has an additional cooling effect on the material. However, the interaction of flammable volatiles with the oxygen-rich flame front can lead to ignition and therefore further energy feed back into the incident heat flux which contributes to the overall fire growth. A schematic illustration of the key processes occurring during decomposition is shown in figure 2.4.

The formation of char from the solid pyrolysis reaction products via cross-linking processes is highly desirable. The carbonaceous residue forms a porous layer that acts as a thermal barrier between the flame and the underlying virgin material due to its very low thermal conductivity. Additionally, the char layer provides some structural integrity to the decomposing material as

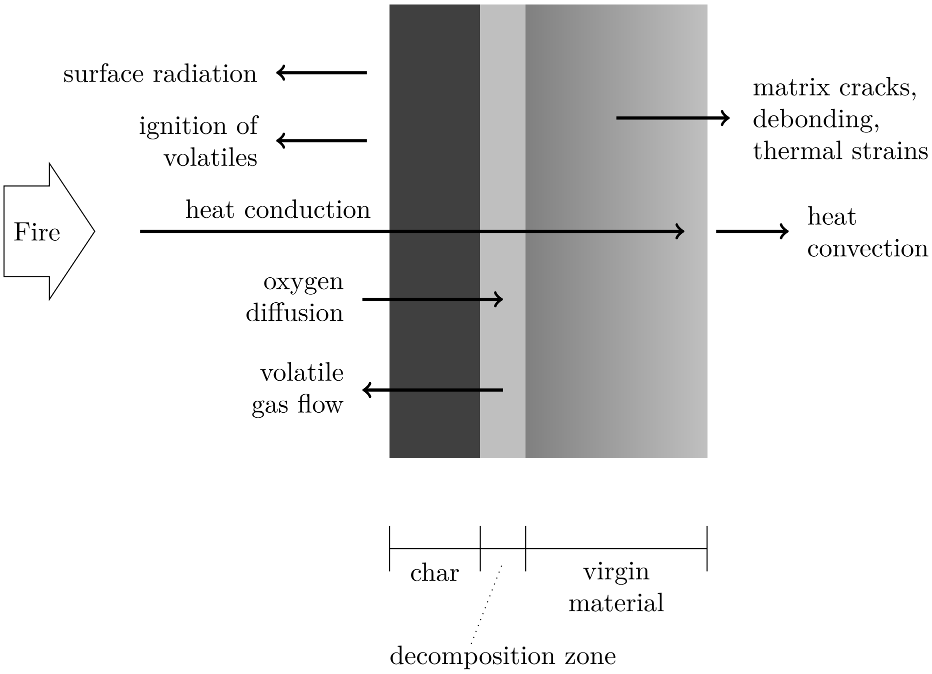

Figure 2.4: Schematic of key processes occurring during the decomposition of polymeric material under one-sided heat exposure.

well as reducing the flaming combustion because a lesser amount of the combustible material can contribute to the production of heat, smoke and/or toxic products. Cracks within the polymer or polymeric matrix occur due to the internal pressure built up from volatiles forming and moisture evaporating. In fibre-reinforced composites another side effect of the decomposition process is the delamination which occurs between fibre and matrix or between skin and core materials in sandwich composites.

The nature of polymer decomposition is dependent on the chemical and physical properties of the affected material, see figure 2.5. Many studies have investigated the fire performance as well as the fire-structural behaviour of a variety of polymeric materials [69–73]. For example, it is well known that phenolic resin has superior fire properties over other thermosets used in fibre-reinforced composites. Due to its highly aromatic structure within the polymer chain, which forms the building blocks of char residue, it yields high amounts of char up to 60 % [74]. Mouritz et al. [75] have investigated the char formation as one factor amongst other fire reaction properties and have shown the phenolic's superiority over epoxy, polyester and vinyl esters which in comparison only yield small amounts of char, between 5 % to 20 % [74], and mostly transform into volatiles. High-performance thermoplastic composites, such as PEEK and PPS used in aircrafts, can exhibit prolonged retention of mechanical integrity as well as higher post-fire residual strength due to a high char yield compared to common thermoset materials as shown by Benoit et al. [76]. The choice of fibre reinforcement influences the fire performance of polymer-matrix composites as organic fibres made from UHMW polyethylene or aramid can contribute towards heat release rate and smoke yield in comparison to non-combustible reinforcment such as glass or carbon fibres. Aramid fibres although thermally unstable provide some flame resistance due to a high char yield in comparison to polyethylene fibres which are highly flammable, see data presented in table 2.1.

In structural applications the mechanical integrity is of considerable concern as this is a temperature-sensitive property. Amongst other investigations, a study conducted by Feih et al. [77] has shown the susceptibility of composite structures to compressive failure as opposed to tensile failure when exposed to fire. Failure behaviour under compressive conditions is dominated by the polymeric matrix which experiences a rapid decrease in mechanical strength due to the generally low glass transition temperatures. Under tension the fibre reinforcement is determinative of the failure behaviour and is essential in maintaining structural integrity so that material failure is delayed because the consequences of the polymer matrix softening are not as detrimental as in case of compressive loading.

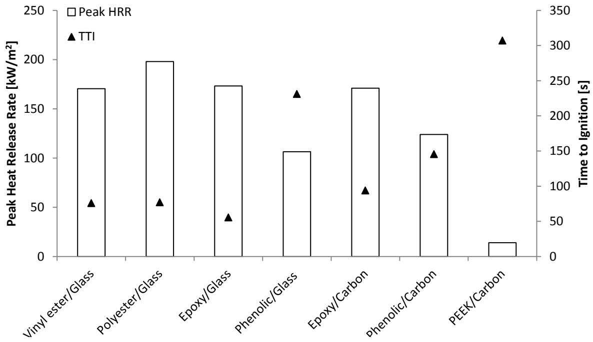

Figure 2.5: Selected fire reaction properties at $50\,\mathrm{kW\,m^{-2}}$ irradiance for various types of 6 mm thick thermoset and thermoplastic composites comprising 60 % glass or carbon fibres. Data from Lyon et al. [78].

Characteristic	Aramid	PE
Time-to-ignition $[s]$	185	31
Peak HRR $[kW/m^2]$	63	691
Average HRR $[kW/m^2]$	50	275
SEA $[m^2/kg]$	66	426

Table 2.1: Selected fire reaction properties at $50\,\mathrm{kW\,m^{-2}}$ irradiance of organic fibres embedded in an epoxy matrix. Data from Brown [79].

2.2 Passive Fire Protection

The susceptibility of the structural performance of lightweight metallic materials and structures comprising organic polymeric components to elevated temperatures necessitates the implementation of fire protection measures. The current fire protection approaches can be divided into two categories: Active and Passive fire protection.

Active fire protection entails manual or automatic fire detection systems as well as response systems in order to assist with the fire suppression. Examples covered under this definition are fire extinguishers, sprinkler systems and fire alarms.

The aim of Passive fire protection systems, in contrast, is to contain fires and retard the spread of a fire through the slowing down of heat transfer into adjacent structures and therefore increasing fire endurance and structural survivability. This, for example, is achieved in buildings through the compartmentalisation principle which makes use of fire-resistant walls, doors and floors. These structures usually feature some sort of measure to increase the fire resistance of the materials and meet the standardised fire safety requirements. The following sections present a short summary of conventional passive fire protection methods.

2.2.1 Flame Retardants for Polymers/Composites

One of the approaches to minimise the fire risk of polymeric materials is to alter their inherent poor fire characteristics. Through the introduction of chemical or physical additives into the polymer formulation, a considerable reduction of heat release rate and delays of time-to-ignition can be achieved [80]. Thus, the flame retardancy of a polymeric material is enhanced through alterations of the combustion behaviour in comparison to the unmodified material. Flame retardant (FR) additives can be classified into three groups [81] according to their mode of interaction with the combustion process during fire exposure:

1. Gas-phase flame retardants

2. Endothermic flame retardants

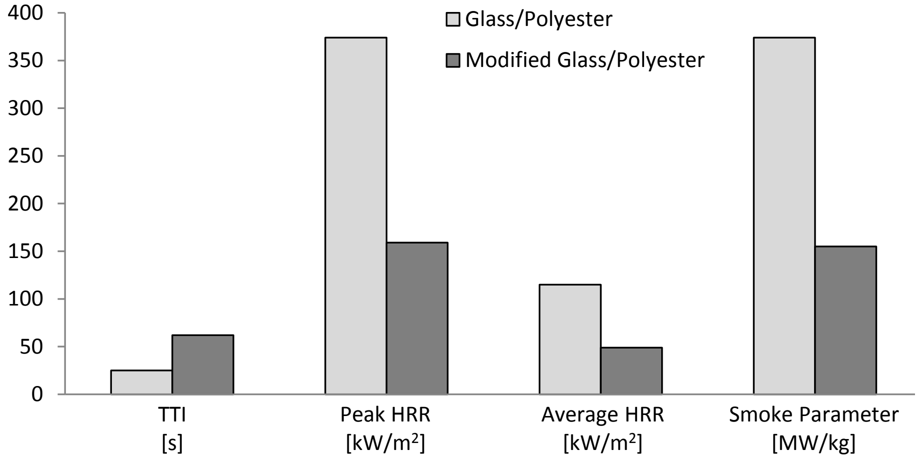

Figure 2.6: Fire reaction properties of a brominated FR glass/polyester composite in comparison to an unmodified specimen. Data taken from Scudamore [84].

3. Barrier or char forming flame retardants

The most common gas-phase additives are halogenated flame retardants, such as chlorine and bromine compounds, or phosphorous-based flame retardants. These materials work primarily in the vapour phase where they form highly active radicals that remove free oxygen and hydroxyl radicals which are formed during pyrolysis of the organic material. Therefore, the combustion process is effectively interrupted by starving the flame of its fuel. The positive impact on the fire characteristics of added bromine FRs to a composite material is presented in figure 2.6. The effectiveness of a halogen-containing FR coating depends on the main halogen type used. The halogen potency decreases in the order of $I > Br > Cl > F$ because of increasing hydrogen-halogen bond energy (from left to right) [82]. Phosphorous containing FR polymers also promote char formation in addition to the reduction of the amount of reactive combustion gases.

The second group of FRs decompose through an endothermic route thereby cooling the condensed phase and effectively decelerating the pyrolysis of the polymer. Additionally, non-flammable and non-toxic gases such as CO_2 and water vapour are released as a side-product of the reaction which dilute the fuel available in the gas phase. Typical representatives of this group are mineral fillers such as aluminium (ATH) and magnesium hydroxides (MDH). The highly endothermic decomposition of ATH commences at 220 °C meaning that the filler is absorbing most of the heat before polymer pyrolysis is initiated whereas the onset of the decomposition of MDH is above 300 °C which makes it an attractive alternative for application in high-temperature environments [83].

Barrier forming flame retardants are made up of polymers reinforced with evenly dispersed nano-scale filler materials. The FR effect arises from the formation of a nanoparticle-rich surface layer which acts as insulation for the incident heat as well as a barrier for mass loss and fuel release from the polymeric material. The most commonly used nano-scale fillers are clay particles (Montmorillonite) as well as carbon nanotubes.

Although all of the listed FR methods greatly improve the fire performance of inherently combustible polymers, they exhibit adverse side effects which need to be taken into consideration. Halogenated flame retardants pose potential toxic effects to the environment and human health and are therefore restricted in their application [85]. Additionally, some halogenated FR generate corrosive products during combustion [86] which can further affect adjacent structures. The addition of FR to polymers has, in general, an adverse effect on the inherent material properties. A careful optimisation of the nature and ratio of the additives for specific polymers has to be carried out with consideration of the end-use application. This is especially true for mineral fillers like ATH that only show profound FR efficacy if applied in high loading of more than 40 wt% of the total composition which diminishes mechanical properties as well as increases the viscosity of the polymer bulk, which in turn poses problems for processing and manufacture [87]. Although barrier-forming nanocomposite polymers lower the peak heat release during decomposition, they do not lower the total heat release despite releasing the polymeric fuel over a prolonged time period [88].

One of the major shortcomings, however, is that FR modified polymers only release their fire retardant effect when thermal decomposition is initiated with temperatures exceeding 250 °C. This does not address the effect of softening of the polymer matrix when the glass transition temperature is exceeded which would lead to structural failure much before thermal decomposition starts [89].

2.2.2 Nanocomposites

Further advances in the flame retardancy of polymeric materials have been made over recent years through the incorporation of nanoscale filler materials into polymer matrices. Considerable improvements in thermal stability and FR characteristics can be observed at low loading levels of typically up to 5 wt% which makes them attractive in comparison to conventional FR methods which need high loadings. Additional advantages arise from the synergetic effects on mechanical, electrical or thermal properties [80, 90]. A variety of nano-fillers are used for FR purposes: layered silicates (montmorillonite, boehmite, LDH), various types of carbon structures (nanotubes, graphene, carbon black) as well as metal oxide nanoparticles (TiO_2) [91–96].

The main mechanism responsible for the flame retardancy effect which applies to nanocomposites in general lies in the formation of a protective layer at the surface of the material during pyrolysis of polymer matrix consisting of agglomerated nanofillers and carbonaceous polymer residues [97, 98]. This forms an effective barrier limiting heat transmission and oxygen diffusion into the bulk material as well as trapping volatiles beneath the surface and hence hinders additional fuel from entering the combustion zone. Creating an even dispersion of nanofillers has proved challenging which in turn affects the FR efficacy of the composite material because an uneven dispersion and consequent non-continuous appearance of the protective surface would impede its functionality [99].

Alongside other studies, Kashiwagi et.al [100] have shown that the incorporation of nanocomposites results in a considerable reduction in the overall and maximum heat release rate in comparison to a neat polymer matrix because of the greatly reduced mass loss rate due to the protective barrier. However, the flammablity parameters, total-heat-released and time-to-ignition, exhibit converse characteristics in that no improvements or even a deterioration in these properties has been observed, as shown in table 2.2 or by Bartholmai [101], which poses an insuperable obstacle for classifaction ratings and suggests the use of nanocomposites is only feasible in conjunction with conventional FR additives.

2.2.3 Surface Fire Protection

The application of surface coatings has proved to be a convenient, cost-efficient and effective fire proofing method as it bypasses many of the difficulties involved in processing and manufacturing of additive modified polymer formulations [102].

Thermal Insulative Barrier

The use of mineral or ceramic wool to provide fire protection for large-scale structures is widespread in civil infrastructure and for marine applications. Insulating mats comprising of accumulated mineral or ceramic fibres of specific density, length and diameter are bonded onto substrates with a high-temperature adhesive and used, for example, in composite hulls, bulkhead structures, or in flame proof walls for buildings. These materials effectively restrict the heat conduction to the

Material	pHRR $[kW/m^2]$	TTI $[s]$	THR $[MJ/m^2]$
PP	2011 ± 80	33	106 ± 4
PP/CB	765 ± 30	25	103 ± 1
PP/MWNT	855 ± 34	23	100 ± 2
PP/EG-1	1129 ± 79	24	105 ± 3
PP/EG-2	1104 ± 45	24	105 ± 1
PP/MLG	570 ± 22	25	96 ± 2
PP/TRGO	532 ± 21	23	97 ± 2

Table 2.2: Cone calorimeter parameters of peak heat release rate, ignition time and total heat released for a variety of 3 mm thick carbon/polypropylene (PP) nanocomposites tested at 50 kW m^{-2} irradiance: carbon black (CB), multiwall nanotubes (MWNT), expanded graphite (EG), multi-layer graphene (MLG), thermally reduced graphite oxide (TRGO). The polymer contained 5 % per weight of nanoparticles. Data from Dittrich et al. [93].

Figure 2.7: Intumescent coating before (left) and after (right) heat exposure in a cone calorimeter at 50 kW m^{-2} irradiance [105]. Commercial intumescent paints typically exhibit an expansion factor between 25 and 250.

underlying structure thus considerably prolonging the onset of thermally induced degradation in the substrate material [103]. The main disadvantage is that they add significant weight when applied in the considerable amounts needed for effictive fire protection whilst fulfilling no structural function. They can also absorb liquids which not only leads to a reduction in thermal insulation characteristics but is also highly undesirable in case of spilt fuels as this can act as an additional fuel source during fire scenarios contributing to the fire growth [104].

Fire Retardant Polymeric Coating

The same principles as presented in sections 2.2.1 and 2.2.2 above can be employed for use in flame retardant surface coatings. In combination with an appropriate organic binder or polymer the FR additive or nanofiller can form an aesthetic layer on a substrate whilst providing finely tuned fire protection characteristics without affecting the bulk material properties.

Intumescent Coating

One of the most widely applied methods is the use of intumescent surface coatings. These coatings expand (intumesce) under heat exposure, see figure 2.7, due to a multitude of chemical reactions being activated by the heat input. The fire protection effect arises from the formation of a porous carbonaceous foam which acts as an insulative and fire resistant heat barrier. Three constituents are required to ensure the intumescence effect:

- an acid source, e.g. Ammonium Polyphosphate
- a char-forming (carbonific) component, e.g. Pentaerythritol

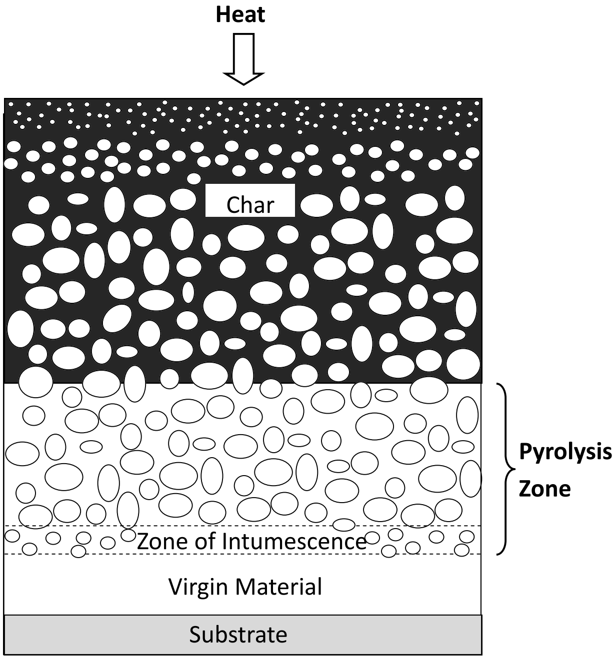

Figure 2.8: Schematic of the different reaction zones forming during the intumescing process. Reproduced from Alongi et al [106].

- a foaming (spumific) agent, e.g. Melamine

The decomposition of the acidic constituent initiates the intumescence reaction. The reaction occurs at temperatures below the polymer pyrolysis temperature, usually at temperatures between 100 °C to 250 °C [107]. During this the carbon source is dehydrated, resulting in the formation of a carbon-rich, highly viscous char melt. Simultaneously, the blowing agent decomposes into non-flammable gases such as carbon dioxide and water vapour which cause the char to foam as the released gases are trapped within the viscous char melt. As the result, a highly porous, multi-cellular char is formed [108, 109] which acts as an effective thermal barrier inhibiting the heat conduction into the underlying substrate as well as providing a diffusion barrier of oxygen which prevents combustion. Figure 2.8 shows these different zones that can be observed during the intumescing process in a schematic cross-section view of an intumescent coated substrate. Intumescent coatings are effective in suppressing flame spread, reducing heat release and lowering smoke density [67, 110, 111]. Increasing the initial coating thickness provides a simple means to achieve an even greater delay of the temperature increase of the underlying structure, see figure 2.9.

However, several disadvantages are associated with the use of intumescent coatings. Environmental exposure (UV, radiation, moisture, salt water) adversely affects their durability thus impairing the fire protection performance linked with ageing [113, 114]. Water absorption and exudation are acknowledged as the major problems affecting chemical and physical stability [115] and the risk of mechanical damage of an intumescent coating is high due to a low resistance to wear and erosion. This can lead to the exposure of the underlying substrate which on the one hand diminishes the fire-proofing purpose and on the other hand can introduce corrosion to the metallic substrates under normal operational conditions which is also a significant problem.

H

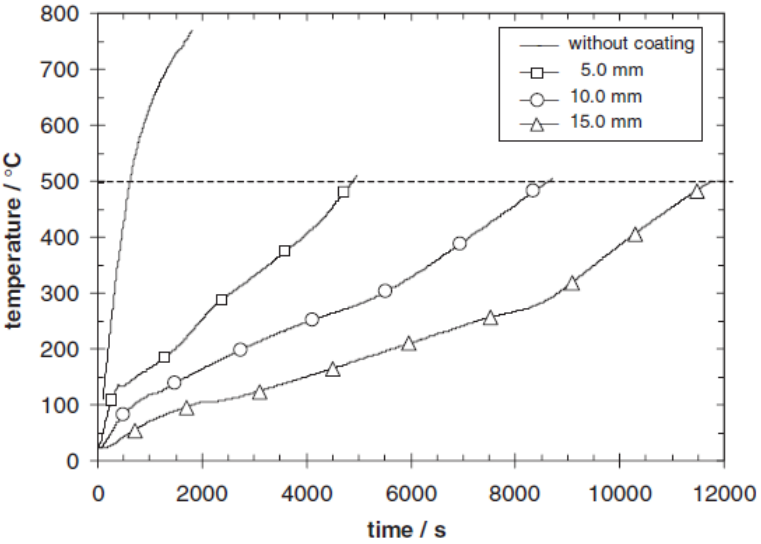

Figure 2.9: Effect of intumescent coating thickness on rear face temperatures of steel plates during a furnace test: the temperature increase is greatly prolonged with increased coating thickness. Reproduced from Bartholmai et al. [112].

2.3 Thermal Modelling

The scientific discipline of modelling the thermal response of materials under heat exposure has increased in importance in the same way that new and innovative materials are increasingly used to replace metal-based structures in conventional applications across all industries. Accurate theoretical predictions are required to provide assistance during the design process of new materials and structures. Simulating the fire performance with these models reduces the need for expensive and time consuming fire testing. Additionally, such models provide the opportunity of developing and assessing innovative materials with tailor-made properties, before prototypes are built.

The focus in this section is the description of thermal models for non-metallic materials. The thermal response of steel or aluminium structures can accurately be characterised by the temperature rise through heat conduction processes and eventually the phase changes through melting. The thermal modelling of non-metallic materials that are partially or fully combustible is a much more complex procedure due to the manifold and occasionally interdependent chemical and physical processes that occur during heat exposure, as described in previous sections. Models developed within the research community typically use finite difference methods or finite element analyses to make predictions about the temperature evolution at any point of a specimen. Additional characteristics that can be evaluated are residual mass content, volume changes, strain development or the production of volatiles.

The theoretical description of the polymer degradation mechanisms has advanced into such detail that molecular dynamic analysis has become a standardised tool in understanding the chemical reactions occurring during polymer decomposition. However, for the present study a holistic approach is chosen for the theoretical characterisation of the fire performance as it is understood that this is the most important aspect, to be able to accurately predict the macroscopic behaviour for the assessment of any developed polymer-metal laminates as an effective fire protection material.

2.3.1 Polymers and Composites in Fire

Various theoretical studies on the fire behaviour of wood [116–119] constitute the framework for the mathematical formulation of the fire behaviour of combustible polymeric materials. These studies include effects of heat conduction, endothermic pyrolysis reactions, convective gas flow as well as variable material properties which depend on the virgin or charred state of the material. Similar processes to those described occur during the decomposition of composite materials due to the organic constituents common both in wood and composites, which means these studies lend themselves to adapt those early mathematical models to composite materials.

Most of the early models include the description of heat transfer in one dimension which is suitable to replicate real case scenarios where material is exposed to uniform, one-sided heating. Advances have been made to accurately predict heat transmission in two and three dimensions [120, 121] in order to analyse spatial temperature distribution caused by localised heating. As most decomposition reactions are ignored, these models are only valid for low heat flux and exposure conditions where material degradation is not yet initiated. The challenge here is to accurately describe heat and volatile mass transport as well as material properties in all three dimensions.

After Pering et al. [122] developed one of the first models to include the effect of mass loss caused by the thermal decomposition of organic matrices in combination with transient heat conduction, Henderson et al. [123] published an advanced model to describe the thermal response of a composite material exposed to one-sided heating. It is based on one-dimensional heat conduction in combination with the influences of mass loss, convective mass flow and the heat of decomposition:

$$\rho c_p \frac{\partial T}{\partial t} = k_x \frac{\partial^2 T}{\partial x^2} + \frac{\partial k}{\partial x}\frac{\partial T}{\partial x} - \dot{m}_g c_{p_g} \frac{\partial T}{\partial x} - \frac{\partial \rho}{\partial t}\left(Q_P + h_s - h_g\right) \tag{2.1}$$

where T, t are the temperature and time,
x is spatial coordinate in through-thickness dimension,
ρ is material density,
c_p is the specific heat,
k is the thermal conductivity,
$\dot{m}_g$ is the mass flow of volatile products,
c_{p_g} is the specific heat of the volatiles,
Q_P is the heat of decomposition,
h_s and h_g are the enthalpies of the solid material and the volatiles, respectively.

The first two terms on the right-hand side of the equation describe the effect of heat conduction with variable thermal conductivity on the temperature rise of the material whereas the third term reflects the internal flow of gaseous decomposition products directed towards the material's hot face thus causing a cooling effect. The last term defines the amount of heat generated or absorbed during the decomposition process in dependency of the material's mass loss where Q_P denotes the heat of pyrolysis and h_s, h_g the enthalpy of the consumed solid material and evolving gases, respectively. Positive terms are designated to exothermic reactions associated with the release of heat while negative terms indicate endothermic reactions and therefore energy absorption. The expression for the mass loss rate $\partial m/\partial t$ is defined via the Arrhenius equation.

$$\frac{\partial m}{\partial t} = -A m_0 \left(\frac{m - m_f}{m_0}\right)^n \exp\left(-\frac{E}{RT}\right) \tag{2.2}$$

where m is material mass at current time t,
m_0 the initial mass at $t = 0$,
m_f the final value of residual mass,
A is the pre-exponential factor,
n is the reaction order,
E is the activation energy for pyrolysis reaction,
R is the ideal gas constant,
T is the temperature.

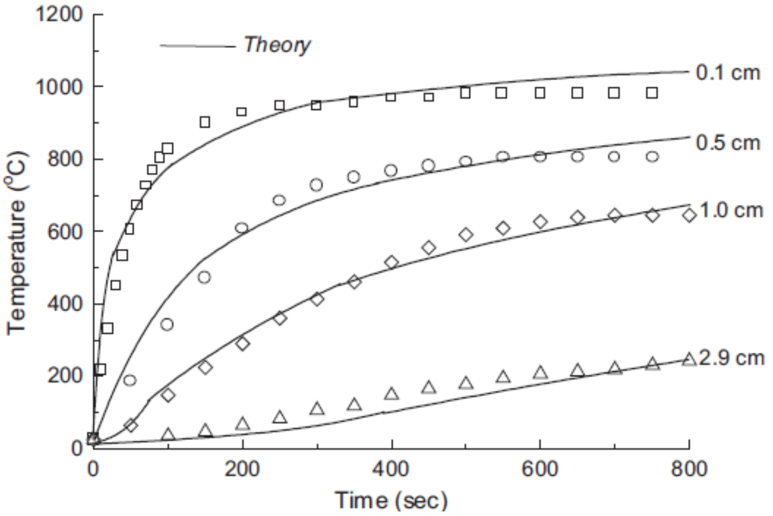

Figure 2.10: Comparison of calculated and experimental temperature curves of a 30 mm thick glass/phenolic composite specimen, exposed to a one-sided heat flux of 280 kW m^{-2}. Reproduced from Henderson et al. [123].

The kinetic parameters pre-exponential factor A, the activation energy E and the order of reaction n can be derived experimentally from thermogravimetric analysis.
The Henderson model can be used to accurately predict the temperature development within decomposing polymer-matrix based materials. Henderson carried out fire exposure tests on glass/phenolic specimens in order to validate the calculated temperature evolution through comparison with experimentally obtained temperature profiles. Good correlation between the experimental and theoretical results was observed as shown in figure 2.10.

Gibson et al. [124] presented a simplified version of the Henderson model. The main assumptions made refer to constant material properties such as thermal conductivity and specific heat capacity as well as constant gas transport parameters during the decomposition process.

$$\rho c_p \frac{\partial T}{\partial t} = \frac{\partial}{\partial x}\left(k\frac{\partial T}{\partial x}\right) - \dot{M}_G \frac{\partial}{\partial x} h_G - \rho A \left(\frac{m - m_f}{m_0}\right)^n \exp\left(-\frac{E}{RT}\right)(Q_P + h_s - h_g) \tag{2.3}$$

Just as in the Henderson model, the Gibson model cannot account for any effects caused due to char formation or further material degradation at high temperatures, e.g. carbon fibre degradation beyond 500 °C [125] or glass fibre deterioration above 900 °C [126]. Despite the apparent restrictions to low and intermediate heat fluxes due to these omitted effects, the Gibson model has been succesfully used to describe the thermal behaviour of various composite types [77, 127, 128] as well as composite sandwich structures exposed to one-sided heating [129].

More recently, more sophisticated models have been developed in order to include additional effects that are related to or caused by the decomposition process. However, the influence of these processes usually has a smaller effect on the temperature development than heat conduction, pyrolysis and gaseous mass flow [130]. Florio et al. [131] proposed a model that adds the effects of thermal expansion and internal pressure rise due to the accumulation of gaseous decomposition products to the basic Henderson equation. It yields important information about the diffusion of the volatiles and the formation of delamination cracks. McManus et al. [132, 133] were the first to combine thermal and mechanical material responses during heat exposure. This model includes the calculation of the total strain within the material arising either from externally applied loads or those internally induced through thermal expansion, gas pressure of volatiles and moisture as well as char formation.

2.3.2 Fire Protection Materials

The modelling of heat transfer across a passive thermal barrier encompasses materials like ceramic fibre blankets or refractory ceramics. As these materials do not undergo physical or chemical changes when exposed to high-temperature environments, simple heat conduction analysis can be applied to calculate temperature evolution across a passive thermal barrier during heat exposure [103].

$$\rho_{pc} c_{p,pc} \frac{\partial T}{\partial t} = k_{pc} \frac{\partial^2 T}{\partial x^2} \tag{2.4}$$

With k_{pc}, $c_{p,pc}$ and ρ_{pc} being the critical parameters which describe the material's properties of thermal conductivity, specific heat and the density of the passive coating and should be inputted as function of temperature in order to reflect the correct temperature dependency of the parameters.

In contrast, the simulation process for thermal coatings classified as reactive fire protection materials is much more complex due to the variety of thermal effects invoked when active intumescent coatings are exposed to a high-temperature environment. The main processes to be accounted for in a heat transfer model for intumescent coatings include the decomposition of active coating compounds, the gas flow of the produced volatiles and the formation and expansion of porous char and basic heat conduction [134].

A concise review on this subject has been published by Griffin [135] outlining the research efforts and the limitations of earlier studies [136–141]. In this study Griffin presents a governing equation for the one-dimensional heat transfer across an intumescent coating taking into account the aforementioned thermally induced effects.

$$\rho_{Int} c_{p,Int} \frac{\partial T}{\partial t} = k_{Int} \frac{\partial^2 T}{\partial x^2} - \nu_x \rho_{gas} c_{p,gas} \frac{\partial T}{\partial x} + \Delta h_{Int} \tag{2.5}$$

$$\Delta h_{Int} = \rho_{0,Int} \left(1 - \omega\right) \sum_k \gamma_k r_k \Delta h_k \tag{2.6}$$

where ν_x is the velocity of volatiles in x-direction, ω is the void fraction,
γ_k is the initial mass fraction of coating consumed during reaction k,
r_k is the rate of reaction k,
Δh_k is the specific enthalpy change for reaction k.

The first term on the right hand side of equation (2.5) describes the heat conduction through the coating whereas the second term denotes the energy balance arising from the cooling effect of volatile gas flow and the last term accounts for the absorbed or evolved energies during the decomposition reactions of the individual chemical compounds. Due to the physical expansion of the coating during heat exposure, the spatial dimension between neighbouring nodal points of the simulation needs to be adjusted

$$x_{i+1,j} - x_{i,j} = \alpha_{ex} \left(m_k\right) \left(x_{i+1,0} - x_{i,0}\right) \tag{2.7}$$

with $\alpha_{ex}(m_k)$ denoting a variable expansion parameter and x representing discrete nodal points at specific loactions $i, i+1$ and times $j, j = 0$.

One of the most significant limitations of the current models, and consequently the greatest challenge to overcome, as pointed out by Griffin and later by Staggs [109] is an accurate reproduction of the expansion behaviour. The introduction of an expansion factor is of widespread use either as parameter directly determined from experimental observations [142] or coupled to the conversion of intumescent components into gaseous products [138]. It is shown in studies, e.g. Kandare [143], that a reasonable correlation between calculated and experimental temperature profiles can be achieved despite acknowledging the shortcomings that are due to the consequences of using a simplified expansion factor.

As the process of expansion is a complex issue due to its non-uniform and non-linear characteristics influenced by atmospheric conditions, type of heat source, the rheological properties of the char melt and coating thickness, a detailed and accurate mathematical description of intumescent swelling is yet to be established.

Studies into the kinetics of the decomposition reactions, such as [144–146], can be an aid to further the understanding of the complex processes involved and contribute towards the development of more sophisticated models.

2.4 Conclusions of Literature Review

Based on the observations presented in the literature review as well as the basic principles outlined in the introduction, it has been shown that a variety of new lightweight materials are viable alternatives to traditional metallic structures. When subjected to elevated temperatures the susceptibility of these lightweight materials to change both their material behaviour and mechanical performance is widely acknowledged, and this is their shortcoming. The mechanisms of the materials' reaction occurring during fire exposure and the consequences thereof have been pointed out for both metallic and combustible materials.

In order to overcome the apparent deficiencies of reduced fire resistance, one solution would be the use of thicker sections of material to exploit the advantage of the slow burn-through effect in e.g. polymer-matrix composites. In theory, this would delay the decomposition long enough to provide adequate and safe escape time. However, in reality this contradicts the principle of the lightweight design approach where as little as possible high-strength material is used in an assembly to fulfill structural requirements and safety factors. Therefore, the only feasible alternative is to use lightweight materials in combination with some form of fire protection method.

Several methods of fire protection commonly implemented have been outlined in previous sections. The beneficial effects and implications of their use in combination with lightweight materials has to be critically assessed. For example, the application of flame retardant additives cannot be considered as a feasible option because these materials exert their fire protection effect only with the onset of decomposition at high temperatures. In consequence, the softening stage at lower temperatures is not inhibited or retarded which has fatal consequences in structural applications such as an aircraft fuselage or ship bulkheads where structural collapse can cause great human and resource losses.

Therefore, surface fire protection offers the only viable alternative to address these shortcomings in prolonging both the onset of the softening (for metallic structures and combustible materials) and the decomposition (in case of combustible materials). Any newly developed fire protection solution has to overcome the drawbacks associated with conventional fire protection methods. Of special importance here is the ability to withstand environmental influences, in particular water absorption and corrosion resistance, considering that the life time of transport vehicles may span several decades. The deadweight of fire protection measures can considerably add to the overall structural weight hindering performance, which is why it is sometimes referred to as parasitic.

In comparison with any existing surface coating, a novel coating or fire barrier should therefore be of lightweight design and preferably combine several functions so that further weight savings are possible. This could for example be realised through the incorporation of lightning strike protection which is currently carried out as an additional metal mesh on the surface of carbon-epoxy composites used in the fuselage of aircraft or in rotor blades for wind turbines.

Chapter 3

PML Design and Manufacture

This study's aim is to investigate and evaluate novel fire-resistant surface barrier for lightweight metal or polymer-based structures which could be applied, ideally, to any transport vehicle type. The lightweight aspect of such a design is essential to the transport sector as it promises cost and emission savings. Therefore materials have to be chosen that, when introduced into the laminate design, can establish a sufficient fire-protection effect without adding significant undesirable weight to the primary structure.

This chapter conatins a brief presentation of the PML design concepts and the materials used as laminate constituents. The manufacturing process, which is an adaptation of widely used processing techniques for multi-component materials such as fibre-reinforced polymer composites, will be outlined.

3.1 Materials

Aluminium foils

Aluminium is an intuitive lightweight choice as a laminate constituent with its long history of use especially in the aerospace sector. Specific aluminium based alloys have been developed to satisfy the need for high structural properties, while providing fatigue and corrosion resistance at the same time, compared to pure aluminium which has low mechanical strength properties.

Commercially available foils range from pure aluminium foils to tailor-made alloy foils with iron, silicon and manganese additives. However, the latter materials have the disadvantage that they are usually not readily available and involve significant cost. Therefore, pure aluminium foils have been the favoured choice of material in this study.

Aluminium foil with the smallest thickness available is commonly used as household or kitchen tin foil. Its thickness typically ranges from 10 µm to 18 µm. The very fabric like behaviour of kitchen foil is unsuitable and undesirable for the processes during the laminate manufacture which involves manual handling and hand lay-up. Its low thickness causes the foil very easily to form creases and kinks; also tearing frequently occurs. Additionally, at this thickness range the aluminium foils feature many rolling defects and numerous pin holes, as shown in figure 3.1, which are highly undesired as the performance of the laminate in fire is strongly dependent on its capability to capture the volatile decomposition products. With increased foil thickness the number of defects significantly reduces and the stiffness increases which improves the handling conditions during manufacture. Therefore, commercially available aluminium foils of 30 µm and 50 µm thickness sourced from *North East Laboratory Supplies* have been chosen as the PML metal constituent in this study.

(a) Pin holes **(b)** Rolling defects

Figure 3.1: Irregularities and visible pin holes in common aluminium household foil.

Polymer Interlayers

Epoxy resins are one of the main types of structural adhesives. Their relatively high strength and wide operational temperature range make them first choice for a wide range of engineering applications. A high performance, aerospace grade epoxy resin system, resin LR-135 and hardener LH-137, supplied by *PRF Composites (UK)*, has been chosen for the manufacture of the multi-layer laminates. Its low viscosity is one of its main properties that is essential for the manufacturing process. Additionally, a room temperature curing cycle followed by a low-temperature post-curing process are very operational-friendly and do not require specifically developed equipment.

Metal Foils with High Melting Points

The use of aluminium in a fire-scenario, where temperatures can easily exceed 1000 °C, may seem counter-intuitive as the melting point for the pure metal lies at around 660 °C. In severe fire conditions where PML would be exposed to temperatures above the melting point of aluminium, degradation caused by the foil melting is to be expected. Nevertheless, the principle mechanisms responsible for the establishment of the PML fire protection effect are not impaired by the damage to the PML because the melting phase only occurs in the final stages after the thermal insulation barrier has fully developed. Additionally, melting of the PML is a gradual process which occurs after the heat front has gradually progressed through the PML. Alternatively, it is thought that through the introduction of metal foils with melting points above flame temperature the fire performance of the laminates can be improved as it would provide an additional non-melting barrier against the flames so that it is able to retard the heat transfer further.

These high-melting foils typically have a much higher density than the aluminium foils which would be in contrast to the lightweight design principles if the laminates were solely made out of these alternative materials, see table 3.1 for comparison. To ensure a good fire-protection effect, the

	T_{melt} [°C]	T_{decomp} [°C]	Density $[\mathrm{kg\,m^{-3}}]$	Conductivity $[\mathrm{W\,m^{-1}\,K^{-1}}]$	Heat capacity $[\mathrm{J\,kg^{-1}\,K^{-1}}]$
Aluminium	660	-	2700	200	910
Stainless Steel	1400	-	7800-8000	16	490-530
Titanium	1665	-	4510	12	540
Epoxy resin	-	300-350	1100-1400	0.18-0.2	800-1200

Table 3.1: Material properties at room temperature.

laminates can be a hybrid of the non-melting foils in combination with the aluminium foils as the non-melting foils are only needed to lessen the destructive character of the fire on the aluminium. Therefore, modified laminates would be manufactured that feature either one 30 µm Stainless Steel foil Type 304 supplied by *Hollinbrow Precision Products (UK) Ltd* or one 30 µm Grade 2 Titanium foil sourced from *Ti-Shop.com* at their front face.

3.2 Experimental Procedure

PML Manufacture

The 30 µm and 50 µm thick aluminium foils are supplied as 300 mm wide rolls. This allows the aluminium rolls to be placed in a small jig and for the foil to be pulled out to the required length during manufacture. The low-viscosity of the mixed epoxy resin (500 mPa s to 1000 mPa s at room temperature) enables the use of a spray gun to apply the resin onto the foils. The advantage over other coating techniques such as using a paint brush or a hand-held squeegee is that it offers a controlled way of applying a homogeneous resin layer with uniform thickness that can easily be repeated to achieve layers of the same thickness in the manufacturing progress.

After the resin is sprayed directly onto the unrolled foil, a Stanley knife can be used to cut the foils to a standard size of $300 \times 300\,\text{mm}^2$. Individual coated foils are then stacked on top of each other according to the desired architectural design whilst a foam roller is applied with pressure to encourage good bondage as well as minimising the amount of air that might be trapped between the two aluminium layers.

At this point the non-melting top layer can be introduced for the assembly of so-called modified PML. The steel or titanium foils are cut to size and treated with a spray coat in the same way as the aluminium foils. The steel or titanium foils then form the top layer of the stacked aluminium-resin laminate.

For consolidation the assembled laminates are pressed with 70 kN for an initial curing period of 2 hours at 60 °C. A post-curing heating cycle at 80 °C for 10 hours as outlined in the manufacturer's datasheet follows the initial 24 hours room temperature cure process in order to develop the full mechanical strength of the resin.

The method of unrolling the foil and cutting after applying the spray-coat reduces the amount of manual handling which in turn minimises the chances of introducing creases and kinks into the foils. A careful handling of the foils is important as any irregularity within one layer will imprint through to the other layers and multiplies the locations where air can become trapped. Air within

Figure 3.2: Fabricated PML a) before and b) after revision of manufacturing process.

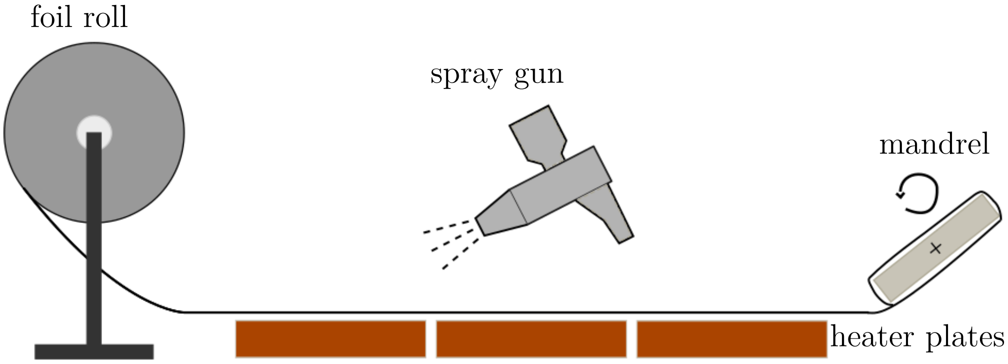

Figure 3.3: Schematic of the PML manufacturing process.

a PML is an unwanted flaw which will compromise the effectiveness of the fire retardancy and reduces overall PML structural integrity.

With ongoing study, advancements to the manufacturing process became necessary to improve PML quality and consistency. A new processing procedure has been developed in order to minimise the amount of manual handling which presents the greatest risk of causing faults within the laminates. The revised procedure, schematically shown in figure 3.3, involves a continuous process. At the start, the aluminium foil is unrolled onto heated plates set at a temperature of 70 °C which assists the initiation of the curing process of the resin after the foil has been spray-coated with the epoxy. After a short resting time, the coated foil is draped onto a mandrel-like device. Through rotational movement of the mandrel the foil is tightly wrapped around the device until the desired number of layers is reached. The same curing procedure as previously described follows.

The laminates manufactured by the revised process were of a higher quality as shown in section 3.2 as a result of there being less manual handling. Higher consistency in weight and thickness ratios of the samples in combination with a fault-free appearance was observed. By way of example, micrographs of a manually assembled PML and a PML manufactured according to the revised technique are shown in figure 3.4, respectively. A number of air pockets and irregularities can be noticed in the manually assembled PML which in contrast are eradicated within the second sample which features evenly distributed resin layers in a highly uniform PML sample.

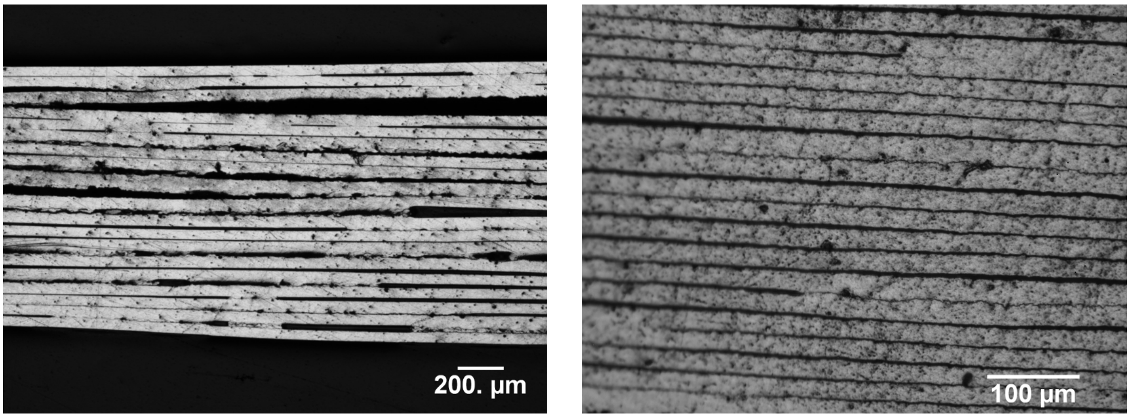

(a) 50 µm PML, 19 layers **(b)** 30 µm PML, 20 layers

Figure 3.4: PML micrographs taken with a light microscope showing laminates with a) inferior quality and b) much enhanced quality due to improvements in the manufacturing process.

Bonding of PML onto a Structure

It is critical to be able to fully integrate the laminates into the primary structure of any proposed application. To this effect, a process has been developed to bond laminates onto various substrate materials. During this study aluminium and carbon-epoxy composite substrates are chosen as the main subjects of investigation because they provide a fair representation of material types used by the transport industry, be it an aircraft fuselage material, a structural member of a ship hull or a train carriage body. The process developed allows PML to be attached to either one or both faces of the primary structure.

In principle, the bonding technique follows the manufacturing process outlined in the above section. For a good interface bonding the surface roughness of the substrate has been slightly increased either via grit blasting (aluminium) or manual abrasion (polymer-matrix composite) before a spray-coat of resin is applied onto which a PML is positioned. During the curing the bonded specimen is clamped between metal plates which allow the sample to be held in place so that slippage is prevented. The standard curing cycle of 24 hours at room temperature and then elevated temperature post-curing would follow.

3.3 PML Architecture

As PML presents a new concept of fire protection technique, there is a need to understand the basic behaviour in fire scenarios. In order to assess principle influences on the fire behaviour various laminate architectures have been produced. Besides the two different foil thicknesses, another principal variable introduced to study the fire protection effectiveness of PML is the number of aluminium foils present within a sample. A PML is manufactured featuring either 10 or 20 layers of metal foil; which includes one non-melting top foil in case of the modified PML samples. Table 3.2 provides an overview of the main PML types and their nomenclature used in this study.

The PML constitutive properties are governed by the relative contributions of each constituent material which is generally expressed as a volume or mass fraction. The volume fractions φ_{al},φ_{res} of the aluminium and epoxy resin within a PML can be derived from the basic relationship of mass fraction and density for a two-component system

$$\varphi_{al} = \frac{\dfrac{w_{al}}{\rho_{al}}}{\dfrac{w_{al}}{\rho_{al}} + \dfrac{w_{res}}{\rho_{res}}} \tag{3.1}$$

with w and ρ denoting the weight fraction and material density of each constitutive element,

	Polymer-metal laminates		Modified Polymer-metal laminates	
		Label		Label
			9 layers + 1 Steel foil	10L/30μm + St
30μm thick Alu foil	10 layers	10L/30μm	19 layers + 1 Steel foil	20L/30μm + St
	20 layers	20L/30μm	9 layers + 1 Titanium foil	10L/30μm + Ti
			19 layers + 1 Titanium foil	20L/30μm + Ti
			9 layers + 1 Steel foil	10L/50μm + St
50μm thick Alu foil	10 layers	10L/50μm	19 layers + 1 Steel foil	20L/50μm + Ti
	20 layers	20L/50μm	9 layers + 1 Titanium foil	10L/50μm + Ti
			19 layers + 1 Titanium foil	20L/50μm + Ti

Table 3.2: Overview over basic PML architectures.

respectively. And vice versa, converting the volume fraction into weight fraction via

$$w_{al} = \frac{\rho_{al}\varphi_{al}}{\rho_{al}\varphi_{al} + \rho_{res}\varphi_{res}} \tag{3.2}$$

Material properties such as PML density, specific heat capacity and other mechanical characteristics can be estimated according to the rule-of-mixture using average epoxy volume fractions of around 6 %.

$$\rho_{\mathrm{PML}} = \varphi_{\mathrm{res}}\rho_{\mathrm{res}} + \varphi_{\mathrm{al}}\rho_{\mathrm{al}} \tag{3.3}$$

$$cp_{\mathrm{PML}} = \frac{\varphi_{\mathrm{res}}cp_{\mathrm{res}}\rho_{\mathrm{res}} + \varphi_{\mathrm{al}}cp_{\mathrm{al}}\rho_{\mathrm{al}}}{\rho_{\mathrm{PML}}} \tag{3.4}$$

For modified PML materials the above equations change accordingly to take into account the contribution of the additional constituent.

$$\rho_{\mathrm{PML}} = \sum_{i=1}^{n} \varphi_{\mathrm{i}}\rho_{\mathrm{i}} \tag{3.5}$$

where φ_i and ρ_i represent the volume fraction and density of the i-th element of a Steel/Aluminium/Epoxy PML or Titanium/Aluminium/Epoxy PML, respectively. The overall specific heat capacity of a modified PML is then defined as

$$cp_{\mathrm{PML}} = \frac{\sum_{i=1}^{n} \varphi_{\mathrm{i}}cp_{\mathrm{i}}\rho_{\mathrm{i}}}{\rho_{\mathrm{PML}}} \tag{3.6}$$

Chapter 4

Material Characterisation

Understanding and analysing the fire performance of Polymer-Metal Laminates requires knowledge of their thermal and physical properties over the whole temperature range to be considered. There is an abundance of information about the material properties of metals over a wide temperature range, whereas characteristic material data for polymers is mostly limited to ambient temperatures. This section provides a description of the experimental work conducted in order to characterise these thermal and physical properties. Focus has been placed on experimental methods that would assist in the understanding of the material's behaviour at ambient as well as elevated temperatures. The experimental findings together with analytical results will form an essential part of a material's properties database from which a thermal model can be developed.

4.1 Epoxy Resin

4.1.1 Glass Transition Temperature

For materials comprising of polymeric constituents, glass transition (T_g) is defined as the temperature range over which a change in the polymer from a glassy to a rubbery state occurs. It is a transformation of the molecular structure which affects thermal as well as mechanical properties. The mechanical properties experience a significant decrease which practically excludes polymers or polymer-matrix materials from being deployed in environments above T_g due to these low structural properties. Thermal properties such as specific heat capacity and thermal transport characteristics show noticable changes, too. The specific heat capacity commonly increases on exceeding the glass transition temperature because of the increased polymer chain mobility which corresponds to a higher level of stored energy whereas thermal diffusivities are reduced due to the intensified scattering of the heat transferring phonons caused by the increased chain movement.

The glass transition temperature for the epoxy used in the developed PML lies between 78 °C to 82 °C as obtained from Differential Scanning Calorimetry experiments.

4.1.2 Thermal Analysis

Combined Thermogravimetric Analysis (TGA) and Differential Scanning Calorimetry (DSC) are used to study the decomposition behaviour of the PRF epoxy resin. In a PerkinElmer STA3000 device a 12 mg resin sample is heated up from room temperature up to 800 °C while its mass loss (TGA) and the heat flow towards the sample (DSC) are recorded. The tests are carried out at three different heating rates of $10\,°\mathrm{C\,min^{-1}}$, $20\,°\mathrm{C\,min^{-1}}$ and $40\,°\mathrm{C\,min^{-1}}$ in a nitrogen atmosphere. The higher heating rate results in a shift of the corresponding curves and curve characteristics towards higher temperatures due to the sample's thermal inertia, see table 4.1 for details.

	T_{onset} [°C]	T_{offset} [°C]	T_{max} [°C]	$T_{95wt\%}$ [°C]	$T_{90wt\%}$ [°C]	$T_{50wt\%}$ [°C]	Char yield [wt%]
HR10	341	426	373	339	348	378	6.49
HR20	355	439	381	353	363	389	6.37
HR40	370	448	406	366	376	404	5.75

Table 4.1: Change in decomposition characteristics of PRF epoxy resin for three heating rates.

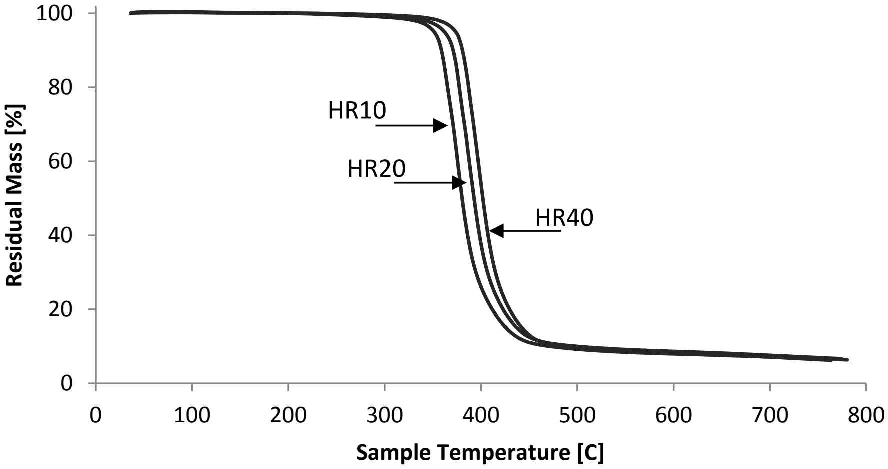

(a) Mass loss

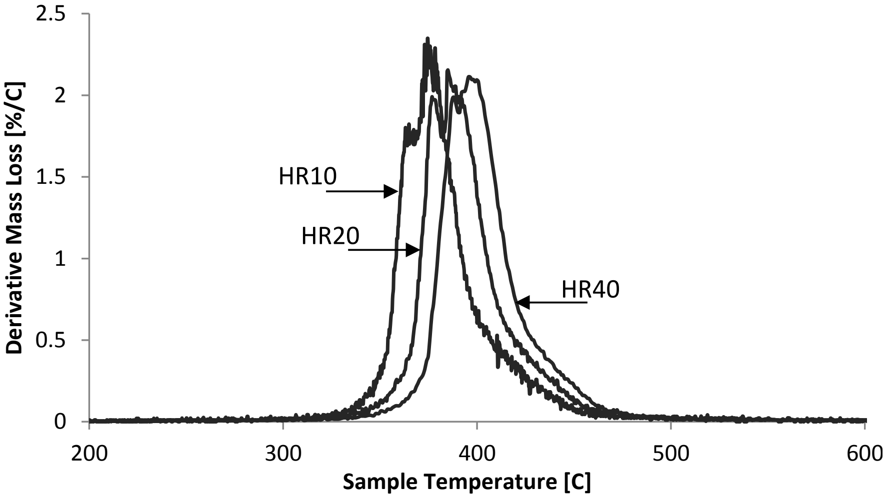

(b) 1st derivative of mass loss curve

Figure 4.1: Thermogravimetric analysis of PRF epoxy resin for three different heating rates: 10 K min^{-1}, 20 K min^{-1} and 40 K min^{-1}.

The TGA curves as shown in figure 4.1a are characterised by a steady mass loss between 300 °C and 500 °C which indicates a single-stage decomposition process. During the decomposition the resin is mostly transformed into hydrocarbon volatiles and lightly combustible gases leaving only a small amount (6 %) of solid charred residue. The first derivative curves dw/dT are used to assess the rate of weight loss and determine the point at which the maximum decomposition rate occurs, see figure 4.1b.

A multi-branch least squares fitting technique [147] is applied to analyse the TGA curves in order to obtain the kinetic parameters E_a and A for the decomposition reaction of the epoxy polymer. Since the heating rates within a decomposing resin vary from a few degrees per minute up to $100\,^{\circ}\mathrm{C\,min^{-1}}$ depending on the spatial temperature distribution within the sample [148], simultaneous analysis of the TGA curves is important. Individual curve fitting provides an independent set of kinetic parameters for every mass loss curve recorded at a specific heating rate. The assumption that taking the average of these individual parameters, in order to obtain one universal set of parameters for the particular polymer analysed, accurately describes the mass loss behaviour does not follow. Thus, the multi-branch fitting is necessary to appropriately consider the wide range of heating rates that occur within a decomposing polymeric resin.

As the pyrolysis reaction follows a first order Arrhenius equation, the kinetic parameters activation energy and rate coefficient of the epoxy resin used within PML can be obtained from the fitting procedure. These values are later used as input data for heat transfer simulations. The GNUPLOT software provides a fitting technique that allows a simultaneous evaluation of all three mass loss curves according to the multi-branch fitting technique which uses the Arrhenius equation

$$\frac{d\rho}{dt} = -A\rho_0 \left[\frac{\rho - \rho_{\mathrm{f}}}{\rho_0}\right] e^{(-E_a/RT)} \tag{4.1}$$

where A and E_a are the two unknown parameters rate coefficient and activation energy, respectively. The following values for A and E_a are obtained during the fitting procedure

$$A = 2.44 \times 10^{14}\ \mathrm{s^{-1}}\quad \pm 10.86\% \qquad\qquad E_a = 2.07 \times 10^{5}\ \mathrm{J\,mol^{-1}\,K^{-1}}\quad \pm 0.32\%$$

Figure 4.2 shows the close correlation of the experimental TGA curves and the data curves simulated with the kinetic parameters obtained from the fitting procedure. The recorded DSC curves, see figure 4.3, clearly show the endothermic characteristic of the decomposition reaction. The onset

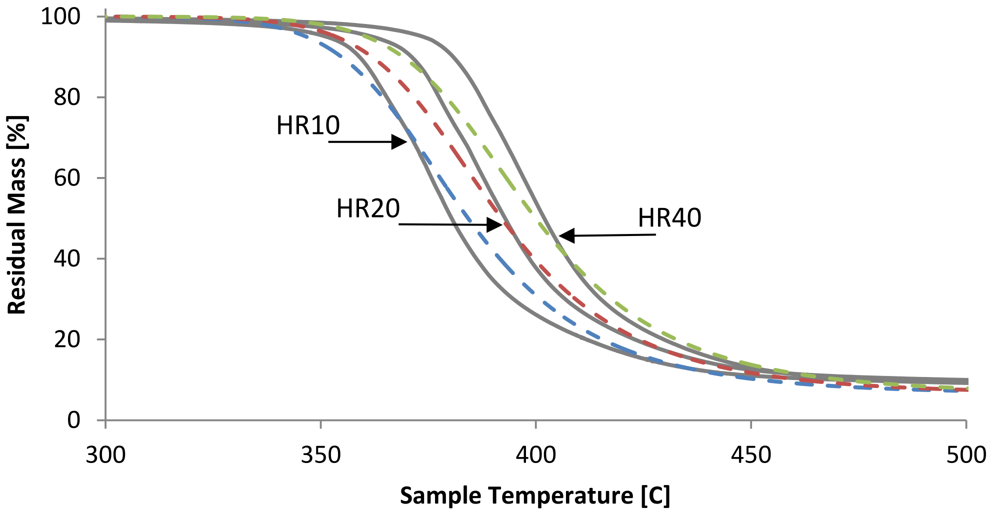

Figure 4.2: TGA fit results obtained with GNUPLOT, curves with increasing heating rate from left to right.

of the decomposition is determined to be around 340 °C. The DSC measurement also allows for the evaluation of the specific heat capacity of the resin as the heat flow rate is proportional to the material's specific heat. In recording the heat flow and comparing it with the heat flow rate into a reference material (e.g. sapphire) tested under the same conditions, the specific heat of the sample is obtained. Of special interest here is the change in value around the resin's glass transition temperature, see table 4.2.

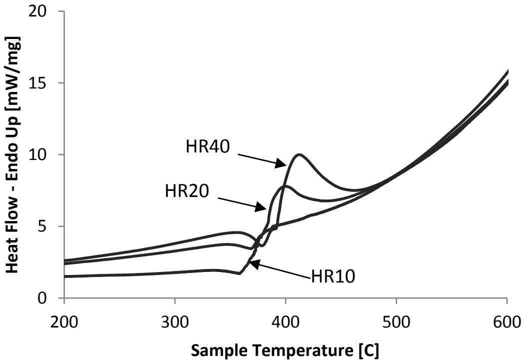

Figure 4.3: DSC analysis of PRF epoxy resin at varying heating rates

Temperature [°C]	Specific heat capacity [J/kgK]
27	934.5
97	1519.7
157	1521.0

Table 4.2: Specific heat capacity of PRF epoxy resin

4.1.3 Thermal Transport Properties

The thermal diffusivity of a material is commonly measured via transient methods like Hot Disk or Laser Flash during which a thermal gradient is applied to a small coupon sample. However, a simple and low-cost step-change technique that has been developed in-house can also be used to determine the thermal diffusivity accurately.

Theory

In general, a thermal experiment during which heat is transferred one-dimensionally through a slab of material can be modelled using LaPlace's equation

$$\frac{dT}{dt} = \alpha_{\mathrm{x}} \frac{d^2T}{dx^2} \tag{4.2}$$

where T is temperature, t is time and x the spatial coordinate. The material property α_x denotes the thermal diffusivity in the through-thickness, x, direction. It can be described through thermal conductivity k_{x}, material density ρ and specific heat c_{p} as follows

$$\alpha_{\mathrm{x}} = \frac{k_{\mathrm{x}}}{\rho c_{\mathrm{p}}} \tag{4.3}$$

The main factor that determines the heat transfer through a material of thickness b is defined as the Fourier number

$$Fo = \frac{\alpha_{\mathrm{x}} t}{b^2} \tag{4.4}$$

The recorded data of the centreline temperature can be expressed as the dimensionless temperature θ

$$\theta = \frac{T_1 - T}{T_1 - T_0} \tag{4.5}$$

where T is the centreline temperature, T_0 is the initial sample temperature, T_1 is the ambient temperature which will be reached at long exposure times. The dimensionless temperature θ ranges from an inital value of 1 to 0 for long experiment times, independent of the direction of the imposed

thermal gradient.
The well-known series solution [149] for equation (4.2) can be truncated to the first term without significant loss of accuracy when $Fo > 0.2$. The centreline dimensionless temperature of a flat plate is then calculated according to

$$\theta = \frac{4}{\pi} e^{\left(-\frac{\pi^2 Fo}{4}\right)} \tag{4.6}$$

This equation has its limitations as it is restricted to situations of perfect heat transfer when the sample surface is instantaneously exposed to the ambient temperature T_1. In practice the exact realisation of such a boundary condition is rarely achieved. A physical measure, the so-called Biot number, has been introduced to evaluate the efficiency of heat transfer through boundary layers. The Biot number, Bi, describes the ratio of the sample's internal resistance to heat conduction to the external resistance to heat convection.

$$Bi = \frac{hb}{k_{\mathrm{x}}} = \frac{hb}{\alpha_{\mathrm{x}} \rho c_{\mathrm{p}}} \tag{4.7}$$

with h denoting the heat transfer coefficient.
When $Bi > 300$ the effect of surface resistance to heat transfer may be ignored and the relationship in equation (4.6) can be used to derive the value of thermal diffusivity. For low Bi numbers, which occur mostly in such step-change experiments, the effect of the surface resistance to heat flow has to be taken into account. Heisler [150] delivered a modified version of the LaPlace equation that is applicable for cases where $Bi < 100$

$$\theta = \frac{T_1 - T}{T_1 - T_0} = C e^{\left(-\zeta^2 Fo\right)} \tag{4.8}$$

$$\text{with} \quad Bi = \zeta \tan\zeta \quad \text{and} \quad C = \frac{4 \sin\zeta}{2\zeta + \sin 2\zeta} \tag{4.9}$$

From the above equations it is apparent that Bi is defined as a function of ζ which poses a problem since ζ is an unknown factor and not vice versa.
Yovanovich [151] has given an approximation for the solution of heat transfer problems within a slab geometry to overcome this intrinsic problem and defined ζ as dependant upon Bi.

$$\zeta = \frac{\pi}{2\sqrt{1 + \frac{C_1}{Bi^{C_2}}}} \quad \text{with} \quad C_1 = 2.24 \ , \ C_2 = 1.02 \tag{4.10}$$

Reorganising equation (4.8) will lead to a final expression that is used to derive the thermal diffusivity from a step-change experiment when the above modifications are considered

$$\alpha_{\mathrm{x}} = \frac{-b^2}{\zeta^2 t} \ln\left(\frac{\theta}{C}\right) \tag{4.11}$$

The last undefined variable is the Biot number. From the outset of the experiment the heat transfer coefficient (HTC) needed in equation (4.7) is not known. However, the same experimental step-change procedure can be used to determine the HTC at various temperatures with a material block of high thermal conductivity. In that case, Bi becomes very low and the analysis of the recorded data can be based on the so-called Lumped System Analysis [152]. For $Bi \leq 0.1$ a uniform temperature distribution throughout the specimen is assumed so that the energy balance is expressed as the energy increase of the sample limited by the heat transferred into the sample during the time interval dt

$$hA\left(T - T_\infty\right) = -\rho V c_{\mathrm{p}} \frac{dT}{dt} \tag{4.12}$$

where h is the convective heat transfer coefficient, A is the surface area, V is the sample volume,

T_∞ is the ambient temperature, T is the sample temperature, c_p is the specific heat capacity. After integration and substitution of the dimensionless temperature θ, the above equation can be written as

$$\ln\theta = \ln\frac{T - T_\infty}{T_0 - T_\infty} = \frac{hA}{\rho V c_p}t \tag{4.13}$$

Therefore, the HTC can be directly obtained from the slope of the curve when the logarithm of the dimensionless time θ versus time t is plotted.

Procedure

A 100 × 100 mm^2 and 12 mm thick epoxy block, as shown in figure 4.4, is prepared featuring a fast-response thermocouple at its centre point that allows the recording of the variation of the centreline temperature. In order to ensure a one-dimensional heat transfer through the thickness of the specimen and prevent an in-plane temperature gradient the specimen edges are insulated with a Syndanio ceramic board bonded on with epoxy resin. The sample is kept in a temperature-controlled furnace for a few hours to achieve a uniform temperature of the sample. The sample is then rapidly moved from the furnace and placed in a temperature-controlled and agitated water bath which is kept at a temperature that is 20 K lower than the sample temperature. A temperature gradient will instantly form at the specimen's surface. The change of the centreline temperature is recorded by a data acquisition system from the time the specimen is submerged until the sample reaches a constant final temperature. In order to investigate the temperature dependence of the thermal diffusivity as well as measuring the heat transfer coefficient for the surrounding medium, experiments have been carried out in temperature intervals of 10 K over a wide temperature range.

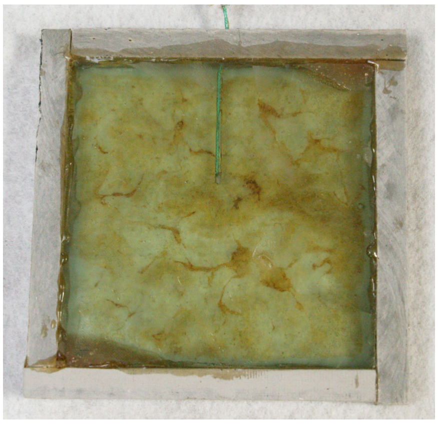

Figure 4.4: Polymer slab specimen after high temperature thermal diffusivity measurement. Discolouration due to exposure to temperatures above 180 °C.

Results

As can be seen from the above derivation of the equations for the analysis of the step-change experiment, it is essential for the accurate measurement of thermal diffusivity values to have defined boundary conditions. Literature values for the convective HTC can give an orientation towards the magnitude but are far too vague to allow for precise calculations. A list of HTC values is commonly given in heat transfer text books [149, 152] indicating the wide range that occurs, arising from the fact that the value of HTC for each individual case is highly dependent on the settings such as temperature, sample geometry, surface orientation or fluid properties.

In order to ensure that the criterion of $Bi \leq 0.1$ is fulfilled, the step-change experiments have been carried out with an aluminium specimen. Aluminium has a very low resistance to heat transfer as its high conductivity prevents the development of a temperature gradient through the sample. A one-dimensional explicit finite difference method has been developed with MATLAB software to validate the experimental HTC values obtained via equation (4.13). It is assumed that if the measured temperature-time curve can be precisely reproduced, the value for the HTC of the surrounding medium is accurate.

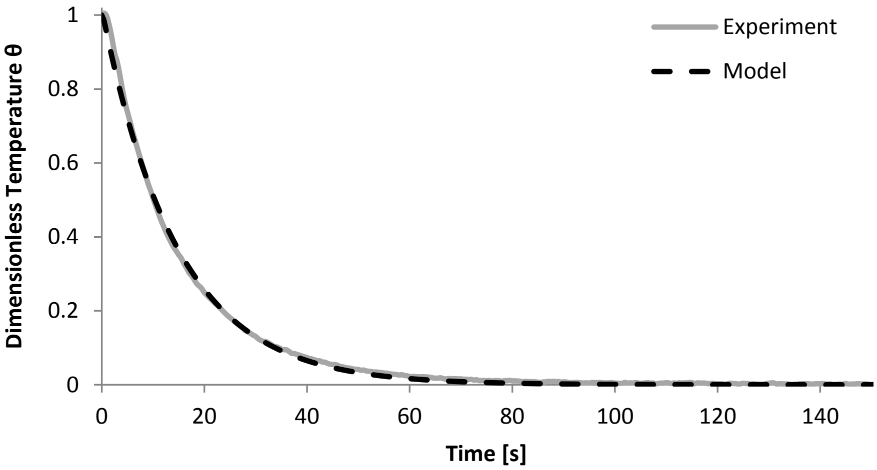

Figure 4.5: Determination of HTC: Comparison of measured and simulated reduction of a specimen's centreline temperature during a cooling experiment.

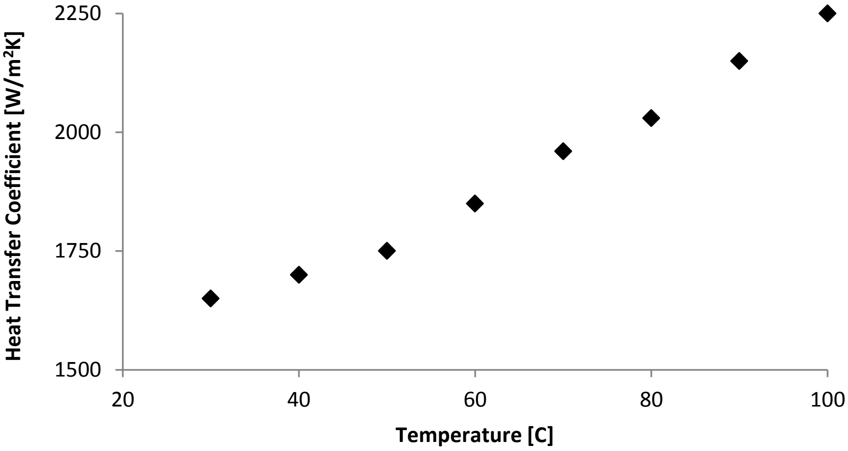

Figure 4.6: Temperature dependence of HTC of the agitated water bath.

The heat is conducted through the sample according to

$$\frac{\rho c_\mathrm{p}}{\Delta t}\left(T_x^{t+1}-T_x^t\right)=\frac{k}{\Delta x^2}\left(T_{x+1}^t-2T_x^t+T_{x-1}^t\right) \tag{4.14}$$

Considering the convective boundary conditions on the exposed surfaces the finite difference equation modifies to

$$\frac{\rho c_\mathrm{p}}{\Delta t}\frac{\Delta x}{2}\left(T_x^{t+1}-T_x^t\right)=\frac{k}{\Delta x}\left(T_{x+1}^t-T_x^t\right)+h\left(T_\infty-T_x^t\right) \tag{4.15}$$

Leaving instrument settings such as rotational mixer speed and water level constant over the testing period, the value for the convective HTC for the described step-change experiment is mainly a function of temperature. Having used a 20 mm slab of 5000er aluminium with known thermal properties, the derived results in figure 4.6 show a steady increase in the HTC with increasing temperature which lies well within the range compared to values found in literature. The developed finite difference method is able to accurately replicate the experimental temperature curve as shown in figure 4.5 in the case of a cooling experiment performed from 60 °C down to 40 °C. The results from the experiments at other temperatures show identical behaviour with similar accuracy. Thus, the measured HTC values are used as valid input values for the determination of thermal diffusivity.

The thermal diffusivity of the PRF epoxy resin has been measured as temperature dependent between room temperature and 100 °C. The reduction in thermal transport property with increasing temperature is shown in figure 4.7. Typical step-change behaviour over the tested temperature range is observed with the main decrease occurring around the resin's glass transition temperature. At 100 °C the thermal diffusivity is reduced to about 70 % of its room temperature value. The room temperature value of $\alpha = 0.1761\,\mathrm{mm\,s^{-1}}$ relates to a thermal conductivity of $k = 0.1943\,\mathrm{W\,m^{-1}\,K^{-1}}$ via equation (4.3). This shows good correlation with theoretical values for epoxy resins which cover a wide range from $k = 0.15 - 0.32$ [153, 154] due to the chemical versatility of epoxy polymers in general.

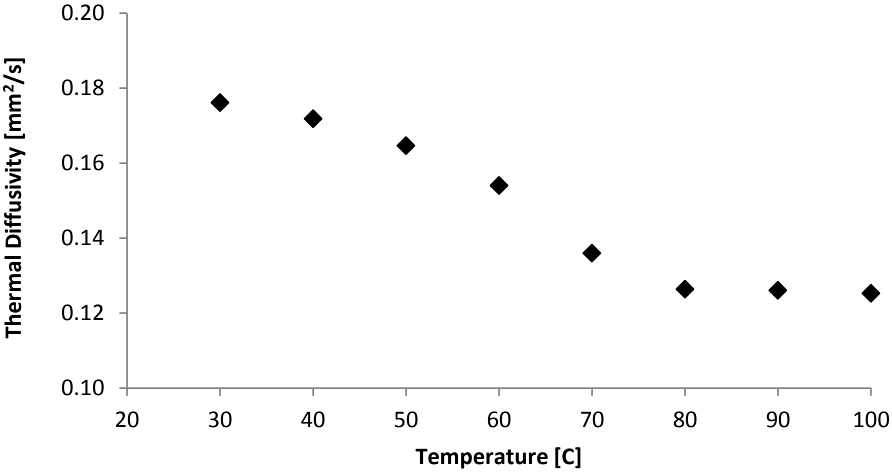

Figure 4.7: Thermal diffusivity of PRF epoxy resin as function of temperature.

4.2 Polymer-Metal Laminates

4.2.1 Thermal Transport Properties

Theoretical Background

The thermal properties of multi-component materials depend on the orientation of the layered material towards the direction of heat flow. This is analogous to electrical resistance systems because properties such as the effective thermal conductivity can be evaluated either in series or parallel. The series model [155] applies in the case of a heat flow perpendicular to the layered sample as schematically illustrated in figure 4.8. The overall thermal conductivity is then calculated according to the following equation (4.16) taking into account the thermal conductivity of each constituent and its volume fraction

$$\frac{1}{k_{\text{overall}}} = \sum_{i=1}^{n} \frac{\varphi_i}{k_i} \tag{4.16}$$

where φ_i is the volume fraction and k_i the thermal conductivity of the i-th element.
Therefore, the calculation of the room temperature thermal conductivity for a typical PML made of aluminium foil and PRF epoxy resin with the respective properties of

$$k_{\text{al}} = 200 \quad \mathrm{W/mK}, \quad k_{\text{epoxy}} = 0.19 \quad \mathrm{W/mK}, \quad \varphi_{epoxy} = 0.06$$

yields a theoretical value of

$$\frac{1}{k_{\text{theory}}} = \frac{1-\varphi}{k_{\text{al}}} + \frac{\varphi}{k_{\text{epoxy}}}$$

$$k_{\text{theory}} = 3.19 \quad \mathrm{W/mK}$$

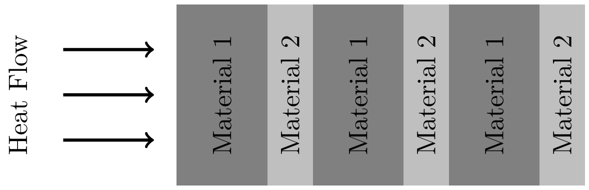

Figure 4.8: Series model for multi-layered materials.

Experimental Procedure

The same experimental technique as described under section 4.1.3 can be used to measure the thermal conductivity of the laminates. A combination of using the agitated water bath up to 100 °C as well as a fluidised sand bath for elevated temperatures up to 250 °C allows the determination of the temperature dependence of the PML's thermal conductivity over a wide temperature range. However, due to technical limitations measurements above the onset of resin decomposition are not possible. Alternatively, the PML specimen can be artificially decomposed under controlled furnace conditions (time and temperature) and the step-change experiment then carried out at room temperature.

Preparation of the samples involved the bonding of two PMLs on the exposed surfaces of a $100 \times 100\,\text{mm}^2$ aluminium block that had been insulated along the edges of its 10 mm thickness. Figure 4.9 depicts a schematic design of such a specimen for the step-change experiment.

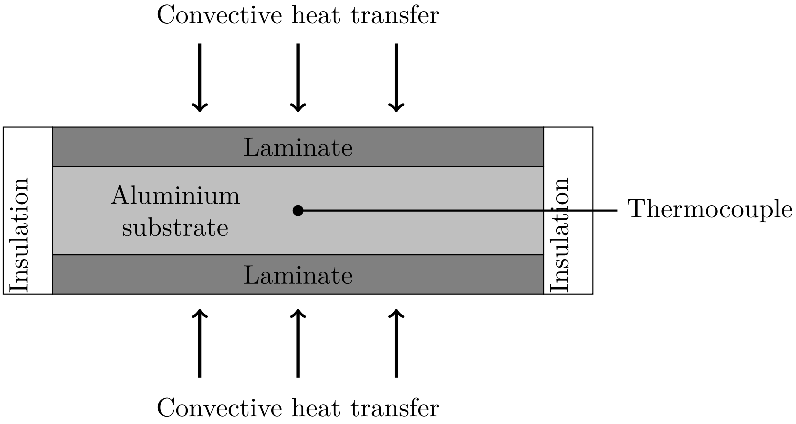

Figure 4.9: Cross-section of a typical PML/aluminium sample used for step-change experiments.

Theory

During the cooling experiment, the amount of heat that is conducted across the laminate layers and then transferred from the PML surface layer into the surrounding water environment via convection can be quantified through the variation of the centreline temperature of the aluminium. A schematic temperature distribution along the specimen's cross-section is shown in figure 4.10. This is possible because the temperature at the interface between laminate and aluminium is assumed to be the same as in the centre since there is no temperature gradient present within the aluminium due to its high thermal conductivity.

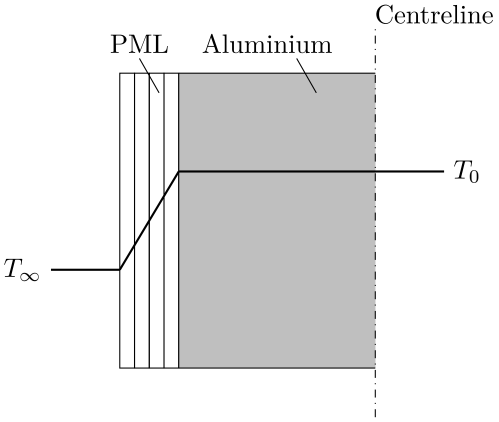

Figure 4.10: Schematic temperature distribution along the cross-section of a PML/aluminium sample during a step-change cooling experiment.

The heat conducted through the laminate is defined as

$$q_{\mathrm{PML}} = \frac{Q}{A} = \frac{k_{\mathrm{PML}}}{\mathrm{a}}\left(T - T_\infty\right) \tag{4.17}$$

with k_{PML} being the laminate's thermal conductivity, a the thickness and $(T - T_\infty)$ the temperature difference to the ambient environment.
Whereas the temperature rise within the aluminium substrate is defined as

$$q_{\mathrm{Al}} = \frac{Q}{A} = -\rho c_{\mathrm{p}} \mathrm{b} \frac{dT}{dt} \tag{4.18}$$

where ρ,c_{p} and b are the aluminium density, specific heat capacity and plate thickness, respectively. dT/dt describes the temperature change over time. Combining the above relationships enables the modelling of the temperature change during a cooling experiment from the following differential equation

$$\frac{k_{\mathrm{PML}}}{\mathrm{a}}\left(T - T_\infty\right) = -\rho c_{\mathrm{p}} \mathrm{b} \frac{dT}{dt} \tag{4.19}$$

Rearranging and integrating leads to

$$t = \frac{\rho c_{\mathrm{p}} \mathrm{ba}}{k_{\mathrm{PML}}} \ln\left(T - T_\infty\right) + C \tag{4.20}$$

The integration constant C is found when the boundary conditions at the start of test are taken as $T = T_0$ at $t = 0$

$$C = -\frac{\rho c_{\mathrm{p}} \mathrm{ba}}{k_{\mathrm{PML}}} \ln\left(T_0 - T_\infty\right) \tag{4.21}$$

and as a consequence

$$t = \frac{\rho c_{\mathrm{p}} \mathrm{ba}}{k_{\mathrm{PML}}} \ln\left(\frac{T - T_\infty}{T_0 - T_\infty}\right) = \frac{\rho c_{\mathrm{p}} \mathrm{ba}}{k_{\mathrm{PML}}} \ln\theta \tag{4.22}$$

The thermal conductivity of the metal laminates can be derived from the above equations. It is common to plot the logarithm of the dimensionless temperature θ versus time. The slope of the obtained curve can be directly related to the thermal conductivity k_{PML} through equation (4.23).

$$k_{\mathrm{PML}} = \rho c_{\mathrm{p}} \mathrm{ba} \frac{\ln\theta}{t} \tag{4.23}$$

Results

Thermal conductivity values for the 10L/50μm PML sample have been obtained from the analysis of thermal step-change experiments carried out over a temperature range from room temperature

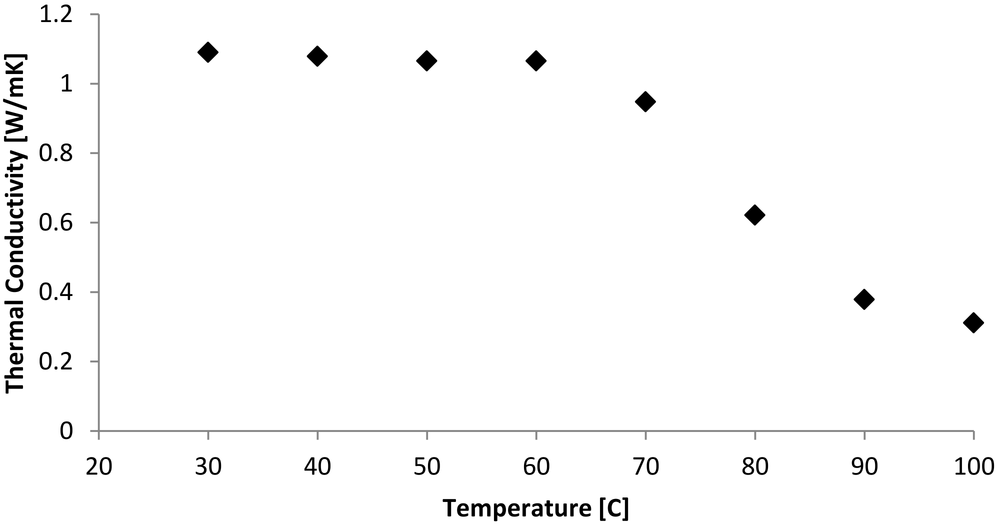

Figure 4.11: Temperature dependence of thermal conducitvity of unexpanded PML.

to 100 °C and 250 °C as well as measurements of the decomposed sample condition.

It is found that at room temperature the PML has a thermal conductivity of $k = 1.09\,\mathrm{W\,m^{-1}\,K^{-1}}$. This is not as low as thermal conductivity values for materials purely designed and optimised for fire insulation purposes such as ceramic fibre blankets ($k \approx 0.04\,\mathrm{W\,m^{-1}\,K^{-1}}$) or intumescent paints ($k \approx 0.03\,\mathrm{W\,m^{-1}\,K^{-1}}$). However, considering that over 90 % of this material is comprised of metal foil, it proves its considerable potential as a fire protection material in comparison with other materials in high temperature applications such as fire clay bricks ($k \approx 1.4\,\mathrm{W\,m^{-1}\,K^{-1}}$) or glass fibres ($k \approx 1.2\,\mathrm{W\,m^{-1}\,K^{-1}}$).

As seen from figure 4.11, with increasing temperatures a reduction of about two thirds from $k = 1.1\,\mathrm{W\,m^{-1}\,K^{-1}}$ to $k = 0.31\,\mathrm{W\,m^{-1}\,K^{-1}}$ at 100 °C can be seen with the major change occurring around 80 °C. The latter observation is not surprising bearing in mind that the limiting factor for any property of a multi-component material is the constituent exhibiting the lowest property value. Therefore, the temperature dependence of the PML thermal conductivity is dominated by the behaviour of the epoxy polymer component. This can be seen when the curves for thermal transport properties for PML and epoxy resin are compared with each other as the same step-change characteristic can be observed with the main decline occurring around the polymer's glass transition temperature of around 80 °C.

In case of a 10L/50μm PML the theoretical value at room temperature is calcuated by the equation (4.16) to $k = 3.39\,\mathrm{W\,m^{-1}\,K^{-1}}$. The apparent difference between the theoretical and experimental value for the thermal conductivity of PML can be explained by the presence of air within the samples. During the manufacturing process it is possible that air is either not completely removed by debulking and compressing, or introduced secondarily because of tiny creases in the foil and air trapped in the resin spraying process.

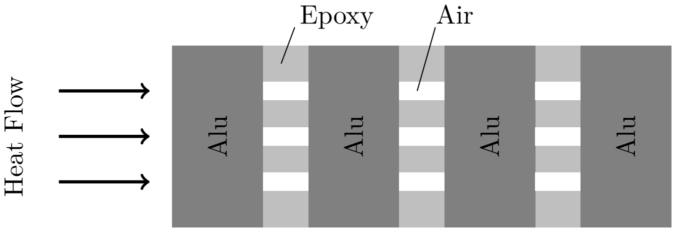

Figure 4.12: Combination of in-parallel and in-series configuration in a PML.

Technique	Sample type	k_{exp}	k_{theory}	apparent φ_{air}
Hot-Disc	10L/30μm	1.07	2.91	7.18%
	20L/30μm	1.06	2.71	7.12%
	10L/50μm	1.17	3.39	6.97%
	20L/50μm	1.03	3.54	7.47%
Step-change	10L/50μm	1.09	3.39	7.38%

Table 4.3: Thermal conductivity for various PML types at room temperature, given in $\mathrm{W\,m^{-1}\,K^{-1}}$.

The aforementioned analogy of an electrical resistance system can be used in reverse to determine the air content within the PML sample under the assumption that the overall thermal conductivity equals the value obtained via step-change experiment $k_{\text{all}} = k_{\text{exp}} = 1.09\,\mathrm{W\,m^{-1}\,K^{-1}}$. For the new three-component material comprised of aluminium, epoxy and air, the general series equation (4.16) needs to be modified to account for the fact that air is contained within the polymeric interlayers, which is illustrated in figure 4.12. Thus the air and epoxy fractions are in parallel with each other, denoted as the denominator of the second term on the right hand side of equation (4.24), which in turn is connected in series to the aluminium foils.

$$\frac{1}{k_{\text{all}}} = \frac{\varphi_{\text{al}}}{k_{\text{al}}} + \frac{\varphi_{\text{layer}}}{\varphi_{\text{epoxy}} k_{\text{epoxy}} + \varphi_{\text{air}} k_{\text{air}}} \tag{4.24}$$

The ratio of the fractions φ_{al} and φ_{layer} is deduced from the thickness of the individual specimen. The parameter φ_{layer} also reduces the number of unknown variables as it equals the sum of φ_{epoxy} and φ_{air}. Solving the above equation with respect to φ_{epoxy} leads to the air volume fraction contained within PML.

$$\varphi_{\text{epoxy}} \left(k_{\text{epoxy}} - k_{\text{air}}\right) + \varphi_{\text{layer}} k_{\text{air}} = \frac{\varphi_{\text{layer}}}{\frac{1}{k_{\text{all}}} - \frac{\varphi_{\text{al}}}{k_{\text{al}}}} \tag{4.25}$$

The amount of air trapped within the 10L/50μm PML is determined to $\varphi_{\text{air}} = 7.38\,\%$.

In order to investigate the variation in thermal conductivity for the different laminate designs additional measurements have been carried out. The Hot-Disc method was used for this purpose because, besides the property determination, it provides an additional means of verifying the results obtained from the step-change experiment. The results for measurements performed at room temperature are listed in table 4.3. All values lie well within a 10 % error margin around an average value of $k = 1.08\,\mathrm{W\,m^{-1}\,K^{-1}}$. The slight variations arise from the differing weight fractions of epoxy resin present within each sample as well as a possible volume fraction of around 7 % trapped air. But more importantly it verifies the results from the much simpler step-change experiment which seems to show it is a quick and inexpensive alternative. Also, since the variations of the thermal conductivity lie within a very small margin it can be assumed that the temperature dependence measured for the 10L/50μm PML type can be taken as reference values for further analysis of all four different PML designs.

At temperatures above 100 °C the PML sustains a further gradual decrease in thermal transport properties. The thermal conductivity is steadily reduced to a low of $k = 0.13\,\mathrm{W\,m^{-1}\,K^{-1}}$ at 230 °C. Although these temperatures are well below the onset of polymer pyrolysis, the epoxy resin within the PML will experience thermal degradation over this temperature range which can affect its material properties. An indication of such behaviour is observed in the slight colour changes of the epoxy resin itself that occur when the polymer is exposed to temperatures as low as 150 °C. With increasing temperatures the effect of thermal degradation will become more pronounced affecting the material's properties still further. However, the biggest factor affecting the reduction in thermal conductivity is related to the air content within the PML samples. As the temperature rises, the trapped air volume increases due to the thermal expansion of the gas. This in turn influences the thermal transport capability since a higher proportion of the thermally resistive gas-air mix causes a reduction in the overall thermal conductivity of the PML. The thermal expansion effect can be observed in the appearance of small blisters at the laminate's surface resulting in a slight overall increase in PML thickness.

Decomposed PMLs display a thermal conductivity of $k = 0.095\,\mathrm{W\,m^{-1}\,K^{-1}}$ which is less than one order of magnitude lower, compared to the room temperature value. The reduction is caused by the pyrolysis of the polymer which almost completely transforms the organic material into decomposition gases yielding only 6 % of char from the total amount of resin present within the PML. In addition, the decomposition gases cause the PML to swell extensively. Due to the swelling, the PML in a decomposed condition comprises of nearly 90 % air-gas mix. The theoretical value for the thermal conductivity of a decomposed PML, based on the observed volume ratios of air, aluminium foil and char, is determined via the series model to $k = 0.03\,\mathrm{W\,m^{-1}\,K^{-1}}$. The apparent difference between the theoretical and experimental results for the decomposed PML is thought to arise from the difficulties of accurately capturing the decomposed condition of the laminates. With the applied experimental technique, the specimens had to cool down before they could be handled. It was noticed that this resulted in a contraction of the expanded PML so that the observed expansion factor underestimates the true expansion during decomposition.

4.2.2 PML Expansion Behaviour

The process of laminate expansion due to resin decomposition is essential to the fire protection effect constituted by PML materials. Knowledge of an accurate description of the swelling behaviour is a necessary prerequisite for correct thermal analysis.

The expansion characteristics of passive fire protection, i.e. intumescent materials, are commonly specified through the introduction of a swelling factor. In early investigations of intumescent coatings, expansion has been simplified and described as a temperature-dependent volumetric parameter obtained from visual observation [156]. As the pyrolysis reaction is the direct cause for the transformation of organic matter into gaseous products and hence a macroscopic mass loss, the expansion performance should be directly related to the mass loss characteristics. Recent approaches achieved a more accurate depiction as the expansion has been successfully linked to the production of decomposition gases during the pyrolysis reaction [143, 157] although secondary effects influencing the swelling behaviour might have been neglected as a result.

Isothermal heat exposure tests represent a simple method that allows the assessment of the swelling capabilities of expandable materials in a controlled thermal environment. For this, PML specimens are placed in a temperature regulated furnace and mass loss and expansion are recorded at specific time intervals. The experiment has been repeated for various points over the temperature range from just above the onset of decomposition up to 500 °C which is indicated as the end of the decomposition reaction by TGA.

The time-dependent mass loss behaviour under isothermal conditions can be reproduced by a simplified kinetic model presented by Lyon [158] which defines the pyrolysis of the chemical polymeric bonds as the rate-limiting parameter for the mass loss of a char-forming polymer. Therein the residual polymer fraction can be expressed

$$\frac{m}{m_0} = y_c + (1 - y_c)\, e^{-k_p t} \tag{4.26}$$

with m/m_0 denoting the ratio of current mass m to initial mass m_0, y_c describing the equilibrium char yield, k_p the pyrolysis rate constant and t representing time.

The mass loss curves reproduced from the above equation show good correlation with the

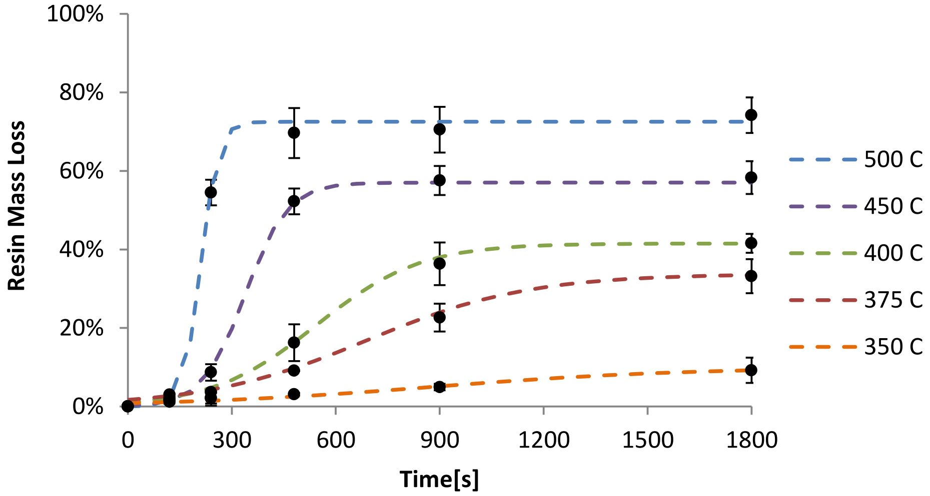

Figure 4.13: Mass loss of the resin contained within PML as function of time during isothermal furnace tests.

experimental data for long exposure times and in the identification of the final mass fraction after the pyrolysis reaction has come to an end. Distinctive discrepancies are noticeable during the initial phase of the reaction due to the thermal lag induced by the furnace environment. The non-conformity arises from the deduction of Lyon's model based on isothermal TGA experiments with near-immediate material response of small-scale samples, whereas the conducted furnace tests represent a different thermal environment which seems to affect the pyrolysis pattern as the residual polymer fraction in the isothermal TGA experiments is much lower than in the corresponding furnace test suggesting incomplete polymer conversion. This does not, however, allow an inference that the determination of the kinetic parameters of TGA heating curves can be derived from the isothermal tests, as additionally proposed in Lyon's work.

Adjustments to the basic equation are necessary in order to accommodate the effect of the thermal inhibition time observed during the furnace experiments. The revised equation for an adequate description of polymer mass loss Δm within a PML is given as

$$\Delta m = \frac{m_0 - m}{m_0} = \frac{\Delta m_{max}}{1 + \exp\left(k\left(t - t_{cr}\right)\right)} \tag{4.27}$$

where temperature-dependent parameters represent the total amount of polymer mass loss Δm_{max}, a reaction constant k and the point of highest mass loss rate t_{cr}. The mass loss curves obtained from the furnace tests are presented in figure 4.13 showing good consistency with the revised modelling procedure of the pyrolysis reaction above 300 °C. The observed PML expansion behaviour is a non-linear function of the recorded polymer mass loss as shown in figure 4.14 where the relationship between PML expansion factor and the logarithm of mass loss are presented. The exponential curve characteristic indicates behaviour based on a power-law dependency which can be expressed in the form of

$$f(x) = y_0 + a(x^b)$$

The application of the above equation during a least-squares fitting procedure leads to a mathematical description of the PML expansion during isothermal furnace tests with good correlation, as shown in figure 4.15.

$$\beta = \frac{d_f}{d_0} = \beta_0 + (\beta_{max} - \beta_0)\left(\frac{m_0 - m}{m_0}\right)^n \tag{4.28}$$

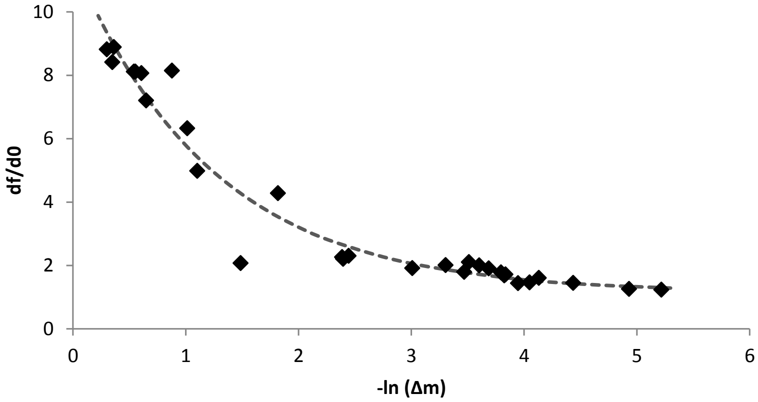

Figure 4.14: PML expansion, i.e. ratio of final to inital PML thickness, shown as function of polymer mass loss recorded during isothermal furnace tests.

where β, β_0, β_{max} are the instantaneous, initial and maximum expansion factor,
d_f/d_0 is the ratio of final to initial PML thickness,
$m_0 - m/m_0$ defines the epoxy mass loss,
n is the reaction's rate constant.

The slight inhibition time is evidently caused by the thermal lag of the decomposition reaction of the polymer within the PML in the first place. Furthermore, enough reaction gases need to be produced in order to cause deformation of the softened PML aluminium foils which ultimately results in macroscopic surface blisters and overall expansion. The average expansion observed is in the range of 9 times the initial PML thickness. Individual measurements show maximum values of the expansion factor of greater than 10. The measured values are slightly underestimating the actual expansion because of the specimens' cooling down phase. During this process the expanded PMLs experience noticeable contraction which leads to a conservative description of the swelling potential of PML materials in the presented model.

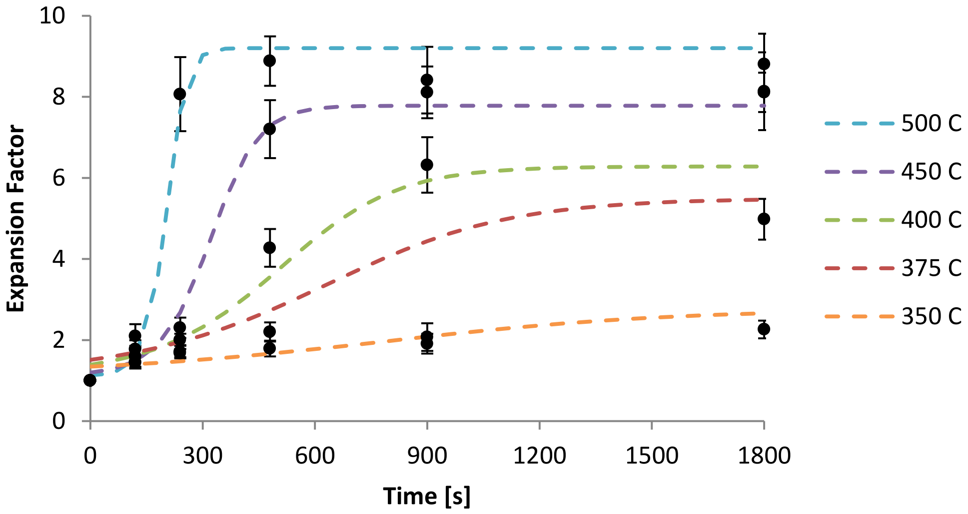

Figure 4.15: Time-dependent change in expansion factor during furnace tests shown as comparison between experimental observation (data points as average of four individual measurements) and calculated parameter as a function of polymer mass loss (dashed curve).

An example of an expanded PML is presented in figure 4.16. The micrograph shows a cross-section of an expanded PML bonded to an aluminium substrate. In contrast to isothermal furnace testing where the sample is exposed to heat to all faces, thermal input had only been applied to the PML surface. Nevertheless, the swelling behaviour is still discernable as distinctive delamination between individual foil layers occurs which leads to the overall observed expansion of the PML thermal barrier.

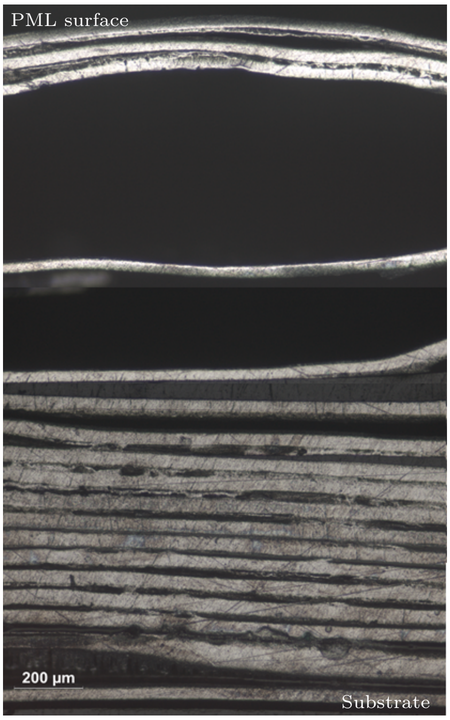

Figure 4.16: Cross-section view of an expanded 20-ply PML on AA2024 substrate after exposure to a radiant heat flux of $50\,\mathrm{kW\,m^{-2}}$ for 9 min, with the heat exposed surface being at the top of the picture. Residual gas pockets resulting from the epoxy decomposition during high temperature exposure are clearly visible.

Chapter 5

Thermal Modelling of PML Structures

The COM_FIRE program was developed at Newcastle University in the mid-1990s as a FORTRAN program [124]. Over the years COM_FIRE has been updated numerous times to include options for different heating sources, broadening the property library of homogeneous composite materials as well as incorporating additional thermal effects to better reflect realistic material behaviour. During this research it was found that COM_FIRE is deficient in that it was unable to predict the temperature evolution in non-homogeneous materials as well as being unable to recognise the cause and effect of expansion within specimens. It is only able to simulate the thermal behaviour of thick fibre reinforced composite materials comprising of a polymer matrix in fire conditions.

In this study a new thermal model has been developed to predict the temperature distribution within PML materials and PML-protected specimens when exposed to elevated temperatures. The newly developed PML_FIRE program, written as a MATLAB program and based on the COM_FIRE program, overcomes the shortcomings in the existing modelling approaches and will accurately simulate the thermal response of PML materials bonded onto a substrate material when exposed to fire conditions. It is possible to use PML_FIRE independently or in combination with COM_FIRE. The new modelling in the program was necessary, in particular, to adapt COM_FIRE to recognise the behaviour of the layered structure of the multi-component materials. Additionally, specific thermal effects that occur during the PML's exposure to fire due to the unique architecture and the formation of the fire protection effect have been incorporated into the new program code.

5.1 Governing Equations

The one-dimensional heat transfer process in the through-thickness direction of a solid material which is heated from one side is described by a non-linear partial differential equation. The rate of change of the internal energy of the material, i.e. temperature increase or decrease, is determined by the rate at which heat is conducted through the solid

$$\rho c_{\mathrm{p}} \frac{\partial T}{\partial t} = \frac{\partial}{\partial x}\left(k \frac{\partial T}{\partial x}\right) \tag{5.1}$$

The temperature increase is indicated on the left-hand side of the equation whereas the heat transfer as conduction through the material is denoted on the right-hand side. At the material's front face, which is directed to the heat source, the heat is transferred from the flame towards the sample through radiation and free convection. No forced heat convection is considered in the analysis.

The net heat flux q, defined as energy per surface area into the front face of the sample, is the combined effect of radiation (first term) according to the Stefan-Boltzmann Law and natural convection (second term) from the heating source

$$q = \frac{Q}{A} = \sigma \left(\epsilon_{\mathrm{fl}} \alpha_{\mathrm{s}} T_{\mathrm{fl}}^4 - \epsilon_{\mathrm{s}} T_{\mathrm{s}}^4 \right) + h \left(T_{\mathrm{fl}} - T_{\mathrm{s}} \right) \tag{5.2}$$

where σ is the Stefan-Boltzman-constant, ϵ_{fl} and ϵ_{s} are the flame and sample emissivity respectively, α_{s} is the sample's absorptivity at the front face, h is the convective heat transfer coefficient, T_{fl} and T_{s} are denoted as the temperature of the flame and the sample, respectively. Similar boundary conditions apply for the back face where the effect of natural convection and radiation is driven by the temperature difference between the sample and the ambient temperature. In a fire situation where the temperature of the heating source easily exceeds 1000 °C radiation is the dominant mode of heat transfer.

The effect of natural convection on the hot face of the sample can be best described as a turbulent boundary layer of air flow for a vertical wall surface [159]. Thus, the heat transfer coefficient is defined as

$$h_{\mathrm{hf}} = 1.31 \sqrt[3]{\theta} \quad \text{with} \quad \theta = T_{\mathrm{fl}} - T_{\mathrm{s}} \tag{5.3}$$

where θ denotes the temperature difference between the surrounding flame environment T_{fl} and the front face of the sample T_{s}. The heat transfer coefficient for the cold face is estimated according to the following equation [159]

$$h_{\mathrm{cf}} = h_{\mathrm{nc}} + 0.03 T_{\mathrm{s}} + 0.0001 T_{\mathrm{s}}^2 \tag{5.4}$$

with h_{nc} being the heat transfer coefficient for natural convection in air which is in the range of $5\,\mathrm{W\,m^{-2}\,K^{-1}}$ to $20\,\mathrm{W\,m^{-2}\,K^{-1}}$. The temperature of the sample at the cold face is represented by T_{s}.

5.2 Numerical Realisation

Discretisation

A one-dimensional explicit Finite Difference (FD) method has been chosen as the numerical approach to simulate the heat transfer through a PML bonded onto a substrate. It allows for the calculation of a temperature change during a certain time interval at any given point x throughout the material by taking into account the temperature development of its neighbouring points $x-1$ and $x+1$, as schematically shown in figure 5.1.

The laminate part of a bonded PML sample is equally divided into nodes to form uniform elements according to the number of laminate layers. One metal foil together with one epoxy layer forms a combined spatial element of thickness x. The spatial elements for homogenous metal or composite substrates can be coarsely distributed, i.e. a less fine mesh is needed. For substrates with a thickness of up to 20 mm the application of a maximum of 50 substrate nodes is standard practice.

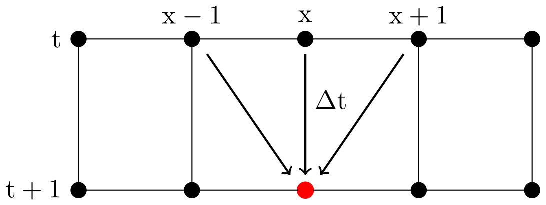

Figure 5.1: Principal determination of nodal temperatures during 1D explicit FD methods.

An alternative to the aforementioned practice of distributing the nodes would be to treat every physical layer as an individual layer within the simulation as outlined in figure 5.2. The significant disadvantage is that this would cause a substantial impact on the computing time. The separation of metal foils and epoxy layers into individual elements leads to a multiplicity of nodes to be evaluated at any one time step in comparison to the approach of combined elements. The fact that the element with the smallest spatial dimension determines the number of time steps results in hugely increased computing time as there exists at least a factor of ten between the spatial dimension of a combined element in comparison to a single epoxy layer element.

Based on these considerations, the overall increase in computing time which would take up to several hours is deemed unacceptable in creating an efficient model that can be used to accurately simulate the thermal response in different fire scenarios and assist in the development of new PML materials.

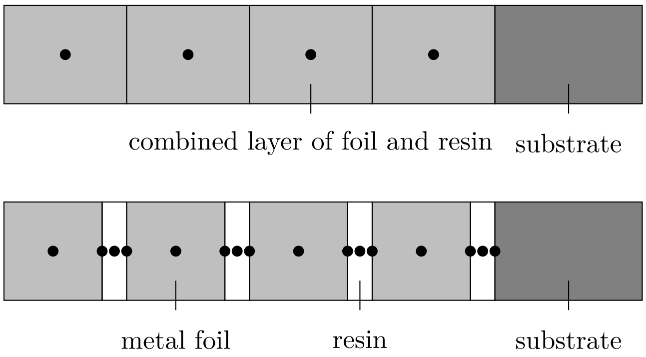

Figure 5.2: Schematic outline of the nodal mesh for combined (top) and individual (bottom) layer approach for a 4-ply PML/substrate specimen.

Finite Difference Equations

For the principal heat transfer through any element within the sample equation (5.1) can then be rewritten in finite difference notation as

$$\frac{\rho c_\mathrm{p}}{\Delta t}\left(T_x^{t+1}-T_x^t\right)=\frac{k}{\Delta x^2}\left(T_{x+1}^t-2T_x^t-T_{x-1}^t\right) \tag{5.5}$$

The temperature development at the boundary node on the hot face is determined as shown below where the first term on the right-hand side describes the heat conduction away from the hot face into the first layer of the laminate, the middle term denotes to the radiation effect and the last term describes the convective heat transfer.

$$\frac{\rho c_\mathrm{p}}{\Delta t}\frac{\Delta x}{2}\left(T_x^{t+1}-T_x^t\right)=\frac{k}{\Delta x}\left(T_{x+1}^t-2T_x^t-T_{x-1}^t\right)+\sigma\left(\epsilon_\mathrm{fl}\alpha_\mathrm{x}T_\mathrm{fl}^4-\epsilon_\mathrm{x}T_\mathrm{x}^4\right)+h_{hf}\left(T_\mathrm{fl}^t-T_\mathrm{x}^t\right) \tag{5.6}$$

Similarly, the boundary conditions for the cold face of the sample can be defined as

$$\frac{\rho c_\mathrm{p}}{\Delta t}\frac{\Delta x}{2}\left(T_x^{t+1}-T_x^t\right)=\frac{k}{\Delta x}\left(T_{x+1}^t-2T_x^t-T_{x-1}^t\right)+\sigma\left(\epsilon_\mathrm{fl}\alpha_\mathrm{x}T_\mathrm{fl}^4-\epsilon_\mathrm{x}T_\mathrm{x}^4\right)+h_{cf}\left(T_\mathrm{fl}^t-T_\mathrm{x}^t\right) \tag{5.7}$$

Introduction of Interfaces

As PML structures are multi-component materials with a wide range of thermal properties it is important to ensure that sustained heat transfer is passed on from one element to the next where different material types meet. This is valid within the PML itself, the foil-resin junction, as well as the transition from PML to the substrate material. Therefore, the set of finite difference equations for any interface node needs to take into account the different material properties as well as the change in spatial dimension from both elements contributing to the interface. Equation (5.5) changes accordingly to formulations given by Croft [160]

$$\frac{(\rho c_\mathrm{p})_\mathrm{segment}}{\Delta t}\left(T_x^{t+1}-T_x^t\right)=\frac{k_1}{\Delta x_1^2}\left(T_{x+1}^t-2T_x^t-T_{x-1}^t\right)+\frac{k_2}{\Delta x_2^2}\left(T_{x+1}^t-2T_x^t-T_{x-1}^t\right) \tag{5.8}$$

Stability Criteria

The Fourier number is a dimensionless number that is used to characterise the heat transfer process. For stability reasons negative coefficients in the finite difference equations are not permitted as it would contradict thermodynamic principles. In order to fulfil this requirement, the stability criterion has to have a value lower than 0.5. A low Fourier number may result in an improvement in accuracy as reducing Fo decreases the time interval for every time step. However, if too low a figure is chosen it dramatically increases the computing time as well as the cumulative error for the predictions in every time step due to the large total number of time intervals. The best solution seems to be, when selecting an appropriate Fo, to compromise between the positive effect of improved accuracy as against the adverse influences of error and time increase, and to find a figure that best satisfies those competing effects.

$$Fo=\frac{\alpha\Delta t}{\Delta x^2}=\frac{k\Delta t}{\rho c_\mathrm{p}\Delta x^2}\leq 0.5 \tag{5.9}$$

5.3 Thermal Effects

Substrate Material

The fire protection effect of PML can only be assessed in relation to the performance of the unshielded substrate material during the heat exposure. Therefore, it is important to correctly reproduce the observed experimental behaviour of the substrate within the simulation. This can be realised as shown under section 5.2 where equations (5.5) to (5.7) describe the heat transfer through a homogeneous material including boundary conditions. Material specific properties such as thermal conductivity k, specific heat capacity c_p, density ρ, absorptivity α_s and emissivity ϵ_s have to be adjusted accordingly. It is preferable to implement them as functions of temperature instead of as a single-value property which might give a rough estimation but is less accurate.

As an example, for a 10 mm aluminium substrate plate the material properties listed in table 5.1 have been implemented into the MATLAB program. The simulated curves for aluminium substrates exposed in a fire test based on these input criteria fit the temperature recordings obtained from the thermocouples very well, see figure 5.3. Additionally, the simulation allows prediction beyond the experimental results as the thermocouples are limited to temperatures below 400 °C. The fire behaviour from room temperature up to the melting point of an aluminium plate can be accurately estimated.

When other substrate materials are used such as GFRP or CFRP polymer-matrix composites, the existing COM_FIRE code is suitable to predict the fire performance of these combustible materials. It contains a vast material library comprising various types of polymer (polyester, vinyl

Property	Definition		Reference
Specific heat capacity in J kg^{-1} K^{-1}	$c_\mathrm{p}=0.41T+903$ $c_\mathrm{p}=0.825T+695.5$ $c_\mathrm{p}=1040$	for $T=[0\,°\mathrm{C},500\,°\mathrm{C}]$ for $T=[500\,°\mathrm{C},660\,°\mathrm{C}]$ for $T=660\,°\mathrm{C}$	[161]
Thermal conductivity in W m^{-1} K^{-1}	$k=T/15+200$	up to $T=660\,°\mathrm{C}$	[161]
Emissivity and Absorptivity	$\epsilon_\mathrm{S}=0.14$	with $\alpha_\mathrm{S}/\epsilon_\mathrm{S}=2.5$	[149, 162]

Table 5.1: Material properties for 99.8 % purity aluminium.

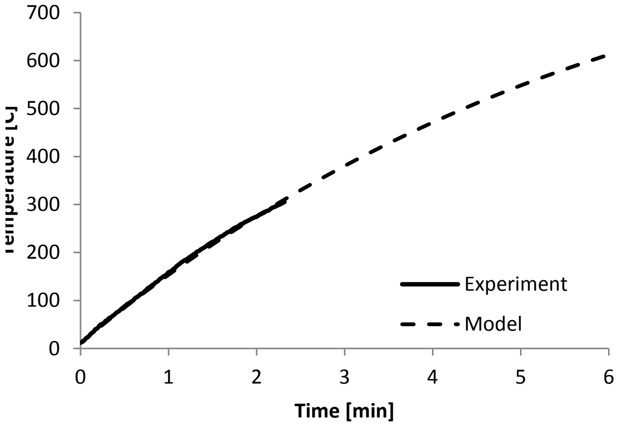

Figure 5.3: Comparison of experimental and modelled temperature response of a 10 mm aluminium substrate exposed to 116 kW m^{-2} heat flux.

ester, epoxy, phenolic) and reinforcement (glass, carbon, aramid) from which it is possible to account for most common fibre-reinforced composite materials.

Temperature-dependent Material Properties

The rule-of-mixture approach is widely used to calculate material properties of multi-component structures. PML exhibits overall material properties arising from the partial contribution of its constituents, metal foil and resin. Thus, effective properties such as PML density ρ_{eff} and specific heat capacity $c_{P,eff}$ can be evaluated using

$$\rho_{eff} = \varphi \rho_{epoxy} + (1-\varphi)\, \rho_{alu} \tag{5.10}$$

$$c_{P,eff} = \frac{\varphi c_{p,epoxy} \rho_{epoxy} + (1-\varphi)\, c_{p,al} \rho_{al}}{\rho_{eff}} \tag{5.11}$$

It is essential for the accurate prediction of a material's thermal response to heat exposure to use the correct material property values as thermal conductivity k_{PML} and specific heat capacity $c_{p,eff}$ are not independent of temperature. Through various experimental methods as described in chapter 4 these properties have been established at certain temperatures from ambient temperatures up to the point when resin decomposition starts. During the simulation the variables are implemented as functions of temperature, based on the experimental points or the rule-of-mixture technique stored within the program and linear interpolation between these points.

Thermal Degradation of Resin

With the onset of polymer decomposition during extended heat exposure, the constantly changing resin composition and the amount of absorbed or generated heat from the degradation process influences the heat transfer through the material. In order to account for these effects the governing FD heat conduction equation has to be extended to be in the form of the Henderson equation (2.1) which offers a mathematical description of the decomposition process. Changes in resin density and therefore mass loss are determined via Arrhenius equation for which the kinetic parameters obtained from the thermogravimetric analysis in section 4.1.2 are used as input parameters. During a simulation run, an evaluation of the resin density and hence the element's effective density is made for every node at every time step in order to take into account changes due to resin degradation and related reaction heat.

Expansion of PML

Arising from the resin degradation is an effect that is essential for the fire protection principle within PML laminates. Due to the layered architecture of the laminates the gases that are produced when the resin is decomposing are trapped between the metal foils. This means that in fire scenarios the laminates are gradually expanding as the degradation progresses, this can be observed by the formation of blisters. Through various experiments, such as the cone calorimeter, the isothermal furnace and small-scale fire testing, the expansion behaviour of the samples has been evaluated. From these observations the PML expansion has been directly linked to the mass loss characteristics based on the production of decomposition gases. In the numerical model the expansion factor is calculated from the equation (4.28) in order to describe the increase of the thickness of a node over a set temperature range.

Melting of Metal Foils

As described before in section 4.3, aluminium foils will eventually melt when they are exposed to fire for a prolonged period of time. The effect of melting can be implemented into the model as a phase change as described in [160]. The amount of energy it takes to melt a certain quantity of aluminium can be expressed as a temperature difference that equals 309 K.

$$\Delta T_{\mathrm{m}} = \frac{H_{\mathrm{m}}}{c_{\mathrm{p}}} \tag{5.12}$$

with H_m denoting the latent heat for melting of aluminium and c_p the specific heat capacity. This means for the FD model that whenever a node reaches the melting point a further increase in temperature is arrested and the node is held at a constant temperature, see figure 5.4. During the following time steps the predicted temperature rise is calculated according to the governing equations and accumulated until the temperature difference ΔT_m is exceeded. Consequently, this node is then fully melted and its temperature will be set to the flame temperature.

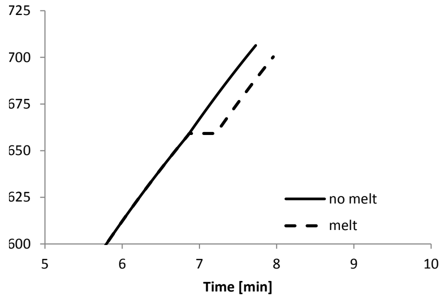

Figure 5.4: Effect of thermal delay due to melting effect in aluminium.

Non-melting Front Face

The developed PMLs consist in their basic structure of alternating layers of aluminium and epoxy resin. As mentioned before the temperatures in a fire scenario usually exceed 1000 °C. This highlights the disadavantage of using aluminium foils which have a melting point of only 660 °C and can therefore withstand the high temperatures for only a limited period of time. Hence, modified laminates have been developed where the front-facing aluminium foil has been substituted with another non-melting metal foil. Laminates modified with a stainless steel foil or titanium foil as a front face were made. The consequent changes which needed to be made to the PML_FIRE model are limited to the introduction of variable material properties for the front-facing layer element, depending on which material is present in the actual laminate. The properties implemented include thermal conductivity k, specific heat capacity c_{p}, density ρ, emissivity ϵ_{s} and absorptivity α_{s}.

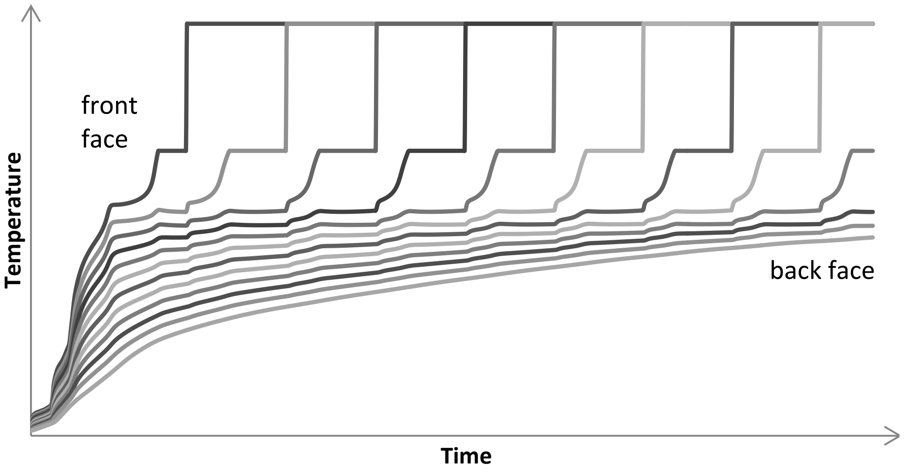

Figure 5.5: Schematic PML_FIRE model output depicting the temperature-time distribution for individual nodes within a specimen under influence of all three major thermal effects.

5.4 Output

One of the main outcomes of the model is the computation of the time-temperature profiles in the through-thickness direction of a specimen for a selected time period of heat exposure. Figure 5.5 displays a schematic example of such temperature distributions for chosen nodal points of a PML/Aluminium specimen. This was simulated using the most advanced version of the PML_FIRE model including the effects of polymer decomposition and consequent PML expansion, as well as metal foil melting. The consequences of these thermal effects are traceable in the calculated temperature profiles in comparison to conventional heat transfer simulations of polymer composite materials which display a continuous temperature increase during the transient stage before reaching stable conditions for long exposure times, as shown by Mouritz and Gibson [130].

After an initial inhibition time, the onset of decomposition leads to the formation of gas pockets within the PML which form sections with low-thermal conductivity properties. This results in the establishment of a thermal gradient within the specimen which is noticeable from the PML_FIRE generated temperature profiles as fanning out of individual nodal temperature curves and the consequent slower increase in the back face temperature in comparison with the heat exposed front face. At high temperatures when the aluminium melting point is reached the melt stage of the simulation starts abruptly resulting in a sharp halt in the temperature rise followed by the substitution of the nodal temperature with the temperature of the flaming environment.

Additional output from the PML_FIRE model includes the display of the remaining resin content RRC which is expressed as a ratio of the residual polymer content to the initial polymer content. It serves as an indicator of the rate of conversion as it shows the continuous decrease in polymer content with an ongoing decomposition reaction until only residual char is left which thus inversely acts as a gauge for the expansion status and overall fire protection efficacy. Independently, the nodal expansion factor calculated during the simulation run is recorded for similar reasons. Furthermore, the actual mass loss during every time step and for specified nodes is produced in order to monitor the smoothness of the decomposition reaction and to detect any occurring anomalies that may indicate computational errors or erroneous results.

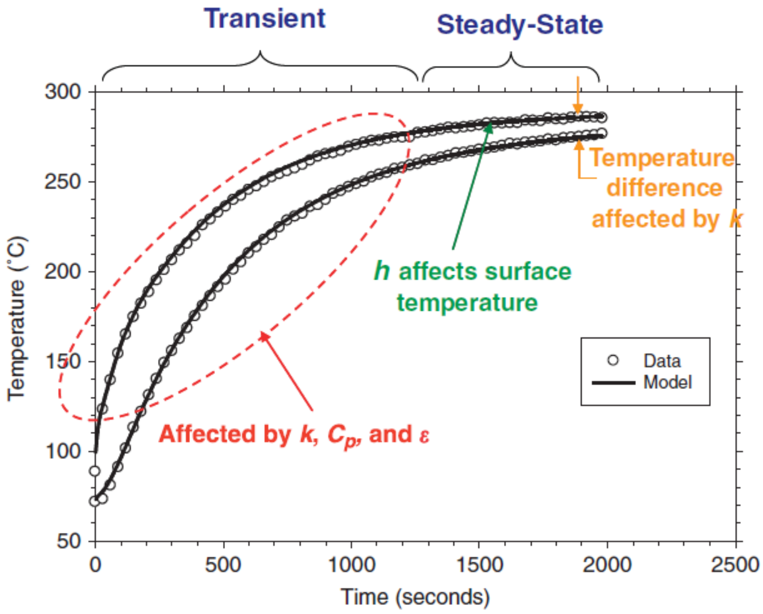

Figure 5.6: Influence of various material and process parameters onto the temperature evolution at different stages during the fire exposure of a fibre-reinforced composite laminate [165].

5.5 Sensitivity Analysis

Investigating the sensitivity of the PML_FIRE model to changes in external and intrinsic parameters aids the understanding of the behaviour of the simulation under various test conditions. The influence of the different thermal effects on the calculated temperature profiles and the model's sensitivity to changes in the scale and manner of the material's properties should be analysed. Through this it is possible to identify the importance of individual parameters as well as the incidence of any interacting or competing relationships that affect the outcome of the thermal predictions.

Few studies [163–166] have investigated the influence of multiple input parameters on the outcome of thermal modelling of fibre-reinforced composites under heat or fire exposure. Based on results from FD calculations as well as FE modelling, strong influences on the calculated temperature profiles are indentified in these studies as arising from changes in intrinsic material properties such as resin density ρ and thermal conductivity k as well as the activation energy E_a used to characterise the polymer decomposition reaction. Furthermore, these studies underline the importance of a detailed knowledge of the material's properties and in particular their temperature dependency as seen in examples of thermal conductivity k and specific heat c_p for which small variations in the actual property values can cause considerable uncertainties in the outcomes of the applied thermal models [163]. The study by Lattimer et al. [165] identified characteristic thermal properties which most affect the temperature evolution during different stages of the heat transfer process. In figure 5.6 the influence of parameters such as thermal conductivity, specific heat, heat transfer coefficient and emissivity on the transient and steady-state sections of a temperature profile are visualised.

5.5.1 Thermal Effects

As presented in previous sections, PML_FIRE is a thermal model based on a number of essential processes that have been identified during experimental observations as the main physical driving forces determining the overall fire performance of specimens during heat exposure. A starting point into a sensitivity analysis of the developed model is the examination of these various basic effects in

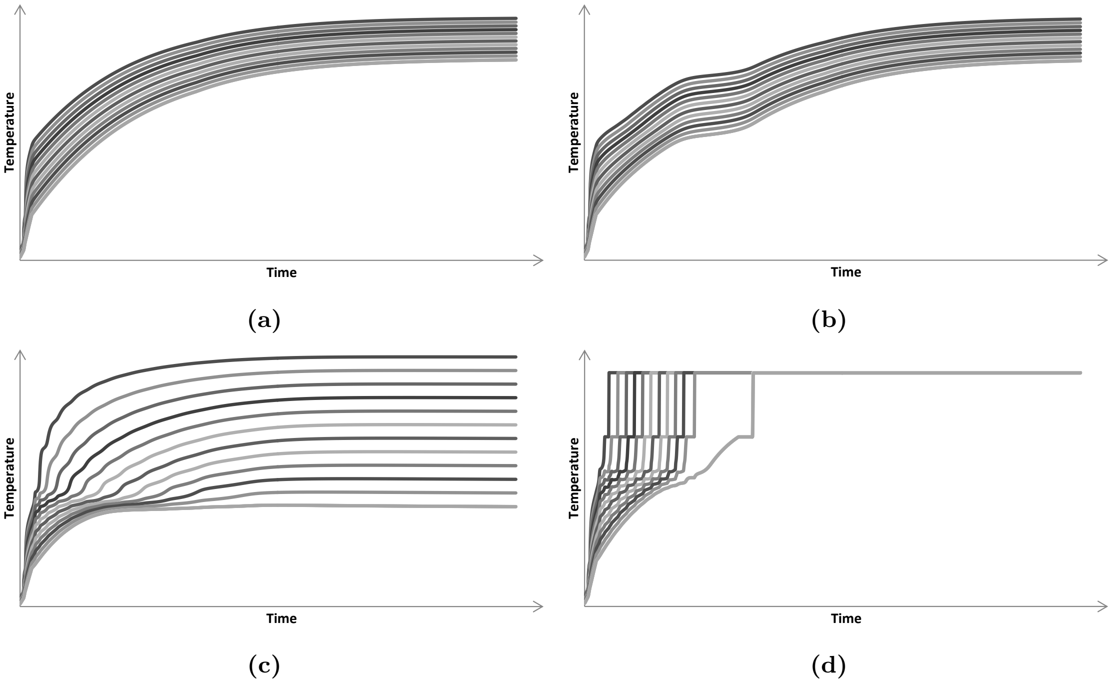

Figure 5.7: Influence of thermal effects (decomposition, expansion and melting) and combinations thereof on the temperature evolution in the through-thickness direction of a PML/Alu specimen: a) basic heat conduction, no thermal effects, b) heat conduction with decomposition, c) heat conduction with decomposition and laminate expansion, d) heat transfer including all three effects.

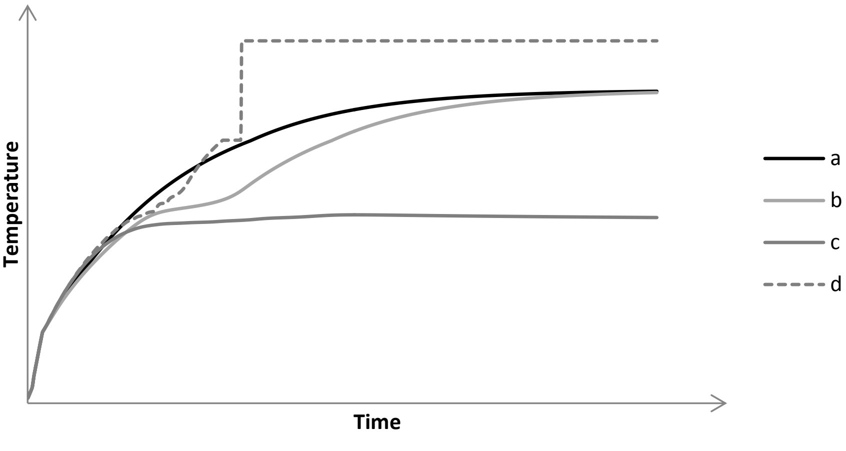

Figure 5.8: Schematic evolution of back face temperatures of a PML/Alu specimen: a) basic heat conduction, no thermal effects, b) heat conduction with decomposition, c) heat conduction with decomposition and laminate expansion, d) heat transfer including all three effects.

order to assess the consequences of the incorporation of the individual routines into the simulation, as well as the implications arising from a combination of these processes in comparison with a non-reactive material exhibiting only basic heat conduction properties. Figures 5.7 and 5.8 show the simulated results of such analysis for a PML/Aluminium specimen subjected to various test cases. In figure 5.7 complete specimen temperature profiles of individual test cases are displayed whereas figure 5.8 illustrates a comparison of specimen back face temperatures for all simulated tests cases, as this is one of the main aspects in fire design engineering.

The reference case is represented by a non-reactive material exhibiting the same constant room temperature properties, k, c_p and ρ, as a real PML/Aluminium specimen thus acting passively during the heat conduction process the specimen is subjected to under the given boundary conditions. From the resulting temperature profile shown in figure 5.7a it can be seen that temperatures continue to increase during the transient period of heat transfer before stable steady-state conditions are reached at long exposure times with a constant temperature gradient in the through-thickness of the specimen.

Any of the thermal effects additionally introduced into the simulation, like decomposition, expansion and melting impose a deviation from the reference behaviour, see figures 5.7b to 5.7d.

The process of decomposition is assumed to have significant consequences on the results of the computation as the material undergoes major changes during the physical process of decomposition which then needs to be reflected in the variation of the material property values during a simulation run. The resulting temperature profile (figure 5.7b), however, shows only small difference compared to the temperature increase of the reference curve (figure 5.7a) after temperatures for the onset of decomposition are exceeded, before a small retardation effect in the nodal temperature curves is observed when the decomposition reaction is completed. The effect only appears slight, particularly, when compared with the effects seen in fibre-reinforced polymers where a minimum of 35 % of the specimen volume is of degradable origin, whereas in the present specimens only 6 % are of polymeric origin.

Adding the routine of specimen expansion to the previous test case is a logical consequence arising from the physical degradation process during which decomposition gases are released as by-products together with the effect of expansion which is the most important design principle of the PML fire protection effect. After temperatures for the onset of decomposition are reached a drastic change in behaviour of the nodal temperature curves can be observed in comparison to the previous test case results, with a steep temperature gradient being predicted to occur. Every polymeric layer, in its degraded state is filled with decomposition gases, which creates a thermal barrier that exhibits very low thermal transport properties contributing to a developing thermal gradient. As a consequence, the specimen's back face temperature curve exhibits almost no further increase after decomposition has been initiated in the layers at the front and remains at a low temperature level in comparison to the previous two test cases.

As with the physical effect and subsequent experimental observations, adding a routine to the PML_FIRE program describing the melting of the metal foils has a significant effect on the predicted temperature distribution. The underlying layers experience a sudden temperature increase after the melting process of the previous node is completed because of the direct exposure to the flame temperature and thus induces cyclical repetition in the neighbouring nodes. This behaviour is disadvantageous because it interferes with or suppresses the process of retaining the decomposition gases and therefore inhibits the insulating effect. Furthermore, if the simulation time is set long enough the melting effect could hypothetically be observed within the aluminium substrate material as well.

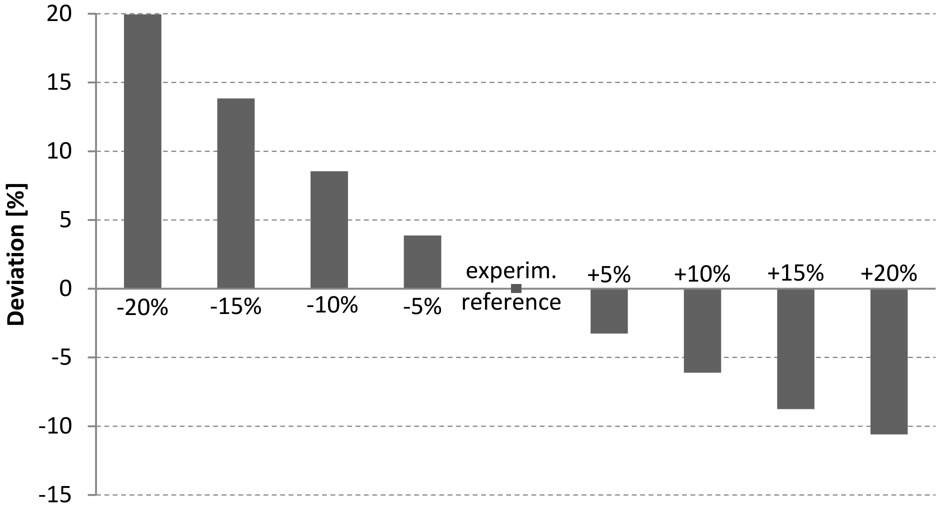

Figure 5.9: Change in parameter T600 due to perturbations of thermal conductivity. Deviation given as relative percentage based on the results obtained for T600 via experimental values for thermal conductivity.

5.5.2 Parametric Study of Material Properties

A parametric study of PML_FIRE on major input variables has been conducted in order to test the sensitivity and the accuracy of selected input parameters and to investigate their effect on the simulated temperature distribution. For that purpose, a parameter $T600$ measuring the time until a temperature of 600 °C at the back face of a specimen is reached has been introduced during the parametric study. This allows a comparison of an infinite number of simulations exhibiting differences in their calculated temperature evolution due to relative changes in input variables. The effect of a number of parameter perturbations is summarised in figures 5.9 and 5.10 for the input parameters of PML thermal conductivity and the overall PML expansion factor. A positive deviation on the vertical axis indicates an increased time period until a temperature of 600 °C is reached, whereas a negative deviation indicates that 600 °C is reached at an earlier time than the reference simulation, which is entirely based on experimental values and properties.

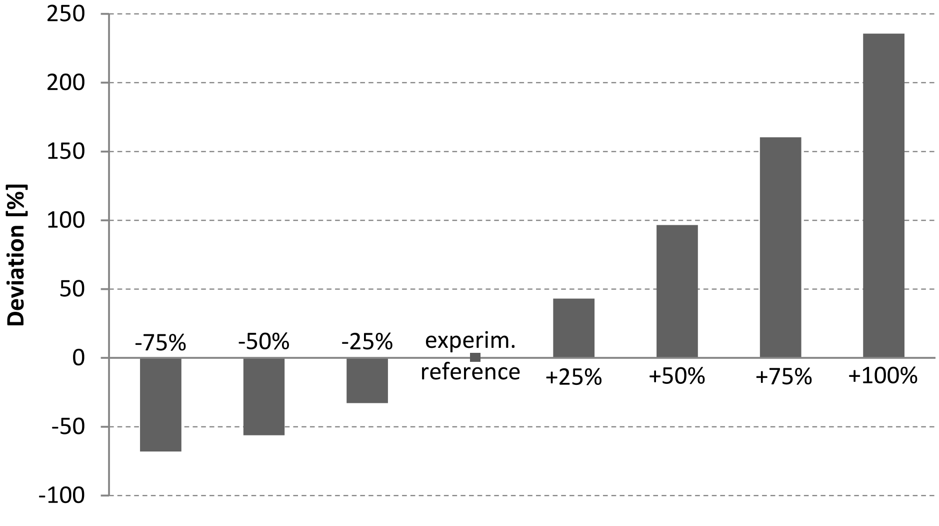

Figure 5.10: Change in parameter T600 due to perturbations of the overall PML expansion factor. Deviation given as relative percentage based on the results obtained for T600 via experimental values for laminate expansion behaviour.

With a widely acknowledged range of ± 10 % for the accuracy of experimentally determined

Polymer	E_a $\left[\mathrm{kJ\,mol^{-1}}\right]$	A $\left[\mathrm{s^{-1}}\right]$	Reference
Epoxy[1]	117	2.16e+6	[167]
Epoxy[2]	182	9.67e+10	[73]
Phenolic[3]	163	4.62e+4	[168]
Phenolic[4]	218	1.30e+16	[169]
Polyester	128	4.00e+8	[170]
Polypropylene	299	8.71e+18	[71]
PEEK	222	1.10e+13	[171, 172]

Table 5.2: Kinetic parameters of various polymers used during the sensitivity analysis.

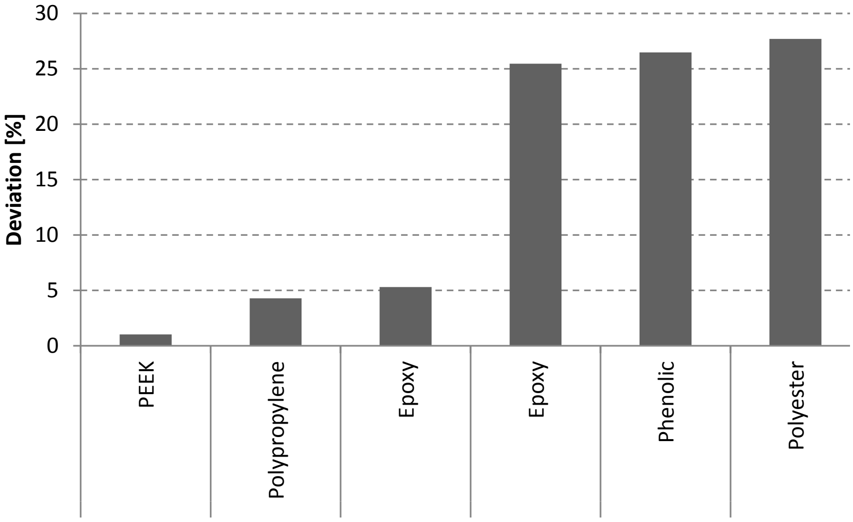

Figure 5.11: Change in parameter T600 through variation of polymer activation energy of decomposition reaction. Deviation given as relative percentage based on T600 results of standard PML specimens containing PRF epoxy resin.

variables, these figures clearly show the significant influence variations in thermal conductivity k and expansion factor β have on T600 for the individual test cases. For thermal conductivity, this means an indirect translation of any variation in input value into a change of the T600 parameter. For the expansion parameter, a pronounced direct dependency of the calculated time values on the actual expansion factor can be observed albeit of non-linear behaviour. The analysis shows that an under- or overestimation of these two input parameters can lead to a considerable variation of the simulation outcome in comparison to experimental results. It emphasizes the importance of experimental accuracy and careful execution of subsequent experiments to limit possible model output errors due to inaccuracies in input properties.

Further changes to input parameters such as resin specific heat c_p and activation energy E_a are observed to have only a minor influence compared with the aforementioned parameters k and β. Although identified in those studies [163–166] as influential to the outcome of the thermal simulations the discrepancy arises from the type of specimen investigated. Whereas these studies investigated the behaviour of fibre-reinforced polymeric composites with a minimum of 35 % polymeric content, during the parametric study of PML_FIRE those parameters characterise properties of the resin constituent the contribution of which, to the overall PML properties, is low according to rule-of-mixtures. Therefore, applied to PML such great parameter influence is not observed as only 6 % of a PML material is actually of polymeric origin. This leads to observations that perturbations of

---

[1] Araldite epoxy resin LY5052 and hardener HY5052
[2] Toray 3900 epoxy resin
[3] Resitan IP502 novolac-type phenolic resin
[4] Fiberite MXBE-350 phenolic resin

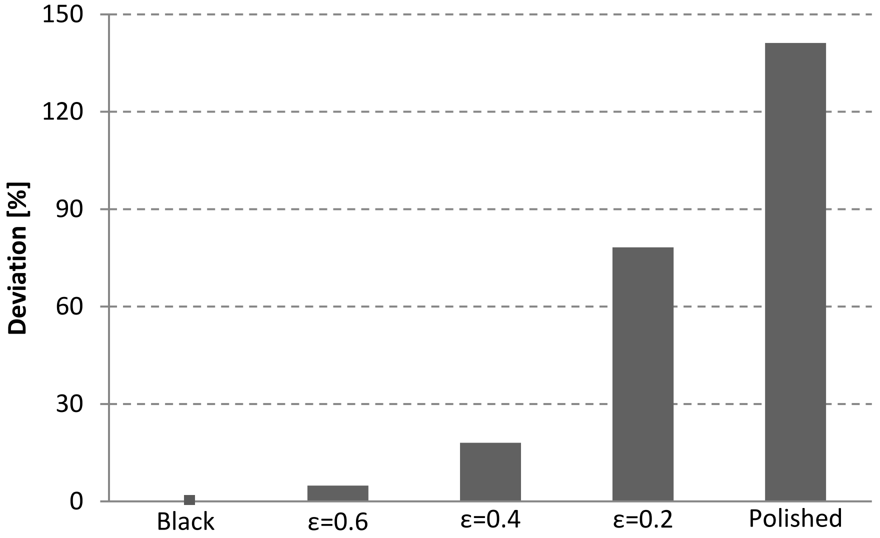

Figure 5.12: Change in parameter T600 through variation of surface emissivity. Deviation given as relative percentage based on T600 results of a blackened specimen surface.

up to ± 20 % to the specific heat capacity of the resin used within a PML would only lead to a variation in T600 of under 5 %. Only drastic changes, such as the assumption of the entire nodes exhibiting only polymeric character, would lead to significant changes in the thermal outcome.

An investigation of the dependency of the kinetic parameters activation energy E_a and rate constant A has been carried out with the prerequisite of substituting the current parameter set with values published in literature for a variety of different polymeric materials used as matrix constituents for fibre-reinforced composite materials. These include epoxies, phenolics, PEEK, polyester and polypropylene [71, 73, 167–172], see table 5.2 for details. The results of the analysis show a low sensitivity of the PML_FIRE model to changes in the rate constant which covered a range of 15 orders of magnitude whereas changes to the parameter of activation energy, ranging from $100\,\mathrm{kJ\,mol^{-1}}$ to $300\,\mathrm{kJ\,mol^{-1}}$, seemed more critical, which is in accordance with the literature studies outined for example by Ramroth et al. [164]. No clear indication of a trend with a variation in activation energy is observed, however, a strong dependency with a deviation up to almost 30 % for T600 for the different material types is noticeable, see figure 5.11. From a physical point of view, the lower activation energy would be favourable with regard to the PML protection efficacy as it would result in the decomposition reaction being initiated earlier, leading to the formation of the thermal gradient at earlier times, in comparison with the reference case with higher activation energy thus elongating the delay of the heat transfer resulting in a slower rise of the specimen back face temperature which could be observed.

One important point is, the conducted parametric study does not reflect the true behaviour of PML manufactured from different resin types as only the kinetic parameters have been varied according to the material simulated. For a realistic simulation of the effect of using different resin types within PML, further changes to other intrinsic material properties such as thermal conductivity k, specific heat c_p, density ρ and swelling capacity β would have to be introduced to the model.

One parameter that determines transmission of heat into the specimen is the property of surface emissivity which is used to define the boundary conditions within the simulation. Depending on the appearance and conditioning of the specimen's front face, the emissivity value needs to be adjusted. During the experimental as well as model analysis two ends of the emissivity spectrum have been considered: on one hand a black painted sample surface promoting maximum heat transfer into the specimen as the reference sample, and on the other hand a polished metal surface of the aluminium with high reflectivity so that only a small portion of the incoming heat is actually transmitted into the specimen. The results shown in figure 5.12 reflect these assumptions wherein strong non-linear behaviour is observed. A continued decrease in the emissivity parameter leads to a positive deviation in the T600 parameter indicating a delay in heat transfer due to a reduced surface transmission with lower emissivity values.

This effect has been experimentally witnessed under different boundary conditions than those assumed during the parametric study. However, the effect of surface preparation on the temperature profiles for the back faces of specimens featuring PML is clearly noticeable, see figure 5.13. Specimens with a pristine metal surface experience much slower temperature increases compared to samples featuring a black painted front face.

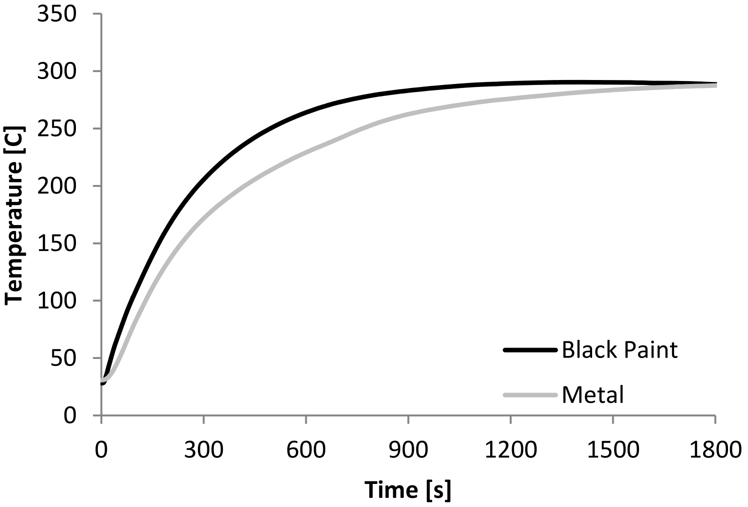

Figure 5.13: Temperature evolution of the rear face for two specimens with different surface emissivities: black paint and pristine metal.

Chapter 6

Fire Performance of Polymer-Metal Laminates

Small-scale fire testing is used for the assessment of the fire protection efficacy of PML materials. It offers an inexpensive and quick option with regard to sample preparation and test operation compared to other widely used fire tests, such as the full-scale furnace test, whilst allowing for a prompt evaluation of the heat transfer and flame resistance characteristics of unprotected and PML protected substrates. The results of a number of fire tests carried out are presented in order to gain an in-depth knowledge of the material's behaviour under heat exposure. Various combinations of external parameters, of energy input and heat source, and material selection contribute to a thorough analysis covering a broad range of fire scenarios. Furthermore, the results of these fire tests are used to validate the development of the PML_FIRE model.

6.1 Experimental

6.1.1 Small-scale Fire Testing

A conventional small-scale Bullfinch burner connected to a propane gas tank provides regulated gas flow at a constant level [173, 174]. The specimen is held upright by a steel picture frame at a specified distance from the burner so that the burner flame strikes the sample surface perpendicular to the flame direction as shown in figure 6.1. The sample has insulation around the edges to avoid

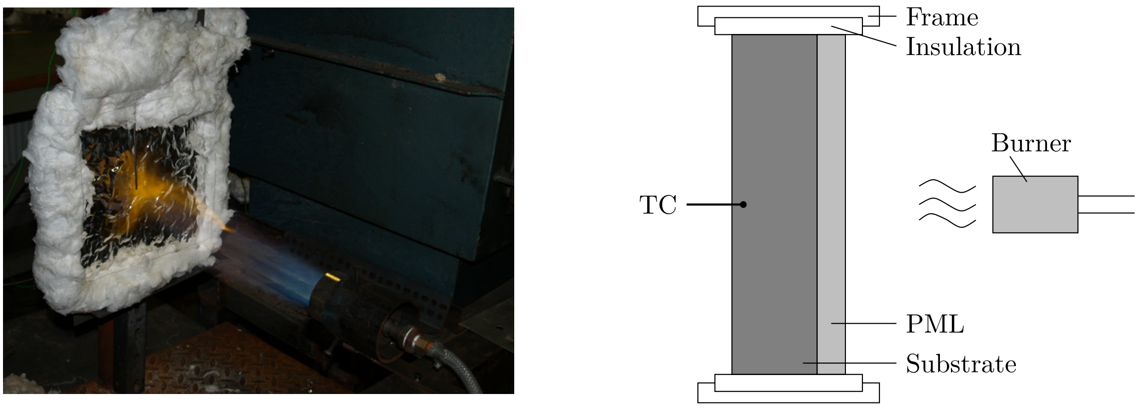

(a) Experimental installation

(b) Test schematic

Figure 6.1: Setup of small-scale burner test experiments for specimens in vertical orientation.

heat loss. The specimen's back face is left uncovered to allow for free heat transfer from convection and radiation at the so-called *cold face* of the sample.

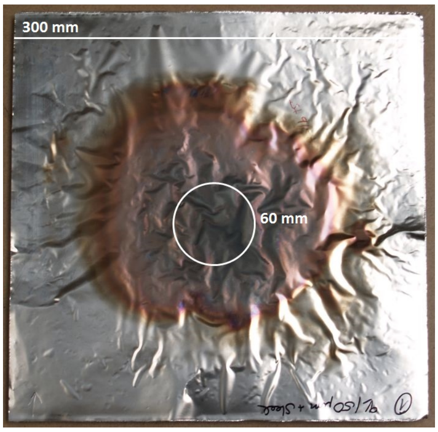

Figure 6.2: Heat affected area (dark coloured region) greatly outsizes actual burner diameter (white circle).

With a burner cross section of 60 mm diameter, a conventional sample size of $100 \times 100\,\mathrm{mm}^2$ that is typically used in small-scale fire testing, would be sufficient for this type of burner test. However, due to the swelling behaviour of PML which is not limited to the area directly impacted by the burner flame, see figure 6.2, specimens of size $300 \times 300\,\mathrm{mm}^2$ were also tested in order to capture the full extent of PML expansion caused by the accumulation of the decomposition gases. This is to avoid adverse effects as seen with samples of smaller dimensions where a splitting of the laminates can occur leading to a partial release of the decomposition gases and thus reducing the fire protection effect.

The flame produces a combustion zone at the front of the specimen which can be characterised through its field temperature. The incoming heat flux as indicated by the field temperature is monitored by type-K thermocouples at the front of the sample to check consistency and record any anomalies. On the back face of the sample additional thermocouples record the temperature rise which is essential to assess the specimen's thermal performance. Furthermore, the back face temperature indicates the risk of heat dissipating into the environment and the potential for ignition of adjacent structures which in turn is a major safety concern when it comes to the safe structural life time of the whole structure or section of it and the consequent effects on evacuation strategies. These fire tests were mainly carried out at a heat flux of $116\,\mathrm{kW\,m^{-2}}$ which is in accordance with ISO-2685 [175] and a standard regulation used by the areonautical industry to assess the fire resistance of materials. However, the heat flux parameter is continuously adjustable so that it is possible to simulate fire scenarios of much higher intensity or much less severity.

A comparison of the cold face temperature profiles measured during the fire testing and the results obtained via the PML_FIRE model allows the validation and necessary adjustment of the fire performance model.

6.1.2 Burner Calibration

The field temperature is one possible way of characterising the severity of the flame during the small-scale fire testing. However, a more controlled option is to perform the burner test at constant heat flux level, with heat flux defined as the amount of thermal energy penetrating a specific area. It offers advantages over simple temperature-controlled tests in that it accounts not only for the radiative contribution of the flame which is sensed by thermocouples but also for the convective element. This is necessary because the propane burner used in the testing produces a flame of high velocity with the convective characteristics becoming more dominant towards higher heat flux levels. Additionally, any energy feedback from the material into the combustion zone as a result of ignition and endothermic reactions would impair the field temperature measurements, distorting the level of adjustments necessary to maintain constant heat flux.

The two major parameters influencing the detectable field temperature and thus the heat flux at the specimen surface during the burner test are the propane gas pressure and the distance between specimen front and burner itself. Increasing the gas pressure results in higher heat flux whereas a greater distance lowers the heat flux.

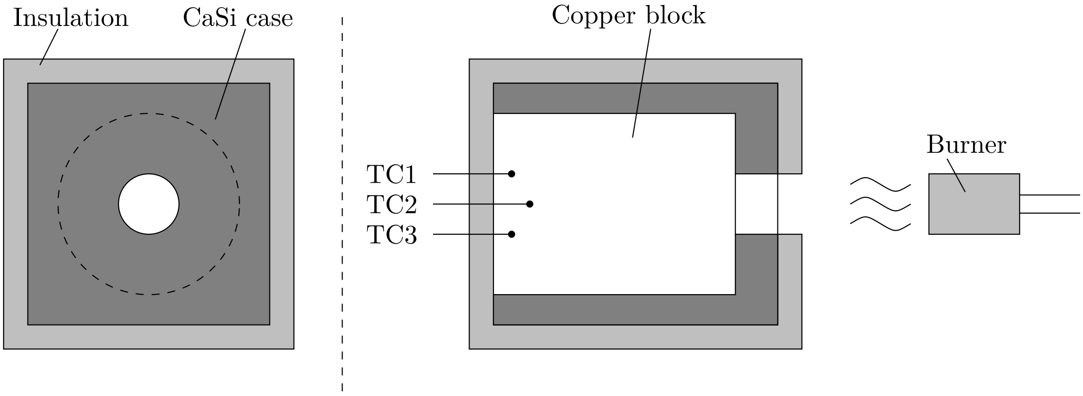

Figure 6.3: Front and cross section view of the copper block heat flux meter used during calibration experiments of the propane burner.

For purely radiative heat transfer conditions, such as those present in cone calorimeter testing, calibration devices like the Schmidt-Boelter meter are commercially available. Due to the much higher ferocity of the actual burner flame in this small-scale test, a calibration method previously devised within this research group provides a more robust apparatus that tolerates radiative and convective heat transfer up to high flux levels.

Due to its high thermal conductivity and its known thermal properties, copper is particularly suitable for use as the sensing material in a heat flux meter. A copper block encased in a ceramic insulation board, save for a small surface area, which is additionally wrapped in ceramic fibre blanket for further insulation, is used during the calibration procedure. During the exposure of the copper block's front face to the burner flame, the temperature rise of the copper, for various test conditions with variable gas pressure and burner-specimen distances, is recorded by thermocouples inserted at different depths at the back of the block. These are indicated as *TC1* to *TC3* in figure 6.3 which depicts the principle test setup for burner heat flux calibration.

The determination of the incident heat flux is based on a principle evaluation of the thermal potential of the copper block in comparison with any occurring thermal losses. Although the heat flux meter is well insulated, heat losses can occur through radiation from the exposed front face and convection between the unexposed copper block surfaces and the insulation layer due to a small air gap. A detailed description of the methodology and the analysis of the different effects are given in the work by Browne [176]. From there it follows that the incident heat flux q is calculated according to

$$q = \frac{Q}{A_{surf}} = \frac{(mc_p)_{cu}\frac{dT}{dt} + A_{surf}\epsilon_{cu}\sigma\left(T_{cu}^4 - T_{amb}^4\right) + A_{ins}h\left(T_{cu} - T_{amb}\right)}{\alpha A_{surf}} \tag{6.1}$$

where Q is the thermal energy input,
m is the copper block mass,
c_p is the specific heat,
dT/dt is the rate of temperature rise,
A_{surf} is the exposed surface area,
ϵ is the emissivity of the block,
σ is the Stefan-Boltzmann constant,
A_{ins} is the unexposed surface area of the meter,
h is the heat transfer coefficient,
T_{cu} and T_{amb} are the instantaneous meter and ambient temperature respectively,
T_{amb} is the ambient temperature,
α is the copper block absorptivity.

Figure 6.4 shows the resultant calibration curve for the propane gas burner which is used as

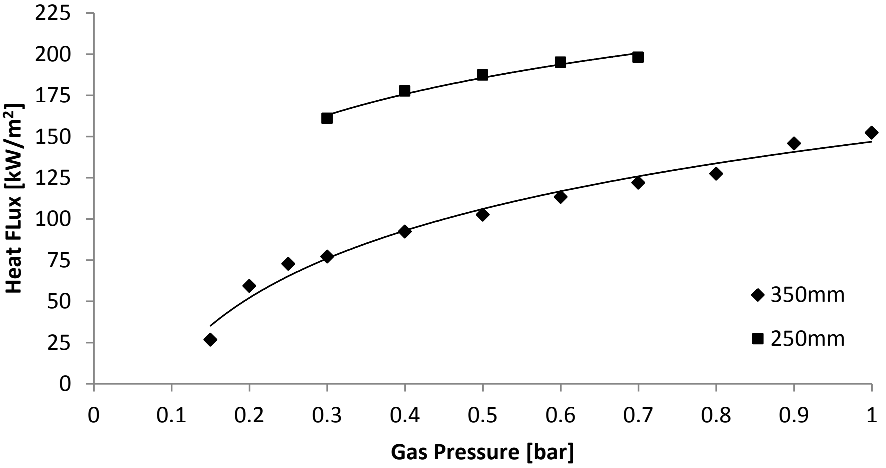

Figure 6.4: Calibration curve of the propane burner used during small-scale fire testing.

the standard reference curve during the small-scale fire testing. The correct heat flux level up to 200 kW m^{-2} can be achieved for individual testing conditions through a combination of different gas pressures and burner-to-sample distances. It is noticeable that at very low gas pressures below 0.2 bar the flame temperature is not stable and therefore the flux meter underestimates the true heat flux. To correct this, the test should be carried out with a greater burner-to-sample distance but with a higher gas pressure in order to achieve a stable heat flux.

6.1.3 Cone Calorimeter Testing

The fire reaction properties of the newly developed thermal barriers are measured according to ISO-5660 using a Fire Testing Technology cone calorimeter. The 100 × 100 mm^2 specimens are positioned in a steel edged frame, horizontally orientated and exposed to a radiant heat flux of 70 kW m^{-2}. Testing the PML on its own or bonded onto a metal substrate does not yield any meaningful results with regard to the fire reaction properties as the amount of combustible material within these specimens is too small to create a signal greater than the general signal noise. Therefore, the PML has to be bonded onto various flammable substrate materials including 2 mm unidirectional carbon epoxy composite (CFRP) of type MTM44-1 supplied by Cytec as well as 2.5 mm Glass Laminate Aluminium Reinforced Epoxy (GLARE) of type G3-5/4-0.4 supplied by University of Delft.

6.2 Substrate Response

As a starting point for the model validation, accurate modelling of the temperature distribution within a specimen substrate is necessary before the correct assessment of the heat transfer through the PML can be calculated by the simulation in a later stage. Aluminium is a non-combustible, inert material so that the heat transfer calculations include only heat conduction as the mode of heat transfer through the substrate, there will be no other thermal effects. Convection and radiation are considered as boundary conditions for both the hot and cold face of the specimen when modelling the thermal behaviour observed during fire testing.

Due to its very high thermal conductivity, the aluminium substrates experience a rapid rise in temperature over a short period of time when exposed to heat, this has been confirmed in fire tests of 10 mm aluminium slabs of type 5083. The recorded back face temperatures of specimens during these tests are presented in figure 6.5 showing the temperature response characteristics for

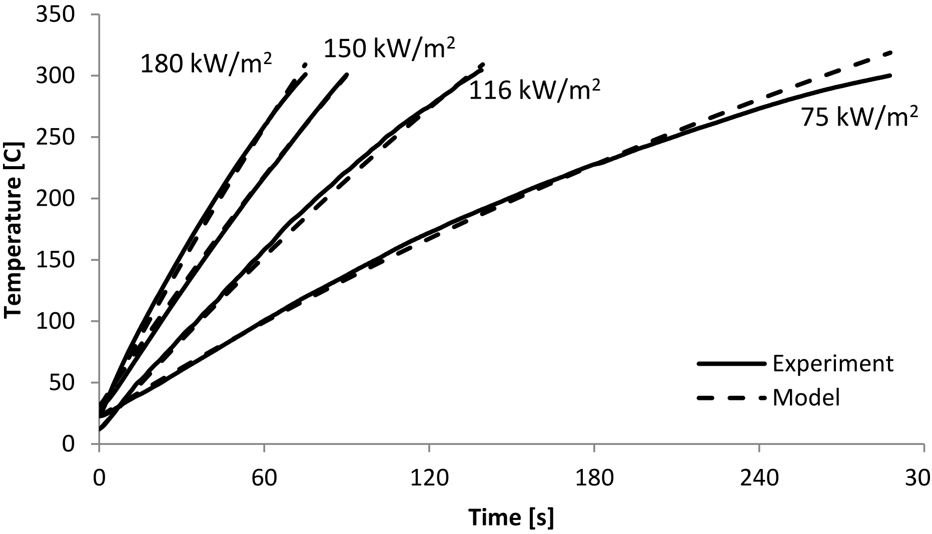

Figure 6.5: Rear face temperature profiles for an aluminium 5083 specimen in fire scenarios of different heat flux levels. The severity of the flame decreases from left to right. Modelled temperature curves are also included for these test cases.

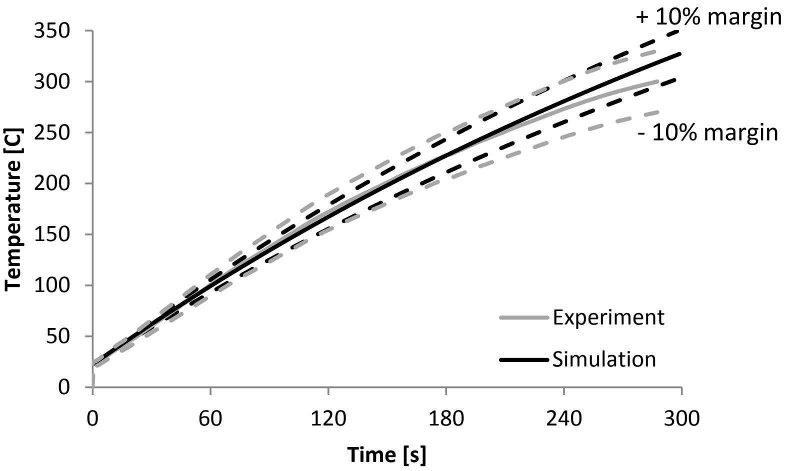

Figure 6.6: Effect of ± 10 % variation in experimental readings (grey curves) as well as in the heat flux input parameter for the PML_FIRE model (black curves).

various heat fluxes. For this short exposure time transient heat transfer is dominant with steadily increasing temperatures occurring. In case of high incident heat flux levels, the temperature rise is almost linear whereas for the lowest heat flux tested a clear deceleration of the heating rate towards the end of test is observed. This is an indicator of the onset of the transition from transient heat transfer to steady-state conditions which for prolonged test durations would result in a decline of the temperature increase as thermal equilibrium is neared and, subsequently, an even temperature distribution throughout the sample is achieved.

It is noticeable that even for the low heat flux of 75 kW m^{-2} the back face temperature reaches a critical level of 150 °C and above within a short period of time, which occurs at even shorter times at higher heat fluxes, see figure 6.5. At theses temperatures softening of the metal occurs which leads to a significant reduction of the material's load-bearing capacity. The rapid loss of the mechanical strength of the aluminium makes it a very temperature-sensitive material which necessitates the application of thermal insulation to prolong safe structural integrity.

The modelling results of these temperature profiles are included in figure 6.5, and it will be observed that a close fit with the experimental temperature readings is achieved. Only in the

$75\,\mathrm{kW\,m^{-2}}$ test does a slight discrepancy between the experimental and the modelled curve appear in results at high temperatures above 250 °C where the slope of the temperature profile decreases. However, the resulting temperature profiles still falls within a 10 % error margin of each other as indicated by the paired solid and dashed lines in figure 6.6.

6.3 Aluminium-based PML

Polymer-metal laminates are designed to provide thermal protection for temperature-sensitive substrate materials in structurally critical applications. The basic PML material is comprised of alternating aluminium and epoxy resin layers in various sample architectures.

Upon fire exposure blisters emerge at the front face of the PML due to decomposition gases evolving from the underlying epoxy interlayers after a short inhibition time from heat being conducted into the material. Since in all the performed tests the flame temperature has exceeded the aluminium melting point, the top metal layer of the PML can only withstand this for a short time period before foil melting occurs which leads to ignition of the decomposition gases that are retained within the formed blisters. The fire performance of PML materials is characterised by this continuous cycle of resin decomposition, blister formation and subsequent exposure of underlying layers due to the melting of the top foils which is accompanied by gas ignition. A sequence of pictures presented in figure 6.7 shows the different stages the basic PML material undergoes when exposed to severe heat. The PML expansion in form of individual blisters as well as the melting damage is clearly visible.

Influence of Number of Layers

The comparison of back face temperatures recorded during the fire testing of uncovered 10 mm thick aluminium substrates and same-type specimens covered with PML is shown in figure 6.8. The effect of thermal insulation that PML materials provide, despite being prone to a destructive appearance, is evident from the temperature difference between unprotected and protected specimens which results in a significant time delay for the PML-covered specimens, before the aluminium substrates reach a temperature at which they will begin to soften and loose structural integrity. Initially, the temperature profiles of all samples exhibit a similar heating rate until decomposition of the polymer within PML is initiated. The rate of temperature increase in PML-covered substrates is retarded as the formation of the thermal barrier occurs, i.e. the expansion of PML greatly slows down the heat conduction with ongoing test duration. In case of a $116\,\mathrm{kW\,m^{-2}}$ heat flux test, it is observed that a minimum temperature reduction of 50 % at three minutes can be achieved for specimens featuring PMLs which means that it takes twice as long to reach the same temperature levels as in unprotected aluminium substrates, leading to prolonged structural life and potential increase in safety time of a factor of two. Increasing the foil number from 10 layers to 20 layers further enhances the insulation effect caused by PML materials. The reason lies with the additional amount of epoxy resin present within the PML which is available for decomposition thus additionally contributing to a further slowing down of the heat transfer across the thermal barrier, see figure 6.9.

Influence of Layer Thickness

The influence that the PML metal foil thickness imposes on the characteristic of the thermal protection effect is not as clear as theoretically anticipated. The high conductivity of the aluminium might cause adverse reactions which can only be explained in conjunction with other factors such as layer numbers.

Increasing the foil thickness from 30 µm to 50 µm appears to have a positive effect on the temperature reduction for 10-layer PML. The thicker foil provides a greater amount of physical

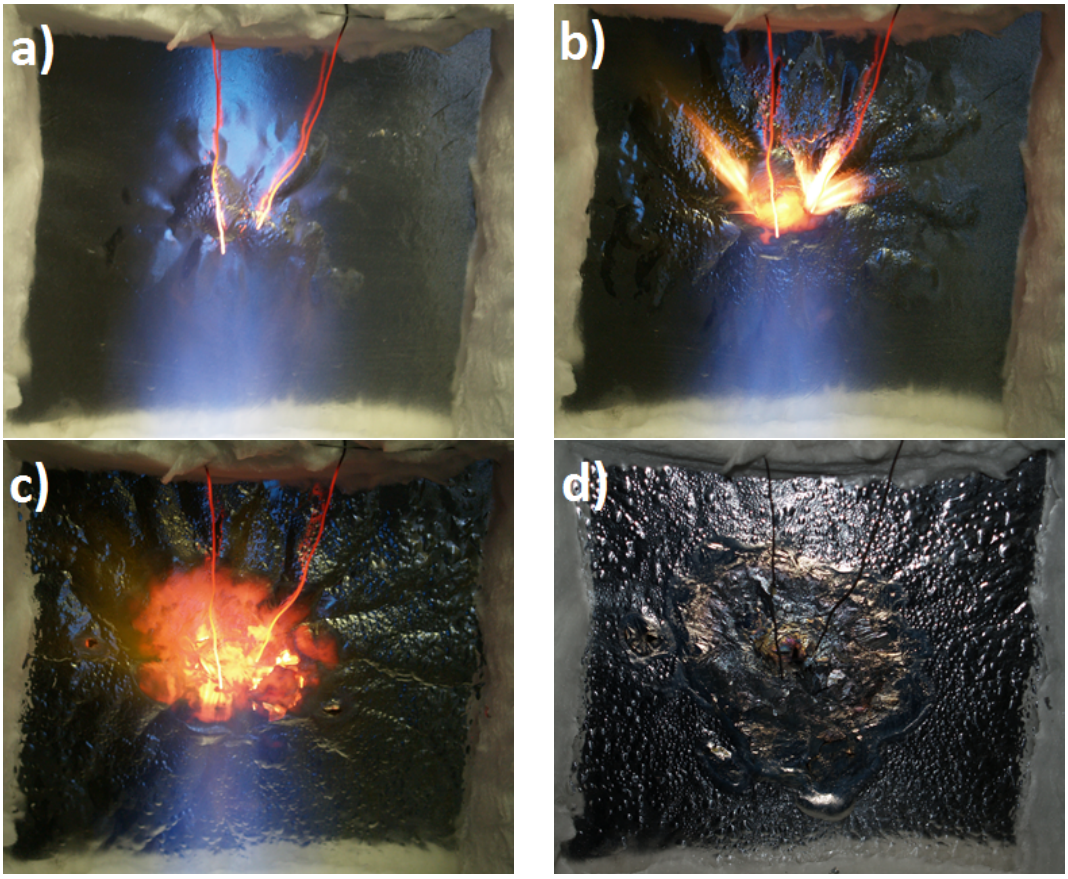

Figure 6.7: Principal fire reaction of PML-covered specimens exposed to 116 kW m^{-2} heat flux. With ongoing test duration not only is heat conducted in the through-thickness direction of a specimen, lateral spread of the affected heat zone beyond the incident flame radius also occurs due to flame buoyancy and high thermal conductivity of the metal foils. Photographs of a 10L/50μm PML specimen are captured at exposure times of a) 110 s, b) 150 s, c) 255 s and d) after the end of test after 335 s.

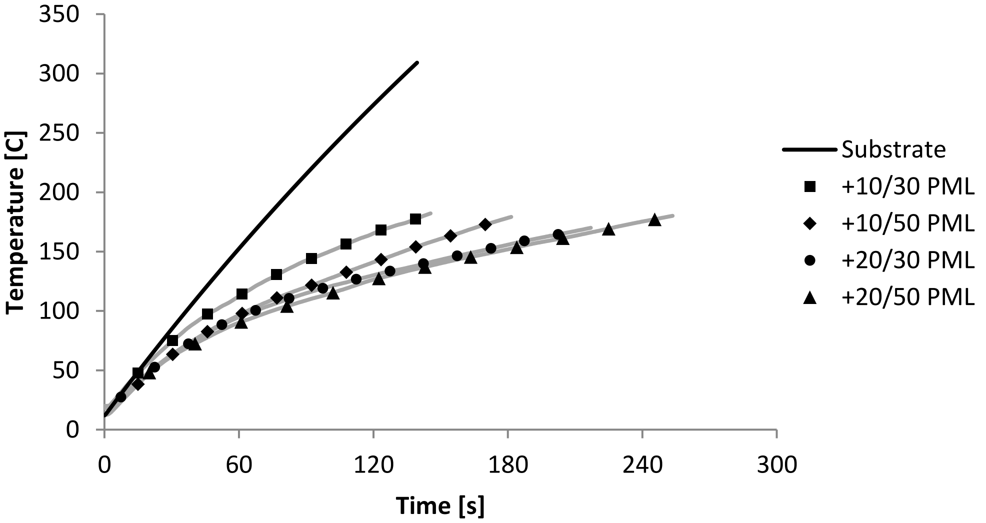

Figure 6.8: Temperature profiles for aluminium substrates with and without PML insulation tested at 116 kW m^{-2} heat flux.

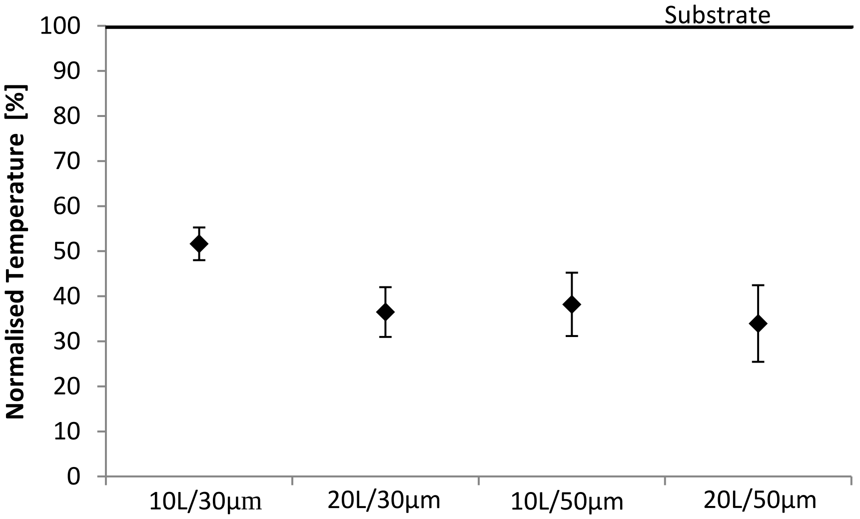

Figure 6.9: Reduction in temperatures in comparison to uncovered substrate, captured at 3 min of fire testing at 116 kW m^{-2} heat flux.

mass which absorbs more energy during the heating up to the same temperature levels as the 30 µm PML as well as higher energy absorption during the actual melting process. This absorbed energy is consequently absent from the heat transfer through the material and therefore contributes to a lower substrate back face temperature. Furthermore, the melting process itself is prolonged which proves advantageous in so far as it most likely provides sufficient time for the formation of the gas-filled blisters, whereas for 30 µm samples the decomposition process and the formation of gas pockets might be interrupted due to melting before the blisters are formed to their full extent which, in consequence, adversely affects thermal lag.

In 20-layer PML samples the effect of an increase in foil thickness on the temperature reduction is less pronounced. As the epoxy resin layer and the consequential decomposition process are the limiting factors for the heat transfer across the PML materials, because of the multiple epoxy layers present in a 20-layer PML, a slight delay in heat conduction through thicker metal foil might be assisted by the low thermal conductivity of the gas-filled layers.

6.4 Performance of Alu-PML in different Fire Scenarios

The influence of the magnitude of the incident heat fluxes on the behaviour of aluminium-based PML has been analysed. In addition to tests carried out at 116 kW m^{-2} heat flux as described in the previous sections, a smaller fire scenario is represented in burner tests performed at 75 kW m^{-2} as well as the imitation of much more severe fire conditions carried out at a heat flux of 150 kW m^{-2}. Some results of these fire exposure tests are compared in figure 6.10.

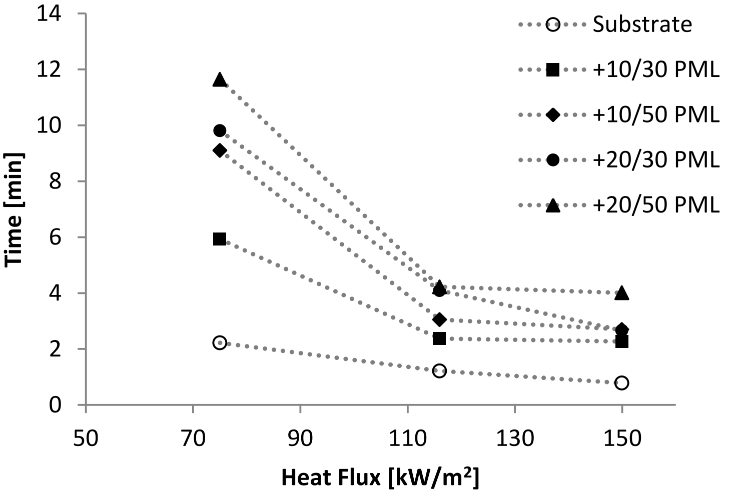

Figure 6.10: Comparison of time spans to reach 180 °C at the rear face of different PML/aluminium specimens obtained during fire tests with varied heat flux levels.

Overall, similar tendencies to tests with a 116 kW m^{-2} flame are observed in experiments with 75 kW m^{-2} and 150 kW m^{-2} heat flux levels. The aluminium substrates experience a fast temperature increase whatever the heating conditions, whereas PML-covered substrates exhibit a much slower rate of heating up due to the thermal barrier formed by the PML material. For all three tested heat flux levels, the 20L/50μm PML offers the best insulation potential of the four PML architectures tested. It is submitted that this is due to the greater number of polymer layers available for decomposition and the thicker metal foils that provide greater resistance against melting and thermal abrasion. In comparison, the 10L/30μm-type PML proves to be the least effective in slowing down the heat transfer resulting in higher specimen back face temperatures and this can most probably be attributed to the fact that this PML is the layer architecture with the least material present. Nevertheless, a 10L/30μm PML bonded to the metal substrate still greatly improves the temperature performance of structures in comparison to unprotected aluminium substrates that are exposed to the same fire conditions.

In case of the 75 kW m^{-2} heat flux tests, all types of PML barrier very effectively slow down the heat transfer into the substrate which is observed in the pronounced thermal lag of the temperature curves as shown in figure 6.11. A time delay in reaching structurally critical temperatures of up to a factor of six times in comparison with unprotected substrates is achieved in the best case scenario. With a radiant flame temperature equivalent of around 800 °C, these fire conditions cause less fire-induced damage to the PML front face. Only the areas directly impacted by the flame diameter are affected by the melting process and the convective character of the flame is also reduced. This allows the full formation and accumulation of decomposition gases between individual metal layers as individual foils provide greater resistance and therefore enhance the fire protection effect.

At 150 kW m^{-2} on the other hand, the burner flame is very turbulent with a highly abrasive character which causes considerable and non-uniform fire damage at the sample front due to melting and ablation similar to the observations made in 116 kW m^{-2} testing. The individual

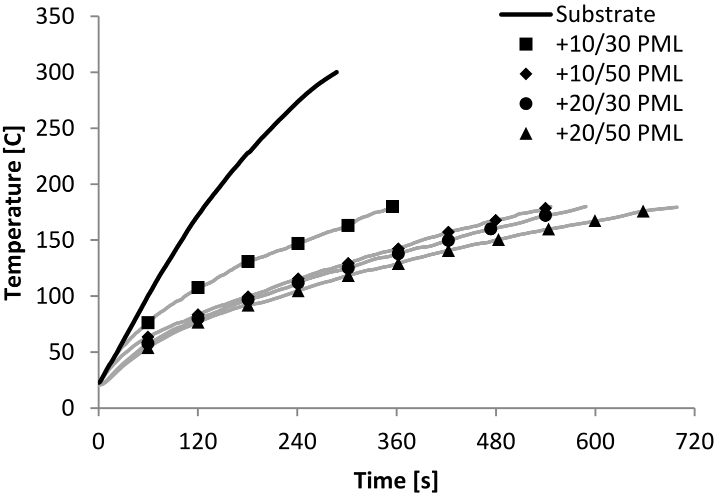

Figure 6.11: Temperature profiles for aluminium substrates with and without PML insulation under 75 kW m^{-2} heat flux.

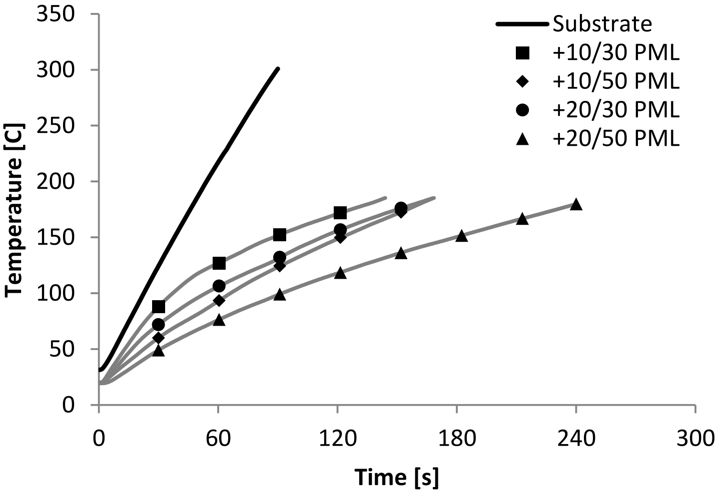

Figure 6.12: Temperature profiles for aluminium substrates with and without PML insulation under 150 kW m^{-2} heat flux.

temperature profiles recorded for the protected and unprotected specimens are shown in figure 6.12 for comparison. Individual metal foils of the PML are eroded within a short time period resulting in considerable disruption and erosion to the PML barrier surface. It is assumed that this non-uniform fire damage affects the heat transfer into the specimen causing thermal losses which would explain why there is not a greater temperature increase in back face temperatures in comparison with 116 kW m^{-2} test results.

6.5 Front-face-modified PML

Incorporation of non-melting materials into the PML architecture has proved to be an effective method to further enhance the fire protection properties of the basic aluminium-epoxy PML. Whereas basic PMLs are affected by the melting process of the aluminium foils, a stainless steel or titanium PML surface layer offers the advantage of resistance against abrasion up to very high heat fluxes as their melting points lie well above 1200 °C.

The observed temperature profiles, as presented in figure 6.13 for the case of 10L/30μm

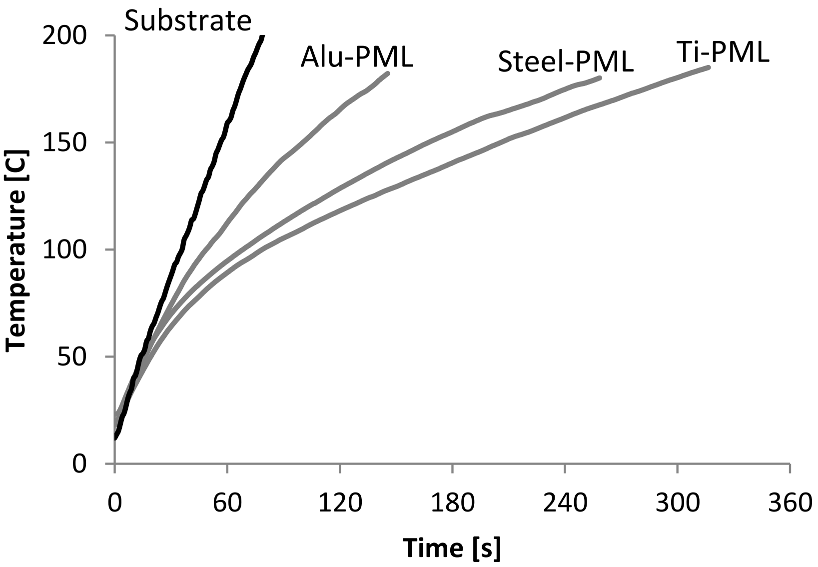

Figure 6.13: Influence of material choice of PML top layer on rear face temperature profiles, tested at 116 kW m^{-2} heat flux.The curve labelled *Alu-PML* refers to a basic 10L/30μm PML, *Steel-PML* to a 10L/30μm + St modified PML and *Ti-PML* to a 10L/30μm + Ti modified PML, all bonded to an aluminium substrate.

laminate types exposed to 116 kW m^{-2} heat flux, of steel- or titanium-modified PML show a clear improvement in delaying the heat transfer through the samples in comparison to basic PML specimens. As the unprotected substrate experiences a rapid temperature increase within the first minute of a 116 kW m^{-2} test the surface layer already reaches temperatures which are critical for structural performance, whereas compared with Steel/PML- and Ti/PML-covered substrates these temperatures are only exceeded after three minutes of testing. The maintained integrity of the modified laminates allows for the full formation of the insulation effect as the decomposition gases are successfully trapped in between the individual metal layers of the laminate, which can be observed by the extensive expansion caused by the blister formation during the experiment. In general it is found that because of the lower thermal conductivity of the titanium foil itself, in comparison with the steel foil, an initial delay in the heat transfer into the laminate is created resulting in a slower rise of back face temperature. This has been observed across the different laminate types at the three tested heat flux levels, see figure 6.14.

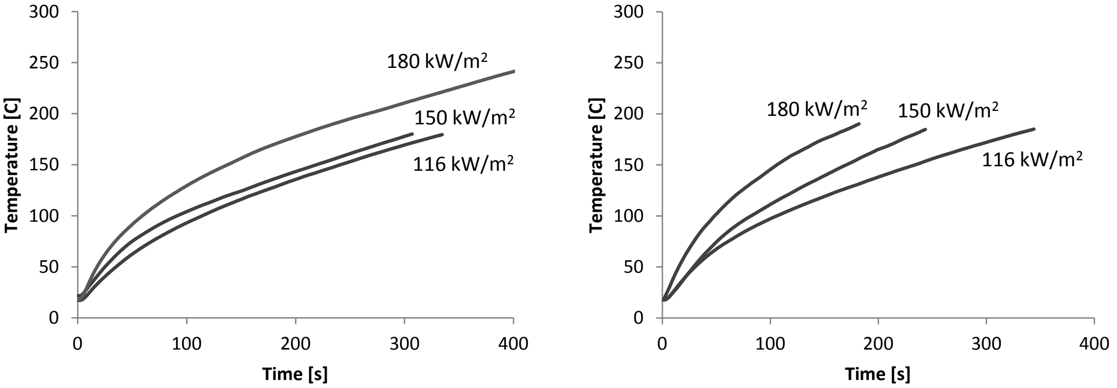

(a) Stainless Steel front

(b) Titanium front

Figure 6.14: Influence of heat flux on temperature profiles in front face-modified PML/aluminium specimens: a) 10L/50μm + St, b) 20L/30μm + Ti.

A summary of the performance of the different laminate types in comparison to an aluminium substrate under different fire scenarios is given in figure 6.15. The data is taken after one minute of testing and should therefore be treated with some caution if predictions are to be extrapolated from this data for longer term heating times. However, these results give an indication of the fire protection efficacy of different PML types in comparison with an uncovered substrate. The use of front face modified PML below a heat flux of $100\,\mathrm{kW\,m^{-2}}$ is economically inappropriate as the basic aluminium PML provides sufficient thermal insulation. At higher heat flux levels, however, when the effect of melting and abrasion becomes more prominent modified PML might prove to be a suitable alternative. Despite the improvements achieved in the test results using non-melting front layers in the PML design, the greater weight and higher cost involved in producing these materials may necessitate compromises when considering their application. Such compromises might limit the use to structures with a significant risk of being exposed to high heat flux fire scenarios, or localised usage where either the structure is most temperature sensitive or there is the greater potential for fires, near an engine for example.

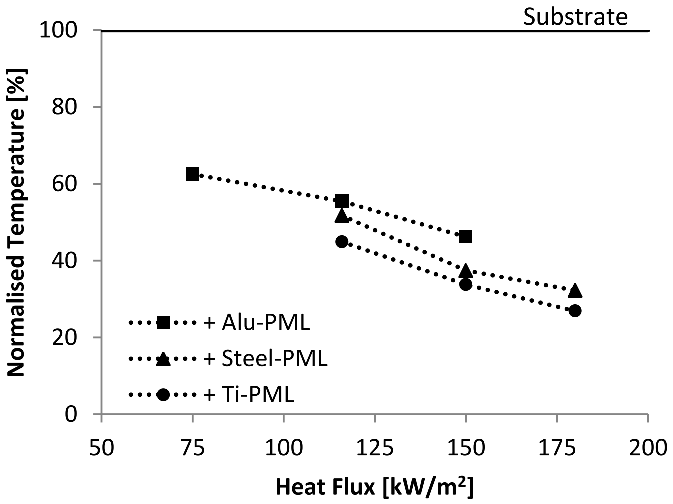

Figure 6.15: Effect of heat flux on temperature reduction for specimens featuring different PML types in comparison to an unprotected aluminium substrate captured at 1 minute of heat exposure.

6.6 Effect of PML on the Fire Characteristics of Combustible Substrates

The main point of interest during an investigation of the fire performance of non-reactive, metal structures is the temperature development within the structure as well as the potential of heat dissipation into adjoining structures or the environment. The increased use of polymer-matrix composite materials in modern-day applications, commonly as a substitute for metal structures, necessitates the assessment of the fire characteristics of these combustible materials besides the basic temperature analysis. During heat exposure these materials will decompose releasing heat and smoke which creates the risk of fire spread as well as impeding the evacuation process during accident scenarios. It is submitted that PML thermal barriers show great potential in reducing the fire risk of such combustible materials due to the PML's fire protection efficacy.

Upon heat exposure all combustible materials experience an initial inhibition time during which heat is transferred into the different layers and the temperature consequently increases until the critical point is reached when enough decomposition gases are produced for ignition.

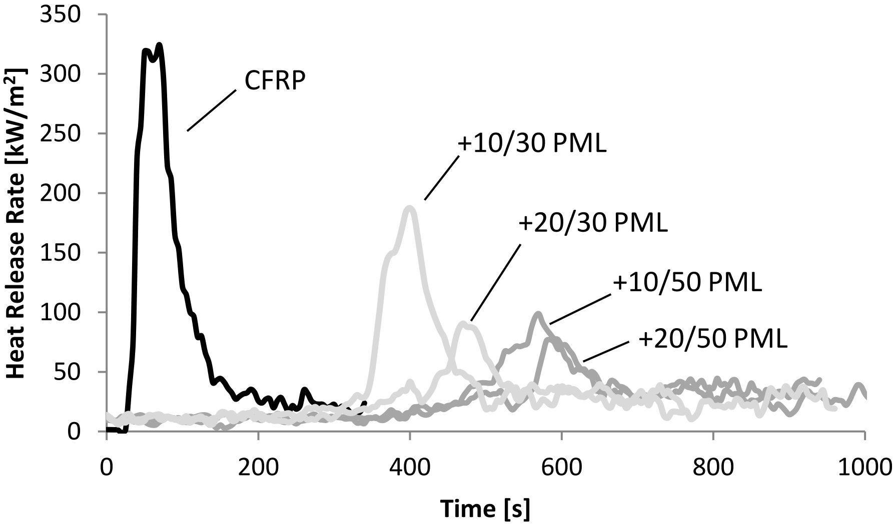

Figure 6.16: Fire reaction characteristics (HRR) of combustible materials protected by PML materials - CFRP substrate.

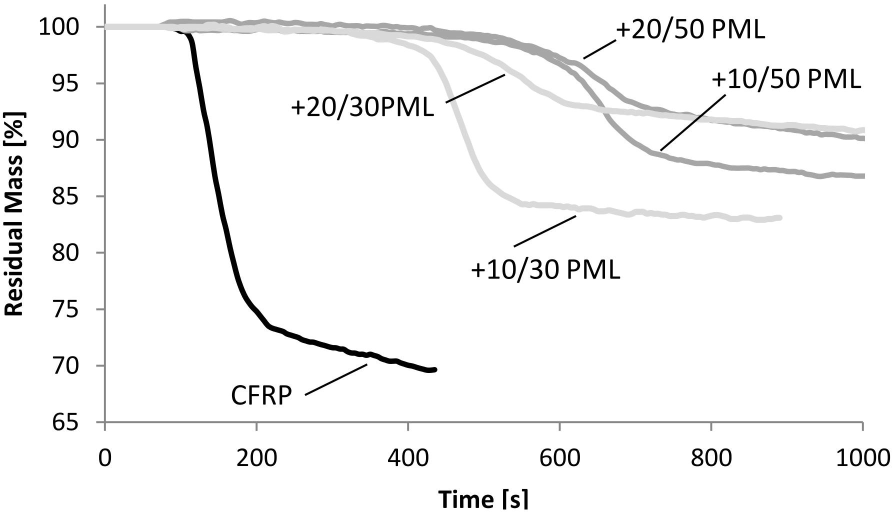

Figure 6.17: Fire reaction characteristics (ML) of combustible materials protected by PML materials - CFRP substrate.

Carbon-Epoxy composite laminates demonstrate only short resistance to ignition due to the high emissivity of the composite which leads to a high portion of the incident heat being transferred into the material. The decomposition temperature of the resin is exceeded within a short time period resulting in intense burning. This is accompanied by a rapid increase in mass loss as the available combustible material is consumed at a high rate releasing high levels of heat, see figures 6.16 and 6.17 for CFRP specimens exposed to $70\,\mathrm{kW\,m^{-2}}$. The ongoing flaming consumption of the material leads to an almost complete depletion of the resin. The residual mass at the end of test is composed of the carbon fibre content and residual char.

GLARE behaves slightly differently because its layered architecture contains dissimilar materials. The high reflectivity of the outer aluminium layer delays the ignition time of the underlying composite layer considerably in comparison to the CFRP. Similar to the CFRP though, an almost complete consumption of the polymer constituent occurs resulting in full delamination of the individual aluminium layers and the charred composite plies of the GLARE material, see figures 6.18 and 6.19.

Additional curves in all four diagrams (figures 6.16 - 6.19) represent either a CFRP or a GLARE substrate protected by PML surface insulation. The superior behaviour of these specimens in

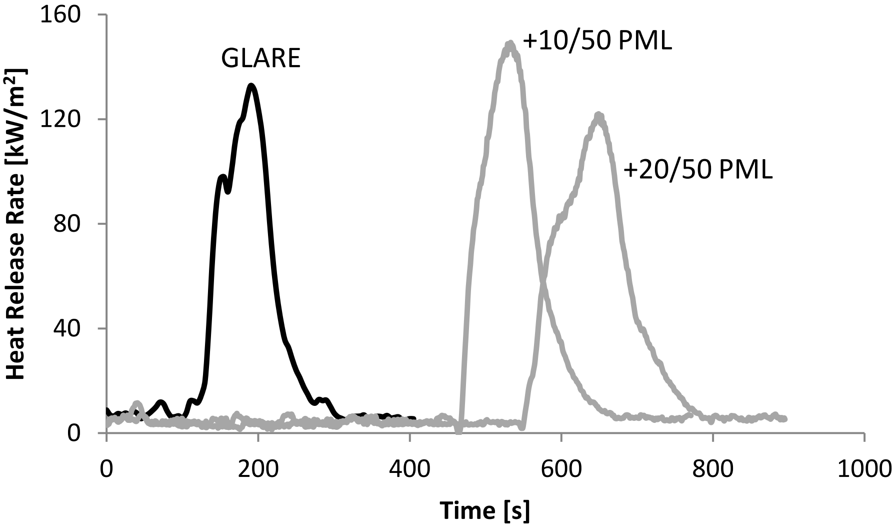

Figure 6.18: Fire reaction characteristics (HRR) of combustible materials protected by PML materials - GLARE substrate.

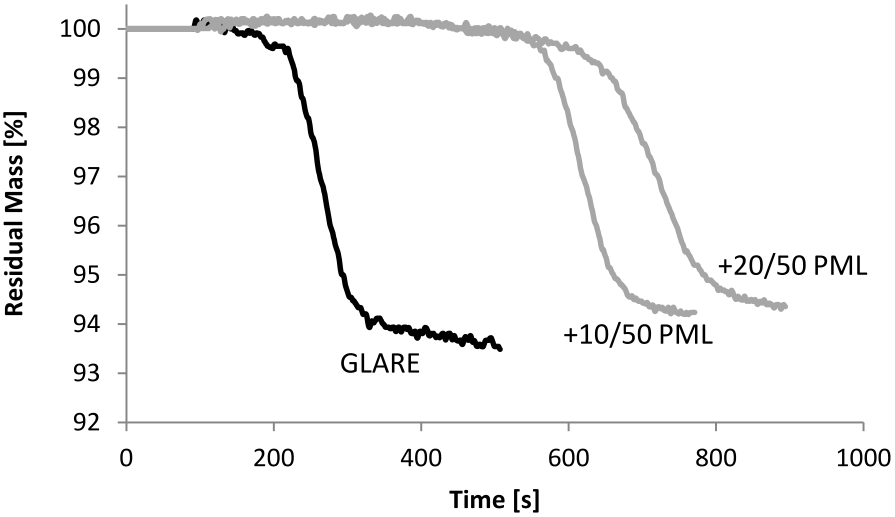

Figure 6.19: Fire reaction characteristics (ML) of combustible materials protected by PML materials - GLARE substrate.

comparison to the unprotected substrates is clearly demonstrated. Under the radiant heat exposure of the $70\,\mathrm{kW\,m^{-2}}$ heat flux, the PML material is able to fully establish its fire protection effect as the adverse effects arising from melting of metal foils or convective surface abrasion do not occur. Hence the unhindered formation of the thermal barrier through decomposition of the PML resin interlayers, and the formation of decomposition gases are fully developed. Although partial melting of the PML surface is observed during later stages of the test, this arises from the ignition of the decomposition gases originating from the substrate rising up from the sample edges which does not occur in real life applications. The process of forming the expanded PML is very effective in slowing down the heat transfer into the underlying substrate which in turn experiences a longer heating up period until the critical temperatures for ignition are exceeded. Consequently, ignition times are observed to be greatly extended, for PML/GLARE specimens a factor of 5 was achieved and for PML/CFRP specimens a minimum factor of 15 has been recorded. This therefore carries with it the great advantage in increasing the time for safe evacuation due to resultant prolonged structural stability as well as reducing the risk of harmful by-products and smoke which also hinders safe evacuation.

Substrate	Insulation	TTI [s]	Peak HRR [kW m^{-2}]	THR [MJ m^{-2}]	MARHE [kW m^{-2}]	FIGRA [kW m^{-2} s^{-1}]	Residual Mass [%]
CFRP	unprotected	26 ± 1	323.90 ± 16.04	25.18 ± 0.60	142.03 ± 6.96	12.46 ± 0.80	69.4 ± 2.5
	+10/30 PML	335 ± 3	187.43 ± 10.06	28.55 ± 1.11	34.16 ± 1.95	0.56 ± 0.03	82.8 ± 3.4
	+20/30 PML	527 ± 4	76.94 ± 4.56	29.17 ± 1.05	20.79 ± 1.23	0.15 ± 0.01	89.2 ± 3.5
	+10/50 PML	495 ± 2	98.73 ± 5.56	26.58 ± 0.74	23.46 ± 1.58	0.20 ± 0.01	86.1 ± 3.3
	+20/50 PML	407 ± 5	90.52 ± 4.41	24.68 ± 0.94	21.57 ± 1.04	0.22 ± 0.02	90.4 ± 2.8
GLARE	unprotected	101 ± 2	132.81 ± 8.14	10.28 ± 0.34	41.12 ± 1.55	1.31 ± 0.08	93.4 ± 0.2
	+10/50 PML	461 ± 3	149.27 ± 10.82	12.57 ± 0.65	19.86 ± 0.69	0.32 ± 0.02	99.8 ± 0.1
	+20/50 PML	544 ± 5	122.01 ± 8.47	12.56 ± 0.75	16.59 ± 0.80	0.22 ± 0.03	99.8 ± 0.1

Table 6.1: Summary of cone calorimeter results of PML-protected and unprotected composite substrates tested at 70 kW m^{-2} irradiance.

Despite similar or slightly higher levels of the total amount of heat released (THR) in the specimens protected by PML, the risk of fire spread and fire growth is greatly reduced as the released heat is spaced out over a longer time period due to the contribution of the PML insulation. This is evident from the MARHE values (maximum average rate of heat emission) which are reduced to below 50 % for GLARE and below 30 % for CFRP specimens in comparison with the respective unprotected substrates, see table 6.1 for more details.

Generalised statements about the influence of the PML surface protection on the burning behaviour of combustible substrates is difficult to make because the measured curve characteristics are very much dependent on the choice of substrate material. For GLARE, a similar burning behaviour of unprotected and protected specimens with a comparable mass loss rate is observed leading to similar charring conditions with similar residual sample weight. Overall, the samples expand in a similar manner and complete delamination of the individual GLARE layers occurs for all tested samples.

For the monolithic CFRP composite substrate, the intensive burning results in an almost complete depletion of the contained polymer as the residual weight is close to the initial fibre weight fraction of 64 %. The mass loss curve shows two distinctive stages of the degradation reaction. Firstly, organic polymer is lost through decomposition which is followed by further char degradation until a residual mass level is reached close to the fibre weight fraction.

In contrast, CFRP substrates featuring PML protection exhibit a different behaviour as the mass loss rate indicates an incomplete consumption of the resin with a maximum of 50 % of the contained polymer being converted into decomposition gases in case of a specimen with a 10L/30μm PML protection. This suggests that due to the introduction of the PML thermal barrier the temperatures are not high enough for extended consumption of the resin but also that the second stage of the decomposition reaction is supressed. A further aspect is the fact that in unprotected CFRP samples the oxygen can easily diffuse through the porous char layers into the bulk of the sample initiating further char degradation. This is in contrast to PML/CFRP specimens where the oxygen can only enter the material via the side edges and which presents a long and limited diffusion route as the top surface of the sample is covered with an impermeable PML.

6.7 Model Validation

From observations during the small-scale burner testing of PML-protected specimens, it can be concluded that the behaviour of the PML surface layers can be categorised into two groups: one being, where the PML surface layer exhibits destructive characteristics with melting and ablation effects; and the other, where the surface of the PML remains fully intact with no impairments visible. For this reason the following sections will discuss each of these cases individually.

6.7.1 Low Heat Flux Environment

An environment characterised as being of *low heat flux* is defined by the absence of irreversible physical damage to the individual layers of an aluminium-based PML thermal barrier. In this case the heat flux the specimen is exposed to is not high enough to initiate any melting or ablation effects on the PML.

The first signs of fire damage to PML have been observed during fire testing at heat fluxes above $75\,\mathrm{kW\,m^{-2}}$. This appears to be in contradiction to the Stefan-Boltzman law for radiative heat transfer which predicts a flame temperature that lies above the aluminium melting point to be equivalent to a heat flux of $44\,\mathrm{kW\,m^{-2}}$. However, it is not surprising that when the very low emissivity of the aluminium metal and its high reflectivity are taken into account, no signs of actual foil melting have been observed in experiments carried out at $70\,\mathrm{kW\,m^{-2}}$, which is equivalent to a

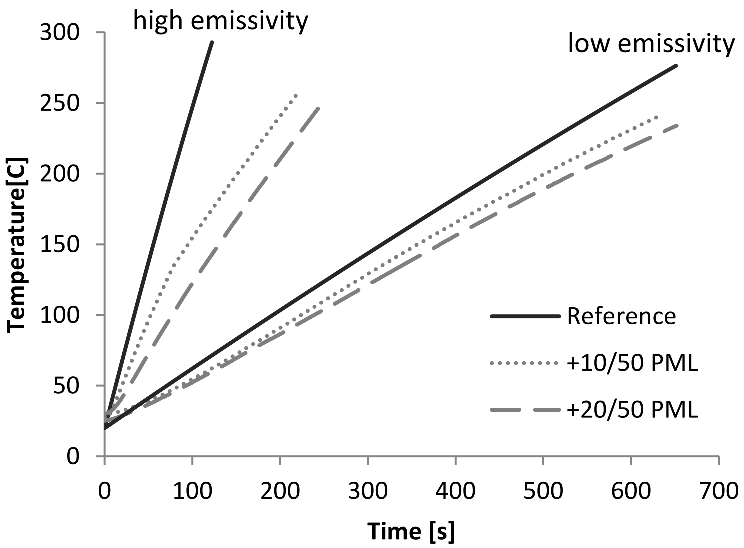

Figure 6.20: Effect of surface emissivity on temperature profiles obtained in low heat flux fire testing with the cone calorimeter at 70 kW m^{-2}. Experimental temperature profiles of aluminium substrates featuring either a 10/50 PML or 20/50 PML with different surface preparation are given. The simulated reference curves (solid line) of an unprotected aluminium substrate are included for completeness.

flame temperature of 796 °C. Because of the inherent low transmission properties of aluminium, the results are much lower hot face temperatures in the worst case scenarios where the specimen surface had been sprayed with black paint in order to maximise the heat absorption into the specimen. In that case, the hot face temperature was measured at around 620 °C which would have been even lower for the case of the pristine metal surfaces of unmodified aluminium-based PML. Therefore, no fire damage of the PML layers will be observed over this heat flux range for test durations up to 30 minutes.

As it is difficult to achieve stable flaming conditions at a reliable constant heating level with the current burner setup for heat fluxes below 100 kW m^{-2}, the following remarks are based on experiments performed with the cone calorimeter which facilitates very controlled and stable testing conditions.

In figure 6.20 the results of cone calorimeter tests carried out at 70 kW m^{-2} heat flux are presented for two different types of PML bonded to an aluminium substrate, each with varied surface preparation. In the graphic, low emissivity refers to a pristine, metal state of the PML surface with a high reflectivity, whereas high emissivity is attributed to a PML surface painted black in order to maximise heat transmission. It is apparent that the original-manufactured surface condition proves advantageous over paint-modified PML specimens in that the former samples exhibit a much slower temperature increase, only reaching similar temperature levels to the latter after much longer testing time. When testing above the critical temperature for the maintainance of structural integrity of aluminium substrates (> 150 °C), a time delay around a factor of 3 is observed in specimens of low emissivity compared to high emissivity specimens. Furthermore, this set of experimental curves for the different PML architectures presents an upper (low emissivity) and lower (high emissivity) limit for the fire protection potential of PML under the applied boundary conditions. The temperature curves for any additional aluminium substrates featuring PML with varied surface preparation, e.g. white paint or brushed metal appearance, will fall into the range spanned by these curves, see figure 6.21.

Small differences in the temperature profiles of thin 10-ply PML specimens compared with thicker 20-ply PML specimens are noticeable, with the thicker PML specimen showing slightly lower heating up rates. The similarity of the curves arises from the low heat flux environment which

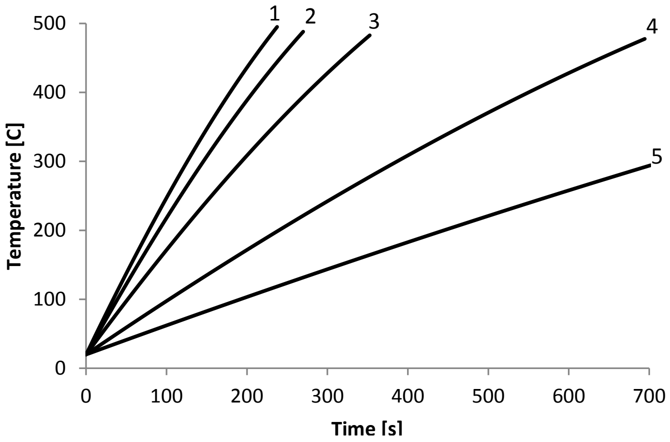

(a) Aluminium plate

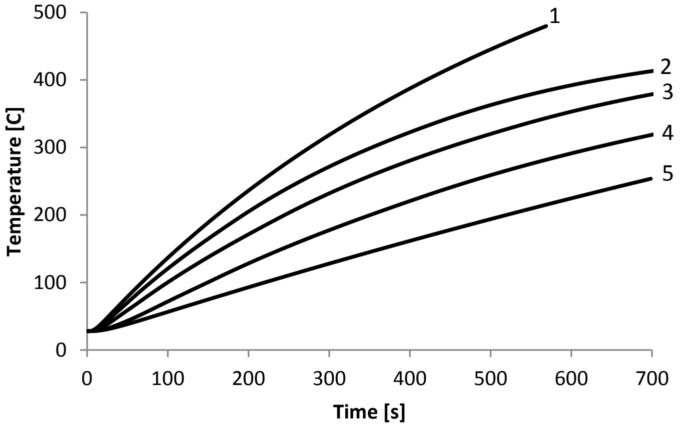

(b) Aluminium with 10/50 PML

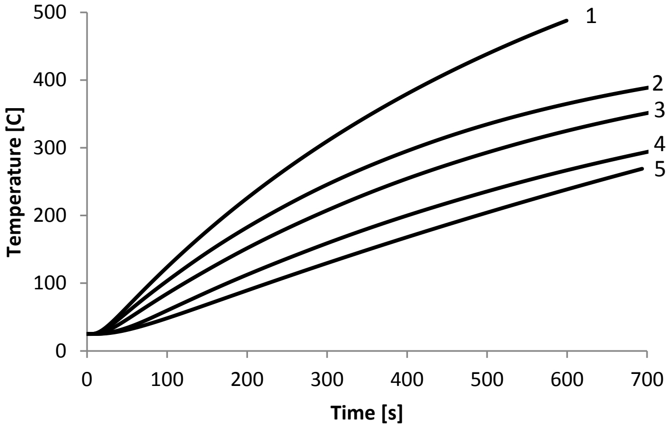

(c) Aluminium with 20/50 PML

Figure 6.21: Influence of varied surface conditions on simulated temperature profiles of a) unprotected aluminium substrate, b) aluminium substrate featuring a 10/50 PML, c) aluminium substrate featuring a 20/50 PML. The emissivity value decreases continuously from curve (1) to curve (5) representing modifications of black paint $\epsilon = 0.9$, white lacquer $\epsilon = 0.69$, 10 % aluminium paint $\epsilon = 0.52$, oxidised aluminium $\epsilon = 0.26$ and pristine metal surface $\epsilon = 0.14$. Reference emissivity values taken from [177, 178].

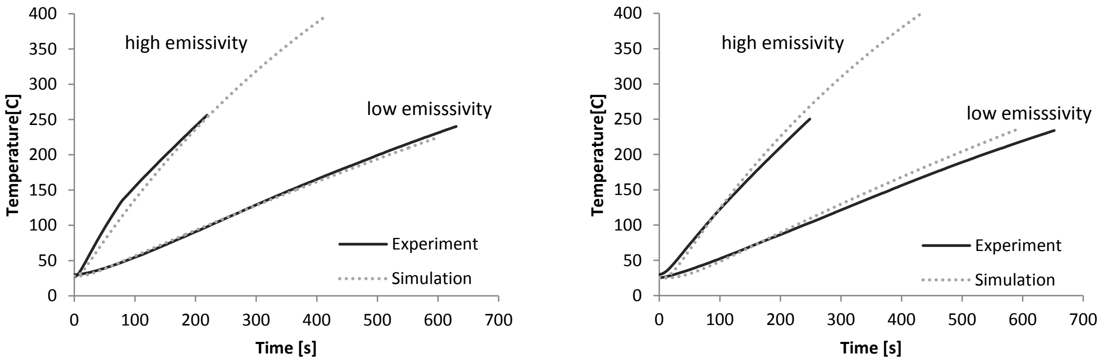

(a) Aluminium substrate featuring a 10/50 PML **(b)** Aluminium substrate featuring a 20/50 PML

Figure 6.22: Comparison of experimental and simulated temperature profiles of PML-protected aluminium specimens with different surface emissivity characteristics exposed to a low heat flux environment.

causes only minimal thermal degradation to be initiated within the PML resulting in an underdeveloped PML fire protection effect. This also explains the affinity of the reference temperature curve which has been produced via simulation of the behaviour of an aluminium substrate without PML protection under the same testing conditions. Yet, for cases of samples with high emissivity, which in principle means an apparently higher heat flux being absorbed into the sample, the fire protection effect becomes more effective due to greater barrier function being formed, leading to greater deviation of the PML sample curves in contrast to the substrate reference curve, so that a greater temperature delay can be observed.

The PML_FIRE model predicts the experimentally determined temperature profiles without further adjustment with good correlation. The input parameters for the hot face boundary conditions have been taken as $\epsilon = 0.14$ as the lower emissivity limit resembling the pristine metal surface, which can be found in literature [149, 162]. The upper limit for the emissivity value in the case of a surface modification painted black is represented by a value of $\epsilon = 0.9$, which is a common assumption [69, 179]. Overall, fitting accuracy of the calculated temperature profiles in comparison with the experimental ones is good, see figure 6.22. Yet, the model seems to exaggerate the temperature response at times.This can be attributed to the assumption that the specimen is fully insulated during the simulation run which is in contrast to experimental conditions where perfect insulation cannot be achieved and thermal losses will inevitably occur.

6.7.2 High Heat Flux Environment

For the modelling of PML-covered specimens exposed to a high heat flux, the emissivity of the unmodified PML surface is set to the same value of $\epsilon = 0.14$ as obtained from the analysis of low heat flux experiments. However, due to the occurrence of the thermal damage to the PML the heat transmission characteristics into the specimen will change with ongoing heat exposure. The highly turbulent nature of the heat flow at the PML surface, together with molten sections of aluminium foil and distorted foil, creates a situation where the effects on heat transmission are impossible to quantify. It is accepted that when setting the emissivity parameter to a constant low value which resembles a pristine metal surface, a significant assumption and simplification is made.

Another factor observed which would greatly influence the calculated temperature profiles is the thermal conductivity of the PML. Initial modelling attempts have used the experimentally obtained temperature dependence of the PML's thermal conductivity which gradually declines from room temperature down to the values of the decomposed material when decomposition is initiated. Figure 6.23 depicts a set of temperature curves obtained with this data set as the dashed curves

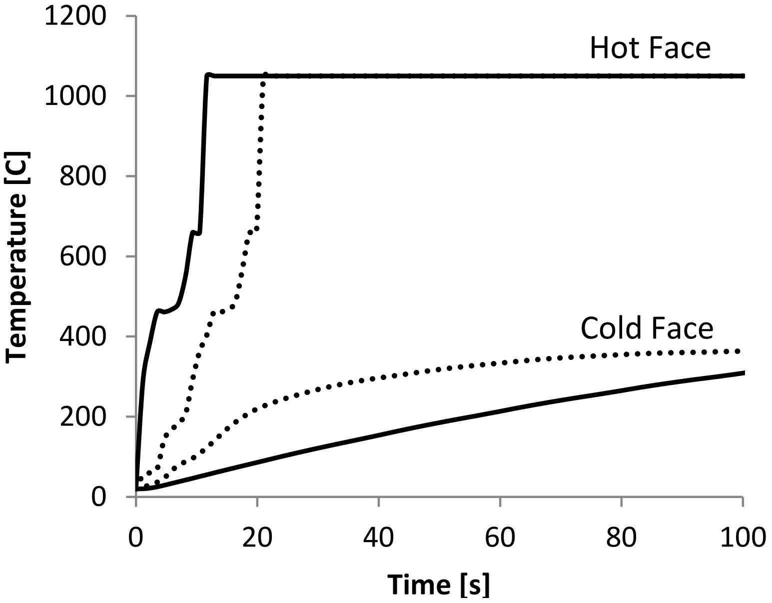

Figure 6.23: Effect of variation in PML thermal conductivity as input parameter for PML_FIRE. The dotted curves representing the experimental temperature dependence, whereas solid curves denote a constant low value of thermal conductivity.

under heat exposure with a flame of 1050 °C. A slow increase in temperature of the hot face and a small thermal gradient across the whole specimen thickness for the initial heating up phase is noticeable. This is in contrast to experimental observations which have shown that within the first ten seconds of the experiment, expansion followed by partial melting of the top PML layers occurs. Furthermore, the predicted steep temperature rise at the specimen's back face does not match the experimental temperature readings. Because the simulated thermal gradient across the specimen's thickness is not great enough to replicate the experimental behaviour, this means that the hot face's heating rate is not high enough and the back face shows a deficient thermal lag.

One potential solution to overcome this problem is to adjust the thermal conductivity parameter to the constant value of $k = 0.095$, associating it with the decomposed state of the material, instead of the temperature dependence which only reaches this value when high temperatures are present within the material. The results obtained from the modified model are presented in figure 6.23 as the solid temperature curves. It will be seen that a much improved correlation of the observed experimental behaviour has been achieved. A wide divergence in the thermal gradient develops from the initial heating phase displaying the considerable thermal insulation potential that PML barriers present. This leads to the slow heating up of the specimen's cold face as shown in the graphic and a much improved thermal lag can be noticed in comparison with the simulated curve.

Applying the adjusted PML_FIRE model to PML-covered specimens, which had been exposed to the flaming conditions of various heat fluxes achieved with the small-scale burner test, results in the temperature profiles shown in figure 6.24 for a 10L/30μm PML/Aluminium specimen and figure 6.25 for a 20L/30μm PML/Aluminium specimen. From the comparison of the experimental and calculated temperature curves it can be deduced that the model is able to capture the thermal behaviour of the samples during these short-term heat exposure experiments over a wide heat flux range with good accuracy. Slightly greater deviations between the curves occur for the case of 20-ply PML specimens in comparison to the 10-ply specimens. However, the experimental and simulated temperatures curves corresponding to one heat flux still fall within a 10 % error margin.

Additionally, the PML_FIRE model can be used to investigate the influence that changes to the PML design have on the overall thermal behaviour of substrate materials protected by PML beyond experimental activities and possibilities. In figures 6.26 and 6.27 results of such analysis are shown

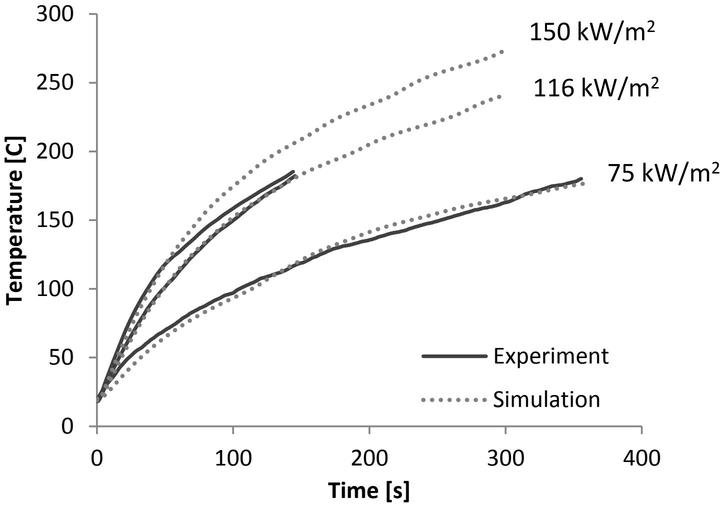

Figure 6.24: Comparison of the experimental and modelled thermal performances of a 10-ply PML under various heat flux conditions.

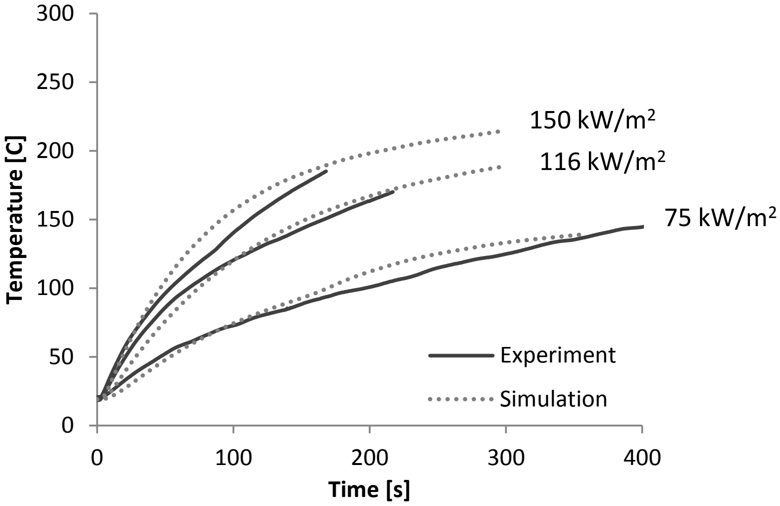

Figure 6.25: Comparison of the experimental and modelled thermal performances of a 20-ply PML under various heat flux conditions.

based on a 10L/30μm PML/Aluminium specimen exposed to a $116\,\mathrm{kW\,m^{-2}}$ heat flux affected by a variation of the input parameters such as PML ply number or the individual aluminium foil thicknesses within the PML. This is partly only for theoretical considerations because, for application in real-case scenarios, a careful compromise between the PML efficacy, the added weight to the substrate together with cost implications have to be considered. In general, it can be concluded that doubling the number of layers provides a greater temperature retardation potential than using foil that is twice as thick. This can be explained by the fact that with an increasing layer number not only is more foil available which imposes a physical barrier against thermal degradation but also the number of organic interlayers is increased which is highly advantageous because a greater expansion potential is available and therefore a more effective barrier formed.

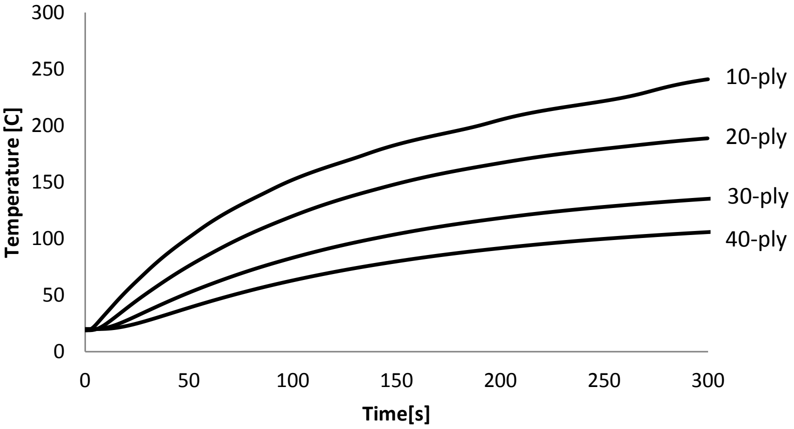

Figure 6.26: Simulated temperature profiles of 30μm PML/aluminium specimens with the PML being manufactured to different overall thicknesses using multiples of foil numbers.

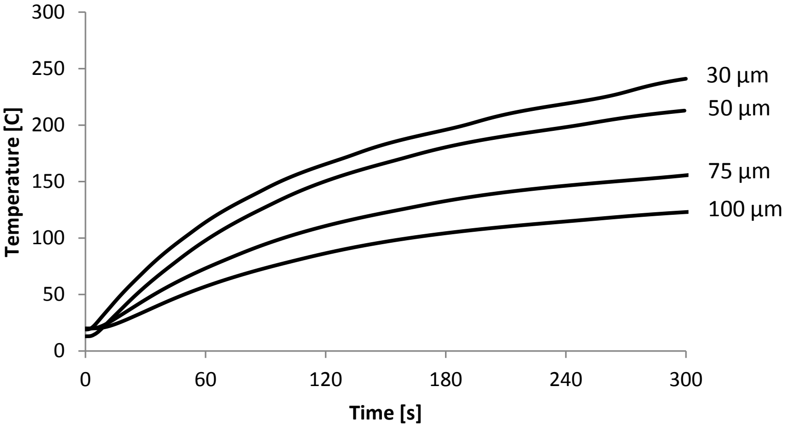

Figure 6.27: Simulated temperature profiles of 10-ply PML/aluminium specimens with the PML manufactured with aluminium foil of varied thickness.

Chapter 7

Application of PML_FIRE: Influence of PML on Fire-structural Performance

The previous chapter has shown the efficacy of PML thermal barriers in retarding the temperature increase of structural materials when exposed to fire, consequently resulting in the improvement of their fire resistance characteristics. However, looking exclusively at the temperature distribution during such thermal system analysis does not mean that these conclusions can be safely used in real-life applications. The materials tested are intended for use in structures that are designed to have regular mechanical loading applied throughout their life time or that will experience structural loading at some point during their life time, e.g. pressurised air cabins, ships' walls or train bodies.

One aim of this study is to investigate whether the introduction of PML thermal barriers could prove advantageous during a structure's life time particular in a fire scenario with regards to structural collapse and/or prolonging the safe evacuation time by preserving the structural integrity, bearing in mind that the mechanical strength of these materials is highly temperature dependent. Characterisation of the mechanical response of specimens, representing either a non-reactive or a flammable substrate type, in combination with PML insulation barriers has been undertaken by experiments exposing samples simultaneously to structural and thermal loading. Briefly comparing the PML system to conventional insulation methods will be undertaken to classify the PML protection efficacy. The PML_FIRE model is used to give an insight into the thermal state of the specimens at the point of structural failure during the analysis of the materials' fire performance under load.

7.1 Experimental

A non-reactive type of substrate material is represented by 6.35 mm thick 2024-T351 Aluminium alloy plates which were cut down into strips of 600 mm length and 50 mm width with the longer dimension corresponding with the direction in which the aluminium plate is rolled during manufacture. Carbon-fibre reinforced epoxy composite material was chosen as the combustible substrate type. The composite material has been manufactured from 24 plies of unidirectional carbon/epoxy prepreg of type AS4/3501-6 supplied by Hexcel to achieve a total specimen thickness close to 6.35 mm. The individual plies were arranged in a symmetric and balanced stacking order to construct a quasi-isotropic composite material featuring a [0/45/90/-45] lay-up resulting in an overall laminate thickness of 6.7 mm and a fibre volume fraction of the manufactured composite laminate of 62 %.

Basic aluminium PMLs of the type 10L/30μm and 20L/30μm were used as thermal barriers.

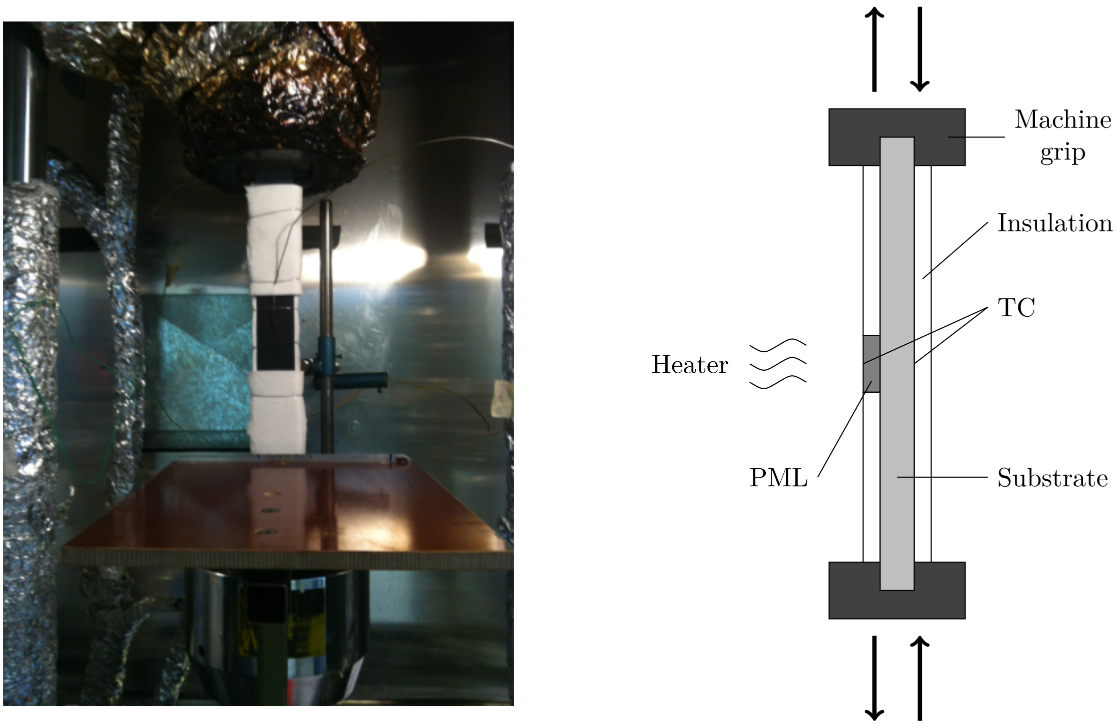

(a)

(b)

Figure 7.1: Test setup for simultaneous mechanical and thermal loading of long slender sample strips: a) Experimental setup prior to test start with an insulated specimen inserted into the machine grips and the heater stage in the picture foreground, b) Schematic of the testing arrangement.

From pre-manufactured sheets, 150 mm long and 50 mm wide PML samples were bonded onto the substrates. All specimens featuring a metal laminate were spray-painted with heat-resistant black paint which maximises the heat absorption into the sample during the fire exposure representing a worst case scenario. A ceramic fibre blanket applied as thermal insulation was wrapped around the edges of the specimen leaving only a 100 mm long window open at the front. For samples with a PML surface barrier, bulldog clips were used to apply pressure on the edges in order to avoid the undesirable delamination of the polymer-metal laminate at the edges which might facilitate the unwanted release of decomposition gases.

A 250 kN load capacity MTS machine was used to determine the specimens' tensile and compressive behaviour under the influence of one-sided heating. The samples were clamped at both ends, leaving a free gauge length of 430 mm. Only a $100 \times 50\,\mathrm{mm}^2$ section at the centre of the sample was exposed to a constant radiant heat of $50\,\mathrm{kW\,m^{-2}}$ from a calibrated coil heater. The rest of the sample was thermally insulated in order to induce the localised heating at the centre of the sample as well as avoiding overheating the machine grips. The machine setup with the heater stage is shown in figure 7.1. Type-K thermocouples attached to the front and the back face of the sample monitored the temperature development throughout the test period.

During the fire-structural testing a constant load was applied to the specimen while it was exposed to the radiant heat source which was placed at 25 mm from the specimen's surface. Tests were carried out at different incident heat flux levels as well as different loading conditions. For the tensile tests the applied load was based on the substrate's yield strength in case of aluminium (348 MPa) and the material's fracture strength for CFRP (588 MPa), which had been determined beforehand in static tensile tests at room temperature. Applied load percentage levels during the fire-structural testing ranged from 80 % to 5 % of the room temperature value for tensile strength. The axial extension of the sample was measured using the machine's cross-head displacement. Load percentage levels for the compression tests were based on the Euler buckling stress of the aluminium alloy (39 MPa) and CFRP composite laminate material (24 MPa) at room temperature, respectively, and were varied between 90 % to 10 %. Again, in-plane deformation of the sample was measured using the machine's cross-head displacement. The horizontal or out-of-plane deformation of the centre point at the back face was additionally monitored by a LVDT device.

7.2 Aluminium Substrate

7.2.1 Temperature Profiles

During the initial transient heating phase of the specimens under irradiance of a 50 kW m^{-2} heat flux, the very high thermal conductivity of the material rapidly transfers the incident heat away from the specimen's surface into the bulk material of the unprotected AA2024 sample causing the back face temperature to increase at a similar rate to the hot face temperature. A small temperature gradient between the sample's front and back of around 45 K is established over time because thermal losses occur as the thermal energy is distributed not only in the through-thickness direction of the sample but also in the vertical direction towards the sample edges and machine grips which gives a considerable heat sink potential.

In contrast, specimens that feature PML surface insulation show very different behaviour in the development of the temperature profiles when compared to the unprotected aluminium substrates. The laminate's inherently very low thermal conductivity prevents a fast heat transfer into the underlying bulk structure which in turn causes the front face to reach high temperatures within a short time period. Due to the thermal barrier that is formed by the PML, the substrate material and consequently the back face is heated up at a much slower rate than the unprotected aluminium specimen. A much greater temperature gradient between hot and cold face of the PML-covered specimen develops for long exposure times under steady-state conditions. A comparison of the observed temperature profiles is shown in figure 7.2. It clearly shows the superior performance of the PML-insulated specimens where temperature reductions of over 100 K can be easily achieved compared with pristine AA2024 samples.

Furthermore, no dependence of the temperature development on the applied stress was observed and no significant difference in temperatures recorded for tension and compression samples tested at a heat flux of 50 kW m^{-2} could be found.

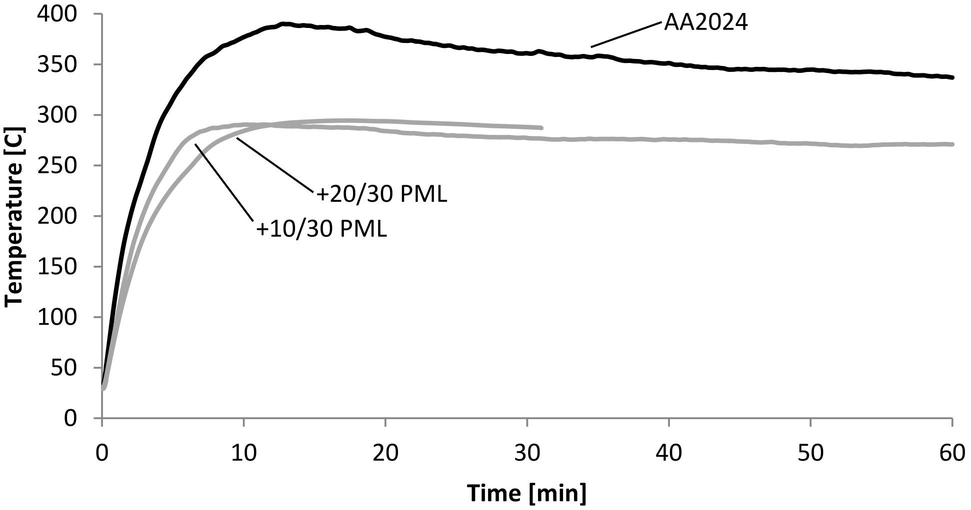

Figure 7.2: Rear face temperature profiles of AA2024 specimens with and without PML insulation when exposed to a radiant 50 kW m^{-2} heat flux.

7.2.2 Fire-structural Performance

For fire-structural testing at constant tensile loading, all samples initially experience the same in-plane displacement because the aluminium strips thermally expand when exposed to heat as indicated by the matching slope of all the displacement curves shown in figure 7.3a. At high loads a sharp increase in the rate of deformation leads to an abrupt plastic failure of the specimen indicating the presence of much higher forces within the sample than the instantaneous yield strength of the material. For tests performed under lower applied stresses, the displacement rate decreases after the initial expansion period leading to extended exposure times until final rupture occurs. Here, the failure mode is dominated by creep-like behaviour as the applied stresses are lower than the material's yield strength. The change in failure mode with decreasing applied stress level can also be noticed during visual inspection of the failed specimens. In figure 7.4 failure caused by creep becomes apparent in the pronounced necking of the samples tested at 30 % stress and below.

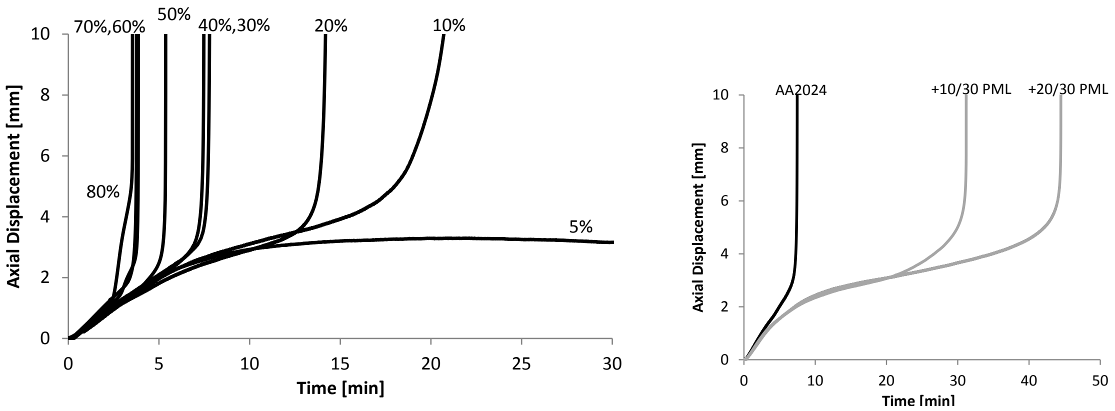

(a) AA2024 **(b)** AA204 and PML specimens

Figure 7.3: Time-dependent deformation during fire-structural tensile testing: a) Individual displacement curves for unprotected AA2024 specimens under constant applied load in the range of 80 % to 5 % of yield strength from left to right, b) Comparison of the recorded deformation in specimens with and without PML protective barrier at an applied load of 40 % yield stress.

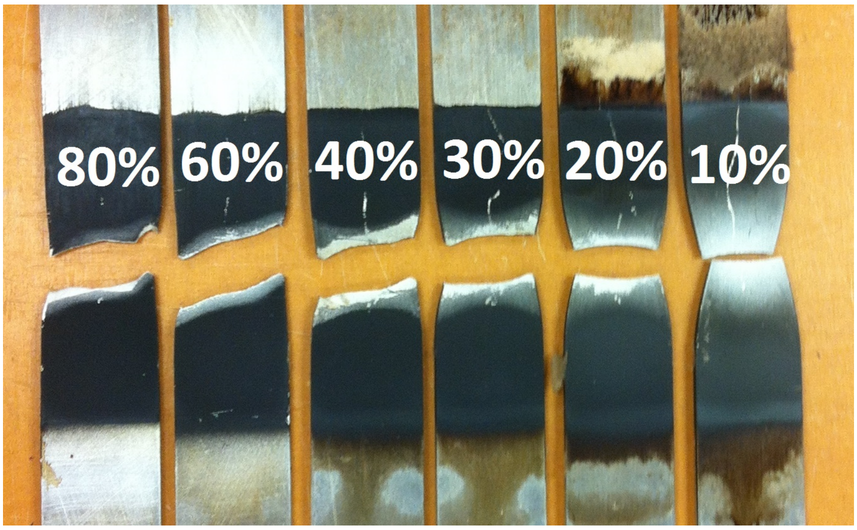

Figure 7.4: AA2024 unprotected specimens tested under tensile loading whilst exposed to one sided heating of 50 kW m^{-2}. Transition from abrupt plastic failure to creep-dominated failure with decreasing applied stress percentage (from left to right).

Under constant compressive loading conditions, three distinctive regions can be identified in the

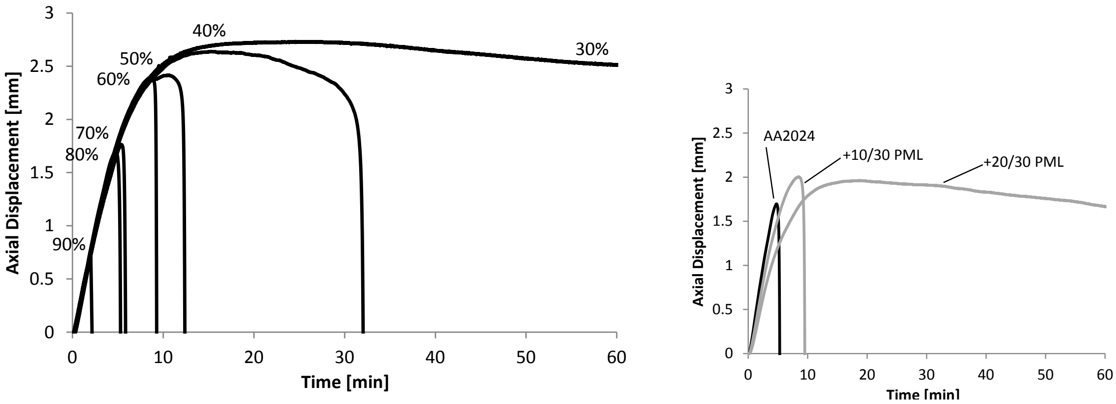

(a) AA2024 **(b)** AA2024 and PML specimens

Figure 7.5: Time-dependent deformation during fire-structural compression testing: a) Individual displacement curves for unprotected AA2024 specimens under constant applied force in the range of 90 % to 30 % of buckling strength from left to right, b) Comparison of the recorded deformation in specimens with and without PML protective barrier at an applied load level of 70 % buckling stress.

behaviour of the unprotected AA2024 substrate samples. These are sections of initial extension, maximum displacement and finally reverse deformation until failure as presented in figure 7.5a. The axial in-plane displacement initially shows a linear increase with time which is associated with the thermal expansion of the aluminium alloy. It can be observed that the rate of increase slows down before maximal expansion is reached. There is no significant out-of-plane deflection for this initial phase. The maximum point is characterised at the onset of plastic failure. The axial displacement decreases beyond this point as the plastic deformation region spreads over the heated zone, whereas at the same time the out-of-plane deformation increases sharply leading to a buckling of the aluminium strip. Under high compression loads the final failure occurs rapidly with a sudden reduction in axial displacement noticeable. In contrast, failure under lower load conditions is prolonged which can be observed in the much slower rate at which the in-plane deformation diminishes together with a gradual increase of the out-of-plane deflection which occurs simultaneously.

Figure 7.6 shows the experimental time-to-failure curves for the aluminium alloy, with and without PML insulation, under tension and compression loading, respectively. It is apparent that a reduction in stress leads to a prolonged time to failure (TTF), i.e. a longer structural lifetime. Specimens with PML insulation show considerably improved failure times compared to unprotected aluminium alloy samples. As expected, samples with a thicker thermal barrier have a longer life time compared to samples featuring a smaller ply number. The specimens were tested to ascertain the load level at which they would not fail. This critical point is established when the test specimens have not failed during 2 hours of the fire-structural test, after which time they are deemed to be structurally safe. These data points are included in the TTF curves although they do not represent the true failure time. However, as set points positioned at 120 minutes on the time axis they give a clear indication of the overall curve trend.

The reason for the improved performance of specimens protected by PML is the lower temperatures reached in samples with thermal protection as shown in figure 7.2. Lower specimen temperatures mean that the reduction in the material's Young's modulus and yield strength is not as advanced as would be expected from exposure to higher temperatures. In tests carried out at low stress levels, the stresses imposed on the specimen are lower than the instantaneous yield strength, resulting in creep-dominated failure behaviour. Testing at high loads where the external stresses are higher, causes elastic/plastic softening. As a consequence, samples with insulation show

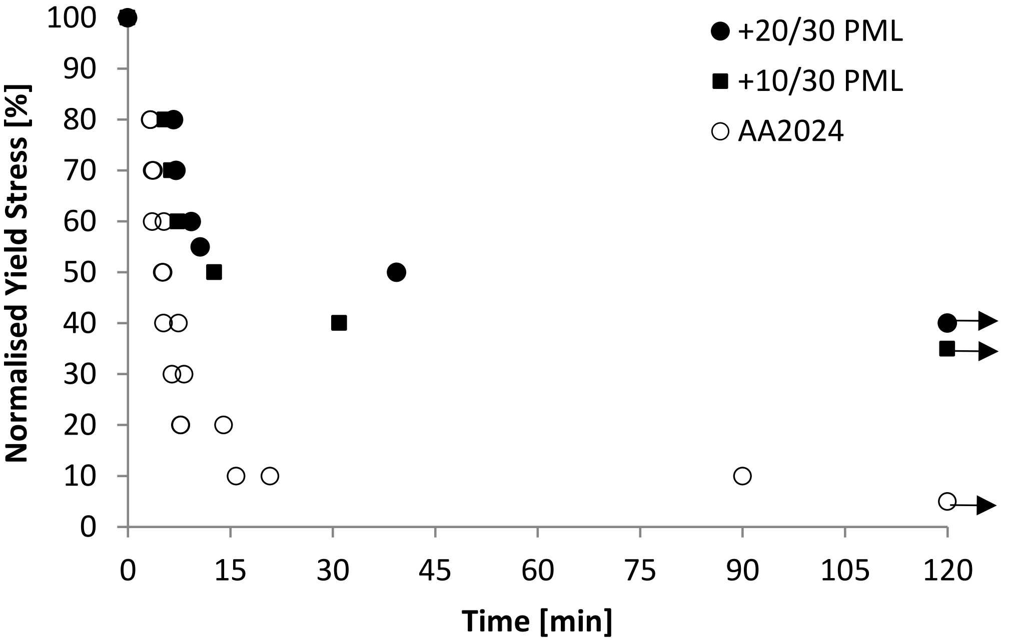

(a) Tension

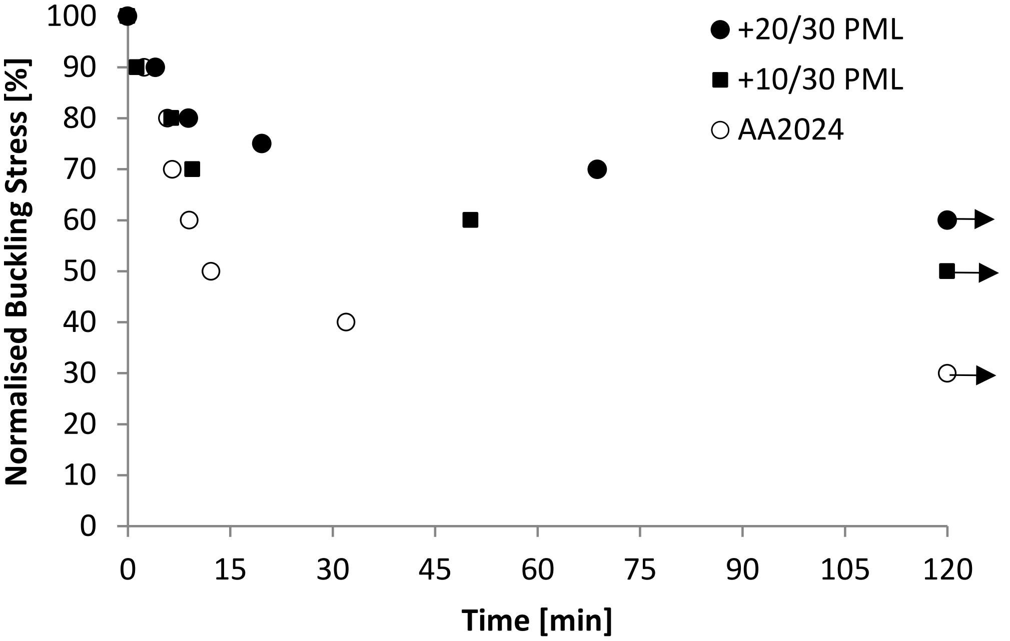

(b) Compression

Figure 7.6: Time-to-failure curves for unprotected and PML-insulated AA2024 specimens under structural loading and simultaneous exposure to a $50\,\mathrm{kW\,m^{-2}}$ heat flux: a) tensile loading, b) compressive loading. The normalised stresses are in reference to the room temperature failure stresses of a pristine AA2024 specimen.

longer failure times at all stress levels as their yield stress has not been reduced as much due to the samples' lower temperatures.

Different failure modes can be observed for the different sample types at specific stress levels for the same reason. As an example, the in-plane deformation of the three different specimen types at constant compressive stress level of 70 % Euler load is shown in figure 7.5b. Rapid failure is noticeable for the unprotected aluminium strip as well as the sample with a 10-ply laminate which shows a greater level of in-plane and out-of-plane displacement than the pristine substrate does. In contrast, the aluminium specimen featuring the thicker PML displays typical creep behaviour indicating that the applied load is lower than the instantaneous yield strength which in turn remains high compared to the strength of the unprotected aluminium specimens at the same load level due to lower temperatures present within the specimen. Overall, with an increase in the applied external load the transition from creep-dominated to elastic/plastic failure can be observed.

Similar behaviour can be observed for the specimens tested under tensile loading conditions. At lower applied stress levels, thermal expansion followed by irreversible creep softening accounts for the in-plane deformation, see figure 7.3b. At higher stress levels a change in the displacement rate occurs after an initial phase of thermal expansion indicating a plastic softening as the material begins to yield. For unprotected aluminium 2024 specimens, the transition from creep softening to plastic softening has been observed to occur between 60 % and 70 % of the applied yield stress when exposed to a heat flux of 50 kW m^{-2}. Interestingly, for samples protected by a thermal barrier this transition shifts to a higher stress level occurring between 70 % and 80 % applied load percentage. This again is due to the lower temperatures reached during the test which delays the effect of reduction in the yield strength and Young's modulus at elevated temperatures. Creep-dominated failure can be observed up to high stress levels when the specimen's yield strength at a specific temperature is finally exceeded.

7.3 Classification of PML Fire Protection Effect

In order to compare the PML thermal barrier system with conventional insulation methods additional test samples were prepared featuring either a thin layer of Superwool ceramic fibre blanket bonded with high-temperature adhesive to AA2024 substrates and commercially available Firefree intumescent paint directly applied onto the AA2024 samples. The thickness of these additional insulation layers ranged from 0.4 mm to 0.6 mm to match the thickness of the PML materials in order to be able to assess the fire protection efficacy of each insulation type.

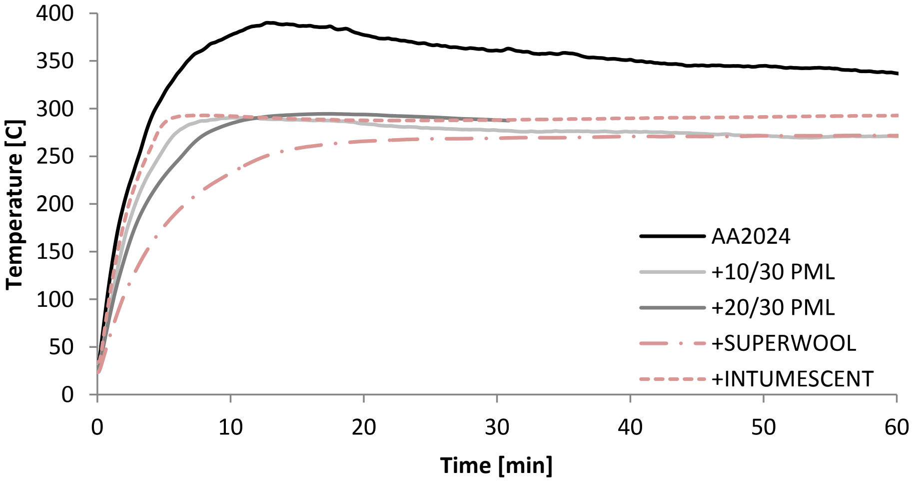

Figure 7.7: Rear face temperature profiles of AA2024 specimens featuring PML in comparison to AA2024 specimens insulated via conventional methods.

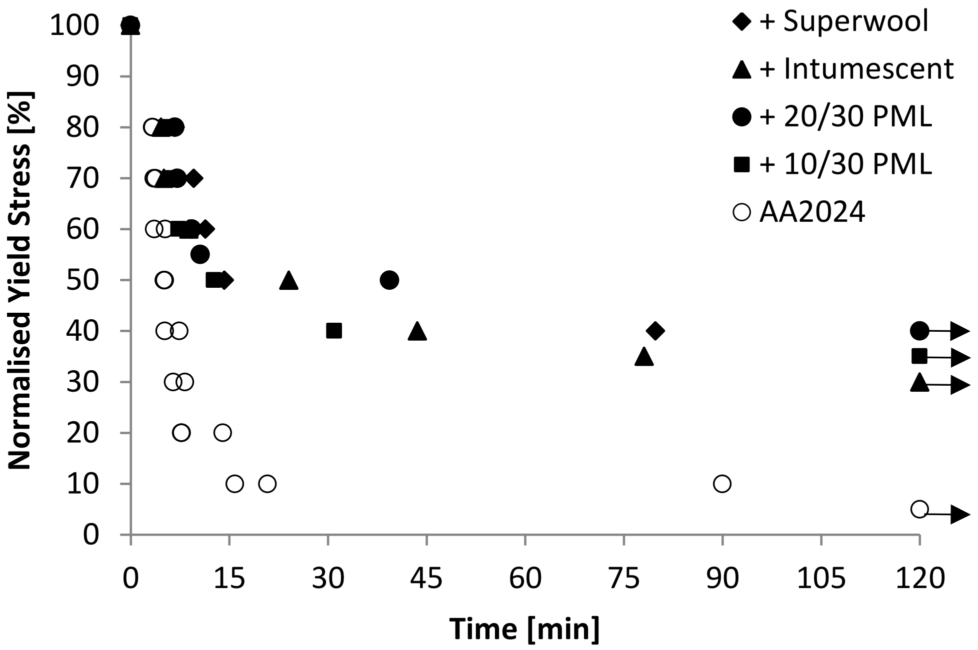

(a) Tension

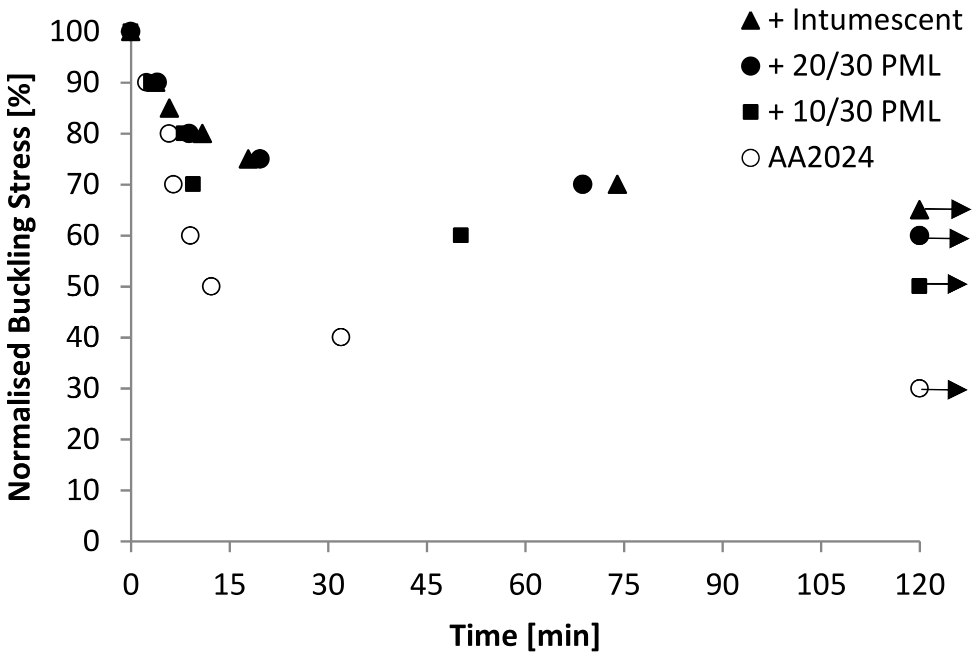

(b) Compression

Figure 7.8: Time-to-failure curves of AA2024 specimens featuring PML in comparison to conventional insulation methods: a) tensile loading, b) compressive loading.

Rear face temperatures which had been recorded during the fire-structural testing of AA2024 specimens featuring all different types of insulation are shown in figure 7.7. From the close affinity of the recorded temperature profiles it can be clearly seen that the two PML systems provide a similar temperature reduction across the sample and thus same insulation efficiency as the conventional insulation methods of inert ceramic blanket or reactive intumescent paint. During the initial transient heating up phase, slightly different rates of temperature increase are noticed which is linked to the different mechanisms involved in the formation of the fire protection effect of each type of insulation. However, steady-state rear face temperatures of 270 °C to 280 °C are reached for long exposure times for all insulated specimens.

As already indicated by the affinity of the temperature profiles, the failure times observed during the testing of all the specimens featuring a thermal barrier show similar characteristics and as anticipated fall onto similar curves (figure 7.8).

7.4 Carbon-Epoxy Composite Substrate

7.4.1 Temperature Development

When exposed to one-sided heating of 50 kW m^{-2} heat flux, the temperature at the front face of an unprotected carbon-epoxy composite sample rapidly increases whereas the back face shows a delayed temperature response. This is because of the material's inherent low thermal conductivity in the through-thickness direction of the CFRP resulting in a pronounced temperature gradient between the front and back faces. With continued irradiation of the specimen the temperature progressively increases through the thickness so that on average at around 600 s exposure time the temperature gradient has diminished and front and rear face have the same temperature.

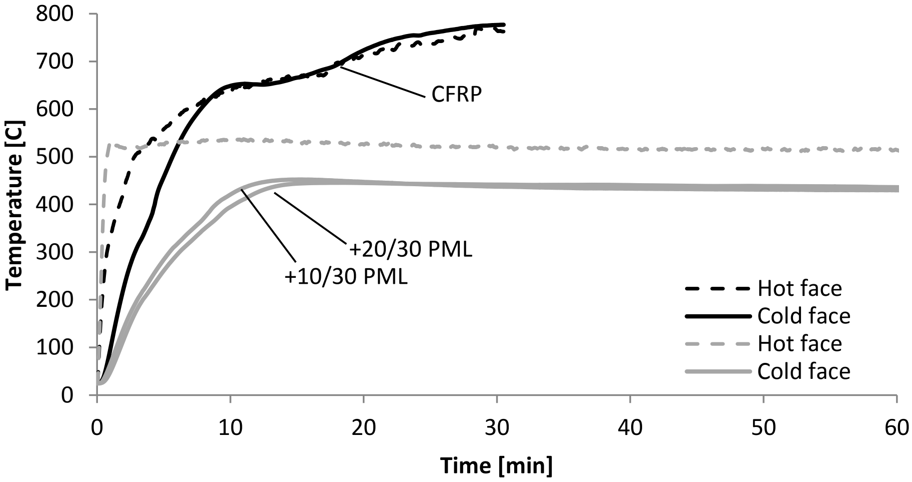

Figure 7.9: Rear face temperature profiles of CFRP specimens with and without PML insulation when exposed to 50 kW m^{-2} heat flux. Dashed lines indicate the temperature curve of the specimen's hot face.

The onset of material decomposition is reached at temperatures in excess of 360 °C. Because of the continued irradiance, the critical point for flaming combustion of the volatiles released during decomposition is passed which leads to continued rise of the CFRP substrate temperature up to 800 °C despite the decomposition reaction being endothermic in character. The sustained smouldering of the combustible material prevents the formation of steady-state conditions, see figure 7.9.

Temperature profiles of PML-covered CFRP specimens exhibit contrasting behaviour. Due to the thermal insulation barrier formed by the PML the temperature increase of the specimen is greatly reduced. A much greater temperature gradient between front and back faces develops, with the back face heating up much slower than in the unprotected CFRP specimens. The great advantage of the application of PML on such a combustible material is the inhibition of the ignition process as the temperatures are not high enough for sustained smouldering which prevents further temperature increase and results in a constant temperature distribution throughout the sample. The PML also provides a shield for oxygen diffusion in addition to the rest of the sample being insulated. In unprotected CFRP substrates the porous char allows oxygen to diffuse into the material towards the decomposition front where ignition is caused. This is prevented with PML thermal barriers. Similar to the AA2024 experiments, the thicker 20-ply PML specimens show a slightly greater front-to-back face temperature gradient during the initial heating up period before similar steady-state conditions as in the 10-ply PML samples with temperatures of around 430 °C at the back face are reached.

7.4.2 Fire-structural Performance

Due to the brittle nature of carbon-epoxy composites the displacement behaviour of these specimens under mechanical loading is characterised by only a small axial deformation, see for example figure 7.10b for a CFRP specimen under tension. The in-plane extension recorded during such fire-structural tension testing is less than 0.5 % strain. Different displacement rates can be detected depending on the applied tensile load percentage with a transition of the failure behaviour occurring between 45 % and 40 % of applied load, which is shown in figure 7.10a. At high tensile loads down to 45 % of the room temperature failure strength, after little initial extension, collective catastrophic fibre failure occurs. For applied stress levels below 40 % the observed displacement rate decreases markedly with a reduction in applied stress. Additionally, the overall sample displacement has increased. Failure of individual composite plies can be recognized which is most distinctive in the 10 % specimen.

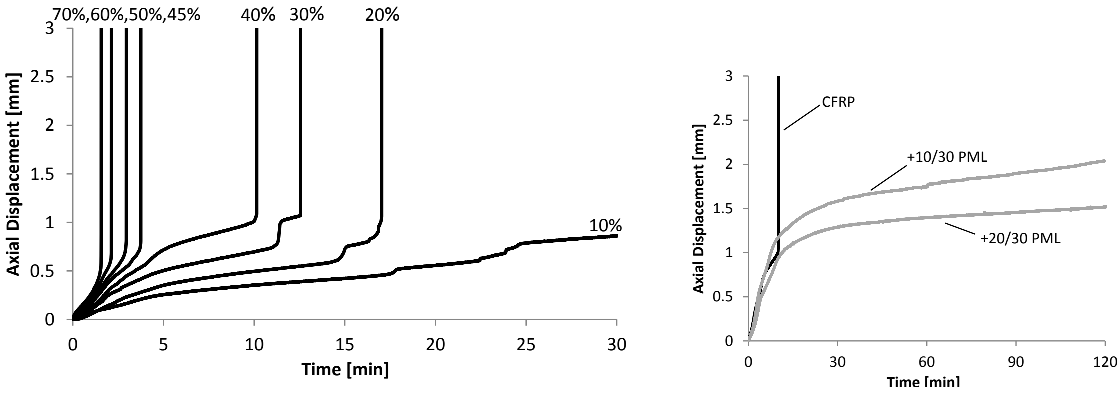

(a) CFRP

(b) CFRP and PML specimens

Figure 7.10: Time-dependent deformation during fire-structural tensile testing: a) Individual displacement curves for pristine CFRP specimens under constant applied load in the range of 70 % to 10 % of tensile fracture strength from left to right, b) Comparison of the recorded deformation in specimens with and without PML protective barrier at an applied load of 40 % tensile fracture stress.

The compressive failure of pristine CFRP specimens is characterised by sudden failure without any axial displacement observed prior to failure, as shown in figure 7.12. PML insulated CFRP specimens show failure behaviour similar to the unprotected samples, both in tension and compression testing. Final compressive failure occurs as a sudden event although with longer failure times. In case of tensile loading, the observed displacement rates are significantly reduced so that failure occurs only after prolonged exposure times. Failure times increase with a reduction in the applied load in

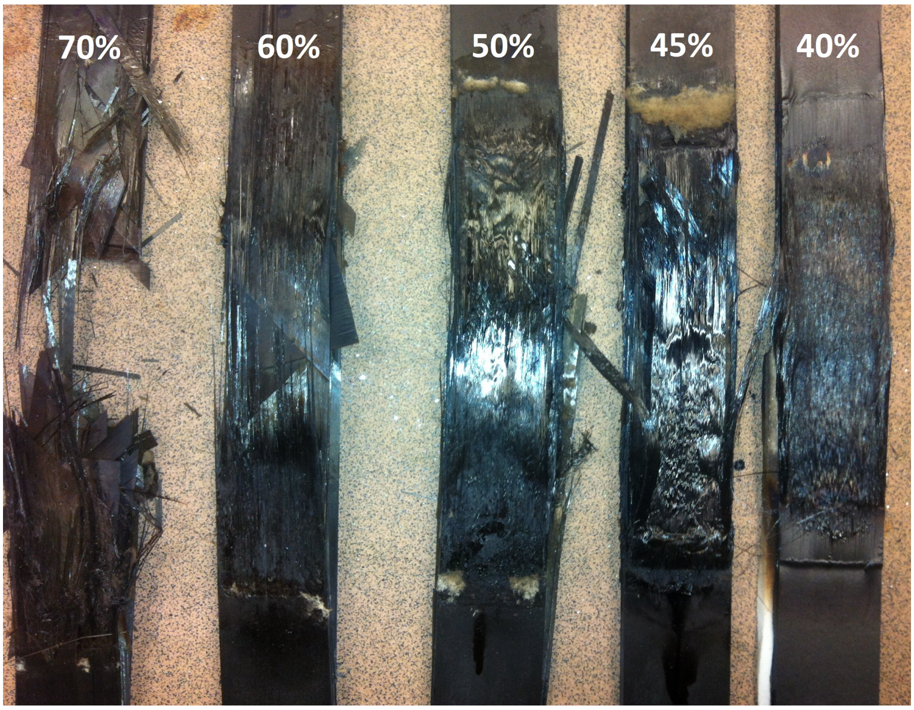

Figure 7.11: Effect of reduction in applied load levels on failure characteristics of unprotected CFRP specimens tested under tensile loading while under exposure to one sided heating of 50 kW m^{-2}.

all cases. Noteworthy in the observation of the failure times for the quasi-isotropic carbon-epoxy samples tested under tensile conditions, is a distinctive plateau that is formed between 45 % and 40 % applied load, see figure 7.14a. It is an indication of a change in failure behaviour and failure mode characteristics.

It is widely recognised that the tensile strength of fibre-reinforced composite materials decreases with increasing temperatures. Therefore, in fire-structural testing the tensile strength of the CFRP material will vary according to the position of the carbon fibre in the through-thickness direction of the sample due to the temperature gradient present leading to an uneven load distribution. The overall strength of the material is assumed to be an average of the load carrying capability of the individual plies depending on their instant thermal status. This is valid for most specimens tested at 45 % load and higher. At these loads, the failure mode is initiated with a softening of the polymer matrix when the glass transition temperature ($\sim$ 200 °C) is exceeded within a short period of exposure time leading to a shift of the load distribution entirely onto the fibre constituents. The inherently high tensile strength of the carbon fibres provides the material's capability to initially support the high loads. Failure occurs when the applied stress is greater than the residual composite tensile strength.

For samples tested at lower tensile load levels failure is dominated by fibre degradation. The applied load is low enough to be sustained for an extended time period despite complete decomposition of the matrix which is caused by continued irradiation and a heating up of the composite. The charred resin has negligible strength but through its rigid structure provides a frame for the carbon fibres which allows them to support the applied load. Eventually the temperature gradient within the sample disappears so that front and back are at the same temperature. This equilibrium temperature is found to be at around 650 °C. At this high temperature thermal degradation in form of oxidation of the carbon fibres occurs which gradually reduces the individual fibre strength leading to an overall reduction of the specimen's strength. The time-to-failure event is determined by the progression of the fibre oxidation under prolonged heat exposure until the stage is reached when the residual strength has declined so much that the applied load cannot be supported and final failure occurs.

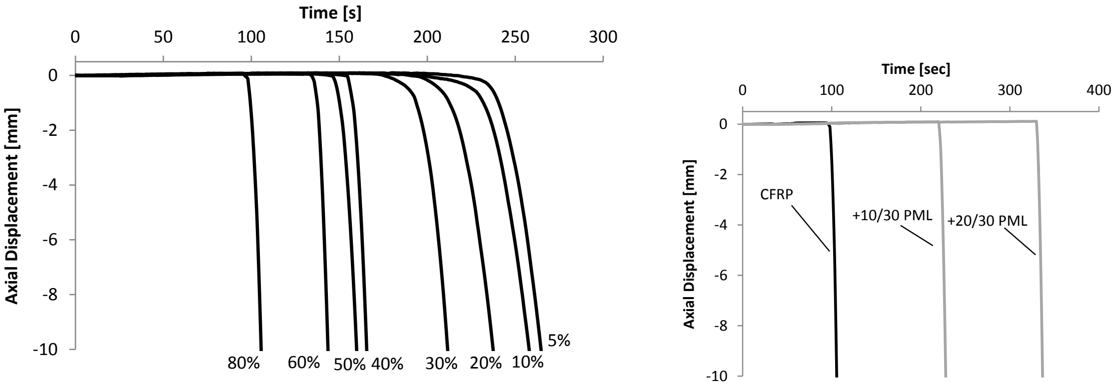

(a) CFRP **(b)** CFRP and PML specimens

Figure 7.12: Time-dependent deformation during fire-structural compressive testing: a) Individual displacement curves for unprotected CFRP specimens under a constant applied load in the range of 80 % to 5 % of the Euler buckling strength from left to right, b) Comparison of the recorded deformation in specimens with and without a PML protective barrier at an applied load of 80 % buckling stress.

Figure 7.13: Effect of reduction in applied load levels (from left to right) on failure characteristics of unprotected CFRP specimens tested under compressive loading while under exposure to one sided heating of 50 kW m^{-2}.

Failure times for PML-protected CFRP substrates tested at high load percentages show similar behaviour to that of the pristine composite substrates but at longer times due to the observed delay in heat transfer. At load levels below 50 % the behaviour deviates from that observed in the unprotected CFRP specimens. Instead of showing a curve featuring a plateau, PML samples exhibit longer and longer failure times which eventually lead to a run-out after 2 hours exposure time below 45 % of applied load. At these load levels the residual strength of the material is high enough to withstand failure for extended times to which the insulation effect of the PML barrier contributes. With a maximum temperature of below 450 °C, fibre oxidation is averted and thus further strength reduction through fibre degradation is prevented. The overall strength of the softened carbon fibres is still high enough to support these applied loads. A distinctive change in failure behaviour between unprotected and protected CFRP specimens can be noticed from visual inspection and comparison of such failed specimens, see figures 7.11 and 7.15. For the unprotected composite fibre pull out caused by delamination for the 45° and −45° plies together with some

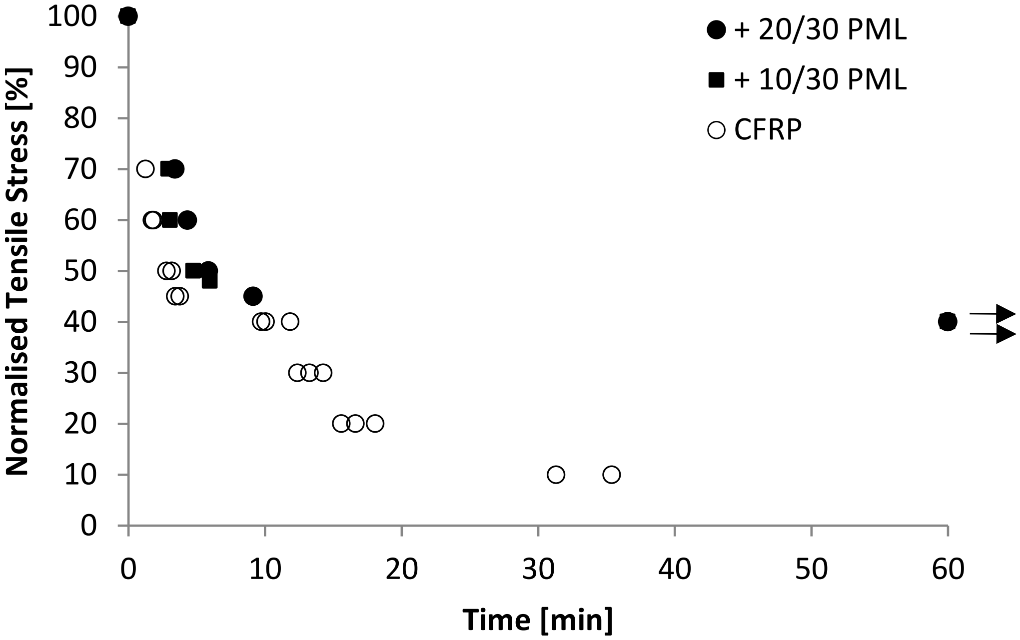

(a) Tension

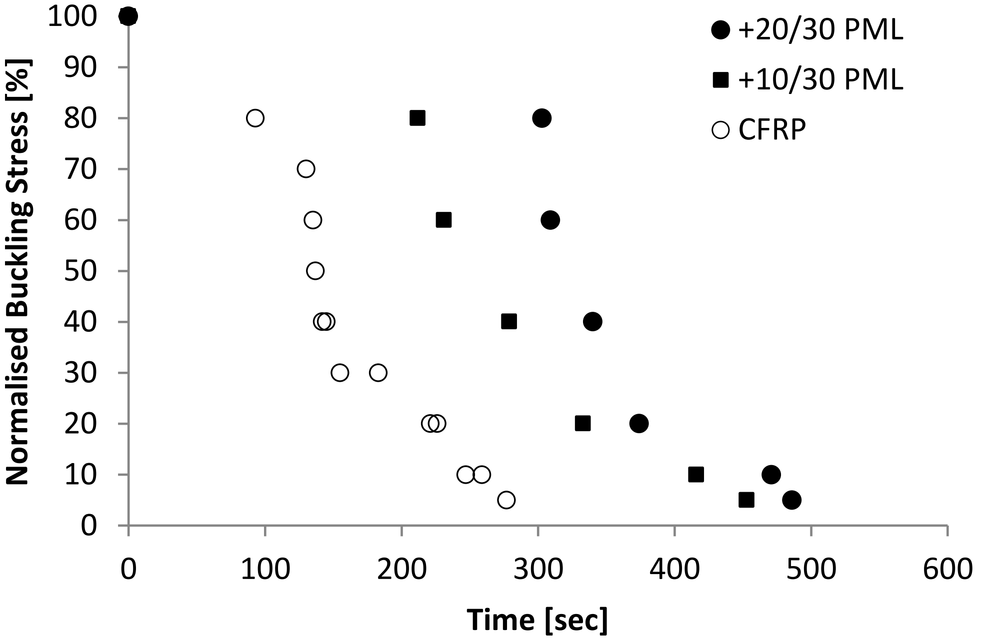

(b) Compression

Figure 7.14: Time-to-failure curves for unprotected and PML-insulated CFRP specimens under structural loading and simultaneous exposure to $50\,\mathrm{kW\,m^{-2}}$ heat flux: a) tensile loading, b) compressive loading. The normalised stresses are in reference to the room temperature failure stresses of the pristine CFRP laminate.

fibre breakage through degradation of the 0° plies can be observed during failure of 70 % and 60 % applied stress. In contrast, for a 10-ply PML insulated CFRP specimen this behaviour is observed for applied stress levels down to 48 %. The specimen tested at 45 % stress shows predominantly fibre breakage through degradation.

In contrast to fire-structural testing under tensile conditions, polymeric composite materials are highly sensitive to compression loading which is reflected, comparatively, in the much shorter failure times, see figure 7.14b. Compressive failure behaviour is dominated by the loss of strength in the polymeric matrix which occurs when its glass transition temperature is exceeded. Due to the matrix softening, delamination of individual laminate plies is initiated which allows the formation of plastic kinking, as shown in figure 7.13. The progression of the heat front in the through-thickness direction of the material consequently reduces the specimen's residual strength until failure occurs. Overall, unprotected CFRP substrates fail within a short time period and the failure curves exhibit only slight improvements in failure time with reduced applied load percentages. CFRP substrates featuring PML show similar trends accompanied by a kinking at longer failure times because of the slower heating up rate of the material.

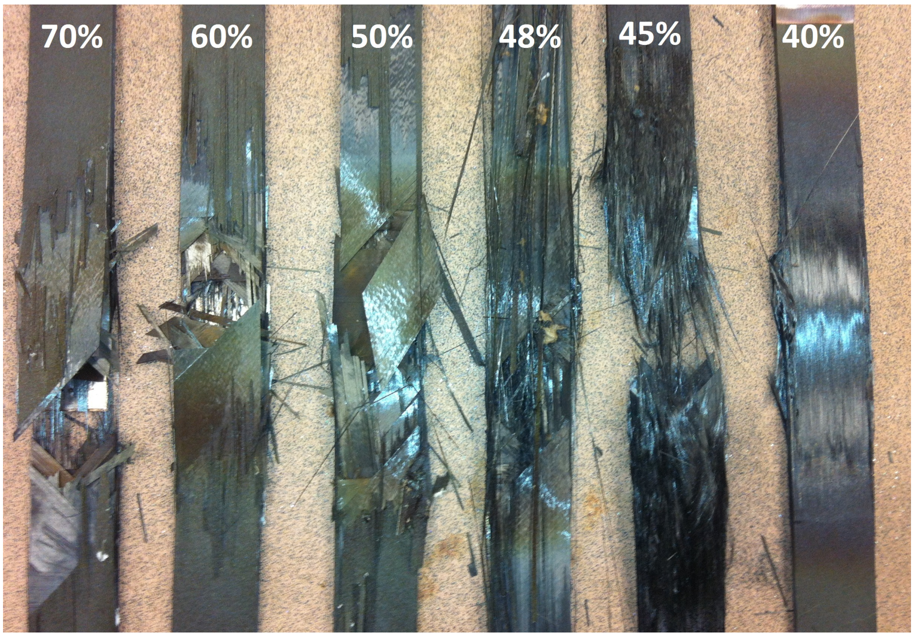

Figure 7.15: Effect of reduction in applied load levels on failure characteristics of CFRP specimen featuring a 10-ply PML tested under tensile loading while under exposure to one sided heating of 50 kW m^{-2}.

7.5 Modelling of Material Peformances

7.5.1 CFRP Laminate Substrate

Modelling the specimen's thermal response is essential to understand and to be able to predict the structural performance of these materials when exposed to one-sided heating. The temperature distribution throughout the carbon-fibre composite material has been determined according to the routines established within the COM_FIRE program. COM_FIRE accounts for the effects of heat conduction under the influence of resin decomposition and volatile mass flow. As most of the thermal properties of the AS4/3501-6 CFRP material were not readily available at the start of this investigation, the necessary property input data has been compiled from the COM_FIRE materials' library; examples of some parameters are listed in table 7.1. Overall, carbon-fibre composite properties have been calculated according to the rule-of-mixtures, based on a fibre volume fraction of 62 %.

Parameter	Resin	Fibre
ρ	$1300\,\mathrm{kg\,m^{-3}}$	$1750\,\mathrm{kg\,m^{-3}}$
c_p	$1850\,\mathrm{J\,kg^{-1}\,K^{-1}}$	$660\,\mathrm{J\,kg^{-1}\,K^{-1}}$
k	$0.35\,\mathrm{W\,m^{-1}\,K^{-1}}$	$0.32\,\mathrm{W\,m^{-1}\,K^{-1}}$
	Composite	
φ_{Fibre}	0.62	
A	$500\,\mathrm{s^{-1}}$	
E_a	$60\,500\,\mathrm{J\,mol^{-1}\,K^{-1}}$	

Table 7.1: Material input data used for thermal simulation of CFRP substrates via COM_FIRE.

The simulated temperature profile across the entire sample thickness of a 6.7 mm CFRP substrate is pictured in figure 7.16. The initial heating-up phase is characterised by a steep temperature increase in the sample followed by a more gradual thermal gradient throughout the sample which is established due to resin decomposition. After about 10 minutes steady-state conditions are reached with the formation of a stable thermal gradient of about 70 °C across the substrate thickness. At this point there are no further reactions to be initiated within the model once the decomposition reaction of the polymeric resin has come to an end. The temperature profile continues on the same level even if the test duration, i.e. heat exposure time, was to be extended beyond the simulation run time of 30 minutes.

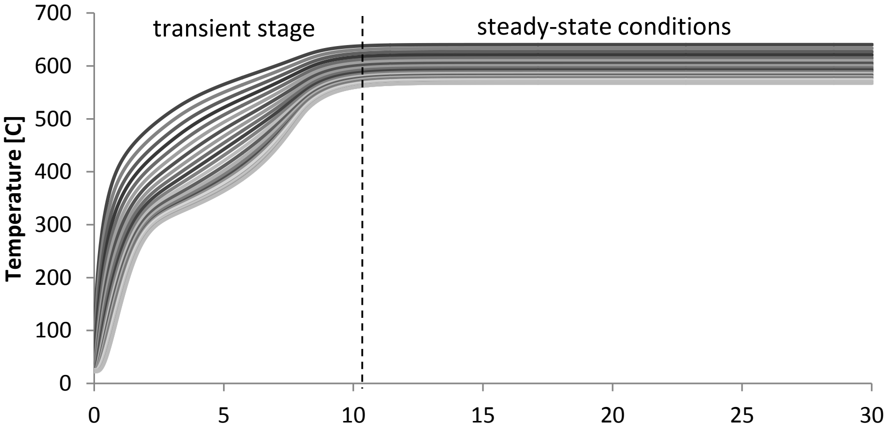

Figure 7.16: Temperature development through the thickness of a 6.7 mm CFRP substrate exposed to one-sided heat flux of $50\,\mathrm{kW\,m^{-2}}$. Each data curve represents the temperature increase for an individual composite laminate ply. The top curve represents the heat source facing front face whereas the lowest curve depicts the temperature rise of the cold face.

Despite using only single-value material properties as input data instead of the more sophisticated and more accurate temperature dependencies, the simulated temperature curve closely fits the experimental thermocouple readings. The model is able to accurately capture the temperature increase during the initial transient stage of the heat conduction process as shown for the front and rear face of an unprotected CFRP specimen in figure 7.17.

With the transition to steady-state conditions after 10 minutes of exposure time, the course of the modelled curves noticeably diverges from the experimental readings. Whilst the exposed specimen experiences a continued temperature increase due to the accumulation of heat arising from the ongoing thermal degradation and continued smouldering, the simulation predicts constant temperature levels between 640 °C and 570 °C throughout the material. This discrepancy is due to the fact that the COM_FIRE program currently does not facilitate incorporating the additional reactions or have the equations programmed in order to capture the behaviour at the later stages of a heat exposure experiment.

Additional information about the degradation process is provided by the COM_FIRE model through the variable *RRC* which describes the progression of the decomposition reaction in the matrix's remaining resin content (RRC). The difference from the *RRC* value to 100 % at any given location within the specimen and testing time represents the amount of organic matter that has been transformed into gaseous by-products during the decomposition reaction. Figure 7.18 visualises the resin degradation profile over the thickness of the composite substrate with every laminate ply being represented by an individual curve in the diagram. The maximum level of 100 % characterises the undamaged material whereas the minimum denotes the end of the decomposition reaction for the individual plies as the condition of residual char is reached. It can be seen that due to the direct exposure to the heat source the front layer of the CFRP material experiences a much faster degradation (curve furthest left) than the back face which in contrast shows a much slower material loss due to the thermal lag (curve furthest right).

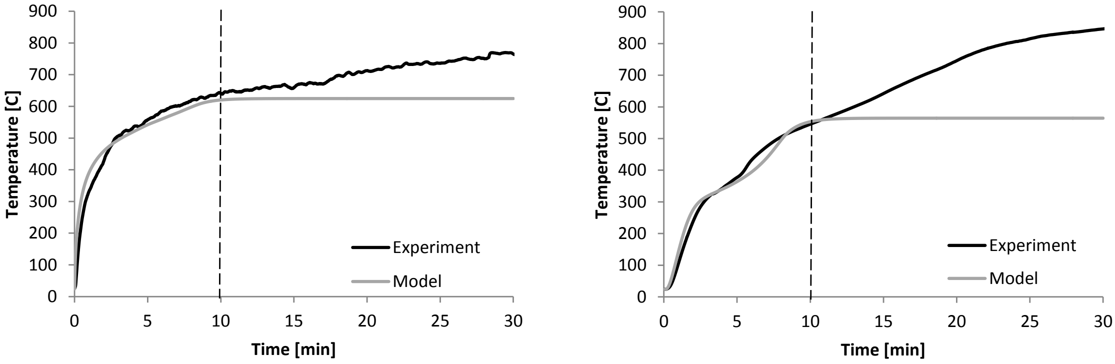

(a) Hot Face **(b)** Cold face

Figure 7.17: Comparison of CFRP temperature profiles obtained during fire-structural testing with results from the simulation run. The vertical line indicates the time boundary beyond which the modelled temperature curves significantly diverge from the experimental one.

Failure Correlation - Compression

The thermal status of the material determines the mechanical performance during a fire-structural heat exposure tests. A simplified way to analyse the experimental behaviour is to compare the thermal characteristics with the structural parameters. This is an alternative to the comprehensive methodology of *Lamina Theory* which uses the thermal and mechanical condition of the individual composite plies in order to successfully describe composite failure under heat influence. However, it requires extensive additional testing to determine the detailed structural material characteristics and their temperature dependencies.

As mentioned in the description of the experimental results in section 7.4.2, the performance of fibre-reinforced polymeric composites during fire-structural testing under compression loading is dominated by the degradation behaviour of the organic matrix. Therefore it is considered legitimate to analyse the temperature and RRC profiles across the material's thickness which are obtained from the COM_FIRE model at the point in time when structural failure had been observed during the experiments. The recorded failure times in case of 50 kW m^{-2} heat exposure experiments are all found to be below the threshold of the transition from transient to steady-state conditions. Above

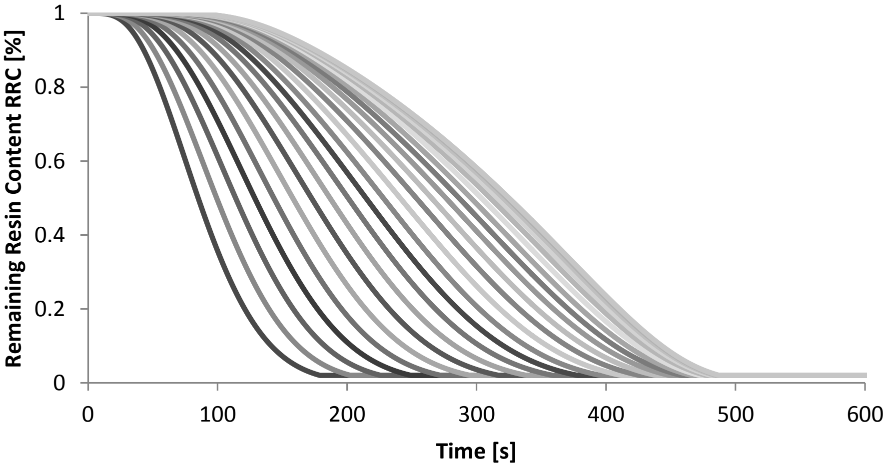

Figure 7.18: Illustration of the degradation progression through the thickness of the CFRP composite material during one-sided heat exposure of $50\,\text{kW}\,\text{m}^{-2}$ by means of the RRC parameter calculated during the simulation.

that threshold major discrepancies between experimental and modelled temperature profiles occur. Thus, an accurate inference of the thermo-structural relationship is assumed when the failure has occurred during the transient stage of the heat transfer process.

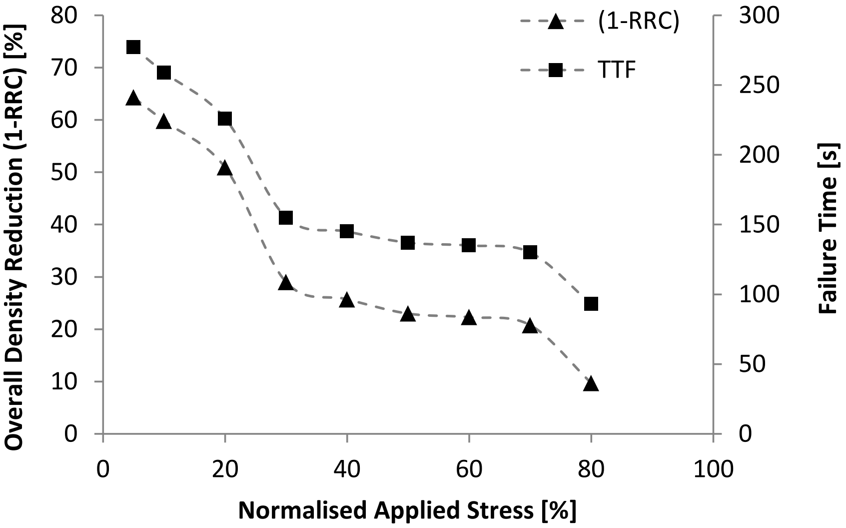

Figure 7.19: Comparison of failure times (TTF) and density reduction(1-RRC) in dependence of the applied compressive load percentage levels during fire-structural testing of unprotected CFRP specimens.

Figure 7.19 shows the time-to-failure curve for the CFRP substrate under compression alongside an overall density reduction defined as the inverse overall RCC parameter which in turn is taken as the average RRC value over every laminate ply at the time of failure. It can be seen that both parameters show identical behaviour in their dependency on the externally applied stresses during the experiments. Consequently, plotting the failure times as a function of the overall RRC of the CFRP material yields a linear relationship between the two parameters, see figure 7.20. As the parameter RRC is only introduced during the simulation procedure it is regarded more sensible and practical to translate this into an overall material density variable according to the rule-of-mixtures criterion. The determination of the overall density parameter as well as the linear relationship

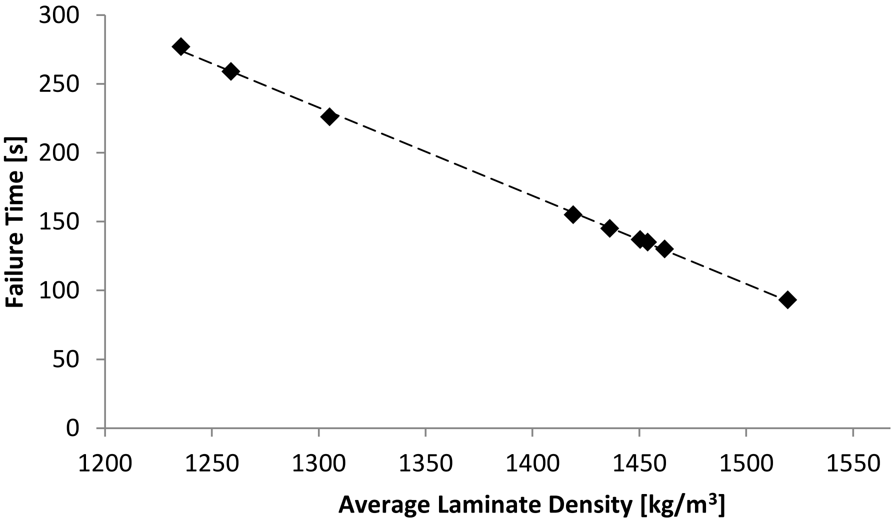

Figure 7.20: Linear relationship between overall CFRP laminate density and structural life time under compression loading.

between the parameters can be expressed via the following equations.

$$\rho_{CFRP} = \varphi_{Fibre} \cdot \rho_{Fibre} + (1 - \varphi_{Fibre}) \cdot \rho_{Resin} \cdot RRC \tag{7.1}$$

$$TTF = -0.64 \cdot \rho_{CFRP} + 1065 \qquad with \quad R^2 = 99.92\% \tag{7.2}$$

Equation (7.2) gives the predicted failure times for specific load levels not tested so far under 50 kW m^{-2} heat flux irradiance. Additionally, it should also be possible to yield reasonable estimates on the range of failure times to be expected for different fire scenarios based on the above conclusions.

It is necessary in all cases to run a simulation with COM_FIRE at the required heat flux level in order to determine the thermal state of the composite material. With the assumption that structural failure resulting from specific applied stress levels is induced at the same level of strength and thus the same state of deterioration in the material as between the different heat fluxes, failure times can be obtained from the corresponding RRC or density profiles. In figure 7.21 such an example is given for the case of a 35 kW m^{-2} heat flux fire scenario which represents a fire originating from small rubbish bin, widely used for aircraft interior material's classifications. The expected shift towards longer structural life times with a reduction of the heat flux from 50 kW m^{-2} to 35 kW m^{-2} becomes apparent.

Failure Correlation - Tension

The behaviour of composite laminates during simultaneous thermal and tensile loading is dominated by the performance of the reinforcing fibres under the temperature influence. The structural survival time of a specimen under heat exposure is dependent upon the lifetime of the fibres and the manner of the reduction in their strength due to increasing temperatures.

The same modelled temperature profile as shown in figure 7.16 is valid for tensile loading conditions as there has been no significant difference observed in the experimental temperature readings during tests carried out on samples under compressive or tensile loading. Because of the high tensile strength of the carbon fibre, the failure times for tension tests occur after much longer heat exposure times, compared with tests carried out under compressive loading. As a consequence, it becomes apparent during the analysis of the failure temperatures (figure 7.22), i.e. the temperatures that are present within the CFRP specimens at the point of failure, that specimen failure only occurs under applied stresses of 70 % down to 45 % during the transient stage

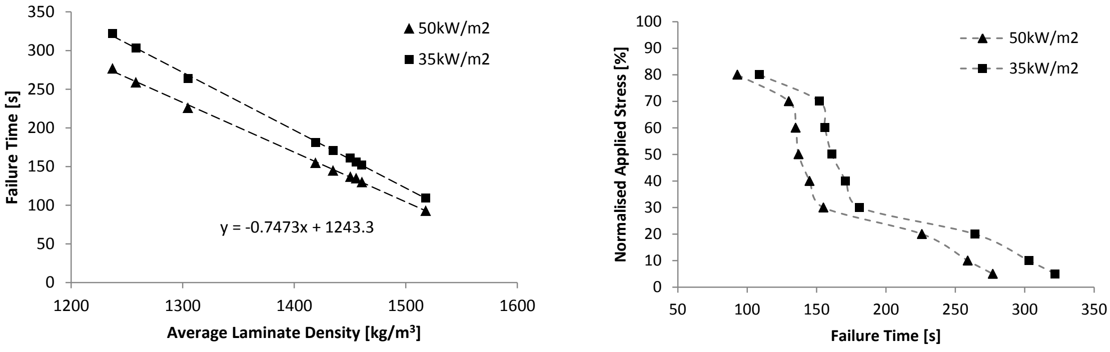

(a) **(b)**

Figure 7.21: Simulated compressive behaviour of a pristine CFRP composite laminate during a 35 kW m^{-2} fire scenario in comparison to experimental data obtained at 50 kW m^{-2} irradiance: a) Time-to-failure as linear function of overall laminate density, b) Extended life time for CFRP specimens tested at the lower heat flux.

of the modelled temperature profile. Failure times for tests carried out at lower applied stresses fall into the region of steady-state conditions which is contrary to experimental observations and does not reflect understood specimen characteristics. At high loading levels the failure is caused by an outright strength reduction of the composite laminate because of the elevated temperatures present within the specimen. However, at 400 °C the inherent material strength of the AS4/3501-6 composite has only been reduced to about 50 % of its room temperature tensile strength which enables the material to withstand lower stress levels during fire-structural testing for extended periods of times.

For cases of specimens experiencing failure during the transient heating up stage of heat exposure, a similar analysis of residual strength and failure times, taking into consideration the temperatures present within the material, is undertaken analogous to the investigation presented for compressive behaviour. Figure 7.23 depicts the dependence of the failure times on the applied stresses for 50 kW m^{-2} heat flux. The reference curve gives the determination of failure times of specific loading cases under these test conditions along this curve. On the assumption that failure for individual loading cases relates to a specific temperature distribution within the specimen at the point of failure, failure times of CFRP specimens exposed to 35 kW m^{-2} irradiance and tensile loading are predicted. The temperature profile of the CFRP material under 35 kW m^{-2} heat flux exposure sees an overall tendency for temperatures to be reached after longer times and with slightly lower temperatures. The transition from transient to steady-state occurs at around 14 minutes with a stable thermal gradient between 591 °C and 525 °C being established. A clear shift to a longer structural lifetime is forecast with the transition to the lower heat flux, which is represented by the second curve in figure 7.23. Improvements of about 15 % may be achieved in the case of 70 % applied tensile stress whereas the failure time for a specimen tested under 45 % applied stress is predicted to increase by about 36 %.

Predictions of failure times of specimens tested under low stress levels are not feasible with this simplified analysis because in these cases degradation of the reinforcing carbon fibres is initiated as the result of the prolonged exposure times and hence high temperature levels within the material. Thus, it is neccessary to perform tensile testing on the CFRP material under isothermal testing conditions to determine the material's strength reduction at elevated temperatures as well as investigating the degradation behaviour and thus high-temperature strength characteristics of the carbon fibres.

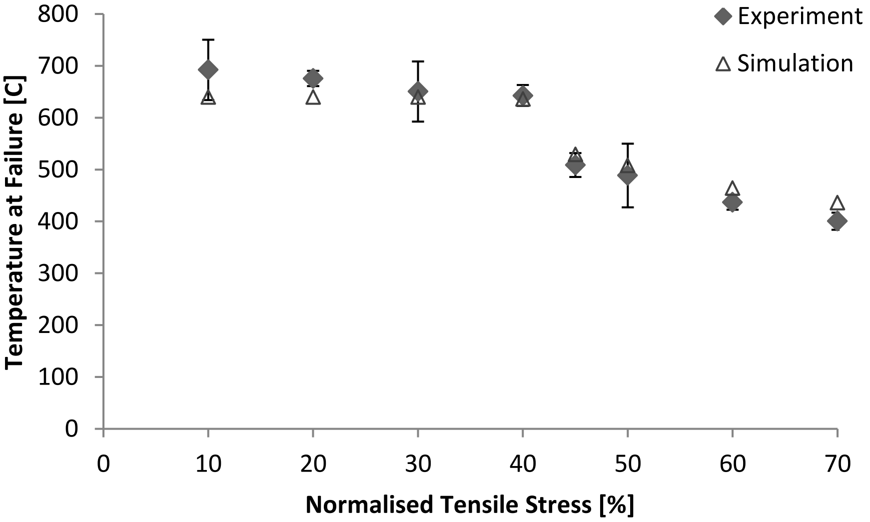

(a) Hot face

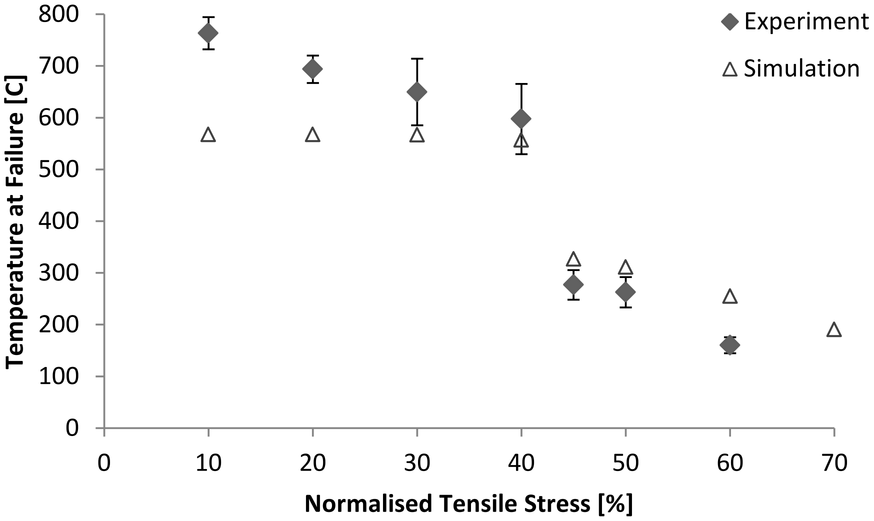

(b) Cold face

Figure 7.22: Illustration of sample temperatures present at the point of failure for the a) hot and b) cold face of the CFRP specimen during tensile loading and simultaneous $50\,\mathrm{kW\,m^{-2}}$ heat flux irradiance. Comparison of experimental (diamond) versus simulated (triangle) data points.

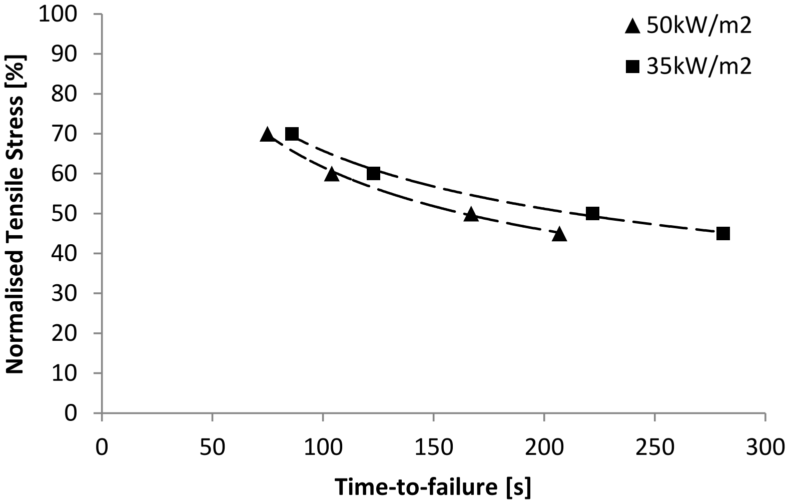

Figure 7.23: Estimation of the fire-structural performance of a CFRP composite laminate during a $35\,\mathrm{kW\,m^{-2}}$ fire scenario when simultaneously loaded under tension. Prolonged failure times for those CFRP specimens exposed to the lower heat flux in comparison to reference samples under $50\,\mathrm{kW\,m^{-2}}$ heat flux irradiance are observed.

7.5.2 CFRP Laminate Substrates featuring PML Protection

The successful replication of the thermal behaviour of unprotected CFRP laminates justifies the incorporation of the routines used in COM_FIRE for pristine composite materials into the newly-developed PML_FIRE model. In order to be able to describe the thermal behaviour of CFRP substrates featuring PML, a combination of the heat principles developed for PML protective layers bonded to aluminium plates and the COM_FIRE routines have been implemented into PML_FIRE.

Figures 7.24 and 7.25 present the experimental and modelled temperature development that the hot and cold faces of PML-protected CFRP laminates of 10-ply and 20-ply experience, respectively, during fire-structural testing at $50\,\mathrm{kW\,m^{-2}}$ irradiance. In contrast to the modelling of the unprotected CFRP specimens where considerable affinity was seen, the predicted temperature curves for 10- and 20-ply PML specimens noticeably deviate from the experimental results. Despite the hot face temperatures agreeing with the modelled temperatures, confirming therefore the correct heat input into the specimen, the modelled rear face temperatures only follow the experimental curve accurately for an initial phase of about 6 minutes for the 10-ply PML and 9 minutes for the 20-ply PML before the curves develop into a plateau at lower temperatures than observed in the experimental profile.

Numerous modelling attempts have been carried out in order to reconcile this discrepancy but a solution explaining this anomaly has been elusive at this stage. The difference in the temperature profiles might be as the result of not capturing a complete picture of the characteristics of each of the individual material sections. This potential explanation is indicated because it seems that the predicted thermal gradient across the PML is too high when compared with the experimental curves. This could also be caused as a result of the differing PML thermal behaviour, where one is bonded to a CFRP composite substrate and the other is bonded to a highly conductive AA2024 substrate which draws thermal energy away from the heated zone of the specimen due to its considerable capacity to act as a heat sink. In contrast, the CFRP material has much lower thermal conductivity and consequently retains the heat nearer the source. It is also possible that due to the simplification of the modelling approach some effects, such as heat accumulation or other side effects caused by the decomposition reaction, might cause higher temperatures than those predicted.

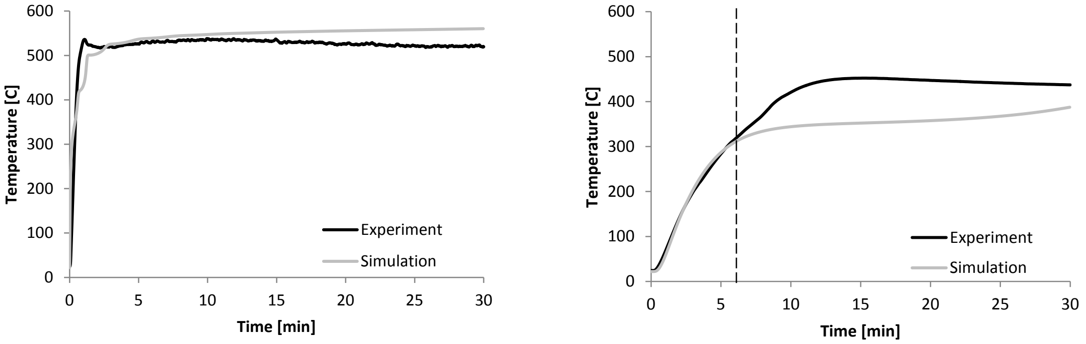

(a) Hot Face **(b)** Cold face

Figure 7.24: Comparison of the experimental (black curve) and simulated (grey curve) temperature profiles for a CFRP specimen covered by 10-ply PML exposed to $50\,\mathrm{kW\,m^{-2}}$.

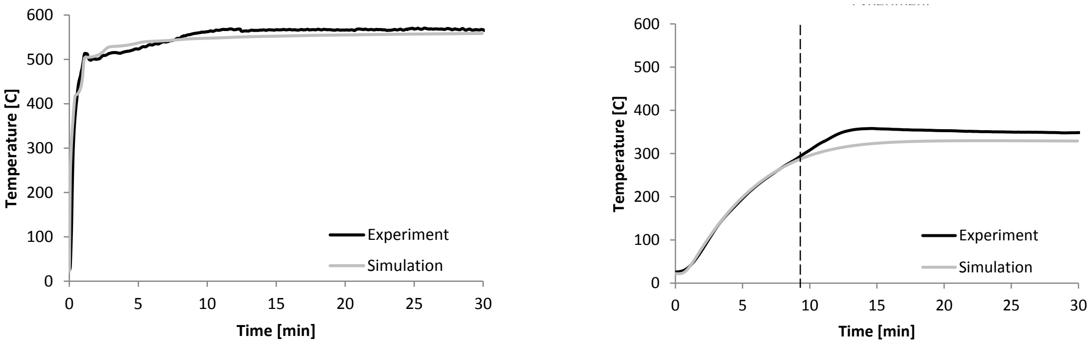

(a) Hot Face **(b)** Cold face

Figure 7.25: Comparison of the experimental (black curve) and simulated (grey curve) temperature profiles for a CFRP specimen covered by 20-ply PML exposed to $50\,\mathrm{kW\,m^{-2}}$.

Failure Correlation

Investigating the failure characteristics of PML-covered CFRP specimens by means of analysing the thermal status of the material at the point of failure is impeded by the aforementioned issues. Predictions for the material's performance when exposed to different fire scenarios are not possible because of the lack of accurate temperature profiles.

However, concordant thermal behaviour is observed for the initial heating up phase of the material until the simulated curve diverges from the experimental results. The failure times observed during fire-structural experiments carried out under compression and $50\,\mathrm{kW\,m^{-2}}$ heat flux all fall within this section of the curve. Figure 7.26 shows the cold face temperatures at the point of failure over the applied range of percentage stress. The close correlation of the experimental and simulated temperature values is noteworthy. There is only a slight deviation occurring at the lowest stress levels for the 20-ply specimen where it is observed that the failure times are located close to the divergent point of the two temperature curves. In contrast, similar conclusions in the case of tensile loading can only be drawn for stress levels down to 40 % and 45 %, see figure 7.26a, due to the long structural survival time that carbon fibres possess which results in failure only after much longer heating times, in comparison with specimens tested at the same stress level under compressive loading.

With regards to the failure performance reverse conclusions can be drawn from the relationship between the failure temperature and the applied stress level. The trend lines of the curves for the individual CFRP specimens featuring either a 10-ply or a 20-ply PML can be used to identify the cold face temperature at the point of failure for specific loads in cases not previously tested. With the temperature determined, the simulated temperature profile can be used to find the corresponding testing time for this temperature which will indicate the estimated failure time under the applied testing conditions. A few examples are shown in figure 7.27 which includes additional data points from the reverse analysis for both types of PML protection bonded to CFRP composite substrates.

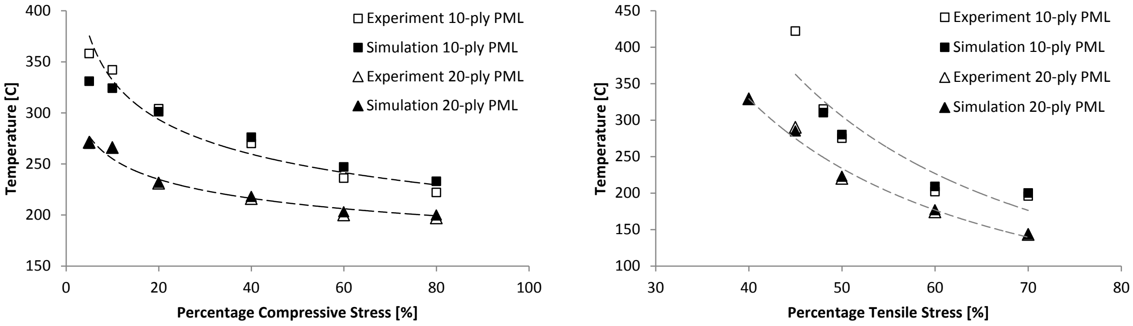

(a) Compression

(b) Tension

Figure 7.26: Comparison of experimental (open symbols) and simulated (closed symbols) temperatures at the point of failure for the two different types of PML protection.

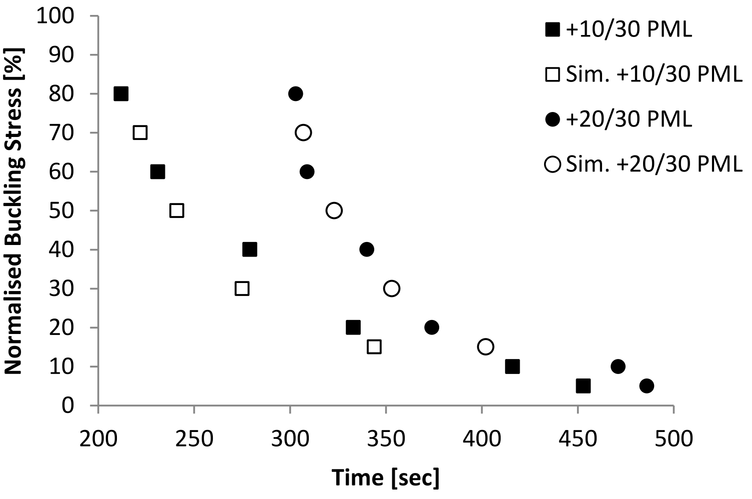

Figure 7.27: Predicted time-to-failure data obtained via reverse analysis based on the temperature at failure. Simulated results are represented by open symbols besides the experimental data points depicted as solid symbols.

7.5.3 AA2024 Substrate

As an example for a nonreactive, passive substrate material, simple one-dimensional heat conduction principles can be applied to model the heat transfer in the through-thickness of an AA2024-T351 specimen when exposed to one-sided heating. The boundary conditions are defined as a radiative heat flux of $50\,\mathrm{kW\,m^{-2}}$ at the hot face and an insulated back face. Yet, once again the simulation results do not agree with the experimental findings with the calculated temperature profile exceeding the maximum experimental temperatures by about 300 °C. This is indicated by the top curve labelled $h = 0$ in comparison to the experimental curve as shown in figure 7.28. This apparent

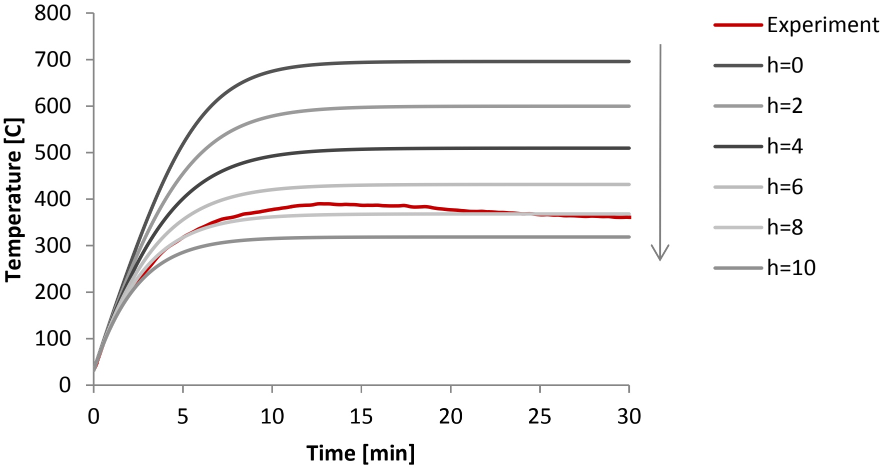

Figure 7.28: Effect of variation in heat loss parameter on the back face temperature of a AA2024 specimen.

mismatch arises from the high thermal conductivity in all directions of the aluminium specimen. The result is that during the heat exposure of the fire-structural tests a significant proportion of thermal energy is transferred away from the specimen's centre towards the vertical ends of the long slender specimens where it is held by the metal grips of the testing machine which present a great heat sink potential. Consequently, a considerable temperature gradient develops along the longitudinal dimension of the aluminium specimen with the thermal energy being drained from the through-thickness direction which, consequently, is unaccounted for in the one-dimensional heat transfer analysis.

An alternate way to overcome this problem would be the application of a two- or even three-dimensional heat transfer analysis in order to account for the complex heat transfer. This would inevitably lead to elaborate coding in combination with an enormous increase in computation time which results in further complications when these principles are to be applied to specimens consisting of a PML protective layer bonded to an AA2024 substrate. However, one-dimensional heat transfer analysis could still be applied as long as the thermal energy that is drawn away by the heat sink is accounted for in the heat transfer equations. One of the options is to introduce a new parameter quantifying the apparent heat loss at every time step and every node of the simulation. This is achieved in the form of a heat transfer coefficient h_{loss} that in relation to the instantaneous temperature difference defines the amount of thermal energy withdrawn due to the heat sink potential of the testing machine.

The quantification of the parameter h_{loss} is impossible to estimate from the experimental setup without a full dimensional analysis, knowledge of the thermal properties of all of the elements as well as extensive multidimensional thermal analysis. A parametric study presents an easier solution in determining this parameter by varying it until a reasonable fit of the experimental temperature curve and the simulated one is achieved. Figure 7.28 shows the development of the temperature profiles dependent upon the heat loss parameter for various simulation runs. The optimum parameter h_{loss} has been found to equal $7.5\,\mathrm{W\,m^{-2}\,K^{-1}}$. The conformity of the simulated temperature profile with the experimental result is shown in figure 7.29. From this graphic it will be seen that for longer testing times the curves slightly diverge, with the simulated curve remaining at a steady-state temperature level whereas the recorded temperature profile shows a slight diminution in temperature. This is most likely to be due to unaccounted heat losses through the insulation material or simply because the rear face has not been perfectly insulated.

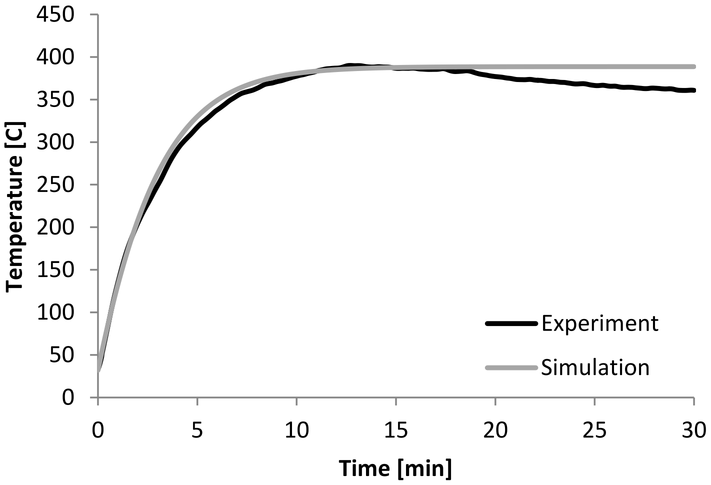

Figure 7.29: Simulated curve and experimental data for temperature increase in a AA2024 specimen subjected to $50\,\mathrm{kW\,m^{-2}}$ heat flux.

Failure Correlation - Tension

Analogous to the simplistic failure analysis presented for the CFRP substrates, similar statements can be made for the investigation of the failure behaviour of aluminium substrates. Two different failure modes have been observed during the fire-structural testing of AA2024 specimen: at high loading levels failure occurs due to the strength reduction in the material associated with a rising temperature, and at low loading levels failure is induced by creep due to extended exposure time at high temperatures. The former failure mode is solely dependent on the temperature distribution within the material as this determines the instantaneous strength of the material. Because of the high thermal conductivity of the aluminium there is virtually no thermal gradient present within the metal specimen. Therefore, the recorded cold face temperature can be directly used as indicator for the material's instantaneous strength which in turn dictates the structural life.

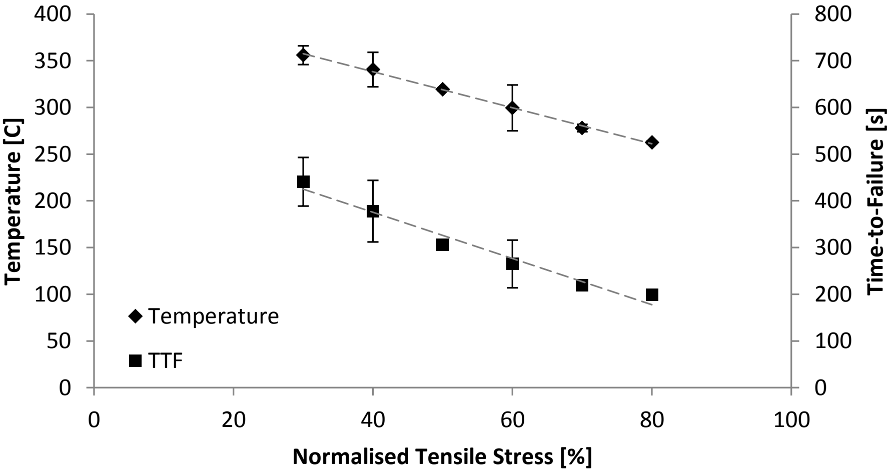

Figure 7.30: Comparison of failure times and temperatures at failure both presented as function of applied tensile stress percentage.

In experiments carried out under tensile loading, the aforementioned assumptions relate to percentage stress levels down to 30 % of the applied load. This can be seen from the temperature profile curve as the recorded failure times for these stress levels occur within the initial transient stage of the heat transfer as well as according to the displacement curves before steady-state conditions are established, which is after about 13 minutes. In contrast, specimens tested at stress levels below 30 % clearly exhibit creep-characteristic behaviour because of the prolonged exposure to stable temperatures of 385 °C. Failure in these samples occurs during the secondary stage of the creep deformation process. Plotting the failure times and the final temperatures at the point of failure as against the applied stress levels reveals a near-linear relationship for specimens experiencing failure during the transient heating up phase, see figure 7.30. Time-to-failure can be expressed directly as a function of the temperature observed at the point of failure, as presented in figure 7.31, which in turn is an indicator for the material's residual strength level as outlined before.

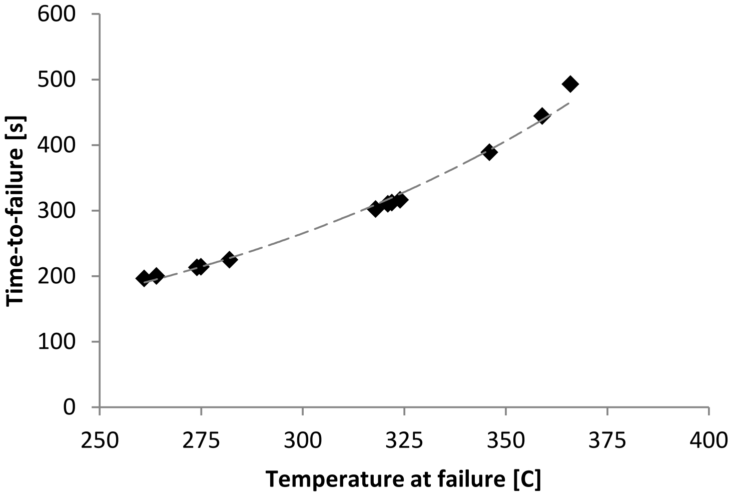

Figure 7.31: Failure times presented as function of the AA2024 specimen's temperature at the point of failure.

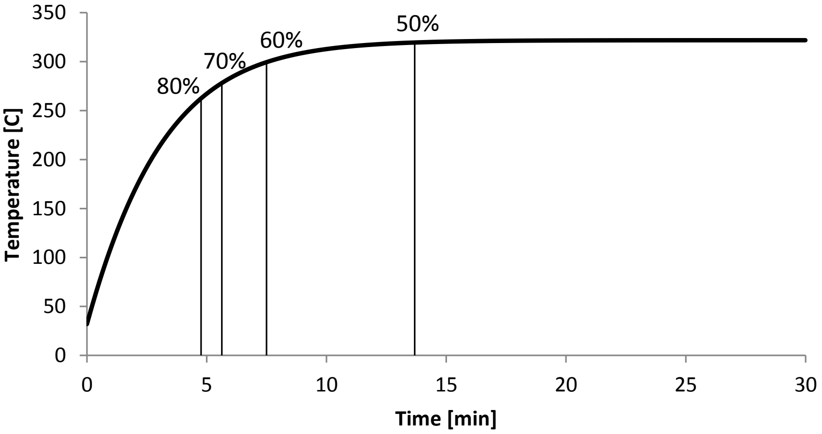

Figure 7.32: Estimated time-to-failure from experiments carried out at different applied tensile stress levels added as indicators to the simulated temperature profile of AA2024 subjected to 35 kW m^{-2} heat flux.

This relationship allows on the one hand for the assessment of other load levels applied during a 50 kW m^{-2} fire-structural experiment and on the other hand for predictions of failure behaviour during the transient stage of temperature increase for fire scenarios with different heat fluxes. In figure 7.32 the predicted failure analysis results have been added to the simulated temperature profile of a AA024 specimen exposed to a 35 kW m^{-2} heat flux. Great improvement of failure times and hence the structural life can be observed in comparison with the failure times presented for specimens exposed to 50 kW m^{-2} (figure 7.30). At a stress level of 80 % the specimen's lifetime is extended by about 44 % for the lower heat flux experiment; at 60 % stress time-to-failure increases by about 70 %.

However, care does need to be taken to assess the limitations of these results. They present the means to estimate the tendency of how much improvement can be achieved. Inaccuracies, however, can occur when the failure times coincide with the transition from transient to steady-state conditions in the temperature profile or fall completely into the region of stable temperature distribution. For the 35 kW m^{-2} heat flux example, this applies to stress levels of 50 % and below, although it cannot be ignored that specimens loaded with 60 % stress level are additionally affected by creep. The predicted failure times might therefore be taken as a minimum safety level as the life expectancy will be significantly affected by the specimen's creep behaviour.

Failure Correlation - Compression

AA2024 presents a better material choice for elements under compressive loads whilst simultaneously exposed to 50 kW m^{-2} heat flux irradiance, in comparison for example, to fibre-reinforced composite laminates. Failure related purely to temperature-dependent strength reduction occurs at stress levels down to 60 % as a result of the applied test load. An overall strong non-linear relationship between failure time and temperature at failure is observed, as shown in figure 7.33. Extensive displacement behaviour is observed for specimens tested below the 60 % stress level which cannot be captured via simplistic temperature-lifetime relationships.

As far as predicting the failure behaviour at 35 kW m^{-2} heat flux irradiance, an improvement of almost 40 % in cases of 90 % loading level is forecast. However, any tests carried out at stress levels below that will exhibit failure times falling into the region of steady-state temperatures together with extended deformation, which cannot be assessed.

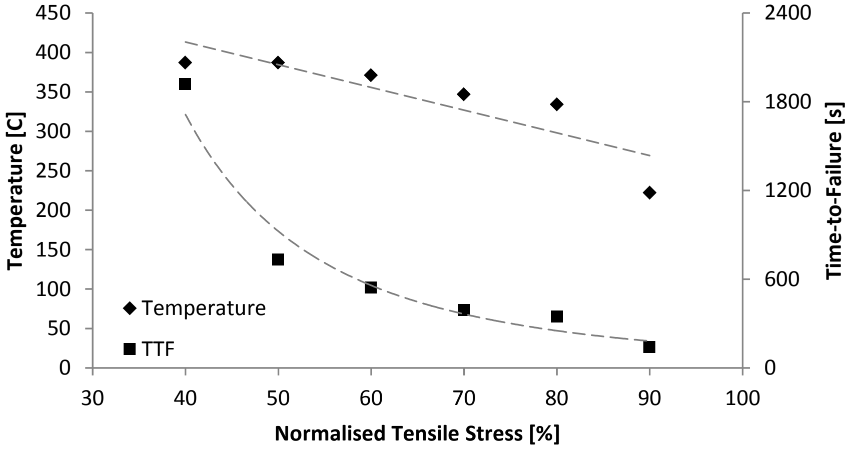

Figure 7.33: Comparison of failure times and temperatures at the point of failure for unprotected AA2024 specimens. Both presented as functions of the applied compressive stress percentages.

7.5.4 AA2024 Substrates featuring PML Protection

The newly-developed PML_FIRE simulation provides the means to model the thermal performance of PML protected AA2024 substrates during fire-structural testing. For this particular test setup, the material's characteristic decomposition behaviour and consequent PML expansion are considered during the heat transfer evaluation. However,the melting of the aluminium foils which is another major factor influencing the temperature behaviour of the speciemns is not accounted for in the program because the heat fluxes applied to the samples during the fire-structural testing below 75 kW m^{-2} heat flux do not provide enough energy to induce foil melting.

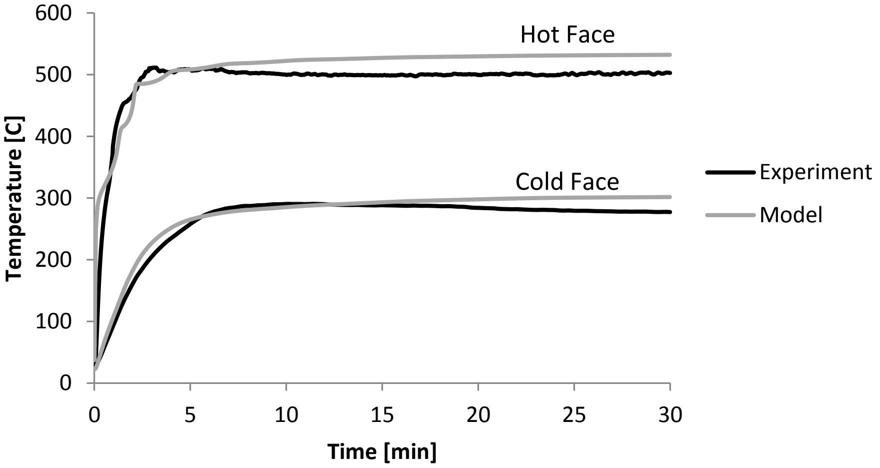

Figure 7.34: Front and rear face temperatures of a AA2024 specimen featuring a 10-ply PML protective surface layer during heat exposure at 50 kW m^{-2}.

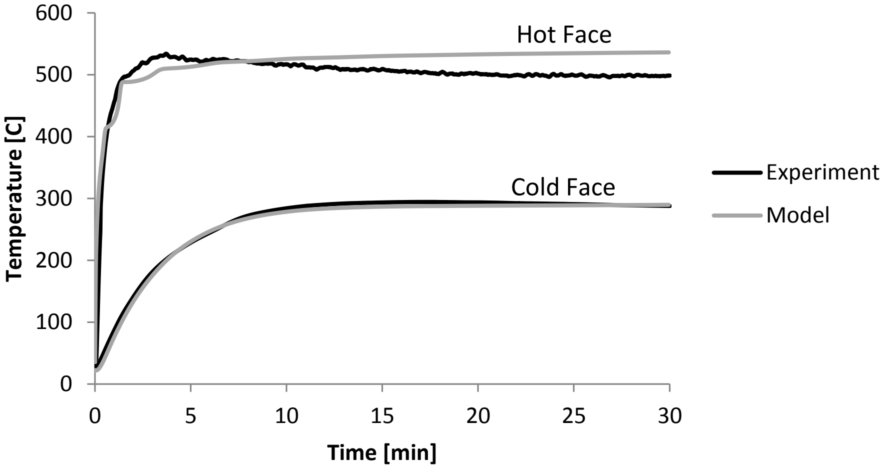

Figure 7.35: Front and rear face temperatures of a AA2024 specimen featuring a 20-ply PML protective surface layer during heat exposure at 50 kW m^{-2}.

The results of the thermal modelling of AA2024 substrates featuring either a 10-ply or a 20-ply PML are presented in figures 7.34 and 7.35. The simulated temperature curves fit the experimental curves with considerable correlation. Steady-state conditions are reached in all cases after an initial transient heating up phase with final temperatures reached after 30 minutes of 301 °C for AA2024 specimens with 10-ply PML and 289 °C for AA2024 specimens with 20-ply PML. Variations were observed in the hot face temperature profiles for both specimen types, the recorded temperatures were diminished slightly for the longer exposure times. This can most probably be attributed to the positioning and securing of the thermocouples. During the experiments the thermocouples were only lightly secured and might have experienced some movement due to the expansion of the PML so that full contact with the hot face was not guaranteed at all times. Also, due to the irregular expansion the thermocouple might have been shielded from the full incoming heat flux and therefore recorded a lower hot face temperature than when in a fully exposed position at the sample front. For the cold face testing, the model replicates almost identically the temperatures for the 20-ply PML specimens whereas the 10-ply PML specimens show a typical tailing off of the temperature curve which can be associated with inefficient heat insulation on the back face of the samples which could cause unaccounted heat losses to occur during longer testing times.

The PML_FIRE model therefore allows the forecasting of temperature profiles for these types of fire-structural test specimens under different heat flux irradiances. In figure 7.36 this is shown

Heat Flux	AA2024 with 10-ply PML	AA2024 with 20-ply PML
35 kW m^{-2}	289 °C	284 °C
50 kW m^{-2}	301 °C	289 °C
70 kW m^{-2}	313 °C	298 °C

Table 7.2: Simulated steady-state temperatures of PML-protected AA2024 specimens reached during long-term exposure of up to 30 minutes in different fire scenarios.

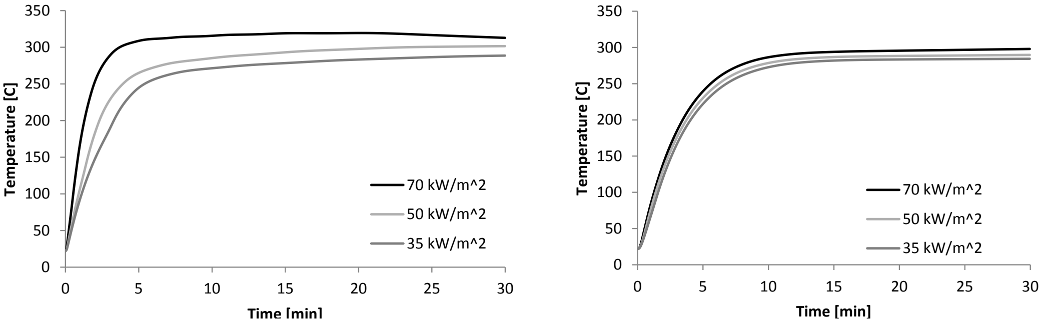

(a) 10-ply PML **(b)** 20-ply PML

Figure 7.36: Modelled temperature profiles of a PML-covered AA2024 specimen subjected to different heat fluxes.

for the heat fluxes of 35 kW m^{-2} and 70 kW m^{-2} in comparison to the reference model curve of 50 kW m^{-2} which is based on the experimental data. Specimens featuring thinner 10-ply PML show a clear tendency, with increasing heat flux, for the initial transient phase to exhibit a higher heating rate before the temperature curve is steady and at a constant level. These results are listed in table 7.2 for steady-state temperatures. Temperature profiles for 20-ply PML specimens show contrasting behaviour in that, although the curves for individual heat fluxes show very similar behaviour, the heating rate increases marginally with a higher level of heat input while the steady-state temperatures at long exposure times only vary by 14 °C whilst covering a heat flux range of 35 kW m^{-2} and 70 kW m^{-2} which would equal a theoretical flame temperature of 637 °C and 809 °C, respectively, according to the Stefan-Boltzman law.

The reason for this arises from the differing insulating effect due to the different thicknesses of the two PML types. For the thinner 10-ply PML, degradation is initiated within all the polymeric layers of the PML with greater fractions being fully decomposed, see table 7.3. For the 20-ply PML a similar number of degraded resin layers are observed as expected when specimens are exposed to the same testing conditions. However, instead of the heat being then directly transferred into the underlying aluminium substrate additional layers are available in the case of the thicker PML which provide an enhanced insulation effect thereby preventing further temperature increases. Looking at

Property	Heat Flux	AA2024 with 10-ply PML	AA2024 with 20-ply PML
Average RRC	35 kW m^{-2}	0.42	0.55
	50 kW m^{-2}	0.31	0.48
	70 kW m^{-2}	0.18	0.39
Number of decomposed plies	35 kW m^{-2}	8 (80 %)	10 (50 %)
	50 kW m^{-2}	6 (60 %)	7 (35 %)
	70 kW m^{-2}	5 (50 %)	6 (30 %)

Table 7.3: Degradation characteristics of PML after 30 minutes exposure to different fire scenarios: Overall PML residual resin content as average over individual ply RRC and number of fully decomposed resin interlayers within PML.

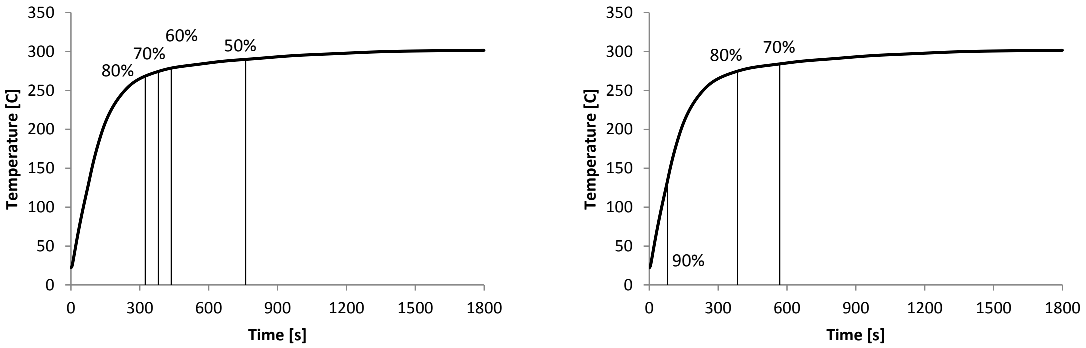

(a) Tension **(b)** Compression

Figure 7.37: Failure times of a AA2024 specimen featuring 10-ply PML tested under $50\,\mathrm{kW\,m^{-2}}$ fire-structural experiments added to the associated temperature profile as indicator of failure mode transition.

the overall average remaining resin content for 10-ply PML type specimens, with increasing heat flux, the induced resin decomposition significantly increases from about 60 % mass loss to more than 80 % in the case of the higher heat flux. This is in contrast to 20-ply PML type specimens where the reduction appears more gradual with more than 50 % of the original resin content not degraded at a low heat flux of $35\,\mathrm{kW\,m^{-2}}$ which figure only diminishes to about 40 % at $70\,\mathrm{kW\,m^{-2}}$.

Failure Correlation - 10-ply PML protection specimens

Figure 7.37 shows the failure times of AA2024 specimens featuring a 10-ply PML added to the corresponding temperature curve for tensile and compressive loading respectively, under the influence of external heat. In addition to the displacement plots shown in earlier sections, these figures clearly indicate that at relatively high loading stress levels, the failure process is already occurring and is partially affected by creep process. Only a few specimens tested at higher stress levels exhibited failure during the transient heating up stage of experimentation which could be directly linked to the temperature-dependent strength reduction of the aluminium substrate. This effect is most pronounced in case of compressive loading where specimens tested at under 70 % showed extensive lifetimes and in some cases would reach the time limit of 2 hours without failing at which point samples were deemed to be safe.

This long-life behaviour restricts the capability to predict failure times for different heat flux experiments according to the simplistic analysis method presented in the early sections for CFRP substrates. This is especially true for cases of lower heat fluxes where there is a greater likelihood that the temperatures which are associated with a reduction in the material's strength will shift towards more steady-state conditions indicating the probable influence by creep deformation occurring at earlier times.

Figure 7.38 summarises the estimated failure times for 10-ply PML/AA2024 specimens under the two different fire scenarios of $35\,\mathrm{kW\,m^{-2}}$ and $70\,\mathrm{kW\,m^{-2}}$ in comparison to the $50\,\mathrm{kW\,m^{-2}}$ experimental set of data. The data points are taken from the transient heating up phase of the specimen. For lower stress levels the influence of creep deformation becomes more pronounced and cannot be assessed with the simplistic strength-temperature failure relationship which eventually causes these specimens to fail after the longer exposure times which are not included in the graphs. Even the lowest data points included in the figures for the predicted heat flux experiments might be an underestimation of the real failure times as these failures would occur in the transition zone from transient heat transfer to steady-state condition which could lead to longer lifetimes due to the onset of creep effects as opposed to outright failure. As concluded before in case of unprotected AA2024 specimens, the extended failure times can only be investigated and then forecast after further analysis and a fuller understanding of the material's creep behaviour.

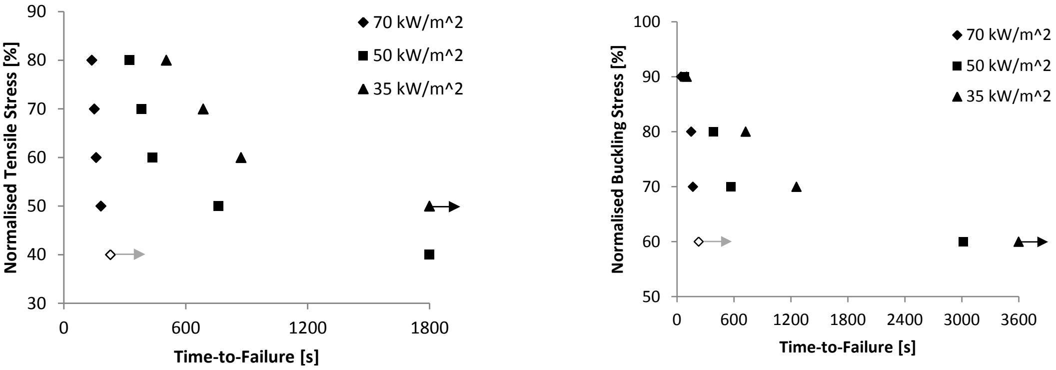

(a) Tension **(b)** Compression

Figure 7.38: Estimated failure times for 10-ply PML/AA2024 specimens exposed to heat fluxes of 35 kW m^{-2} and 70 kW m^{-2} in comparison to experimental data for 50 kW m^{-2} heat exposure experiments.

Failure Correlation - 20-ply PML protection specimens

The same observations as above can be made for AA2024 specimens featuring a 20-ply PML. Analysis might be even more hindered due to the greater insulation potential in comparison to the thinner 10-ply PML specimens. Failure under the same loading level occurs after longer exposure times with the transition point, that is the point at which failure occurs at the boundary of the transient and the steady-state period, moving to higher applied stress levels, see figure 7.39. In consequence, the simplistic failure analysis methodology becomes less reliable due to the limited amount of data points available because only specimens tested at 70 % or higher can be considered. Estimated failure times for heat fluxes lower than 50 kW m^{-2} tend to rapidly tail off during prolonged testing times and this is especially true for cases of compression loading, see figure 7.40.

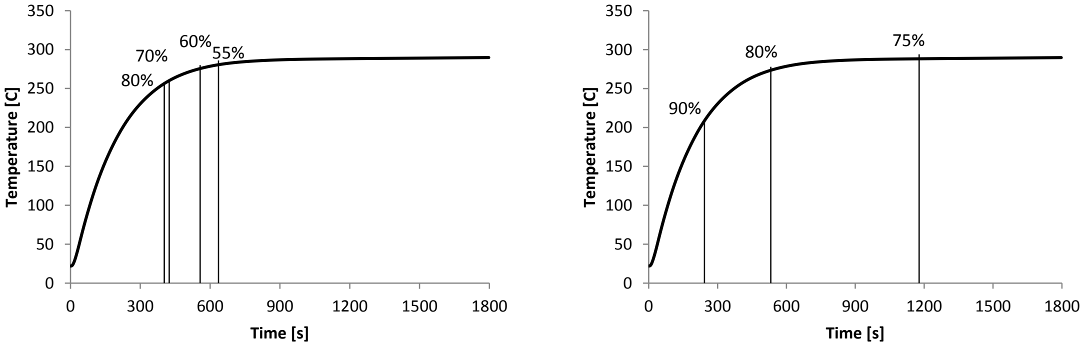

(a) Tension **(b)** Compression

Figure 7.39: Failure times of a AA2024 specimen featuring 20-ply PML tested under 50 kW m^{-2} fire-structural experiments added to the associated temperature profile as indicator of failure mode transition.

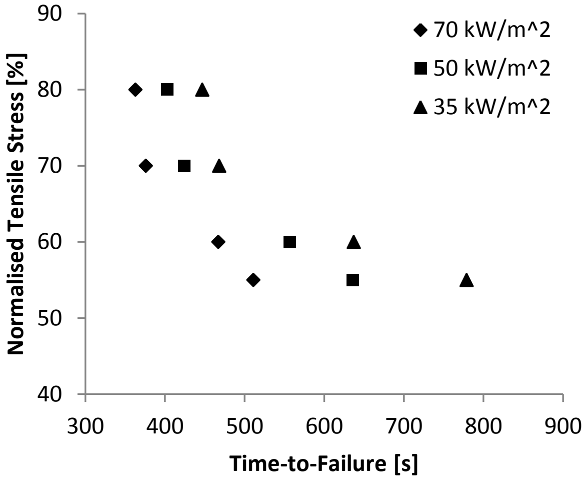

(a) Tension

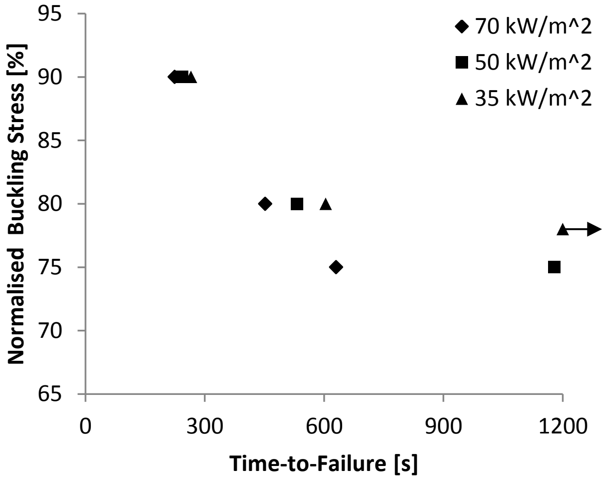

(b) Compression

Figure 7.40: Estimated failure times for 20-ply PML/AA2024 specimens exposed to heat fluxes of $35\,\mathrm{kW\,m^{-2}}$ and $70\,\mathrm{kW\,m^{-2}}$ in comparison to experimental data for $50\,\mathrm{kW\,m^{-2}}$ heat exposure experiments.

Chapter 8

Conclusions

8.1 Summary of Major Findings

The aim of the research presented in this work was to develop a novel fire protection material. Multi-layer polymer metal laminates (PML) comprising of thin aluminium foils separated by even thinner organic polymer layers on the micrometre-scale have been proved to be an effective thermal barrier material which provides an insulating protective layer thereby prolonging the structural integrity of the underlying substrate. Various experimental and numerical methods have been used during this study to prove PML's capability as an effective surface thermal barrier and have shown the excellent fire protection efficacy that PML materials possess. The main conclusions drawn from the investigation into the thermal and fire performance properties of PML are presented in the following sections.

8.1.1 Material Characterisation

- The temperature range and the kinetic parameters of the decomposition reaction for the epoxy resin used as polymer interlayers within PML were determined as these characteristics dictate the overall swelling behaviour of the PML materials.

- From isothermal heating tests, a mathematical description of the PML expansion behaviour was derived as a function of polymer mass loss. A maximum expansion factor of just below 10 was observed which is similar to or greater than commercial intumescent coatings.

- Thermal step-change experiments have proved to be a low-cost and simple method for determining the thermal transport properties from ambient temperatures up to much elevated temperatures. These tests were performed on neat epoxy resin as well as the PML material. The PML's room temperature thermal conductivity was found to be around $1\,\mathrm{W\,m^{-1}\,K^{-1}}$ despite consisting of more than $90\,\%$ of highly conductive aluminium.

- The observed decline in the polymer's thermal conductivity with increasing temperature and the major reduction observed around its glass transition temperature is replicated in the temperature dependence of the PML transport property as the epoxy resin is the dominant influence of the two PML constituents. At high temperatures the PML's transport properties are greatly reduced to less than $10\,\%$ of the room temperature value offering great potential for slowing down heat transfer.

8.1.2 Thermal Response Model

- An improved one-dimensional FD model has been established to simulate the thermal response of PML-insulated substrates under heat exposure. The model is capable of predicting the temperature evolution of non-reactive substrates (metals) as well as combustible materials (fibre-reinforced composites) that are typically used in many lightweight applications.
- The proposed simplified approach during the discretisation step has proved to be adequate in successfully modelling temperature profiles that achieve good correlation with experimental results.
- The newly developed PML_FIRE model incorporates temperature dependent functions for thermal and constitutive properties, the occurrence of polymer decomposition, the overall effect of PML expansion as well as the effects of foil melting, verified as results of experimental analysis.
- A parametric study has been used to assess the sensitivity of the model to perturbations from selected input parameters. Most of the influence on the calculated temperature profiles have been demonstrated by the PML's thermal conductivity, expansion factors and surface emissivity.

8.1.3 Fire Performance of PML

- Small-scale propane burner tests were carried out to assess the fire performance of PML-covered substrates in comparison with unprotected specimens over a wide heat flux range ($70\,\mathrm{kW\,m^{-2}}$ to $180\,\mathrm{kW\,m^{-2}}$) and for several PML architectures. These test results have also formed the basis for the thermal model validation as a consequence of the wide variety of test scenarios and combinations of materials constituted in this research.
- Overall, PML materials provide great potential as thermal insulation barriers as they invoke slower heating rates and much greater time delays in heat transfer as the result of its decomposition properties compared with unprotected specimens.
- Certain aspects of PML design have been proved to be more advantageous for the fire protection efficacy of PML:

  Ply number > Foil thickness
  Titanium front > Stainless Steel front > basic Alu-PML
  Pristine metal surface > painted surface

- For combustible materials, PML provides a means of reducing the risk of fire spread and fire growth because typical fire characteristics such as ignition time, heat release and smoke production are improved through application of PMLs to such substrates.

8.1.4 Influence of PML on Fire-structural Performance

- The great improvements achieved by increasing the failure times of PML-insulated substrates observed during heat exposure under tensile or compressive loading has been shown to be due to the thermal lag and the temperature reduction effected by the PML surface barrier.
- PMLs have been demonstrated as being especially effective in combination with combustible substrates because the iginition of released decomposition gases can be prevented by the PML's barrier effect which reduces the overall risk of fire spread into the environment as well as achieving an overall improvement of the fire-structural performance of the substrate.

- Fire-structural tests have shown that PML materials display similar or superior behaviour over conventional insulation methods with regards to reducing temperature development and extending structural failure times when compared, for example, with superwool and intumescent specimens.

- A simplified approach has been developed for deriving failure times by evaluating the specimen's thermal state at the point of structural failure which can now be simulated by the PML_FIRE model for various fire scenarios.

8.2 Recommendations for Future Work

This study is the first into the feasibility and efficacy of multi-layered PML materials used as thermal insulation barriers. However, despite the very significant achievements and promising results so far there is still room for improvements through optimisation of the PML materials as well as further development of the new the PML_FIRE thermal response model. Some of the aspects are presented below.

From an experimental point of view, further advancements in the fire performance of PML can be achieved through an optimisation analysis of various polymer types that can be used as PML interlayers which will cover different temperature degradation ranges, exhibit differing decomposition reaction characteristics and expansion potential. It is thought worthwhile to explore the potential of using thermoplastic polymers such as high-strength polyimides or PEEK. One immediate benefit would be that this would simplify the manfacturing process greatly as the post-curing step would be made obsolete.

The results of this study have produced graphs for the prediction of underlying substrate failure times, however, a comprehensive investigation into the temperature dependence of the mechanical properties of the substrate materials, such as strength and stiffness, and creep parameters for metals, needs to be carried out to improve the simplified approach presented in this study for the prediction of failure times. The outcomes could consequently be used in combination with the PML_FIRE model to deliver more detailed and accurate failure predictions.

Furthermore, focus should not just concentrate on the fire protection effect and the fire retardant properties of PMLs. When PML materials are considered for fire protection modifications to existing structures in field applications, the PML behaviour with regard to a variety of other properties, e.g. impact, long-term environmental exposure or fatigue, will need to be taken into account. A simple example of use with minimal insulation cost and potential cost savings would be as lightning strike protection for aeroplanes. Here, PML layers could act as a multi-functional material combining lightning strike and fire protection which would make the use of highly conductive meshes with fibre-reinforced composite materials which is the current technique obsolete.

With regard to the PML_FIRE modelling aspect of this research, it is considered that with an increase in computational capacity it should, even in the short term, be possible to advance the simplified discretisation process presented here. If every physical layer within the PML could be represented by individual nodes during the simulation process, a more exact simulation of the thermal response behaviour should be possible. This would provide a means of capturing in more detail the true behaviour and contribution of the individual PML constituents and interpret the impact on the overall temperature development, which should eradicate some of the current discrepancies between experimental and calculated temperature profiles.

Also, in order to use the PML_FIRE model as a true design tool, continued work should focus on building an extensive data library with a focus on establishing details of a variety of substrate materials and PML architectures.

References

[1] E.A. Starke and J.T. Staley. Application of modern aluminum alloys to aircraft. *Progress in Aerospace Sciences*, 32:131–172, 1996.

[2] T. Dursun and C. Soutis. Recent developments in advanced aircraft aluminium alloys. *Materials & Design*, 56:862–871, 2014.

[3] J-P. Immarigeon, R.T. Holt, A.K. Koul, L. Zhao, W. Wallace, and J.C. Beddoes. Lightweight materials for aircraft applications. *Materials Characterization*, 35(1):41–67, 1995.

[4] J.C. Halpin. *Composite Materials*, chapter 2 - Opportunities for Polymeric-Based Composite Applications for Transport Aircraft. Springer London, 2011.

[5] C. Veiga, J.P. Davim, and A.J.R. Loureiro. Properties and applications of titanium alloys: A brief review. *Reviews on Advanced Materials Science*, 32(2):133–148, 2012.

[6] J.C. Williams and E.A. Starke. Progress in structural materials for aerospace systems. *Acta Materialia*, 51(19):5775–5799, 2003.

[7] L.B. Vogelesang and A. Vlot. Development of fibre metal laminates for advanced aerospace structures. *Journal of Materials Processing Technology*, 103(1):1–5, 2000.

[8] T. Sinmazcelik, E. Avcu, M.O. Bora, and O. Coban. A review: Fibre metal laminates, background, bonding types and applied test methods. *Materials & Design*, 32(7):3671–3685, 2011.

[9] W.T. Freeman. The use of composites in aircraft primary structure. *Composites Engineering*, 3(7-8):767–775, 1993.

[10] C. Soutis. Carbon fiber reinforced plastics in aircraft construction. *Materials Science and Engineering: A*, 412(1-2):171–176, 2005.

[11] W.W. Wright. Polymers in aerospace applications. *Materials & Design*, 12(4):222–227, 1991.

[12] AIRBUS S.A.S. Taking the lead: A350XWB. Presentation, 2006.

[13] C. Soutis. Fibre reinforced composites in aircraft construction. *Progress in Aerospace Sciences*, 41(2):143–151, 2005.

[14] Modernairliners.com. http://modernairliners.com/Boeing787_files/Specifications.html. Accessed: 2015-03-05.

[15] G. Marsh. Can composites get firmly on the rails? *Reinforced Plastics*, 48(7):26–30, 2004.

[16] V.P. McConnell. Rail - an evolving market for FRP components. *Reinforced Plastics*, 52(11):24–29, 2008.

[17] Composites gain ground in Europe's rail industry. *Reinforced Plastics*, 42(1):28–31, 1998.

[18] Siemens AG. Velaro. Top performance for high-speed. Brochure, 2014. siemens.com/mobility.

[19] BS EN 12663-2. *BSI British Standards*, 2010. Railway applications. Structural requirements of railway vehicle bodies. Freight wagons.

[20] BS EN 15227. *BSI British Standards*, 2009. Railway applications. Crashworthiness requirements for railway vehicle bodies.

[21] BS EN 45545-2. *BSI British Standards*, 2013. Railway applications. Fire protection on railway vehicles. Requirements for fire behaviour of materials and components.

[22] M. Robinson. Composites make tracks in railway engineering. *Reinforced Plastics*, 39(11):20–26, 1995.

[23] R. Martin. *Ageing of Composites.* Composites Science and Engineering. Elsevier Science, 2008.

[24] A.P. Mouritz, E. Gellert, P. Burchill, and K. Challis. Review of advanced composite structures for naval ships and submarines. *Composite Structures*, 53(1):21–42, 2001.

[25] G. Di Bella, L. Calabrese, and C. Borsellino. Mechanical characterisation of a glass/polyester sandwich structure for marine applications. *Materials & Design*, 42:486–494, 2012.

[26] G. Marsh. Marine composites - drawbacks and successes. *Reinforced Plastics*, 54(4):18–22, 2010.

[27] J. Klimke and D. Rothmann. Carbon composite materials in modern yacht building. *Reinforced Plastics*, 54(4):24–27, 2010.

[28] Marine Supplement. Material trends for FRP boats. *Reinforced Plastics*, 47(9):23–34, 2003.

[29] G. Marsh. 50 years of reinforced plastic boats. *Reinforced Plastics*, 50(9):16–19, 2006.

[30] L. Dokos. Adoption of marine composites - a global perspective. *Reinforced Plastics*, 57(3):30–32, 2013.

[31] G. Marsh. Composites boost superyacht performance. *Reinforced Plastics*, 53(2):28–30, 2009.

[32] SOLAS Chapter II-2. *International Maritime Organisation*, 2002. International Convention for the Safety of Life at Sea.

[33] FAR 25: Appendix F6. *FAA Federal Aviation Administration*, 2003. Test Method To Determine the Flammability and Flame Propagation Characteristics of Thermal/Acoustic Insulation Materials.

[34] ISO 5660-1. *ISO International Organization for Standardization*, 2015. Heat release, smoke production and mass loss rate – Part 1: Heat release rate (cone calorimeter method) and smoke production rate (dynamic measurement).

[35] B. Schartel, M. Bartholmai, and U. Knoll. Some comments on the use of cone calorimeter data. *Polymer Degradation and Stability*, 88(3):540–547, 2005.

[36] V. Babrauskas and R.D. Peacock. Heat release rate: The single most important variable in fire hazard. *Fire Safety Journal*, 18(3):255–272, 1992.

[37] ASTM E162. *The American Society for Testing and Materials*, 2015. Standard Test Method for Surface Flammability of Materials Using a Radiant Heat Energy Source.

[38] UL 94. *Underwriters Laboratories USA*, 2013. Standard for Tests for Flammability of Plastic Materials for Parts in Devices and Appliances.

[39] NASA-STD-6001. *National Aeronautics and Space Administration*, 1998. Flammability, Odor, and Offgassing Requirements and Test Procedures for Mateerials in Environments that Support Combustion.

[40] ASTM E1321. *The American Society for Testing and Materials*, 2013. Standard Test Method for Determining Material Ignition and Flame Spread Properties.

[41] ISO 5658-2. *ISO International Organization for Standardization*, 2006. Reaction to fire tests. Spread of flame. Lateral spread on building and transport products in vertical configuration.

[42] ISO 4589-1. *ISO International Organization for Standardization*, 1996. Plastics – Determination of burning behaviour by oxygen index – Part 1: Guidance.

[43] ISO 4589-2. *ISO International Organization for Standardization*, 1996. Plastics – Determination of burning behaviour by oxygen index – Part 2: Ambient-temperature test.

[44] ISO 4589-3. *ISO International Organization for Standardization*, 1996. Plastics – Determination of burning behaviour by oxygen index – Part 3: Elevated-temperature test.

[45] ASTM D2863. *The American Society for Testing and Materials*, 2013. Standard Test Method for Measuring the Minimum Oxygen Concentration to Support Candle-Like Combustion of Plastics (Oxygen Index).

[46] ISO 5659-2. *ISO International Organization for Standardization*, 2012. Plastics – Smoke generation – Part 2: Determination of optical density by a single-chamber test.

[47] ASTM E119. *The American Society for Testing and Materials*, 2015. Standard Test Methods for Fire Tests of Building Construction and Materials.

[48] ISO 834-1. *ISO International Organization for Standardization*, 1999. Fire-resistance tests – Elements of building construction – Part 1: General requirements.

[49] UL 1709. *Underwriters Laboratories USA*, 2011. Standard for Rapid Rise Fire Tests of Protection Materials for Structural Steel.

[50] Fire Testing Technology. http://www.fire-testing.com/hydraulic-tilting-test. Accessed: 2015-02-03.

[51] MarineLink.com. http://www.marinelink.com/news/machinery-spaces-large362157.aspx. Accessed: 2015-03-03.

[52] Intertek India Private Limited. http://www.indiamart.com/intertek-indialimited/building-products.html. Accessed: 2015-03-03.

[53] E.J. Fogle, B.Y. Lattimer, S. Feih, E. Kandare, A.P. Mouritz, and S.W. Case. Compression load failure of aluminum plates due to fire. *Engineering Structures*, 34:155–162, 2012.

[54] M.T. Davidson, I.E. Harik, and D.B. Davis. Fire impact and passive fire protection of infrastructure: State of the art. *Journal of Performance of Constructed Facilities*, 27(2):135–143, 2013.

[55] J. Suzuki, Y. Ohmiya, T. Wakamatsu, K. Harada, S. Yusa, and M. Kohno. Evaluation of fire resistance of aluminum alloy members. *Fire Science and Technology*, 24(4):237–255, 2005.

[56] BS EN 1999-1-2. *BSI British Standards*, 2007. Eurocode 9. Design of aluminium structures. Structural fire design.

[57] B. Faggiano, G. De Matteis, R. Landolfo, and F.M. Mazzolani. Behaviour of aluminium alloy structures under fire. *Journal of Civil Engineering and Management*, 10(3):183–190, 2004.

[58] J.E. Dorn. Some fundamental experiments on high temperature creep. *Journal of the Mechanics and Physics of Solids*, 3(2):85–116, 1955.

[59] T.Z. Harmathy. A comprehensive creep model. *Journal of Fluids Engineering*, 89(3):496–502, 1967.

[60] J. Maljaars, F. Soetens, and H.H. Snijder. Local buckling of aluminium structures exposed to fire. part 1: Tests. *Thin-Walled Structures*, 47(11):1404–1417, 2009.

[61] J. Maljaars, F. Soetens, and H.H. Snijder. Local buckling of aluminium structures exposed to fire. part 2: Finite element models. *Thin-Walled Structures*, 47(11):1418–1428, 2009.

[62] S. Feih, E. Kandare, B.Y. Lattimer, and A.P. Mouritz. Structural analysis of compression deformation and failure of aluminum in fire. *Journal of Structural Engineering*, 137(7):728–738, 2011.

[63] E. Kandare, S. Feih, B.Y. Lattimer, and A.P. Mouritz. Larson-miller failure modeling of aluminum in fire. *Metallurgical and Materials Transactions A: Physical Metallurgy and Materials Science*, 41(12):3091–3099, 2010.

[64] J. Maljaars, L. Twilt, and F. Soetens. Flexural buckling of fire exposed aluminium columns. *Fire Safety Journal*, 44(5):711–717, 2009.

[65] A. Afaghi Khatibi, E. Kandare, S. Feih, B.Y. Lattimer, S.W. Case, and A.P. Mouritz. Finite element modelling of tensile deformation and failure of aluminium plate exposed to fire. *Computational Materials Science*, 95:242–249, 2014.

[66] L.A. Burns, S. Feih, and A. P. Mouritz. Compression failure of carbon fiber-epoxy laminates in fire. *Journal of Aircraft*, 47(2):528–533, 2010.

[67] A.G. Gibson A.P. Mouritz. *Fire Properties of Polymer Composite Materials*. Solid Mechanics and its Applications. Springer Netherlands, 2006.

[68] A.G. Gibson. The integrity of polymer composites during and after fire. *Journal of Composite Materials*, 38(15):1283–1307, 2004.

[69] B.Y. Lattimer, J. Ouellette, and J. Trelles. Thermal response of composite materials to elevated temperatures. *Fire Technology*, 47(4):823–850, 2011.

[70] R.C. Easby, S. Feih, C. Konstantis, G. La Delfa, V. Urso Miano, A. Elmughrabi, A.P. Mouritz, and A.G. Gibson. Failure model for phenolic and polyester pultrusions under load in fire. *Plastics, Rubber and Composites*, 36(9):379–388, 2007.

[71] A.G. Gibson, M.E. Otheguy Torres, T.N.A. Browne, S. Feih, and A.P. Mouritz. High temperature and fire behaviour of continuous glass fibre/polypropylene laminates. *Composites Part A: Applied Science and Manufacturing*, 41(9):1219–1231, 2010.

[72] P. Patel, T.R. Hull, R.E. Lyon, S.I. Stoliarov, R.N. Walters, S. Crowley, and N. Safronava. Investigation of the thermal decomposition and flammability of PEEK and its carbon and glass-fibre composites. *Polymer Degradation and Stability*, 96(1):12–22, 2011.

[73] M.T. McGurn, P.E. DesJardin, and A.B. Dodd. Numerical simulation of expansion and charring of carbon-epoxy laminates in fire environments. *International Journal of Heat and Mass Transfer*, 55(1-3):272–281, 2012.

[74] C.L. Beyler and M.M. Hirschler. *SFPE Handbook of Fire Protection Engineering*, chapter 7 - Thermal Decomposition of Polymers. 3rd edition, 2002.

[75] A.P. Mouritz, Z. Mathys, and A.G. Gibson. Heat release of polymer composites in fire. *Composites Part A: Applied Science and Manufacturing*, 37(7):1040–1054, 2006.

[76] B. Vieille, C. Lefebvre, and A. Coppalle. Post fire behavior of carbon fibers polyphenylene sulfide- and epoxy-based laminates for aeronautical applications: A comparative study. *Materials & Design*, 63:56–68, 2014.

[77] S. Feih, Z. Mathys, A.G. Gibson, and A.P. Mouritz. Modelling the tension and compression strengths of polymer laminates in fire. *Composites Science and Technology*, 67(3-4):551–564, 2007.

[78] R.E. Lyon, P.N. Balaguru, A. Foden, U. Sorathia, J. Davidovits, and M. Davidovics. Fire-resistant aluminosilicate composites. *Fire and Materials*, 21(2):67–73, 1997.

[79] J.R. Brown, P.D. Fawell, and Z. Mathys. Fire-hazard assessment of extended-chain polyethylene and aramid composites by cone calorimetry. *Fire and Materials*, 18(3):167–172, 1994.

[80] A.B. Morgan. *Long-Term Durability of Polymeric Matrix Composites*, chapter 2 - Additives, Nanocomposites, and Barrier Coatings. Springer US, 2012.

[81] A.B. Morgan and J.W. Gilman. An overview of flame retardancy of polymeric materials: Application, technology, and future directions. *Fire and Materials*, 37(4):259–279, 2013.

[82] S. Bocchini and G. Camino. Halogen-containing flame retardants. In *Fire Retardancy of Polymeric Materials, Second Edition*, pages 75–105. Informa UK Limited, 2009.

[83] T.R. Hull, A. Witkowski, and L. Hollingbery. Fire retardant action of mineral fillers. *Polymer Degradation and Stability*, 96(8):1462–1469, 2011.

[84] M.J. Scudamore. Fire performance studies on glass-reinforced plastic laminates. *Fire and Materials*, 18(5):313–325, 1994.

[85] D. Santillo and P. Johnston. Playing with fire: The global threat presented by brominated flame retardants justifies urgent substitution. *Environment International*, 29(6):725–734, 2003.

[86] S. Lu and I. Hamerton. Recent developments in the chemistry of halogen-free flame retardant polymers. *Progress in Polymer Science*, 27(8):1661–1712, 2002.

[87] S. Liu. Flame retardant and mechanical properties of polyethylene/magnesium hydroxide/montmorillonite nanocomposites. *Journal of Industrial and Engineering Chemistry*, 20(4):2401–2408, 2014.

[88] A. Dasari, Z. Yu, G. Cai, and Y. Mai. Recent developments in the fire retardancy of polymeric materials. *Progress in Polymer Science*, 38(9):1357–1387, 2013.

[89] B.K. Kandola, W. Bhatti, and E. Kandare. A comparative study on the efficacy of varied surface coatings in fireproofing glass/epoxy composites. *Polymer Degradation and Stability*, 97(11):2418–2427, 2012.

[90] F. Laoutid, L. Bonnaud, M. Alexandre, J.-M. Lopez-Cuesta, and Ph. Dubois. New prospects in flame retardant polymer materials: From fundamentals to nanocomposites. *Materials Science and Engineering: R: Reports*, 63(3):100–125, 2009.

[91] J. Gilman. Flammability and thermal stability studies of polymer layered-silicate (clay) nanocomposites. *Applied Clay Science*, 15(1-2):31–49, 1999.

[92] P. Kiliaris and C.D. Papaspyrides. Polymer/layered silicate (clay) nanocomposites: An overview of flame retardancy. *Progress in Polymer Science*, 35(7):902–958, 2010.

[93] B. Dittrich, K. Wartig, D. Hofmann, R. Mülhaupt, and B. Schartel. Flame retardancy through carbon nanomaterials: Carbon black, multiwall nanotubes, expanded graphite, multi-layer graphene and graphene in polypropylene. *Polymer Degradation and Stability*, 98(8):1495–1505, 2013.

[94] R.H. Pour, M. Soheilmoghaddam, A. Hassan, and S. Bourbigot. Flammability and thermal properties of polycarbonate /acrylonitrile-butadiene-styrene nanocomposites reinforced with multilayer graphene. *Polymer Degradation and Stability*, 120:88–97, 2015.

[95] H. Yang, J. Gong, X. Wen, J. Xue, Q. Chen, Z. Jiang, N. Tian, and T. Tang. Effect of carbon black on improving thermal stability, flame retardancy and electrical conductivity of polypropylene/carbon fiber composites. *Composites Science and Technology*, 113:31–37, 2015.

[96] A. Laachachi, E. Leroy, M. Cochez, M. Ferriol, and J.M. Lopez Cuesta. Use of oxide nanoparticles and organoclays to improve thermal stability and fire retardancy of poly(methyl methacrylate). *Polymer Degradation and Stability*, 89(2):344–352, 2005.

[97] J.W. Gilman, R.H. Harris, J.R. Shields, T. Kashiwagi, and A.B. Morgan. A study of the flammability reduction mechanism of polystyrene-layered silicate nanocomposite: layered silicate reinforced carbonaceous char. *Polym. Adv. Technol.*, 17(4):263–271, 2006.

[98] T. Kashiwagi, E. Grulke, J. Hilding, K. Groth, R. Harris, K. Butler, J. Shields, S. Kharchenko, and J. Douglas. Thermal and flammability properties of polypropylene/carbon nanotube nanocomposites. *Polymer*, 45(12):4227–4239, 2004.

[99] T. Kashiwagi, F. Du, K.I. Winey, K.M. Groth, J.R. Shields, S.P. Bellayer, H. Kim, and J.F. Douglas. Flammability properties of polymer nanocomposites with single-walled carbon nanotubes: effects of nanotube dispersion and concentration. *Polymer*, 46(2):471–481, 2005.

[100] T. Kashiwagi, F. Du, J.F. Douglas, K.I. Winey, R.H. Harris, and J.R. Shields. Nanoparticle networks reduce the flammability of polymer nanocomposites. *Nature Materials*, 4(12):928–933, 2005.

[101] M. Bartholmai and B. Schartel. Layered silicate polymer nanocomposites: new approach or illusion for fire retardancy? investigations of the potentials and the tasks using a model system. *Polym. Adv. Technol.*, 15(7):355–364, 2004.

[102] S. Duquesne, S. Magnet, C. Jama, and R. Delobel. Intumescent paints: fire protective coatings for metallic substrates. *Surface and Coatings Technology*, 180-181:302–307, 2004.

[103] S. Feih, A.P. Mouritz, Z. Mathys, and A.G. Gibson. Fire structural modeling of polymer composites with passive thermal barrier. *Journal of Fire Sciences*, 28(2):141–160, 2009.

[104] B.K. Kandola and A.R. Horrocks. *Fire Retardant Materials*, chapter 5 - Composites. Woodhead Publishing, 2001.

[105] S. Duquesne, M. Jimenez, and S. Bourbigot. Aging of the flame-retardant properties of polycarbonate and polypropylene protected by an intumescent coating. *Journal of Applied Polymer Science*, 131(3), 2014.

[106] J. Alongi, Z. Han, and S. Bourbigot. Intumescence: Tradition versus novelty. a comprehensive review. *Progress in Polymer Science*, 51:28–73, 2015.

[107] G. Camino, L. Costa, and G. Martinasso. Intumescent fire-retardant systems. *Polymer Degradation and Stability*, 23(4):359–376, 1989.

[108] I.S. Reshetnikov, M.Y. Yablokova, and N.A. Khalturinskij. Intumescent Chars. In *Fire Retardancy of Polymers*, pages 88–103. Elsevier BV, 1998.

[109] J.E.J. Staggs, R.J. Crewe, and R. Butler. A theoretical and experimental investigation of intumescent behaviour in protective coatings for structural steel. *Chemical Engineering Science*, 71:239–251, 2012.

[110] B.K. Kandola and A.R. Horrocks. Flame retardant composites, a review: The potential for use of intumescents. In *Fire Retardancy of Polymers*. Woodhead Publishing, 1998.

[111] E. Kandare, C. Chukwudolue, and B.K. Kandola. The use of fire-retardant intumescent mats for fire and heat protection of glass fibre-reinforced polyester composites: Thermal barrier properties. *Fire Mater.*, 34(1):21–38, 2009.

[112] M. Bartholmai and B. Schartel. Assessing the performance of intumescent coatings using bench-scaled cone calorimeter and finite difference simulations. *Fire and Materials*, 31(3):187–205, 2007.

[113] H. Vahabi, R. Sonnier, and L. Ferry. Effects of ageing on the fire behaviour of flame-retarded polymers: a review. *Polymer International*, 64(3):313–328, 2015.

[114] M. Jimenez, S. Bellayer, B. Revel, S. Duquesne, and S. Bourbigot. Comprehensive study of the influence of different aging scenarios on the fire protective behavior of an epoxy based intumescent coating. *Industrial & Engineering Chemistry Research*, 52(2):729–743, 2013.

[115] A. Kodaira Y. Sakumoto, J. Nagata and Y. Saito. Durability evaluation of intumescent coating for steel frames. *Journal of Materials in Civil Engineering*, 13(4):274–281, 2001.

[116] C.H. Bamford and D.H. Malan. The combustion of wood, part 1. *Cambridge Philosophical Society Proceedings*, 42:166–182, 1946.

[117] H. Kung. A mathematical model of wood pyrolysis. *Combustion and Flame*, 18(2):185–195, 1972.

[118] E.J. Kansa, H.E. Perlee, and R.F. Chaiken. Mathematical model of wood pyrolysis including internal forced convection. *Combustion and Flame*, 29:311–324, 1977.

[119] B. Fredlund. Modelling of heat and mass transfer in wood structures during fire. *Fire Safety Journal*, 20(1):39–69, 1993.

[120] C.A. Griffis, J.A. Nemes, F.R. Stonesifer, and C.I. Chang. Degradation in strength of laminated composites subjected to intense heating and mechanical loading. *Journal of Composite Materials*, 20(3):216–235, 1986.

[121] W.S. Johnson, J.E. Masters, T.K. O'Brien, J.A. Milke, and A.J. Vizzini. Thermal response of fire-exposed composites. *Journal of Composites Technology and Research*, 13(3), 1991.

[122] G.A. Pering, P.V. Farrell, and G.S. Springer. Degradation of tensile and shear properteis of composites exposed to fire or high temperature. *Journal of Composite Materials*, 14(1):54–68, 1980.

[123] J.B. Henderson, J.A. Wiebelt, and M.R. Tant. Model for the thermal response of polymer composite materials with experiemtnal verification. *Journal of Composite Materials*, 19(6):579–595, 1985.

[124] A.G. Gibson, Y. Wu, H. W. Chandler, J. A. D. Wilcox, and P. Bettess. Model for the thermal performance of thick composite laminates in hydrocarbon fires. *Revue de l'Institute Francais du Petrole*, 50(1):69–74, 1995.

[125] Y. Yin, J.G.P. Binner, T.E. Cross, and S.J. Marshall. The oxidation behaviour of carbon fibres. *Journal of Materials Science*, 29(8):2250–2254, 1994.

[126] S. Bourbigot and X. Flambard. Heat resistance and flammability of high performance fibres: A review. *Fire and Materials*, 26(4-5):155–168, 2002.

[127] M.R.E. Looyeh, P. Bettess, and A.G. Gibson. A one-dimensional finite element simulation for the fire performance of grp panels for offshore structures. *International Journal of Numerical Methods for Heat and Fluid Flow*, 7(6):609–625, 1997.

[128] N. Dodds, A.G. Gibson, D. Dewhurst, and J.M. Davies. Fire behaviour of composite laminates. *Composites Part A: Applied Science and Manufacturing*, 31(7):689–702, 2000.

[129] S. Feih, Z. Mathys, A.G. Gibson, and A.P. Mouritz. Modeling compressive skin failure of sandwich composites in fire. *Journal of Sandwich Structures and Materials*, 10(3):217–245, 2008.

[130] A.P. Mouritz, S. Feih, E. Kandare, Z. Mathys, A.G. Gibson, P.E. Des Jardin, S.W. Case, and B.Y. Lattimer. Review of fire structural modelling of polymer composites. *Composites Part A: Applied Science and Manufacturing*, 40(12):1800–1814, 2009.

[131] J. Florio, J.B. Henderson, F.L. Test, and R. Hariharan. A study of the effects of the assumption of local-thermal equilibrium on the overall thermally-induced response of a decomposing, glass-filled polymer composite. *International Journal of Heat and Mass Transfer*, 34(1):135–147, 1991.

[132] H.L.N. McManus and G.S. Springer. High temperature thermomechanical behavior of carbon-phenolic and carbon-carbon composites, I. Analysis. *Journal of Composite Materials*, 26(2):206–229, 1992.

[133] H.L.N. McManus and G.S. Springer. High temperature thermomechanical behavior of carbon-phenolic and carbon-carbon composites, II. Results. *Journal of Composite Materials*, 26(2):230–255, 1992.

[134] A.P. Mouritz, S. Feih, E. Kandare, and A.G. Gibson. Thermal–mechanical modelling of laminates with fire protection coating. *Composites Part B: Engineering*, 48:68–78, 2013.

[135] G.J. Griffin. The modeling of heat transfer across intumescent polymer coatings. *Journal of Fire Sciences*, 28(3):249–277, 2009.

[136] V.G. Zverev, V.D. Golédin, V.V. Nesmelov, and A.F. Tsimbalyuk. Modeling heat and mass transfer in intumescent fire-retardant coatings. *Combust Explos Shock Waves*, 34(2):198–205, 1998.

[137] G.N. Isakov and A.Y. Kuzin. Modeling of heat and mass transfer in multilayer heat- and fire-insulating coatings under interaction with a high-temperature gas flow. *Combust Explos Shock Waves*, 34(2):191–197, 1998.

[138] C. Di Blasi and C. Branca. Mathematical model for the nonsteady decomposition of intumescent coatings. *AIChE Journal*, 47(10):2359–2370, 2001.

[139] C. Di Blasi. Modeling the effects of high radiative heat fluxes on intumescent material decomposition. *Journal of Analytical and Applied Pyrolysis*, 71(2):721–737, 2004.

[140] M. Gillet, L. Autrique, and L. Perez. Mathematical model for intumescent coatings growth: application to fire retardant systems evaluation. *Journal of Physics D: Applied Physics*, 40(3):883–899, 2007.

[141] F. Zhang, J. Zhang, and Y. Wang. Modeling study on the combustion of intumescent fire-retardant polypropylene. *expresspolymlett*, 1(3):157–165, 2007.

[142] R.J. Asaro, B. Lattimer, C. Mealy, and G. Steele. Thermo-physical performance of a fire protective coating for naval ship structures. *Composites Part A: Applied Science and Manufacturing*, 40(1):11–18, 2009.

[143] E. Kandare, G.J. Griffin, S. Feih, A.G. Gibson, B.Y. Lattimer, and A.P. Mouritz. Fire structural modelling of fibre–polymer laminates protected with an intumescent coating. *Composites Part A: Applied Science and Manufacturing*, 43(5):793–802, 2012.

[144] M. Jimenez, S. Duquesne, and S. Bourbigot. Kinetic analysis of the thermal degradation of an epoxy-based intumescent coating. *Polymer Degradation and Stability*, 94(3):404–409, 2009.

[145] S.M. Neininger, J.E.J. Staggs, A.R. Horrocks, and N.J. Hill. A study of the global kinetics of thermal degradation of a fibre-intumescent mixture. *Polymer Degradation and Stability*, 77(2):187–194, 2002.

[146] E. Kandare, B.K. Kandola, and J.E.J. Staggs. Global kinetics of thermal degradation of flame-retarded epoxy resin formulations. *Polymer Degradation and Stability*, 92(10):1778–1787, 2007.

[147] S. Feih. Finding kinetic parameters from tga curves with a multi-branch least squares fit. Technical Report CRC-ACS TR05002, Cooperative Research Centre for Advanced Composite Structures Limited, 2005.

[148] S. Feih, Z. Mathys, A.G. Gibson, and A.P. Mouritz. Modelling the compression strength of polymer laminates in fire. *Composites Part A: Applied Science and Manufacturing*, 38(11):2354–2365, 2007.

[149] H.D. Baehr and K.S. *Heat and Mass Transfer.* Springer Berlin Heidelberg, 2006.

[150] M.P. Heisler. Temperature charts for induction and constant-temperature heating. *Transactions of the ASME*, pages 227–236, 1947.

[151] M. Yovanovich. Simple explicit expressions for calculation of the Heisler-Grober charts. In *Guidance, Navigation, and Control and Co-located Conferences.* American Institute of Aeronautics and Astronautics, 1996.

[152] Y.A. Cengel. *Heat Transfer: A Practical Approach.* McGraw-Hill, 2007.

[153] S.H. Goodman. *Handbook of Thermoset Plastics (Second Edition)*, chapter 6 - Epoxy Resins. William Andrew Publishing, Westwood, NJ, 2nd edition edition, 1999.

[154] J.H. Lienhard. *A Heat Transfer Textbook*. Dover Books on Engineering. Dover Publications, 2011.

[155] S. Sahin and S.G. Sumnu. *Physical Properties of Foods*. Food Science Text Series. Springer, 2007.

[156] A. Bhargava and G.J. Griffin. A two dimensional model of heat transfer across a fire retardant epoxy coating subjected to an impinging flame. *Journal of Fire Sciences*, 17(3):188–208, 1999.

[157] M. Gomez-Mares, A. Tugnoli, G. Landucci, F. Barontini, and V. Cozzani. Behavior of intumescent epoxy resins in fireproofing applications. *Journal of Analytical and Applied Pyrolysis*, 97:99–108, 2012.

[158] R.E. Lyon. Pyrolysis kinetics of char forming polymers. *Polymer Degradation and Stability*, 61(2):201–210, jan 1998.

[159] T.D. Eastop and A. McConkey. *Applied Thermodynamics*. Longman, London and New York, 1978.

[160] D.R. Croft and D.G. Lilley. *Heat transfer calculations using finite difference equations*. Applied Science Publishers, 1977.

[161] S. Lundberg. Material aspects of fire design. Technical Report TALAT 2502, European Aluminium Association, 1994.

[162] F. Mazzolani. *Aluminium Alloy Structures, Second Edition*. Taylor & Francis, 1994.

[163] P. Krysl, W.T. Ramroth, L.K. Stewart, and R.J. Asaro. Finite element modelling of fibre reinforced polymer sandwich panels exposed to heat. *International Journal for Numerical Methods in Engineering*, 61(1):49–68, 2004.

[164] W.T. Ramroth, P. Krysl, and R.J. Asaro. Sensitivity and uncertainty analyses for FE thermal model of FRP panel exposed to fire. *Composites Part A: Applied Science and Manufacturing*, 37(7):1082–1091, 2006.

[165] B.Y. Lattimer, J. Ouellette, and J. Trelles. Measuring properties for material decomposition modeling. *Fire Mater.*, 35(1):1–17, 2011.

[166] P.T. Summers, B.Y. Lattimer, S. Case, and S. Feih. Sensitivity of thermo-structural model for composite laminates in fire. *Composites Part A: Applied Science and Manufacturing*, 43(5):783–792, 2012.

[167] E.D. McCarthy, B.K. Kandola, G. Edwards, P. Myler, J. Yuan, Y.C. Wang, and E. Kandare. Modelling flaming combustion in glass fibre-reinforced composite laminates. *Journal of Composite Materials*, 47(19):2371–2384, 2013.

[168] A.R. Bahramian. Pyrolysis and flammability properties of novolac/graphite nanocomposites. *Fire Safety Journal*, 61:265–273, 2013.

[169] J. Trelles and B.Y. Lattimer. Modelling thermal degradation of composite materials. *Fire and Materials*, 31(2):147–171, 2007.

[170] A. Galgano, C. Di Blasi, C. Branca, and E. Milella. Thermal response to fire of a fibre-reinforced sandwich panel: Model formulation, selection of intrinsic properties and experimental validation. *Polymer Degradation and Stability*, 94:1267–1280, 2009.

[171] P. Patel. *Investigation of the Fire Behaviour of PEEK-based Polymers and Compounds.* PhD thesis, University of Central Lancashire, 2011.

[172] P. Patel, T.R. Hull, R.E. Lyon, S.I. Stoliarov, R.N. Walters, S. Crowley, and N. Safronava. Investigation of the thermal decomposition and flammability of peek and its carbon and glass-fibre composites. *Polymer Degradation and Stability*, 96(1):12–22, 2011.

[173] A. Gibson, T. Browne, S. Feih, and A. Mouritz. Modeling composite high temperature behavior and fire response under load. *Journal of Composite Materials*, 46(16):2005–2022, 2012.

[174] P. Tranchard, F. Samyn, S. Duquesne, M. Thomas, B. Estebe, J.-L. Montes, and S. Bourbigot. Fire behaviour of carbon fibre epoxy composite for aircraft: Novel test bench and experimental study. *Journal of Fire Sciences*, 33(3):247–266, 2015.

[175] ISO 2685. *ISO International Organization for Standardization*, 1998. Aircraft – Environmental test procedure for airborne equipment – Resistance to fire in designated fire zones.

[176] T.N.A. Browne. *A model for the structural integrity of composite laminates in fire.* PhD thesis, University of Newcastle Upon Tyne, 2006.

[177] Omega.com. http://www.ib.cnea.gov.ar/ experim2/Cosas/omega/emisivity.htm. Accessed: 2015-09-22.

[178] R. Albatici, F. Passerini, A.M. Tonelli, and S. Gialanella. Assessment of the thermal emissivity value of building materials using an infrared thermovision technique emissometer. *Energy and Buildings*, 66:33–40, 2013.

[179] E. Kandare, S. Feih, A. Kootsookos, Z. Mathys, B.Y. Lattimer, and A.P. Mouritz. Creep-based life prediction modelling of aluminium in fire. *Materials Science and Engineering: A*, 527(4-5):1185–1193, 2010.